ALMA MATER STUDIORUM
UNIVERSITÀ DI BOLOGNA

DOTTORATO DI RICERCA IN

CHIMICA

Ciclo XXXVIII

Settore Concorsuale: 03/C1 - CHIMICA ORGANICA

Settore Scientifico Disciplinare: CHIM/06 - CHIMICA ORGANICA

NATURAL AND SYNTHETIC MODULATORS OF LIPID PEROXDATION: PRO-AROMATIC CYCLOHEXADIENES AS ANTIOXIDANTS AND FREE FATTY ACIDS AS PRO-OXIDANTS

Presentata da: Zongxin Jin

Coordinatore Dottorato:
Prof. Cristina Puzzarini

Supervisore:
Prof. Riccardo Amorati

Co-supervisore:
Dr. Andrea Baschieri

Esame finale anno 2026

Abstract

Lipid peroxidation (LP) is a critical oxidative process characterized by free radical chain reactions that lead to the degradation of lipids, playing a significant role in biological systems and food science. In biological contexts, LP is implicated in ferroptosis, an iron-dependent form of programmed cell death associated with neurodegenerative diseases, ischemia-reperfusion injury, and tumor cell resistance to chemotherapy. In food systems, LP contributes to the oxidative rancidity of edible oils, reducing shelf life and nutritional quality. This thesis investigates the modulation of LP through two complementary approaches: the antioxidant activity of pro-aromatic natural terpenes and the pro-oxidant effects of free fatty acids (FFAs), as detailed in two chapters based on experimental studies conducted in heterogeneous model systems and edible oil matrices.

Chapter 2 focuses on the essential oil component γ-terpinene (γ-T), a monoterpene with a unique 1,4-cyclohexadiene structure, which exhibits antioxidant properties through a novel radical exporting ("slingshot") mechanism. This mechanism involves hydrogen atom transfer (HAT) from bis-allylic CH_2 groups, forming a stabilized alkyl radical that rapidly reacts with molecular oxygen to produce a peroxyl radical with conjugated double bonds. Subsequently, an intramolecular 1,4-HAT releases a hydroperoxyl radical (HOO•), leading to aromatization into p-cymene. This process effectively inhibits LP in heterogeneous systems such as micelles and liposomes, and demonstrates remarkable protective activity against ferroptosis in human neuroblastoma (SH-SY5Y) cells at submicromolar concentrations. Collaborative biological experiments, supported by data interpretation, highlight γ-T's potential as a therapeutic agent for ferroptosis-related pathologies. The kinetic parameters of this antioxidant activity were assessed using oxygen uptake measurements, providing insights into the rate constants of chain propagation and termination, which are critical for designing effective antioxidant strategies.

Chapter 3 explores the pro-oxidant role of FFAs, such as palmitic acid, in accelerating LP in edible oils at 130 °C, a temperature relevant to food processing and storage. Using an advanced optical oxygen probe to monitor O_2 consumption, the study quantifies the kinetics of autoxidation in vegetable oil matrices, including high linoleic sunflower oil (HLS), high oleic sunflower oil (HOS), and stripped high linoleic sunflower oil (SHLS). FFAs, formed through triacylglycerol hydrolysis during oil processing, were found to enhance thermo-oxidative degradation in a concentration-dependent manner, promoting the formation of hydroperoxides (LOOH) and secondary oxidation products such as epoxides and aldehydes. These secondary products contribute to off-flavors, nutritional loss, and potential toxicity. The influence of FFAs on antioxidant efficacy was also investigated, revealing complex interactions with natural and synthetic antioxidants (e.g., BHT, TBHQ, and phenolic compounds). Spectroscopic techniques, including 1H-NMR and FT-IR, were employed to characterize oxidation products and confirm mechanistic pathways, such as Fenton-like reactions, which drive an unprecedented dissociative electron transfer occurring between antioxidants and peroxides. The study further examines the impact of specific oxidation by-products, like methyl oleate epoxide, on LP propagation.

Together, these investigations provide a comprehensive understanding of LP modulation, bridging fundamental chemical kinetics with practical applications. The findings highlight γ-T's potential as a novel antioxidant for mitigating ferroptosis in clinical settings and suggest strategies for counteracting FFA-induced oxidative instability in edible oils, enhancing food preservation and safety. The integration of kinetic analyses, oxygen consumption measurements, and spectroscopic data offers a robust framework for developing targeted interventions in both biological and industrial contexts.

Acknowledgements

First, I would like to express my deepest gratitude to the China Scholarship Council (CSC) for providing essential financial support throughout my PhD journey. I am profoundly thankful to my supervisor, Professor Riccardo Amorati, for welcoming me into his research group and offering unwavering guidance and support, which were instrumental in the successful completion of my PhD projects and thesis. My sincere appreciation also extends to my co-supervisor, Dr. Andrea Baschieri, and Professor Luca Valgimigli for their invaluable assistance with the synthesis components of this thesis.

I am grateful to Professor Christian Bergamini, Dr. Francesca Valenti, Dr. Chiara Diquigiovanni, and other colleagues in the Department of Pharmacy and Biotechnology for their contributions to the biological aspects of my research. Additionally, I wish to thank Professor Grzegorz Litwinienko and Professor Laura Goracci for providing me with the opportunity to conduct research for two months at the Faculty of Chemistry, University of Warsaw, and the Department of Chemistry, Biology, and Biotechnology, University of Perugia, respectively, where I collaborated with researchers from diverse backgrounds.

Finally, I extend my heartfelt thanks to all my colleagues in our research group for their constant support, encouragement, and assistance, which were crucial in helping me complete my research.

Statement of Originality

I hereby certify that the work described in this thesis is the original work of the author, with exceptions for work performed by collaborators noted in the acknowledgement. The work in this thesis draws upon a great deal of published research. Any published (or unpublished) work by others is cited and fully acknowledged within the references.

Zongxin Jin

Table of Contents

List of Scheme

List of Figure

List of Table

List of Abbreviations

7-HDC: 7-Dehydrocholesterol
COX: cyclooxygenase
BSO: L-buthionine sulfoximine
CoA: coenzyme A
TF: Transferrin:
TFR1: Transferrin Receptor 1
GPX4: glutathione peroxidase 4
GSH: reduced glutathione
γ-T: γ-Terpinene
α-T: α-Terpinene
Myr: myrcene
Cym: p-Cymene

AIBN: 2,2′-Azobis(isobutyronitrile)

AAPH: 2,2'-azobis(2-amidinopropane) dihydrochloride

Trolox: (±)-6-hydroxy-2,5,7,8-tetramethylchromane-2-carboxylic acid

α-TOH: α-tocopherol

PMHC: 2,2,5,7,8-pentamethyl-6-chromanol

INT: iodonitrotetrazolium chloride

DMSO: Dimethyl sulfoxide

BHT: butylated hydroxytoluene

TBHQ: tert-Butylhydroquinone

PG: propyl gallate

HLS: High linoleic Sunflower oil

HOS: High oleic Sunflower oil

SHLS: Stripped High linoleic Sunflower oil

GT: Glyceryl Triacetate

PA: Palmitic acid

CA: Cinnamic acid

DCP: Dicumyl Peroxide

CHP: Cumene hydroperoxide

KSCN: Potassium thiocyanate

PE: Methyl palmitate

OX: Oxidized Stripped sunflower oil

ME: Methyl palmitate Epoxide

PhCl: Chlorobenzene

PUFA: polyunsaturated fatty acids

Q: *ortho- para*-benzoquinones

QH•: semiquinone radical

QH2: hydroquinone/catechol

RH: Hydrocarbons

ROO•: Peroxyl radicals

ROOH: Hydroperoxides

ROS: reactive oxygen species

HOO•: Hydroperoxides

$O_2•^-$: superoxide

S: substrate

1 Introduction

1.1 Lipid Peroxidation and Ferroptosis

Lipids are a group of organic chemicals which including fats, waxes, sterols, monoglycerides, phospholipids and others. They fundamental exist in dietary products, vegetable oils, particularly those rich in mono-unsaturated fatty acids (MUFA) and poly-unsaturated fatty acids (PUFA), have become the most important nutrition in daily life with the growth-demanding.[1]

Lipid peroxidation (LP), a complex chemical process that leads to the oxidative degradation of lipids, was firstly investigated in early 20th century. It also has been proposed to underlie numerous effects observed in biological systems, primarily because, once initiated, it proceeds via a free radical chain reaction mechanism. On the other hand, the oxygen radicals which formed in the living organisms, are responsible for the lipid peroxidation, leading to a sequence of reactions when not terminated. Therefore, LP is a very attractive topic for explaining many diseases and the side effect and drug-toxic.[2] Main reason is that the lipid peroxides producing the toxic secondary messengers which play an important role in multiple pathologies and cell death. One clinical area where LP is significant is degenerative disease of the brain and the central nervous system (CNS), because brain consumed a large amount of oxygen and generates too much reactive oxygen species (ROS) as the byproducts while synthesizing the ATP. Due to the highly content of PUFAs in the membrane phospholipids of CNS, the free fatty acids could rapidly be incorporated. The combined results provide a environment which contains all the materials for LP.[3]

The interest in LP has recently intensified, since the formal recognition of ferroptosis as a new distinct form of programed cell death in 2012. This form was driven by LP and is closely associated to the pathophysiology of various degenerative diseases and the tumor cell resistance to chemotherapy.[4]

Ferroptosis is a regulated cell death mechanism implicated in severe diseases such as neurodegeneration and ischemia–reperfusion injury.[5] Its molecular basis lies in the impairment of lipid hydroperoxide detoxification by glutathione peroxidase 4 (GPX4). GPX4 is a selenoprotein that uses glutathione to catalyze the reduction of lipid hydroperoxides to the corresponding alcohols. When hydroperoxides coexist with labile iron, they generate uncontrolled free radicals through the Fenton reaction, triggering peroxidation of the phospholipid bilayer. This process ultimately leads to loss of membrane integrity and cell death.

In recent years, significant progress has been made in elucidating the mechanisms underlying ferroptosis. Initially, the system X_c^- (a plasma membrane antiporter, mainly composed of: SLC7A11 and SLC3A2)–GSH–GPX4 pathway was identified as a key suppressor of ferroptosis. Subsequent studies have established that phospholipid hydroperoxides (PLOOHs)—a class of lipid-based ROS—act as the principal executioners of ferroptotic cell death.[6] Furthermore, the mechanisms underlying the synthesis of PLOOHs—particularly the biosynthesis and activation of polyunsaturated fatty acids (PUFAs), which serve as precursors to PLOOHs—have been extensively investigated in the context of ferroptosis.

GPX4 is a central regulator of ferroptosis, a distinct form of non-apoptotic, iron-dependent cell death characterized by lipid peroxidation. This cell death pathway was identified through a high-throughput screen by the Stockwell group[7], revealing compounds like erastin and RSL3 that induce ferroptosis by inhibiting system x_c^- and GPX4, respectively. GPX4, a selenoenzyme, detoxifies PLOOHs using glutathione (GSH) or other thiol donors. Genetic studies, including Gpx4 knockout mouse models, demonstrated that loss of GPX4 function leads to lipid peroxidation and neurodegeneration. (See Scheme 1)

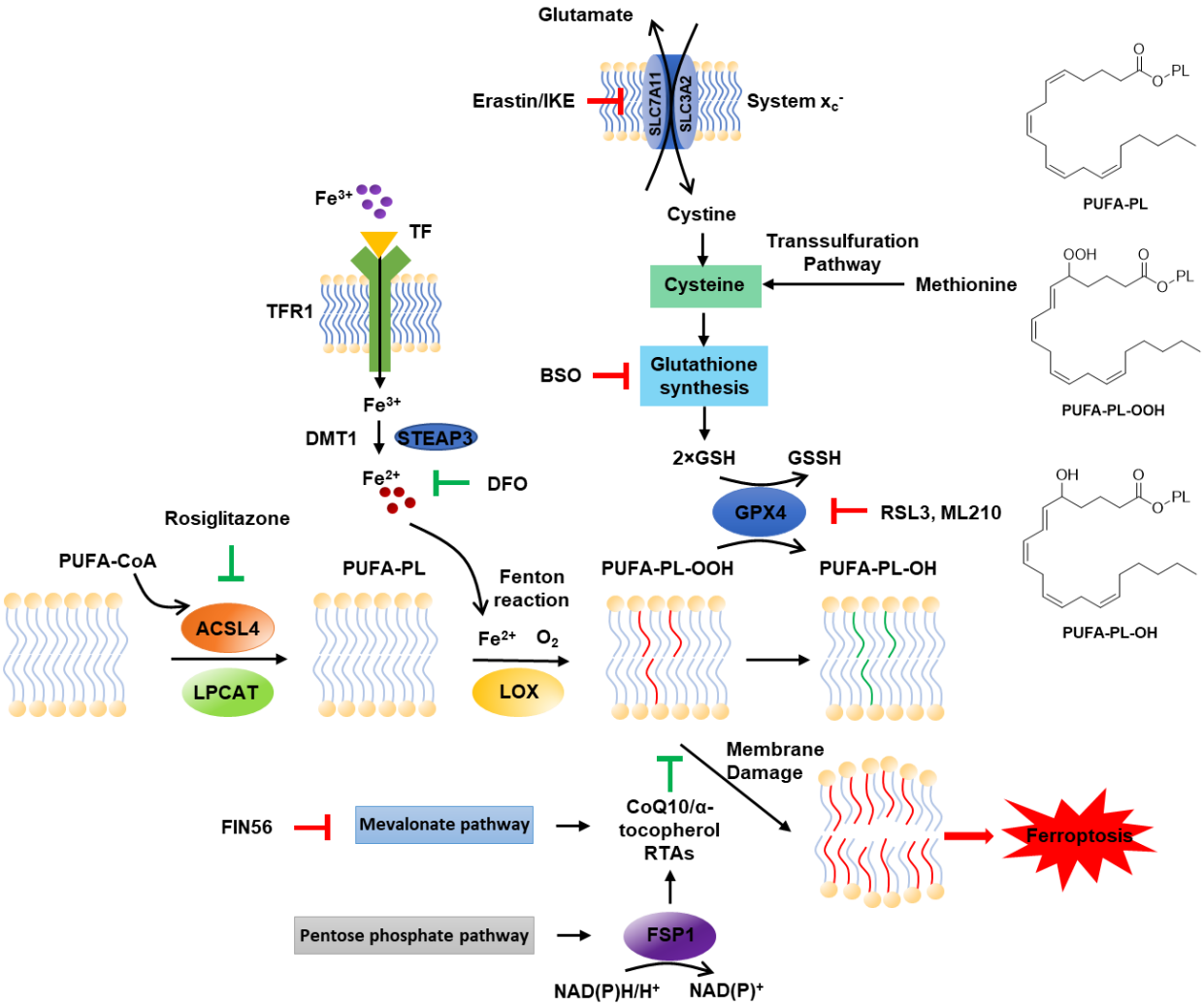
Glutamate
Erastin/IKE
SLC7A11
SLC3A2
System x_c^-
Cystine
Transsulfuration Pathway
Cysteine
Methionine
BSO
Glutathione synthesis
2×GSH
GSSH
GPX4
RSL3, ML210
PUFA-PL
PUFA-PL-OOH
PUFA-PL-OH
Fe^{3+}
TF
TFR1
DMT1
STEAP3
Fe^{2+}
DFO
Rosiglitazone
PUFA-CoA
ACSL4
LPCAT
Fenton reaction
O_2
LOX
Membrane Damage
FIN56
Mevalonate pathway
CoQ10/α-tocopherol RTAs
Ferroptosis
Pentose phosphate pathway
FSP1
$NAD(P)H/H^+$
$NAD(P)^+$

***Scheme 1.1**, Key regulators and pathways contributing to ferroptotic cell death. Cyst(e)ine availability—through uptake via the system xc- or the transsulfuration pathway—is critical for glutathione (GSH) biosynthesis. The degree of lipid bilayer unsaturation, influenced by the enzymatic activities of ACSL4 and LPCAT, in combination with iron-dependent lipid peroxidation, promotes ferroptosis. GPX4 serves as the central regulator, efficiently inhibiting the auto-initiation of lipid peroxidation. Numerous ferroptosis activators and inhibitors have been identified, targeting different aspects of this pathway. ACSL4, acyl-CoA synthetase long-chain family member-4; BSO, L-buthionine sulfoximine; CoA, coenzyme A; TF, Transferrin; TFR1, Transferrin Receptor 1; DMT1, Divalent Metal Transporter 1; STEAP3, Six-transmembrane epithelial antigen of the prostate 3; DFO, deferoxamine; FSP1, ferroptosis suppressor protein 1; GPX4, glutathione peroxidase 4; GSH, reduced glutathione; GSSG, oxidized glutathione; LOX, lipoxygenase; LPCAT, lysophosphatidylcholine acyltransferase; PUFA, polyunsaturated fatty acid; RTA, radical trapping antioxidant.*

Phospholipid peroxidation is another mechanism that causes ferroptosis. The removal of a bis-allylic hydrogen atom from polyunsaturated fatty acyl moieties in phospholipids (PUFA-PLs) is necessary to start lipid peroxidation. This process produces a phospholipid radical (PL•), which then forms a phospholipid peroxyl radical (PLOO•) by reacting with molecular oxygen. Phospholipid hydroperoxides (PLOOH) can be created when the PLOO• radical removes hydrogen atoms from nearby PUFA-PLs.[8] These lipid peroxides cause widespread membrane damage and eventually cell death if GPX4 is unable to detoxify them. Important enzymes like ACSL4 and LPCAT3 increase the amount of PUFAs in cells by facilitating their incorporation into membrane phospholipids. Although the composition of the membrane depends on this remodeling, it also makes cells more vulnerable to ferroptosis. ACSL4's potential as a therapeutic target is thus highlighted by the correlation between its expression and ferroptosis sensitivity in some cancers, such as triple-negative breast cancer.

Iron is indispensable to the execution of ferroptosis, primarily due to its role in catalyzing lipid peroxidation through the Fenton reaction. Upon GPX4 inhibition, PLOOHs interact with ferrous (Fe^{2+}) and ferric (Fe^{3+}) ions to generate lipid radicals (PLO•, PLOO•),

propagating damaging oxidative chain reactions.[8] Ferrous iron is particularly potent due to its higher solubility and reactivity. Additionally, iron is required for the activity of key enzymes such as lipoxygenases (LOXs) and cytochrome P450 oxidoreductase (POR), which further promote lipid peroxidation. Iron chelator, such as deferoxamine (DFO), play a crucial role in modulating ferroptosis by reducing intracellular labile iron levels.

Coenzyme Q oxidoreductase FSP1 represents another regulation of ferroptosis. FSP1 functions as an NADH/NADPH-dependent CoQ_{10} oxidoreductase, utilizing NADH or NADPH to reduce coenzyme Q_{10} (CoQ_{10}, ubiquinone) to its active antioxidant form, $CoQ_{10}H_2$ (ubiquinol). CoQ_{10} is a lipophilic molecule predominantly located in the inner mitochondrial membrane. Its reduced form, $CoQ_{10}H_2$, functions as a lipophilic antioxidant by scavenging free radicals to prevent lipid peroxidation. Additionally, it can indirectly regenerate another important antioxidant, α-tocopherol, thereby enhancing the cellular capacity to neutralize free radicals.[9]

1.2 Vegetable Oils and Lipid peroxidation

Vegetable oil, an indispensable component of human diet has become the majority source of edible lipids, accounting for more than 75% of the world's total lipid consumption.[10] Among them, around 75% of vegetable oils are extracted from the endosperm of oilseeds, such as soybean and rapeseed, while the remaining 25% is obtained from the mesocarp (peel) of oil-rich fruits, primarily oil palm and olive.[11] Vegetable oils have become the main source of fatty acids and essential fatty acids, as well as an important medium for cooking. They not only provide energy but also play a key role in maintaining normal body temperature, protecting body tissues, and transporting fat-soluble vitamins.[12]

1.2.1 The chemical compositions of oil

The chemical composition of vegetable oils is different depending on their origins. The main chemical components in vegetable oils are Fatty acid, the fundamental role to protect the organism and the structural building block of cell membrane to suppliers of energy and signalling molecules; Phytosterols, a plant derived sterols with similar structure as

cholesterol regarding the physiological functions and structures of vertebrate animals[13]; Tocopherols, major fat-soluble vitamin present in vegetable oils, acts as a potent antioxidant by inhibiting the peroxidation of unsaturated lipids through chain-breaking reactions[14]; Phenolic compounds are important secondary metabolites presented in different foods and play an important role in prevention of various diseases, such as cancer, and hyperlipoidemia.[15] and other minor components, like squalane or β-Carotene.[12] The most common vegetable oils in EU, are olive oil, groundnut, sunflower oil and soybean oil, and etc. For example, sunflower oil is consisted with triglycerides, which are ester derived from glycerol and fatty acids, fatty acid contains ≈ 16% of oleic acid (C 18:1, OA), ≈ 68% of linoleic acid (C 18:2, LA), 6% of Palmitic acid (C 16:0, PA), 5% of stearic acid (C 18:0, SA) and small quantities of SFAs and USFAs; 500 ~ 1200 ppm of Tocopherols (mainly α-TOH), 3000 ~ 5000 ppm of Phytosterols.[16] Other oils contain specific bioactive components, such as omega-3 fatty acids, which are known to benefit heart health and reduce inflammation. These are particularly abundant in flaxseed oil and canola oil.[17]

Fatty acids play multiple roles in the organism of human and animal. They are fundamental components of human nutrition and physiology and they serve as the primary building blocks of lipids, providing a dense source of energy and forming essential structural elements of cell membranes. Beyond their role in energy metabolism, fatty acids are crucial for maintaining membrane fluidity, regulating signaling pathways, and supporting the function of vital organs. Fatty acids normally could be classified into three catalogs with respect to their structures, saturated fatty acid (SFA), Polyunsaturated fatty acid (PUFA) and Monounsaturated fatty acid (MUFA).[18] It has been found that regular intake of SFAs increases cholesterol levels, and elevated cholesterol levels are associated with increased mortality from coronary heart disease.[19] MUFA can prevent cardiovascular diseases by several mechanisms and PUFA is the most important fatty acid which contains two or more double bounds in the molecules. Meanwhile, PUFAs is a very important substance, also can prevent cardiovascular diseases, cancer and chronic diseases.[20]

1.2.2 Lipid peroxidation on PUFAs

Among the oxidative damaging biomolecular targets, damage to lipids, especially PUFAs and the derived triglycerides and phospholipids, are primary due to the radical chain propagated peroxidation. Radicals such as ROO•, HO•, HOO•, and RO• can abstract a hydrogen atom from the allylic or bis-allylic positions of PUFAs. These sites are particularly reactive because the resulting radical is delocalized across both double bonds, which lowers the bond dissociation energy (BDE). Specifically, the C–H bond of a bis-allylic group has a BDE of about 76 kcal·mol^{-1}, compared to 85.6 kcal·mol^{-1} at an allylic position,[21] thereby facilitating alkyl radical formation and initiating lipid peroxidation. This alkyl radical reacts with another oxygen very fast, forming a new peroxyl radical and abstract another H-atom from PUFA, thus propagating the oxidation chain and leading to the progressive lipid oxidation, unless external antioxidants terminate such radical chain radical.[22] See Scheme 2.

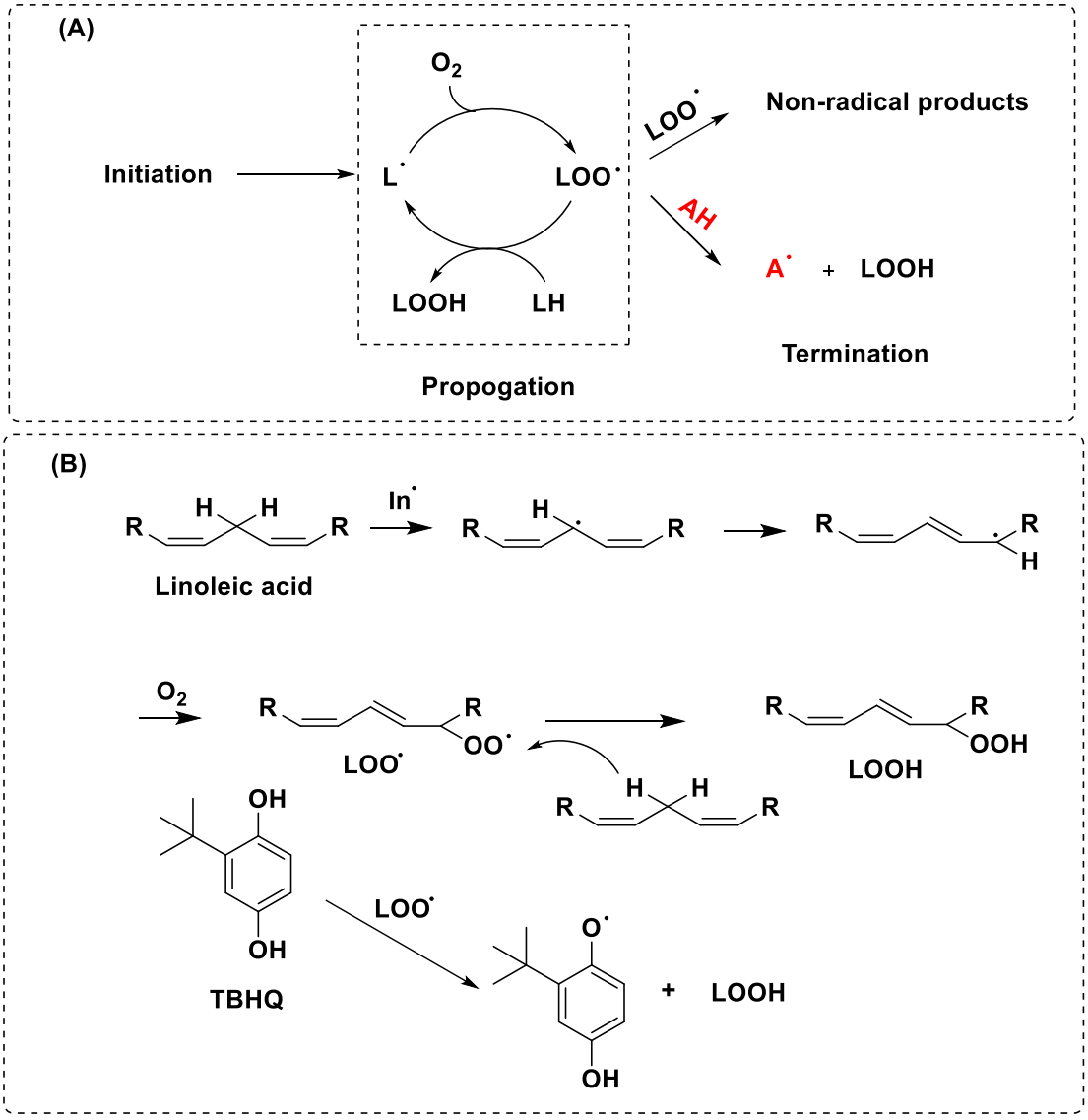

***Scheme 1.2**, A) The main mechanism of autoxidation, B) The main steps of lipid peroxidation*

The main mechanism and steps of lipid peroxidation was introduced in scheme 2. Therefore, here we focus on the hydroperoxides (LOOH) and secondary oxygenated compounds like epoxides, aldehydes, ketones, and diols—which contribute to undesirable effects.[23] During lipid oxidation, the primary products formed are ROOH, which result from the reaction of unsaturated fatty acids with reactive oxygen species. Although relatively stable in the initial stage, LOOH readily decomposed into a wide range of secondary oxygenated compounds. These secondary products are largely responsible for

the undesirable effects associated with lipid peroxidation, including off-flavors, loss of nutritional quality, and potential toxicological risks.[24]

Hydroperoxides are important non-radical intermediates in lipid peroxidation, and their identification can provide valuable mechanistic information, such as whether the primary reaction is mediated by singlet oxygen or by oxygen radicals. Certain cholesterol-derived hydroperoxides (ChOOHs) have been effectively used in this regard in both model systems and cellular studies. Due to their higher polarity compared to parent lipids, LOOHs can disrupt membrane structure and function, which alone may cause cellular damage. Moreover, LOOHs can participate in redox reactions, and their nature and intensity often determine whether peroxidative damage is exacerbated or prevented. The exacerbation of damage may result from iron-catalyzed one-electron reduction of LOOHs, leading to radical-mediated chain peroxidation, whereas prevention may occur through selenium-dependent peroxidase-catalyzed two-electron reduction of LOOHs to relatively non-toxic alcohols.[25]

1.3 Chemistry Mechanism of LP

Lipid peroxidation is the most important type of radical-oxidized damage in the biology system, including the interplay with ferroptosis and the secondary damage of other biochemicals, like proteins. The radical chain reactions triggered by oxidative degradation have been studied for many years, and their mechanisms have been widely understood, particularly regarding the protection of lipids by phenolic and polyphenolic compounds. This is summarized in Eq.(1-7) where LH represents any oxidized lipid molecule and AH indicates antioxidant, while X• and LOO• represents respectively initiating species and the chain-carrying lipid-derived peroxyl radical, LOOH represents lipid hydroperoxides.[22] Since chain-breaking antioxidants act primarily on a kinetic basis (as described in Eqs. (6) and (7)), effectively outcompeting the oxidative chain propagation steps (Eqs. (3) and (4)), understanding the kinetics of lipid peroxidation is essential for the rational design of

effective antioxidant strategies, rather than relying on time-consuming trial-and-error methods.[26]

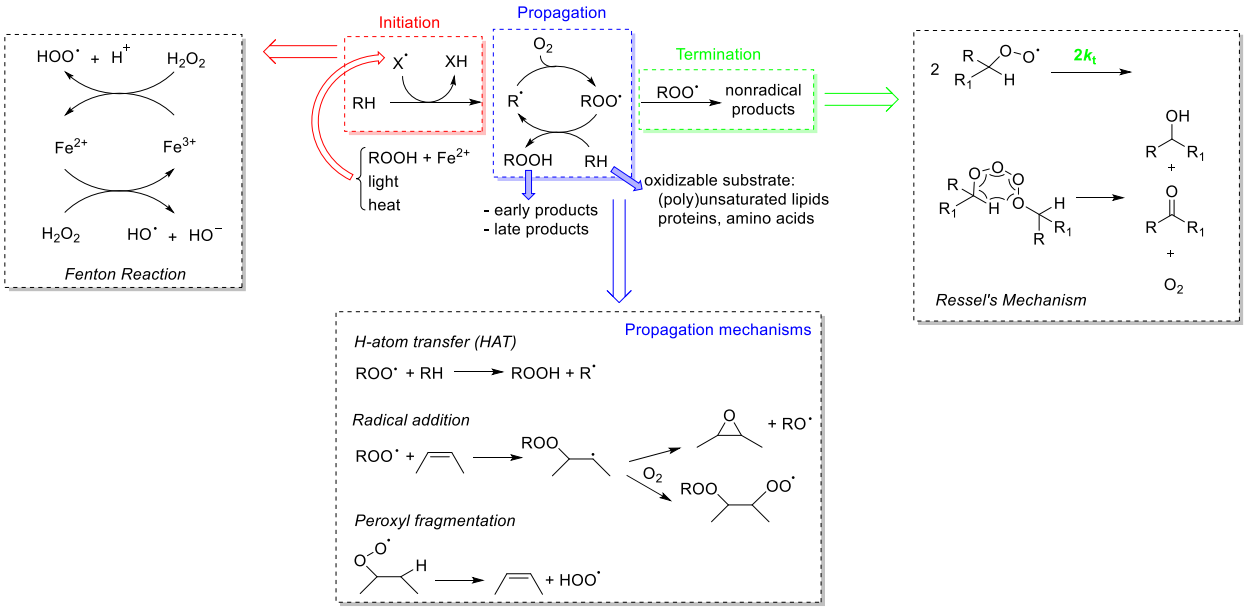

Scheme 1.3, *Mechanism of peroxidation.*

Normally, the lipid chain reaction could divide into three stages, first is **Initiation**. The formation of the first lipid-derived radicals, can consist in attacking by numerous radical species. The most common species are alkoxyl radical (LO•) or a hydroxyl radical (HO•), additionally, hydroperoxyl radicals (HOO•), the neutral form of metabolically produced superoxide radical anion could also initiate the chain reaction.[22]

Propagation of the oxidized chain always occurs two steps, first step is the lipid-derived radical with O2 to form alkylperoxyl radical (LOO•) is quite fast. Thus, the second step gave the main kinetic propagation, the reaction of LOO• with a new lipid molecule form a new lipid-derived radical L•. The k_p is the most important parameter to evaluate the antioxidant strategies. The main products throughout the propagation phase are hydroperoxides (ROOH), which are the primary products of lipid peroxidation (LP)[27], as well as new alkyl peroxyl radicals, which serve as chain-carrying species in the LP process. Chain termination occurs when two radicals quench each other, forming non-radical (diamagnetic) species that are no longer capable of sustaining the chain reaction. Uninhibited LP proceeds via secondary peroxyl radicals, and the most well-established

termination mechanism is the Russell mechanism[28], which involves the formation of a tetroxide intermediate that subsequently decomposes into carbonyl compounds and molecular oxygen.

$$\overset{R_i}{\rightarrow} X\cdot \quad (1)$$

$$X\cdot + LH \rightarrow L\cdot \quad (2)$$

$$L\cdot + O_2 \overset{fast}{\longrightarrow} LOO\cdot \quad (3)$$

$$LOO\cdot + LH \overset{k_p}{\rightarrow} LOOH + L\cdot \quad (4)$$

$$2LOO\cdot \overset{2k_t}{\longrightarrow} non\ radical\ products \quad (5)$$

$$LOO\cdot + AH \overset{k_{inh}}{\longrightarrow} LOOH + A\cdot \quad (6)$$

$$LOO\cdot + A\cdot \overset{fast}{\longrightarrow} LOOA \quad (7)$$

The susceptibility of a specific lipid substrate to peroxidation can be explained by a kinetic parameter known as oxidizability, expressed as $k_p/(2k_t)^{1/2}$. This parameter determines the urgency of antioxidant protection required for that particular lipid substrate. It is defined by the rate constant of chain propagation (k_p, see Eq. 4) and the rate constant of chain termination ($2k_t$, see Eq. 5). Moreover, the effectiveness of any given antioxidant can be predicted by comparing its inhibition rate constant (k_{inh}) with the k_p value of the lipid to be protected — in other words, by comparing the rate described in Eq. 6 with that in Eq. 4.[26]

1.3.1 The products of Lipid Peroxidation

The products of lipid peroxidation can be classified into early products—formed directly during the radical chain reactions—and late products, which result from the degradation or transformation of the early ones. However, this distinction is not always clear-cut, as some compounds can be generated through both pathways.[22,29]

1.3.1.1 Early Product

Early products are mainly represented by hydroperoxides, especially in the case of PUFAs. For example, regarding the linoleate ester residues, the complete product distribution has been shown in Scheme 4, indicating that the relative positions of the double bond and its cis/trans isomers depend on the rate at which the peroxide radical is quenched by H-atom donors.[30] Therefore, during triglyceride peroxidation, trans-trans hydroperoxides are typically formed in greater amounts than cis-trans hydroperoxides. However, in the presence of antioxidants, this ratio can be altered, and the relative concentration of cis-trans hydroperoxides may become higher [31].

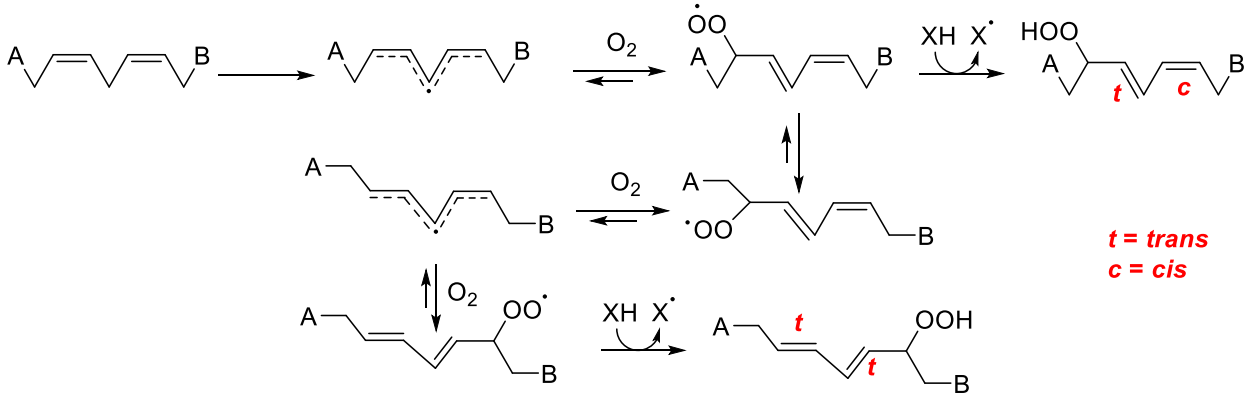

Scheme 1.4. *Simplified mechanism of the formation of early oxidation products from linoleate residues. A and B represent the two ends of the fatty acid, and XH is a generic H-atom donor.*

Product distribution could be very complex when the lipid is highly unsaturated as it can happen the intramolecular radical addition to double bonds to generate cyclic products. See Scheme 5, In the absence of a fast hydrogen atom donor (such as α-tocopherol, α-TOH), arachidonic acid can undergo 5-exo cyclization of peroxyl radicals during autoxidation, with a unimolecular rate constant of approximately 800 s^{-1}, which outcompetes the β-fragmentation reaction ($k_\beta \approx 140\ s^{-1}$)[27]. This process results in the formation of an endoperoxide that still bears a carbon-centered radical (Scheme 5). The endoperoxide can then undergo a second 5-exo cyclization, generating another alkyl radical, which proceeds through further autoxidation steps to yield endoperoxide products or intermediates. These compounds are stereoisomers of certain prostaglandins (such as PGG_2 and $PGF_{2\alpha}$)

produced by cyclooxygenase (COX)[30] and are therefore commonly referred to as isoprostanes.

In 7-Dehydrocholesterol (7-HDC), the autoxidation reaction can proceed either through ROO• addition, leading to the formation of epoxides (In Scheme 5), or via hydrogen atom abstraction—preferentially from the C9–H position[30,32]. The resulting peroxyl radical undergoes 5-exo cyclization at the C5 position to yield a stabilized allylic radical. This radical continues to autoxidize, producing a mixture of α-5,9-endoperoxides and α- & β-6-hydroperoxides[32,33], as illustrated in Scheme 5. In general, the formation of endoperoxides is observed when the geometry of the unsaturated lipid allows for 5-exo cyclization, which can generate either strain-free or resonance-stabilized radicals.

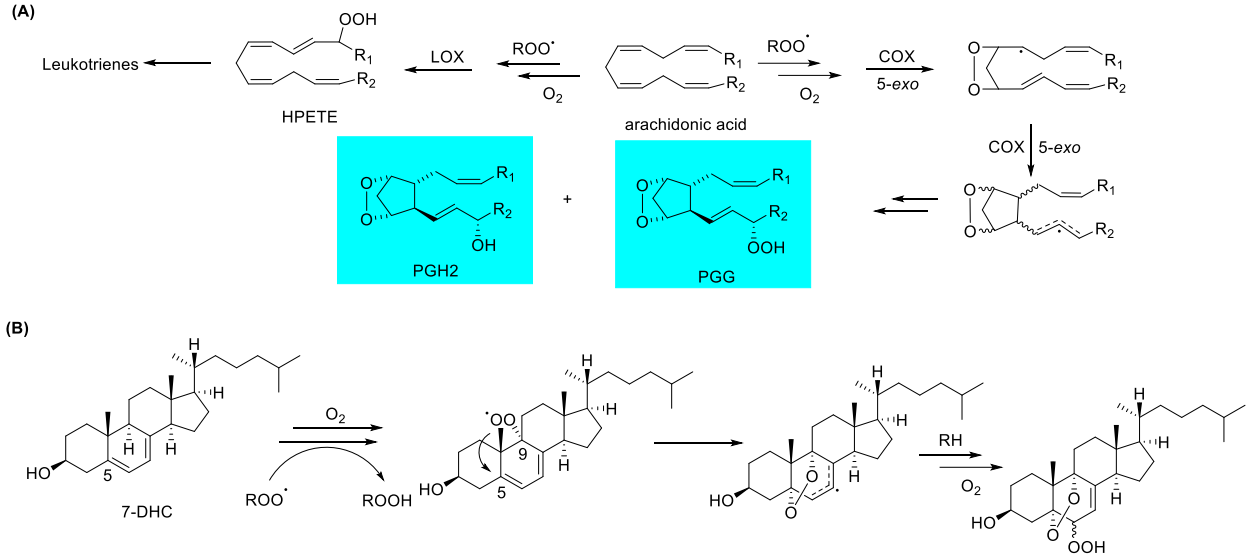

Scheme 1.5, *Formation of endoperoxides during the propagation of lipid peroxidation of arachidonic acid (**A**) and 7-dehydrocholesterol (**B**).*

1.3.1.2 Late Products

The formation of late products is mainly drive by homolytic or heterolytic reaction of hydroperoxides. Thus, the level of hydroperoxide only increased at the beginning of the LP, subsequently decreasing as it is converted into more stable secondary products, which often accumulate during the lipid peroxidation process.[34] Although, the reaction network leading to form secondary products was still extremely complex, however two main

pathways of hydroperoxide decay are well recognized: Hock fragmentation and fenton reaction. The latter is catalyzed by reduced transition metals (such as Fe^{2+}), leading to the formation of alkoxy radicals, which may subsequently rearrange to α-hydroxyalkyls or fragment into alkyl radicals and aldehydes (see Scheme 6B). This reaction is crucial in the initiation of peroxide reactions, as trace metals and hydrogen peroxides are invariably present in lipid materials.[35]

The Hock fragmentation of the primary hydroperoxide in the presence of acid catalyst is the most classical mechanism and through a non-radical pathway transform into two aldehydes. (See Scheme 6A) The natural aldehydes are formed mainly during the reaction of LP depending on the various fatty acid being oxidized. Hydrogen peroxide can also react with alkenes to form epoxides, which can be subsequently attacked by water or acid to produce diols or diesters, respectively[36]. In addition to carbonyl compounds and epoxides, the advanced oxidation of aldehydes can yield other minor products, such as furans, hydroxyl aldehyde condensation products, as well as short-chain acids like acetic and formic acid,[34] which are the primary water-soluble volatiles detected by the Rancimat method.[37]

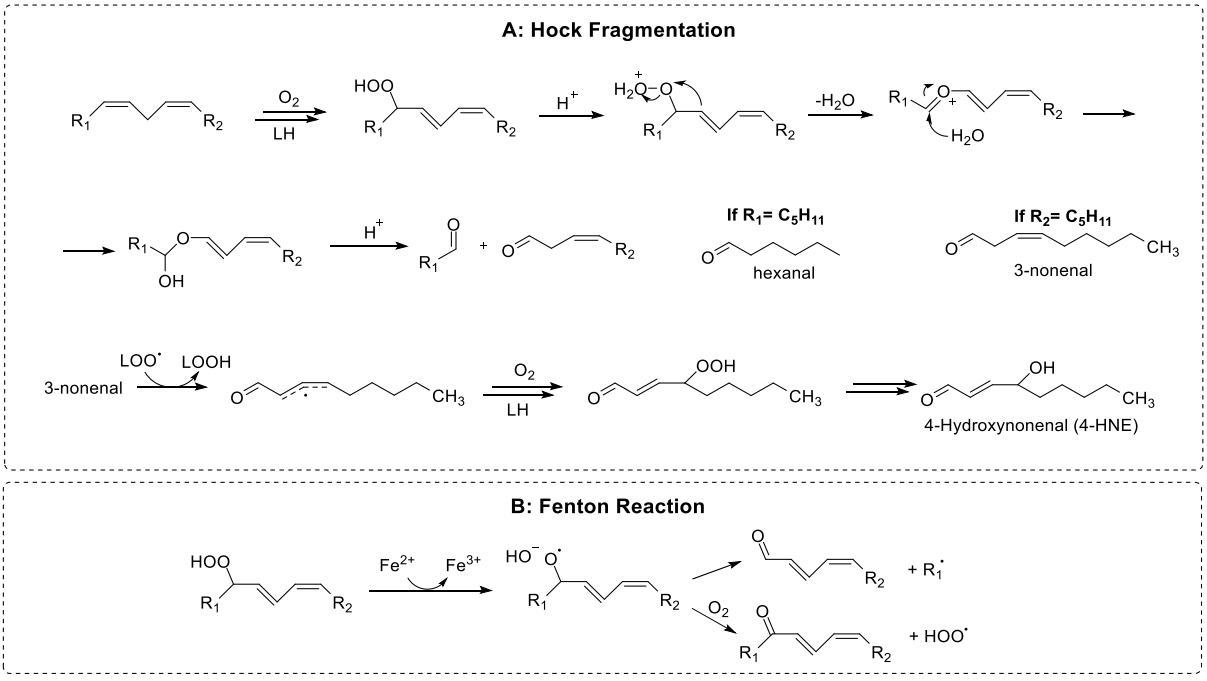

Scheme 1.6, *Examples of mechanisms leading to the formation of late products of lipid peroxidation.*

Epoxide is the secondary oxidation product, mainly formed through the decomposition of LOOH or epoxidation of double bonds, and it can further react to yield aldehydes and diols. For example, the addition reactions of ROO• radicals with C=C double bonds and hydrogen atom transfer (HAT) reactions occur in competition, with the polarity effect of the transition state generally favoring the addition pathway[38]. The resulting alkyl peroxy radicals rapidly undergo homolytic substitution (S_H^i) reactions, leading to the formation of epoxides and the release of alkoxy radicals (RO•), as illustrated in scheme 7. These alkoxy radicals can then attack other lipid molecules, thereby propagating chain reactions.

Aldehydes and ketones are typically generated during the late stages of LP, with 4-hydroxynonenal (4-HNE) being the most representative product. Owing to the presence of unsaturated bonds and their structural similarity to α,β-unsaturated aldehydes and ketones, these compounds are highly electrophilic and exhibit strong reactivity toward nucleophiles, including DNA and amino acids. Such interactions contribute not only to cellular damage but also to their role as signaling molecules, thereby linking their biological function with potential toxicity.[39] Malondialdehyde (MDA) is a dicarbonyl compound and one of the most widely recognized markers of LP, largely due to its ease of detection. It is commonly measured by derivatization with thiobarbituric acid, producing a colored adduct that can be quantified spectrophotometrically or by high-performance liquid chromatography (HPLC), in what is known as the thiobarbituric acid reactive substances (TBARS) assay.[40]

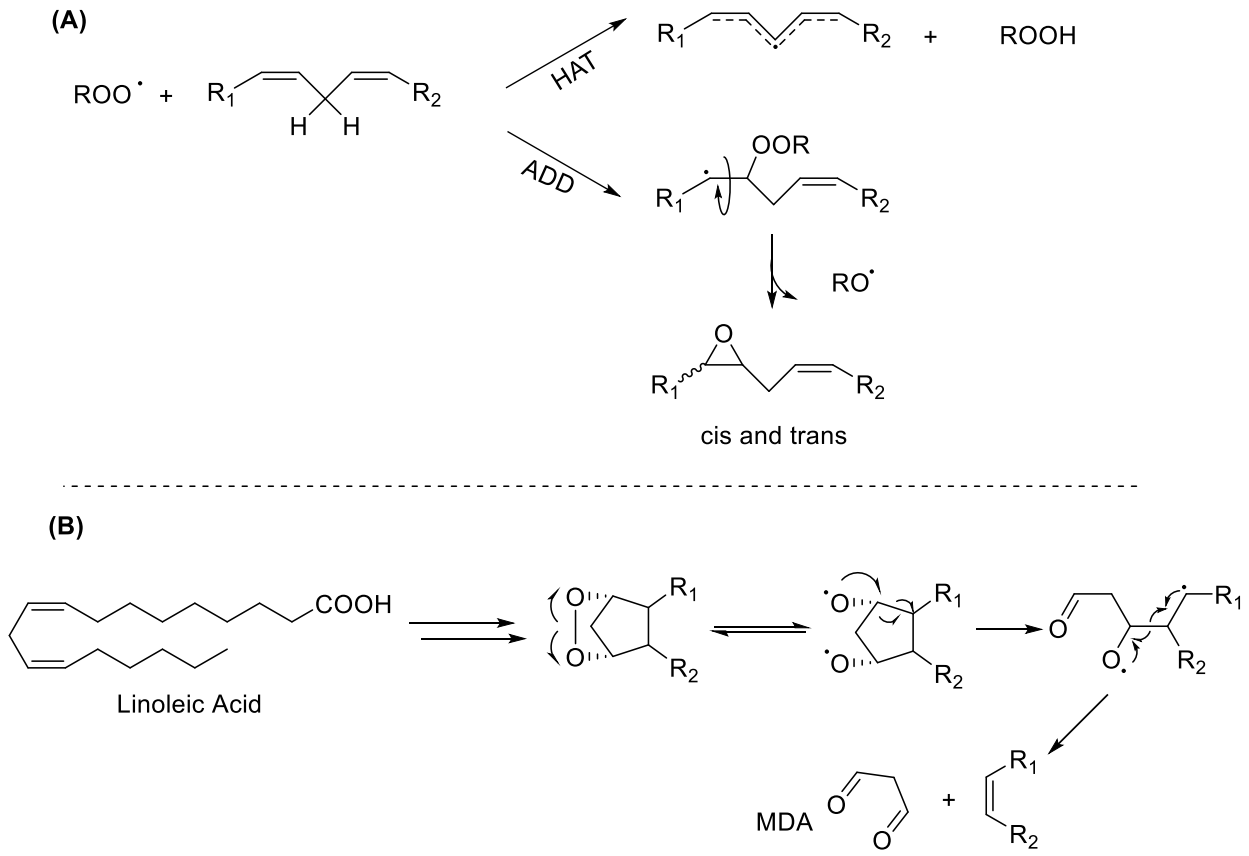

Scheme 1.7, *A) Formation of epoxides during the peroxidation of PUFA, B) malondialdehyde (MDA) from isoprostane pathway*

1.3.2 Method to determine the antioxidant activity

The methods and instruments to measure the antioxidant activity have made a remarkable progress in recent decades. Early methods for evaluating antioxidant efficiency focused on their ability to inhibit the formation of specific lipid oxidation products, thereby directly measuring lipid peroxidation. Over time, a wide range of chemical assays—often coupled with highly sensitive and automated detection technologies—have been developed to assess antioxidant activity through various mechanisms. These include, for example, free radical and reactive oxygen species (ROS) scavenging, reducing power, and metal chelation. Moreover, the substrates used in these assays have expanded beyond simple food model systems to include chemical compounds, biological materials, cell lines, and even living tissues. [41] These testing methods each have their own advantages and disadvantages

based on the detection of different mechanisms. Such as the Oxygen Radical Absorption Capacity (ORAC) test based on the transfer of a hydrogen atom[42], The Cupric Reducing Antioxidant Power (CUPRAC) test based on the transfer of one electron, the mixed tests, like the [2,2-di(4-tert-octylphenyl)-1-picrylhydrazyl] (DPPH) test[43].

1.3.2.1 Oxygen Uptake Apparatus

Monitoring the kinetics of antioxidants can track the consumption of their reactants, typically oxygen, or the formation of intermediate oxidation products.[44,45] Oxygen consumption experiment should be conduct in a closed system and can be monitored one of several methods, such as such as by a polarographic probe. The most accuracy method for measure the kinetic study of antioxidant is the differential pressure transducer. [46] The apparatus is shown below (figure 1A), it consists of two identical reaction vessels (the reference vessel and the sample vessel) are setting at 30ºC, which are connected to both sides of a variable reluctance differential pressure sensor membrane by HPLC tubing. The three-way valve achieves balance and isolation between the two channels, connecting air and the two channels, and ensures oxygen balance between air and the solution through the continuous stirring of a magnetic stirrer. The sensor response (measured in mV/V) is converted to oxygen consumption (M) using a conversion factor, which is determined in separate calibration experiments. Oxygen consumption plots are recorded as the function time, as shown in Figure 1B, where the line A is the autoxidation of substrate in the absence of antioxidant, the others are the inhibits traces obtained after adding antioxidants with different activities.

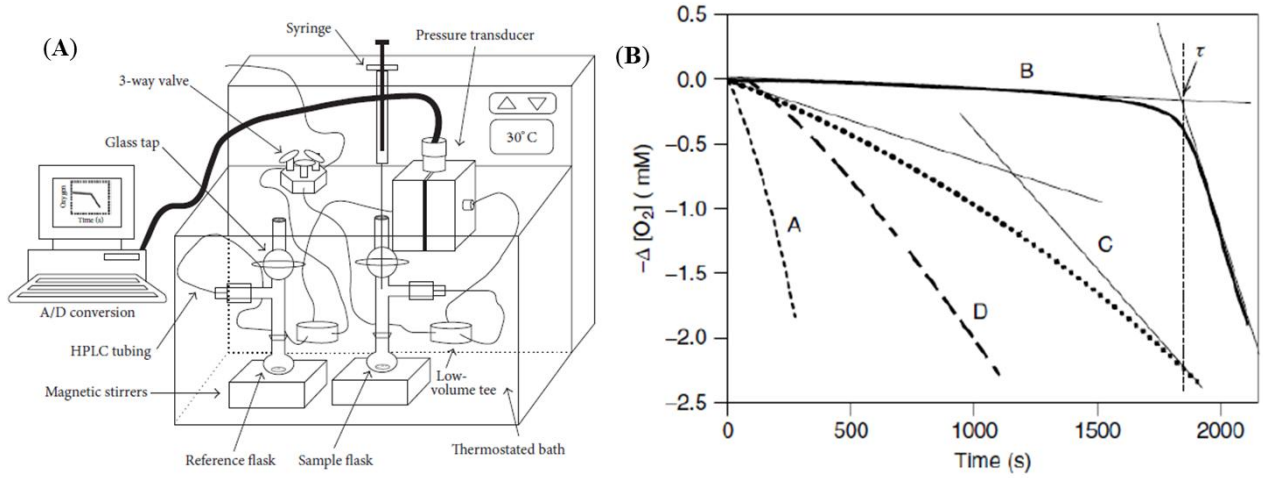

Figure 1.1, *Differential oxygen uptake apparatus for autoxidation kinetics*

1.3.2.2 Measurement of antioxidant ability at high temperature

In both industry and academia, lipid substrate oxidation is typically assessed using parameters such as iodine value, anisidine value, peroxide value, and oxidative stability index (OSI). However, these methods rely on measuring byproducts, provide only partial insights, and are often experimentally demanding. To better understand lipid oxidation reactions at elevated temperatures, our laboratory developed a method based on optically detecting O_2 consumption of substrates during isothermal treatment at 130 °C.[47] Monitoring O_2 uptake is one of the most reliable approaches for studying autooxidation reactions, as it minimizes interference from other processes and allows the determination of key kinetic parameters that describe substrate behavior under these conditions. Figure 1 illustrates the instrumentation employed. O_2 consumption is measured in a round-bottom flask fitted with a short glass condenser. An optical oxygen probe and thermometer are introduced through a silicone rubber septum in the sealing system. The probe operates on the principle of luminescence quenching of a sensing dye: the dye is excited with red light, and the resulting luminescence, measured in the near-infrared region, is quenched by molecular oxygen in a fully reversible manner, altering its intensity and lifetime. This configuration enables direct measurement of oxygen concentration with minimal interference from other gases. The robust oxygen probe, manufactured by PyroScience

GmbH (Aachen, Germany), is connected to a FireSting O_2 control unit equipped with a thermometer probe for continuous temperature correction. The probe tip is maintained at approximately 30 °C by the glass condenser, while the device itself is suitable for monitoring oxygen consumption at reaction temperatures up to 180 °C (See Figure 2).

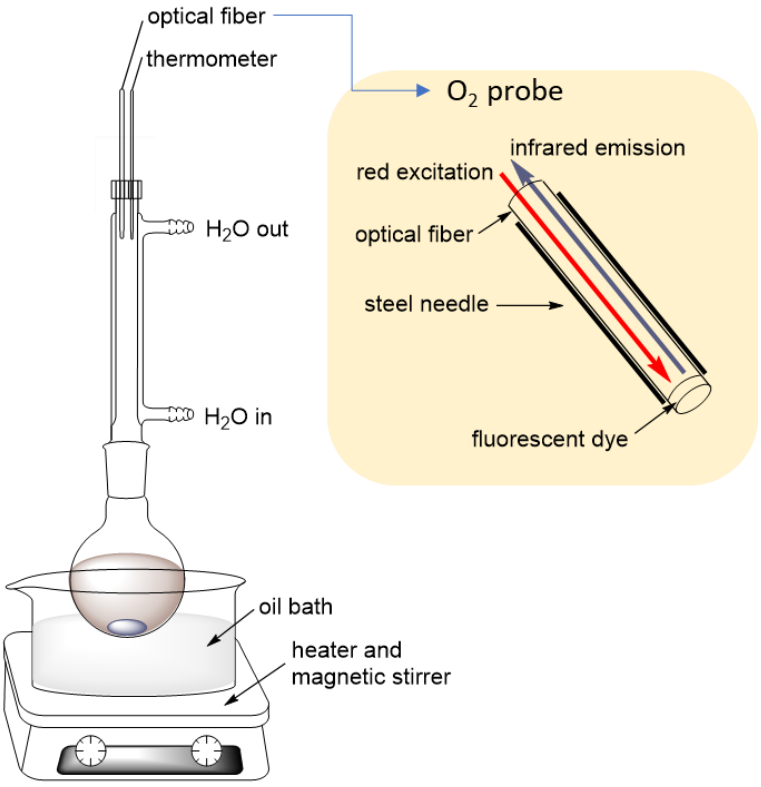

***Figure 1.2**, Apparatus for measuring oxygen consumption and scheme of the optical O_2 probe*

1.3.2.3 Measure the antioxidant activity

The oxygen consumption reflects the extent of the propagation oxidation reaction. At the beginning of the autoxidation without antioxidant, linear plot of oxygen consumption (Plot A in Figure 1.1), the peroxidation of lipid substrate RH (see Equation 4), at the initiation constant (R_i) is constant, follows Equation 8. it is determined by the ratio of the growth rate constant to the square root of the termination rate constant. [48]

$$-\frac{d[O_2]}{dt} = -\frac{d[RH]}{dt} = -\frac{d[ROOH]}{dt} = \frac{k_p}{\sqrt{2k_t}} \times \sqrt{R_i} \times [RH] + R_i \qquad (8)$$

Where [RH] is the initial concentration of the oxidized substrate, R_i is the initiation rate; $k_p/(2k_t)^{1/2}$ is the oxidizability of substrates.

If the antioxidant is effective, an initial phase of inhibition is observed, during which oxidation is significantly delayed. This is followed by a phase that resembles the typical autoxidation curve once the antioxidant has been consumed or deactivated. For a visual representation, refer to plot B in Figure 1. During the inhibition period, antioxidant inhibit the propagation stage of autoxidation by quenching the peroxyl radical to prolong the inhibition period (τ). Thus, the stoichiometric factors n can be determined followed Equation 9.[46] The initial slope of oxygen consumption during inhibition provides Equation 10, determining the inhibition rate constant k_{inh} by assuming that each ROO• free radical is captured by antioxidants and their corresponding free radicals.

$$R_i = \frac{n[AH]}{\tau} \tag{9}$$

$$-\frac{d[O_2]}{dt} = \frac{k_p[RH]R_i}{nk_{inh}[AH]} \tag{10}$$

If the suppression period in Figure 1 is not clearly indicated as in plot B, or if the initial part of the graph cannot be used to obtain the oxygen consumption rate (plot C), then Equation 11 may be utilized. [46,49]

$$\Delta[O_2] = [O_2]_{t=0} - [O_2]_t = -\frac{k_p[RH]R_i}{k_{inh}}\ln(1-\frac{t}{\tau}) \tag{11}$$

There are also some cases like in plot D, where the efficiency of the antioxidant is so small that inhibition period cannot be observed clearly: Equation 12 was drived by Denisov and Khudyakov to determined kihn in such cases.[50,51,52]

$$\frac{d[O_2]_0/dt}{d[O_2]_{inh}/dt} - \frac{d[O_2]_{inh}/dt}{d[O_2]_0/dt} = \frac{nk_{inh}[AH]}{\sqrt{2k_tR_i}} \tag{12}$$

Where the $d[O_2]_{inh}/dt$ is the rate of the oxygen consumption measured from plot, in the presence and absence of the antioxidant.

1.4 Antioxidants and Their Classification

Antioxidants are important compounds able to block the radical-mediated oxidation of many organic materials, including food, plastic, cosmetics, and biomolecules in living organisms. The quest for novel and more active antioxidants is nowadays an active research field. Antioxidants which can slow down the lipid peroxidation and stop the formation of secondary lipid peroxidation, have so many application in food storage, especially to maintain the organoleptic features of vegetal oils and their derivatives, and in plastic and lubricant stabilization.[53] Meanwell, antioxidant can reduce the oxidation of protein and amino acid, as well as the interaction of lipid-derived carbonyls with proteins that changes protein function.[54] Another way to define an antioxidant is as a substance that either directly neutralizes reactive oxygen species (ROS), boosts the body's antioxidant defenses, or inhibits the production of ROS. Antioxidant compounds help extend shelf-life by scavenging free radicals and slowing down lipid peroxidation, which is a major factor contributing to the deterioration of food and pharmaceutical products during processing and storage.[55]

Antioxidants inhibit oxidation by neutralizing free radicals, during which they themselves become oxidized. They mainly work in two mechanisms, preventive and chain-breaking.[56]

Preventive antioxidants act earlier by preventing the formation of new free radicals. They do this by scavenging the initial radicals before they start the chain reaction, or by stabilizing transition metals (such as iron and copper), which can catalyze radical formation. In this way, they reduce the overall rate of oxidation and stop the chain from starting. (Scheme 8)[57] **Chain-breaking antioxidants** (like quercetin and vitamins C and E) interrupt the propagation phase of free radical reactions. When a free radical steals an electron from a molecule, it creates a new radical, which then continues to react with other molecules, generating more radicals in a chain reaction. Chain-breaking antioxidants can donate an electron to these radicals, stabilizing them and stopping the chain reaction, or the radicals can otherwise decay into harmless products.[58]

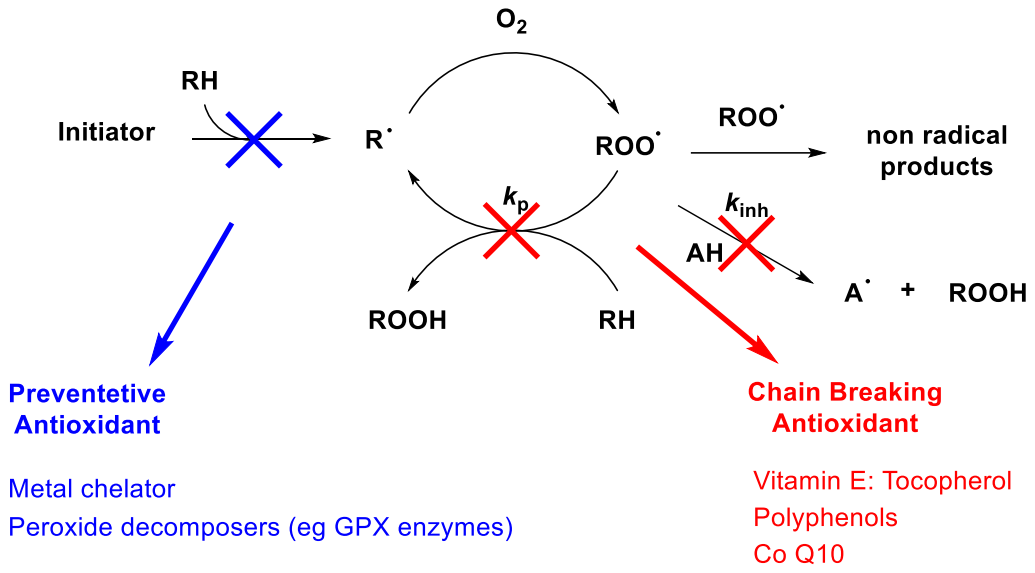

Scheme 1.8, *The general role of antioxidants in lipid peroxidation*

In addition, antioxidants systems contain antioxidant enzymes (e.g., SOD, GPx and CAT etc.), nutrient-derived antioxidants (e.g., vitamin C, vitamin E, glutathione and uric acid etc.), metal binding proteins (e.g., ferritin, lactoferrin and albumin) and other antioxidants present in variety foods.[59] These antioxidants belong to the group of natural antioxidants, which can be obtained from plants, foods, and even animals. Moreover, Synthetic antioxidants are chemically synthesized compounds that do not naturally occur in nature. They are commonly added to foods as preservatives to help prevent lipid oxidation and extend shelf life.

1.4.1 Natural Antioxidant

Natural antioxidants are generally divided into two sorts enzymatic and non-enzymatic.[60] For non-enzymatic antioxidants, they always divide into water-soluble antioxidants and lipo-soluble antioxidants.

Water-soluble antioxidant

Vitamin C, which includes ascorbic acid and its oxidized form, dehydroascorbic acid, plays many important biological roles in the human body. It is a water-soluble vitamin found in citrus and other fruits, berries and vegetables. Vitamin C is an essential nutrient

in man, monkeys, and guinea pigs, these animals do not have ability to synthesis this compound.[61,62] Block et al. (2004)[63] found that vitamin C can reduce levels of C-reactive protein (CRP), which is a marker of inflammation and a potential predictor of heart disease. Additionally, ascorbic acid is capable of scavenging superoxide and hydroxyl radicals, and it can also regenerate α-tocopherol (vitamin E), as reported by Davey et al. (2000)[64]. Vitamin C mainly exists as ascorbate anion (AH^-), which can be oxidized to form the ascorbyl radical and dehydroascorbic acid at physiological pH. The mechanism of Vitamin C as antioxidant is that it scavenges reactive oxygen species (ROS) such as superoxide, singlet oxygen, and peroxyl radicals and can directly neutralize free radicals in the aqueous phase and regenerate vitamin E from its oxidized form (tocopheroxyl radical), thus protecting lipid membranes.

Phenolic compounds represent a large group of secondary metabolites that are widely distributed throughout the plant kingdom. They are classified into different groups based on their core structure and further subdivided according to the number and position of hydroxyl groups, as well as the presence of other substituents. Among polyphenols, the most widespread and diverse group is the flavonoids which consists of two phenyl rings and one heterocyclic ring.[65] It possess various biological activities, among which the most important are their antioxidant effects, capillary-protective properties, and their ability to inhibit different stages of tumor development.[66] Phenolic compounds are also able to scavenge the reactive oxygen species (ROS) because of their electron donation properties. Their antioxidant effectiveness depends on their stability in different systems, as well as the number and position of hydroxyl groups. As for different substituents of phenylic compounds, in general, Compounds with electron-donating substituents exhibit stronger antioxidant capabilities than those with electron-withdrawing substituents.. Price and Casuscelli, (1998)[67] identified quercetin and kaempferol 3-O-sophoroside as the main flavonol glycosides present in broccoli florets. In addition, compounds such as 1,2′-disinapoyl-2-feruloylgentiobiose, 1,2-disinapoylgentiobiose, 1-sinapoyl-2,2-diferuloylgentiobiose, an isomeric form of 1,2,2′-trisinapoylgentiobiose, and chlorogenic acids have also been identified in broccoli. Nielson and Olsen (1993)[68] demonstrated that

cabbage contains a mixture of more than 20 compounds, among which seven were identified as 3-O-sophoroside-7-O-glucosides of kaempferol and quercetin, with or without additional acylation by hydroxycinnamic acids.

Liposoluble antioxidant

Carotenoids are yellow, orange and red neutral pigments present in plenty of plant leaves, fruits, and flowers, as well as the colors of some birds, insects, fish, and crustaceans. Only plants, bacteria, fungi and algae can synthesize carotenoids, but some animals incorporate carotenoids due to their diets. Meanwell, carotenoids are among the most common pigments and more than 600 different derivatives were characterized until now, and β-carotene is the most outstanding one in the family of carotenoid.[69] Among the various radicals formed under oxidative conditions in the body, carotenoids react most efficiently with peroxyl radicals. These radicals are generated during lipid peroxidation, and their scavenging by carotenoids interrupts the chain reactions that ultimately lead to damage in lipophilic compartments. Owing to their lipophilicity and strong ability to scavenge peroxyl radicals, carotenoids are believed to play a crucial role in protecting cellular membranes and lipoproteins from oxidative damage.[70] Lower serum β-carotene levels have been associated with higher rates of cancer and cardiovascular diseases, as well as an increased risk of myocardial infarction among smokers (Rice-Evans, Sampson, Bramley, & Holloway, 1997).[71]

Vitamin E is a fat-soluble vitamin known primarily for its powerful antioxidant properties. It plays a critical role in protecting cell membranes from oxidative damage caused by free radicals. Vitamin E exhibits eight compounds related in molecular structure that includes four tocopherols and four tocotrienols, particularly, α-tocopherol the most important also common chemical can be found in body and different supplements.[72] The primary mechanism gives α-tocopherol their antioxidant ability is the donation of hydrogen bonds, through which α-tocopheroxyl radical is formed. The source of Vitamin E is mainly oils, nuts and cereal grains, there is only a few contents of vitamin E in vegetables. Vitamin E shows the protective effect on heart diseases through inhibiting the oxidation of low-density lipoprotein (LDL).[73] Chronic inflammation contributes to the development of

chronic diseases such as cancer and diabetes. It is characterized by the excessive production of reactive oxygen and nitrogen species, along with various proinflammatory mediators. The mechanic studies demonstrated that some specific forms of vitamin E such as γ-tocopherol and tocotrienols exerts anti-inflammatory effects by inhibiting COX-2- and 5-LOX-mediated eicosanoid production and by suppressing the NF-κB and JAK–STAT6 or JAK–STAT3 signaling pathways in various cell types.[74]

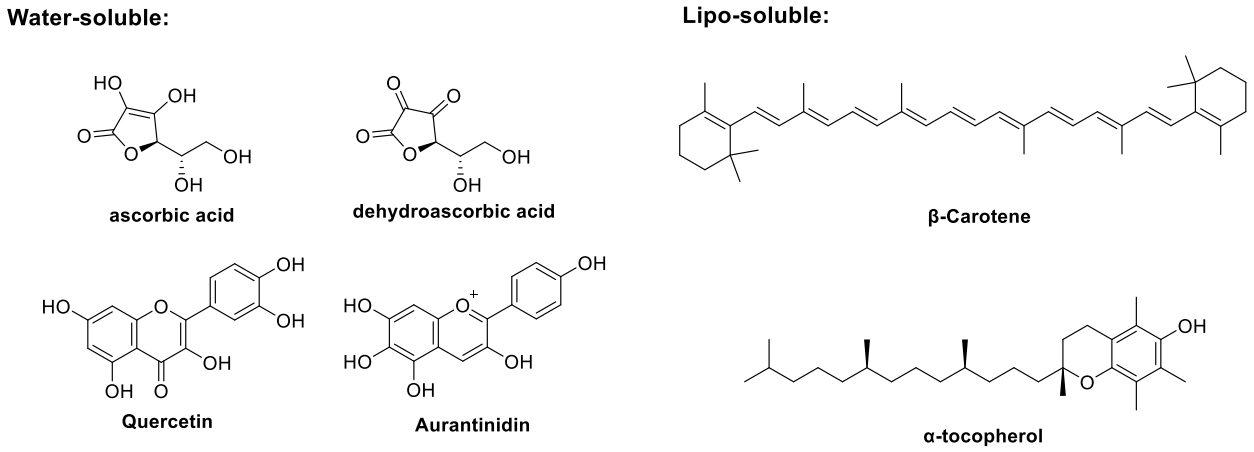

Scheme 1.9, *Water-soluble and Lipo-soluble Natural antioxidants*

1.4.2 Synthetic Antioxidant

Synthetic antioxidants are man-made chemical compounds designed to prevent or slow down the lipid peroxidation and it also widely used in food, oils and other systems. These antioxidants mainly act primarily through two different mechanisms and are classified as primary and secondary antioxidants. Primary antioxidant can prevent the formation of free radicals, also can be categorized as free radical terminator (butylated hydroxyanisole [BHA], butylated hydroxytoluene [BHT] and tertiary butyl hydroquinone [TBHQ])[75], oxygen scavenger (sulphites, glucose oxidase and ascorbyl palmitate) and chelating agents (heavy metal like iron, copper). Secondary antioxidants, such as thiodipropionic acid and dilauryl thiodipropionate, act by decomposing the hydroperoxides formed during lipid oxidation into stable, non-radical end products.[76] (see scheme 10) These antioxidants can be used in the process and preservation of fruits, vegetables and soft drinks. For example, BHA usually is added to fats and oils, like cereals, snack foods and packaging materials;

BHT is similar to BHA generally used in potato chips and other fatty foods; TBHQ, very effective at preventing the oxidative deterioration is also used as the stabilizer in different vegetables oils and animal fats.

Some synthetic antioxidants have been used in the treatment of different diseases, for example, 5-amino-salicylic acid, a synthetic antioxidant, has been shown to be the most effective drug for treating chronic inflammatory conditions of the bowel.[77] Taj and co-workers also synthesized benzamide derivatives that exhibited both antioxidant and anti-Alzheimer activities. The most active compound in this series showed strong inhibition of acetylcholinesterases (ACEs) and demonstrated the highest radical scavenging activity in the DPPH assay.[78] Probucol was a lipid-lowering medication; however, it is also a highly potent antioxidant that protects LDL from oxidation. Despite its efficacy, it was discontinued due to safety concerns, including its tendency to lower High-density lipoprotein (HDL) cholesterol levels and cause QT interval prolongation, clinical studies have been continually performed to re-evaluate its applicability as adjunct therapy in cardiometabolic diseases.[79]

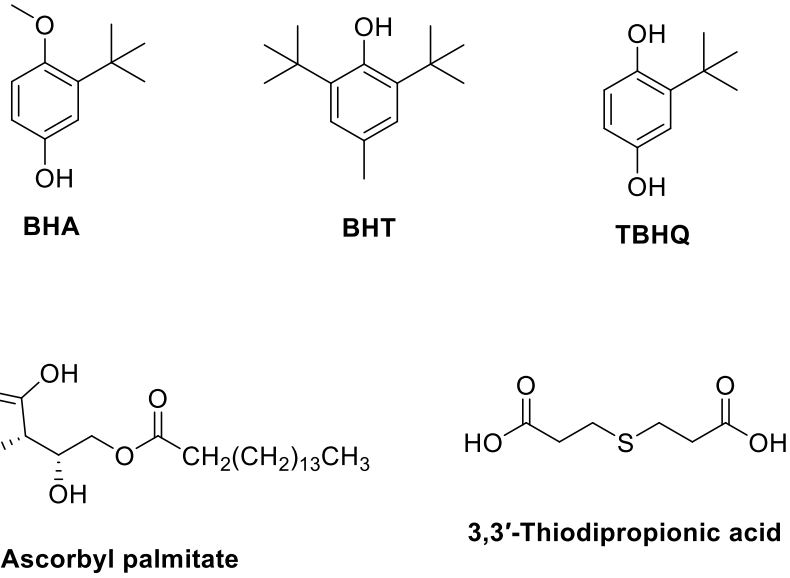

Scheme 1.10, *Synthetic antioxidants*

1.5 Free Fatty acid

Free fatty acids (FFAs) are biologically important energy substrates, and their release from adipose tissue by lipolysis is regulated by the body's energy needs. Elevated free fatty acid levels in obesity contribute to type 2 diabetes, hepatic steatosis, and various cardiovascular diseases.[80] In oils, FFAs originate mainly from the hydrolysis of triacylglycerols during processing and storage. FFAs are primarily formed during oil production, storage, and handling of the raw material. Elevated levels of FFAs are undesirable because they not only accelerate lipid oxidation but also promote hydrolytic rancidity, resulting in the development of off-flavors and unpleasant odors. For instance, short-chain FFA can arise from the secondary oxidation of unsaturated aldehydes as well as from the cleavage of lipid hydroperoxides.[81] Waste cooking oil (WCO) has a higher content of FFAs because high temperatures and air exposure during frying promote the hydrolysis and oxidation of triglycerides, thereby increasing the FFA content in the oil.

N. Frega et. have shown that FFAs are strong prooxidants which is susceptible to thermooxidative degradation in some vegetable oils in 1999. The intensity of its effect was related to the concentration of FFAs.[82,83] According to Colakoglu (2007), incorporating 1% stearic acid into soybean oil led to increased oxygen uptake and higher peroxide levels during oxidation at 55 °C over a 24-hour period, compared to soybean oil without the additive.[84] In 2011, Thaddao Waraho, D found that free fatty acids exhibit potent prooxidant activity in both bulk oils and oil-in-water emulsions. Incorporating oleic acid into oil-in-water emulsions has been shown to significantly enhance the formation of lipid hydroperoxides and hexanal, even at concentrations as low as 0.1% of the total lipid content[85,86]. Chaiyasit et al[87]. observed that oleic acid could concentrate at the oil–water interface in bulk oil, leading to a reduction in the pH of the aqueous phase, which in turn facilitated the acid-catalyzed breakdown of lipid hydroperoxides.

In addition, several methods have been developed for detecting free fatty acids (FFA). In 1964, Robert R. Lowry reported the copper soap method, in which copper forms a colored complex with FFAs, and the concentration is then quantified using UV spectrophotometry[88]. More recently, in 2014, Christina S. introduced an NMR-based

method for determining FFA values, providing a fast and simple alternative to classical quality indices such as acid, peroxide, and saponification values prescribed by the European Pharmacopeia. This NMR method was further adapted for the analysis of waxes and oleyl oleate, while also addressing solvent effects and, in the case of castor oil, the influence of the oil matrix on line broadening and the chemical shift of carboxyl signals.[81]

1.6 Pro-aromatic Terpenes: Cyclohexadienes

1.6.1 Natural pro-aromatic Terpenes

Terpenes (or terpenoids) are the largest and most diverse group of natural compounds, classified by their isoprene units (mono-, di-, tri-, tetra-, and sesquiterpenes). Predominantly found in plants—especially in essential oils from sources like tea, thyme, cannabis, Spanish sage, and citrus fruits (see Fig. 3)—they exhibit numerous medicinal properties.[89] Notable activities include antiplasmodial (similar to chloroquine), antiviral (especially monoterpenes), anticancer, and antidiabetic effects, with the added benefits of varied administration routes and reduced side effects[90]. Historically used in folk medicine, certain terpenes like curcumin possess broad pharmacological actions (anti-inflammatory, antioxidant, anticancer, etc.) and are gaining popularity in functional foods. Ongoing research aims to develop terpenes as lead molecules in modern drug design.[91]

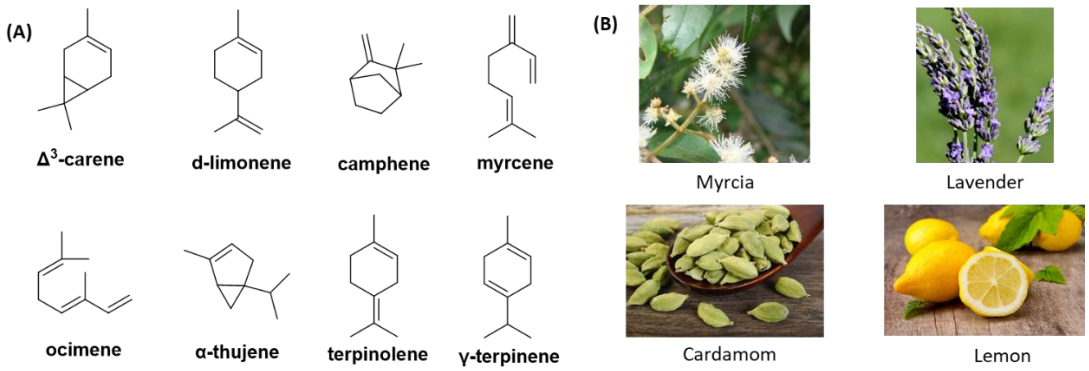

Figure 1.3, *(A): The Structure of Different Natural Terpenes; (B): The plants Contains Natural Terpenes.*

Cyclohexadienes also known as CHD, a family of cyclic hydrocarbons derived from cyclohexane by introducing two double bonds into the ring structure. They have two main isomers, 1,3-cyclohexadiene (1,3-CHD) and 1,4-cyclohexadiene (1,4-CHD). As for 1,3-cyclohexadiene, it was more studied from its conjugated diene, which give a very stable chemical stability. The conjugated structure allowed 1,3-CHD to participate some reactions such as Diels-Alder cycloaddition,[92] making a significant intermediate in synthetic chemistry. 1,4-CHD, on the other hand, contains two isolated (non-conjugated) double bonds. 1,4-CHD and its derivatives are easily aromatized the driving force being the formation of an aromatic ring. The conversion to an aromatic system may be used to trigger other reactions, such as the Bergman cyclization.[93]

The main products of 1,3-cyclohexadiene (1,3-CHD) and 1,4-cyclohexadiene (1,4-CHD) are α-terpinene (α-T) and γ-terpinene (γ-T), both of which are naturally occurring compounds found in essential oils. They are primarily present in plants such as cumin, cardamom, and various citrus species. In recently years, many research prove that the essential oil could be a natural alternative to represent the synthetic antioxidants.[94] Essential oils are complex mixtures of volatile compounds mainly extracted from aromatic and medicinal plants through steam distillation. The antioxidant activity of essential oils rich in phenolic compounds (such as those extracted from thyme, oregano, and cloves) is explained by their chemical similarity to phenolic antioxidants.[95] However, the essential oil contains the nonphenolic component like limonene, linalool, and citral also exhibit antioxidant ability at specific conditions, the reason is these compounds can interfere with the autoxidation radical chain by promoting the decay of peroxyl radicals.[47] Such as α-T and γ-T have demonstrated protective effects against lipid peroxidation in systems like methyl linoleate and egg yolk phospholipids[96], and have also been shown to reduce the peroxidation of low-density lipoproteins[97]

In our previous study, we observed that γ-T had the ability to prolong the antioxidant activity of phenolic antioxidants like α-tocopherol and 2,2,5,7,8-pentamethyl-6-chromanol (PMHC) during the autoxidation process of lipids in homogeneous solutions, whereas its effect on the autoxidation rate is relatively weak when used alone.[98] In addition, γ-T could

generate an hydroperoxyl radical (HOO•)[99] when it aromatizes, that is able to donate a H-atom to the radical of the antioxidant and reverse the radical into the original antioxidant.[98] In a recent study, we demonstrated that γ-T effectively reduces lipid peroxidation (LP) in water-containing biphasic systems, such as micelles and phospholipid membranes, without requiring catalytic decomposition of HOO• or $O_2^{\bullet -}$. The antioxidant mechanism was highlighted the ability of γ-T to convert lipophilic LOO• into hydrophilic species **(**HOO•/$O_2^{\bullet -}$**),** thereby facilitating their rapid diffusion out of the lipid phase undergoing peroxidation (see Scheme 11). While this mechanism falls under chain-breaking antioxidant activity, it differs from classical radical trapping in that the radicals are not neutralized but instead exported into the aqueous phase, where they can no longer propagate lipid oxidation.[100]

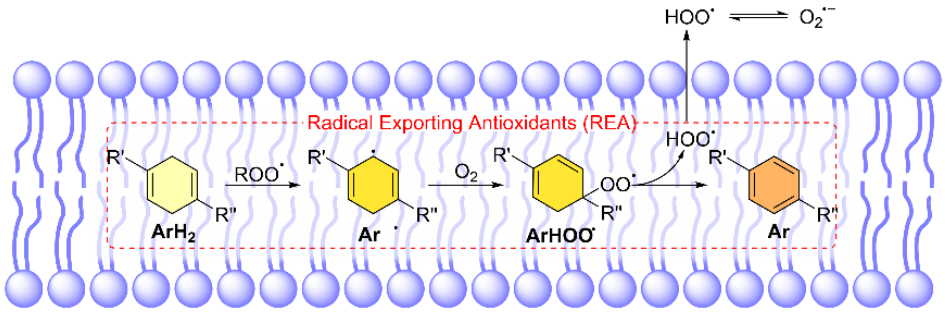

Scheme 1.11, *Mechanism of lipid peroxidation with possible antioxidant mechanisms*

1.6.2 Synthesized pro-aromatic Terpenes

Compared to natural terpenes, there is relatively little documentation regarding synthesized pro-aromatic terpenes. Synthesized pro-aromatic Terpenes are terpene derivatives engineered to contain structural motifs (such as 1,4-cyclohexadiene rings) that can oxidize to yield highly stable aromatic products. This aromatization driving force often facilitates unusual radical pathways—for example, intra-1,4-HAT and can result in the efficient release of reactive species like HOO• during autoxidation.

To obtain synthesized pro-aromatic terpenes, the key reaction employed is the Birch reduction. The reaction mechanism proceeds as follows: A solution of sodium in liquid ammonia forms the intensely blue electride salt $[Na(NH_3)_x]^+ e^-$. The solvated electrons add

to the aromatic ring, generating a radical anion, which subsequently abstracts a proton from the alcohol. This sequence repeats at either the *ortho* or *para* position (depending on the substituents) to yield the final 1,4-diene product. The remaining double bonds in the product do not stabilize further radical additions, thus preventing over-reduction (see Scheme 12).[101]

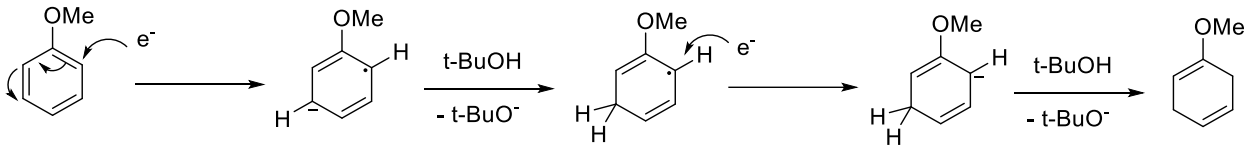

Scheme 1.12, *Mechanism of Birch Reduction*

This reaction was firstly discovered by Arthur Birch in 1944, the reaction of benzenoids affords 1,4-CHD. The reaction is run in liquid ammonia with an alkali metal and an added alcohol at -33ºC (Scheme. 13A).[102] The liquid ammonia is difficult to keep for a long period, usually, to removal 1L of liquid ammonia only needs 12 h. Besides, to prevent the generation of by-products, the temperature should be constant at -33ºC. To overcome these challenges, researchers made more efforts, for example, the Benkeser group (Scheme. 13B) employed lithium in neat ethylamine, ethylenediamine, or mixtures of primary and secondary amines, without the use of additional solvents. This method resulted in a mixture of over-reduced products.[103] The Dolby group achieved the reduction of three substrates to the corresponding Birch-type products in yields ranging from 45% to quantitative (Scheme. 13C), using lithium, ethylenediamine, n-propylamine, and tert-butanol.[104] The Baran group reported an electrochemical reduction of electron-rich arenes (Scheme. 13D) employing 3.5–10 equivalents of tri(pyrrolidin-1-yl)phosphine oxide and 3 equivalents of 1,3-dimethylurea, both of which required removal from the product via column chromatography.[105]

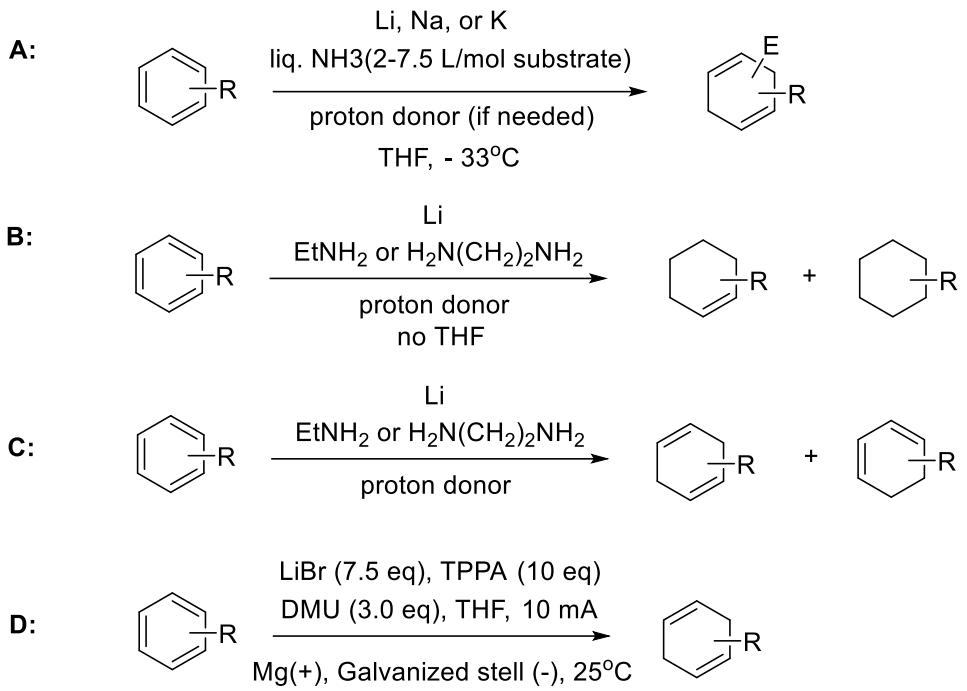

Scheme 1.13, *Previous Birch reductions and this work, (A) General Birch reduction. (B) Benkeser's ammonia-free reduction. (C) Dolby reduction. (D) Baran's electrochemical reduction*

1.7 Superoxide and the detecting fluorescent probe

1.7.1 ROS and superoxide

Life is sustained by oxygen—specifically, dioxygen (triplet O_2)—which is essential for cellular energy metabolism. Its strong oxidizing properties enable the production of adenosine triphosphate (ATP) through oxidative phosphorylation in mitochondria.[106] However, during the process of metabolism and respiration also could generate some sub-product, Reactive Oxygen species (ROS), and when imbalanced or produced in excess, they can lead to biological toxicity.[107] There are other exogenous agents also could stimulate their generation, such as UV irradiation, Food, drugs and Toxins.[108]

The significant ROS in biology aspect is listed in Table 1. It mainly contains the high reactive free radicals such as superoxide $O_2^{\bullet-}$, in the electron-trasnport chain and its protonated (neutral) form, the hydroperoxyl radical (HOO•); highly reactive hydroxyl /

alkoxyl radicals (HO• / RO•) formed from decomposition of peroxides and more lipid soluble peroxyl radicals (HOO• / ROO•)[109].

Table 1.1 Main reactive oxygen species (ROS)

Radical Species		Non-Radical Species	
hydroxyl radical	HO•	hydrogen peroxide	H_2O_2
superoxide radical	O_2^-•	Singlet oxygen	$^1O_2$
aloxyl radical	RO•	Ozone	O_3
hydroperoxyl radical	HOO•	Peroxide	ROOH
peroxyl radical	ROO•	Hypochlorite	HOCl
nitrogen oxide/dioxide radical	NO•/NO_2•	Peroxy nitrite/ peroxynitrous acid	$ONOO^-$/ONOOH
thiyl radical	RS•	Nitrous oxide and nitroxyl anion/cation	$NO/NO^-/NO^+$

Superoxide, as mentioned, is a radical that is not particularly reactive as an oxidant. It is produced in relatively large quantities by mitochondria because, during respiration, electrons may escape from the mitochondrial electron transport chain and react with O_2, forming O_2^-•.[110] In a specific condition, superoxide exists in a different way, briefly, at pH < 4.8, superoxide is mostly protonated and exists as HO_2•[111]. Superoxide, is from in our living system, may act as a signaling agent, a toxic species, or a harmless intermediate that decomposes spontaneously. Its level is mainly limited in vivo by two kinds of enzymes, superoxide reductase (SOR) and superoxide dismutase (SOD), they can catalyze O_2^-• to give O_2 and H_2O_2.[111]

1.7.2 The properties of superoxide

Although hydroperoxyl radicals, the protonated form of superoxide, have been known for a long time, their unusual role in radical-chain reactions is still far from being fully clarified.

The HOO• radicals have an uncommon two-face oxidizing and reducing activity, thus their formation during a radical chain leads to unexpected effects.[112]

Regarding H-atom abstraction, HOO• behaves similarly to ROO•. HOO• can propagate the oxidative chain reaction during the autoxidation of 1,4-cyclohexadienes and other easily oxidizable substrates[113]. Additionally, HOO• is capable of abstracting the phenolic hydrogen atom from α-tocopherol, with a rate constant $k_H = 1.6 \times 10^6\ M^{-1}s^{-1}$ in chlorobenzene (PhCl) [114], which is very close to that reported for ROO• under the same conditions ($k_H = 2.7 \times 10^6\ M^{-1}s^{-1}$).[114]

The unusual chemical property of HOO• lies in their hydrogen-donating ability. The bond dissociation free energy (BDFE) of the O–H bond in HOO• has been estimated at 51.2 kcal/mol in water and 45.1 kcal/mol in the gas phase[111]. Similarly, $O_2^{\bullet-}$ is a strong one-electron reducing agent, with $E°(O_2/O_2^{\bullet-}) = –0.35$ V vs NHE. The BDFE of HOO• is considerably lower than that of typical phenolic and non-phenolic antioxidants (74–84 kcal/mol), demonstrating—on thermodynamic grounds—the feasibility of regenerating antioxidants from their corresponding radicals. [111]

1.7.3 Producing of hydroperoxyl radicals during autoxidation

The efficient generation of $O_2^{\bullet-}$ or HOO• requires that the oxidizable substrate possess specific structural features—namely, a hydrogen atom located at the 4-position relative to the terminal oxygen of the peroxyl group. This arrangement enables an intramolecular 1,4-hydrogen atom transfer (intra-1,4-HAT), leading to the formation of HOO•. However, the effect of 1,4-HAT will be more or less depending on the structural features of the molecule. [115] Some examples of HOO• generation, subdivided by type of functional group are shown below (In Scheme 14).

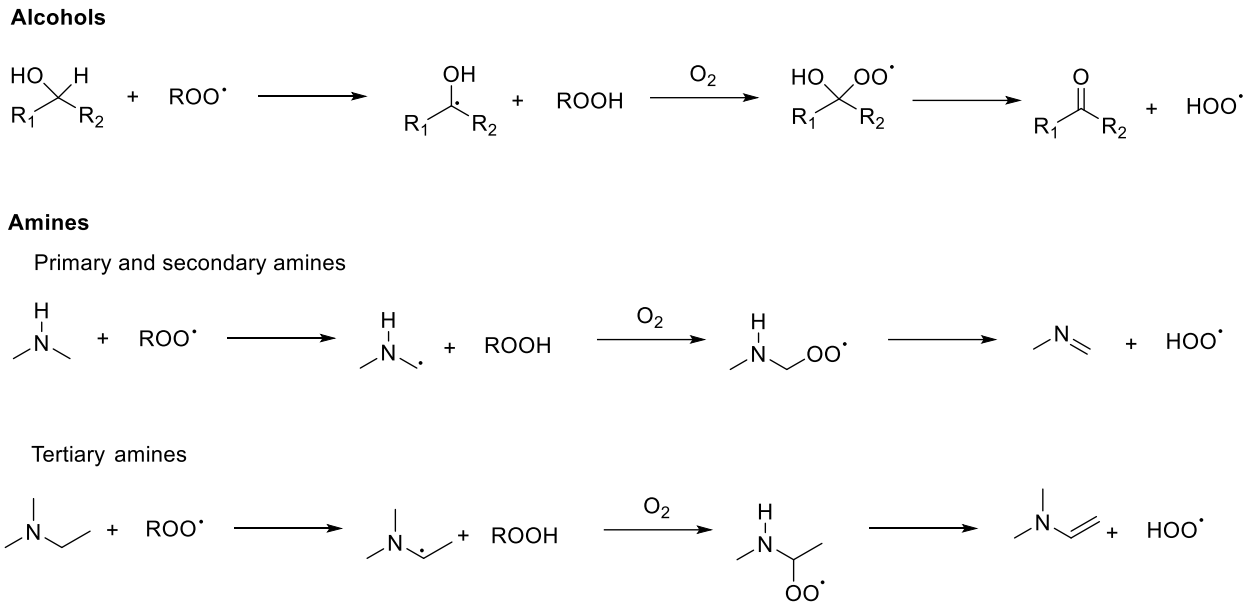

Scheme 1.14, *general mechanism of HOO• elimination by 1,4-HAT from alkyl peroxyl radicals, and typical reaction pathway in alcohols and amines.*

Reports on the antioxidant effects of superoxide dismutase (SOD) on the autoxidation rate indicate that, during the autoxidation of methyl linoleate in micelles, a fraction of the accumulating peroxyl radicals is present in the form of HOO•/O_2•$^-$ species[116]. Given the biological relevance of polyunsaturated lipid peroxidation, these preliminary observations underscore the need for further investigation into the mechanisms underlying HOO• formation.

1,4-Cyclohexadiene derivatives such as γ-T[111], a common terpene found in the essential oils, represent a unique class of alkenes that generate high yields of HOO• during autoxidation.[111, 112] γ-T reacts with radicals exclusively via hydrogen atom transfer (HAT) from its bis-allylic CH_2 groups, forming a highly stabilized alkyl radical. This radical rapidly reacts with O_2 to yield a peroxyl radical containing conjugated double bonds. Subsequently, HOO• is released through an intra-1,4-HAT, driven by the formation of the aromatic product p-cymene. [117] (See Scheme 11) Likely, 1,3- Cyclohexadiene, the isomer of γ-T, α-T which has conjugated double bonds, only partially propagates the oxidation chain via HOO•[118]. Its autoxidation mainly yields epoxides and diketones, the latter most likely arising from the decomposition of alkyl hydroperoxides.

Biologically, certain oxidizing enzymes can also produce $O_2\bullet^-$ as a byproduct. For example, xanthine oxidase (XO) catalyzes the oxidation of hypoxanthine to xanthine, and subsequently xanthine to uric acid, generating $O_2\bullet^-$ in the process[119]. Similarly, nicotinamide adenine dinucleotide phosphate oxidase (NOX) catalyzes the oxidation of NADPH to $NADP^+$, producing $O_2\bullet^-$[120].

Part I

Pro-aromatic Natural Terpenes as Unusual "Slingshot"Antioxidants with Promising Ferroptosis Inhibition Activity

2 Main Work of Part 1

2.1 Preface

In this chapter, the main work was about the essential oil component γ-terpinene (γ-T), a natural monoterpene with a unique highlyoxidizable pro-aromatic 1,4-cyclohexadiene skeleton, inhibit the peroxidation of Polyunsaturated lipids in a heterogenies models (micelles and liposomes). The basic mechanism is that γ-T reacts with radicals by H-atom transfer from the bis-allylic CH_2 groups forming a stabilized alkyl radical which reacts with O_2 to generate a peroxyl radical with conjugated doble bonds. Subsequently, hydroperoxyl radical (HOO•) is released through intra-1,4-HAT mechanism, eventually, aromatizes to p-cymene. This mechanism we called “slingshot” mechanism and it also explains why γ-terpinene shows a protective activityagainst ferroptosis, being effective at submicromolar concen-trations in human neuroblastoma (SH-SY5Y) cells. The experiments presented in Section *1.4.3* were carried out in collaboration with Dr. Luca Pincigher and Dr. Francesca Valenti, who performed the biologic experiments and analyses, while I contributed to data interpretation. Part this chapter was published in Jin, Zongxin, et al. "Pro-aromatic Natural Terpenes as Unusual “Slingshot” Antioxidants with Promising Ferroptosis Inhibition Activity." Chemistry–A European Journal 30.72 (2024).

2.2 Research objectives

Natural pro-aromatic terpenes, the largest natural products mainly existing in plants, have beneficial interactions among organisms, they defend many species of plants, animals and microorganisms against predators, pathogens and competitors and they have been shown to possess various properties relevant to medical, food, and cosmetic applications. Some studies have reported that essential oils containing γ-terpinene (γ-T) exhibit antioxidant activity. However, only a limited number of investigations have explored the mechanisms by which γ-T and its CHD derivatives act in heterogeneous systems. Lipid peroxidation (LP) is a radical-chain process that compromises membrane integrity and underlies ferroptotic cell death. Conventional chain-breaking antioxidants inhibit LP by trapping lipid peroxyl radicals (LOO•), forming stable species incapable of propagating the chain reaction. To overcome these challenges, here, we explore an alternative mechanism involving the generation of hydroperoxyl radicals (HOO•) from pro-aromatic 1,3- and 1,4-cyclohexadienes (ArH_2). Using a combination of kinetic studies in solution, micelles, and phosphatidylcholine (PC) liposomes at varying pH, together with biological assays with HPG2 cells and human neuroblastoma (SH-SY5Y) cells, we evaluated the LP-inhibiting activity of ArH_2 and compared it with that of structurally related aromatic and non-cyclic analogues. Synthetic 1,4-cyclohexadienes bearing either a C_{12} alkyl chain or an EtCOOH group were used to probe the role of lipophilicity in modulating antioxidant activity in liposomes and cells. Superoxide ($O_2^{\bullet -}$) formation was confirmed by a colorimetric assay. Finally, we discuss the data collected for pro-aromatic compounds in the broader context of antioxidants that during their activity, produce HOO• / O2•−, providing evidence that the “radical-export” mechanism is one of the most relevant mechanism used by nature to protect biological membranes.

2.3 Results

2.3.1 Autoxidation Inhibition Studies

In the first part of this study, we investigated the lipid inhibition activities of the natural pro-aromatic compounds γ-T and α-T, which feature pro-aromatic 1,4- and 1,3-cyclohexadienic cycles, respectively. As negative controls, we used para-cymene (Cym), an aromatic compound, and β-myrcene (Myr), an unsaturated terpene containing two non-cyclic conjugated double bonds. All of these molecules are major constituents of essential oils, readily obtainable from sources such as tea tree oil, cardamom oil, thyme oil, cumin seed oil, and bay oil. The chemical structures are shown in Scheme 2.1.

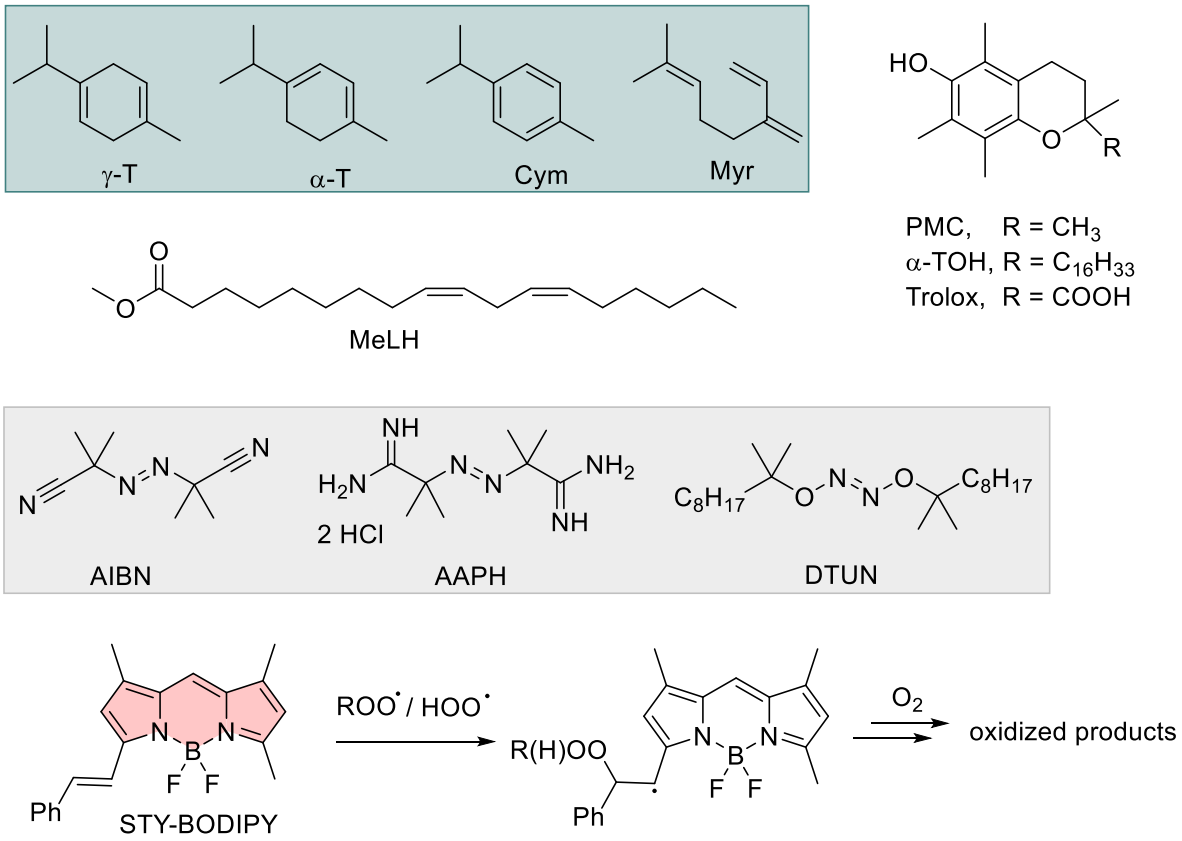

Scheme 2.1, *Main molecules during Autoxidation Inhibition Studies*

Other molecules used in this study were essential for conducting the experiments. 2,2,5,7,8-pentamethylchroman-6-ol (PMC), α-tocopherol (α-TOH), and Trolox are classic vitamin E derivatives widely employed as reference antioxidants in oxidative studies. Due to its C16 alkyl side chain, α-TOH is typically used as a reference antioxidant in non-aqueous

systems. In contrast, Trolox contains a carboxylic acid group, which confers higher solubility in aqueous systems, making it suitable as a reference under such conditions.[121] In contrast, PMC is a lipophilic antioxidant that is typically used in organic systems; however, due to its short alkyl chain, it can also be applied in aqueous systems. Methyl linoleate is wildly employed as a model subtract in lipid oxidation studies due to its well-defined structure and high susceptibility to autoxidation. Its two bis-allylic methylene groups possess relatively weak C–H bonds, making them particularly prone to hydrogen abstraction and subsequent peroxyl radical formation.[122] To initiate oxidation in micellar systems, water- or lipid-soluble radical initiators are often employed to generate a constant flux of primary radicals under controlled conditions. Azobisisobutyronitrile (AIBN) is a lipid soluble azo compound that decomposes thermally to produce carbon-centered radicals, which react with O_2 to form peroxyl radicals. 2,2'-Azobis(2-amidinopropane) dihydrochloride (AAPH) is a water soluble and decomposes to yield hydrophilic radicals in the aqueous phase; (E)-1,2-bis((2-methyldecan-2-yl)oxy)diazene (DTUN) is a synthesized initiator[123], which is lipid soluble diazene and generates peroxyl radical directly in the hydrophobic phase.

STY-BODIPY is a lipophilic fluorescent probe using for lipid oxidation studies. It has a BODIPY core, which has fluorescence (maximum is around 562 nm). It can as signal carriers that co-autoxidize along with a hydrocarbon substrate and indicates the rate constant of inhibition of RTAs both in organic and aqueous solution. Its mechanism of action is illustrated in the Scheme. The STY-BODIPY molecule undergoes an addition reaction with HOO•/ROO•, resulting in a loss of fluorescence, and subsequently reacts with oxygen to produce further oxidation products.[111]

To evaluate the antioxidant properties of these terpenes, this part of work was divided into 4 parts. Briefly, the terpene will be conducted as additives in four different systems. 1) autoxidation of methyl linoleate (MeLH) in homogeneous solution (chlorobenzene), representative of LP in bulk oils;[22] 2) autoxidation of tetrahydrofuran (THF) in buffered water, representative of oxidation of water soluble or water dispersed biomolecules such as proteins;[124] 3) autoxidation of MeLH in a micellar system in buffered water,

representative of LP in small lipid aggregates relevant for cosmetic, pharmaceutical and food applications;[125] 4) autoxidation of monolamellar liposomes of egg-yolk phosphatidylcholine, which mimic cellular membranes.[123]

2.3.1.1 Autoxidation of methyl linoleate (MeLH) in homogeneous solution

MeLH was used as the model substrate in the LP studies. In the first system, we measured the O_2 consumption of the pro-aromatic terpenes γ-T and α-T, along with their negative controls Cym and Myr, using the instrument described in scheme 11. α-TOH (10 μM) was included as the reference antioxidant. Experimental details are provided in *Section 2.7*. The O_2 consumption trace is shown in Figure 2.1A. The inhibition rate constant for α-TOH was consistent with literature values, approximately 3.2×10^6 M^{-1} s^{-1}[126]. As expected, both γ-T and α-T showed a measurable effect in slowing oxygen consumption, meanwhile, the antioxidant capacity of 1,4-CHD was superior to that of 1,3-CHD, whereas Myr, used as a negative control, exhibited minimal inhibition. In addition, an interesting phenomenon was found, the rate of O_2 consumption increased when higher concentrations of α-T were added to the system.

Adding γ-T to MeLH in PhCl solution, in the presence of the azoinitiator AIBN at 30 °C, the rate of oxygen consumption R_{ox} is reduced, indicating an antioxidant effect (see Figure 2.1). The maximum antioxidant effect is reached at approximately 25 mM γ-T. At higher concentrations, the rate of oxygen consumption increases, up to exceeding that of MeLH alone (pro-oxidant effect). a-T shows a similar trend, but with a smaller antioxidant effect at low concentrations and a faster transition to the pro-oxidant phase (Figure 2.1B). P-Cym and Myr have modest effects on the oxidation of the system and don't show antioxidant effects (Figure 2.1B and C).

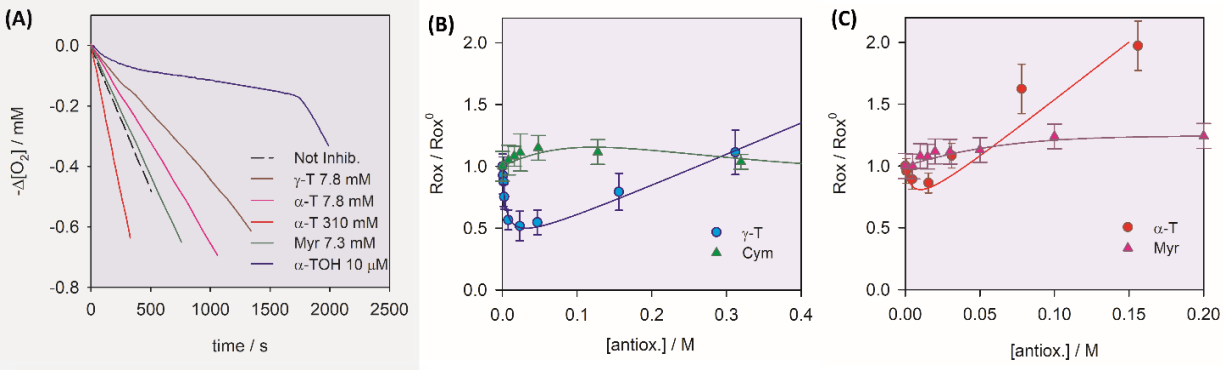

Figure 2.1, *O_2 consumption traces (A) and relative oxidation rates Rox/Rox^0 (B, C) as function of the concentration of the terpenes during the autoxidation of: MeLH (0.8 M) in chlorobenzene initiated by AIBN (A-C)*

2.3.1.2 Autoxidation of tetrahydrofuran (THF) in buffered water

In this part, THF was used as the model substrate in the aqueous solution. We measured the STY-BODIPY consumption of the pro-aromatic terpenes γ-T and α-T at 37°C, along with their negative controls Cym and Myr by UV-vis with temperature control. Trolox (4 μM) was included as the reference antioxidant. Experimental details are provided in *Section 2.7*.

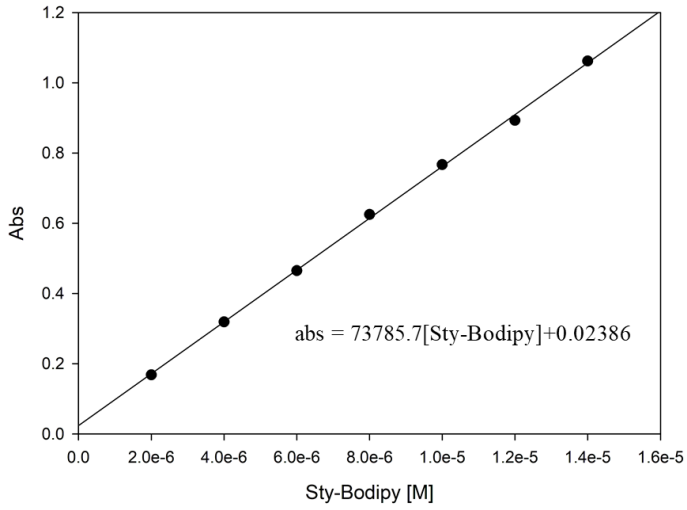

Figure 2.2, *Rate of STY-BODIPY consumption as a function of STY-BODIPY concentration in AAPH-initiated (1 mM) co-autoxidations of STY-BODIPY and THF (3.1 M) in PBS buffer at 37 °C*

Thus, plotting a rate of STY-BODIPY consumption versus time such as plot D, should draw a plot containing the relation to the absorption versus its concentration. (Figure 2.3) In this system, the antioxidant activity of γ-T and α-T was first measured in PBS buffer at pH 7.4 (Figure 2.3D). As expected, both exhibited moderate antioxidant capacity. Notably, γ-T achieved significant antioxidant activity without requiring particularly high concentrations. Furthermore, consistent with the results observed in the organic phase, the antioxidant activity of p-cymene and myrcene showed little variation with increasing concentration.

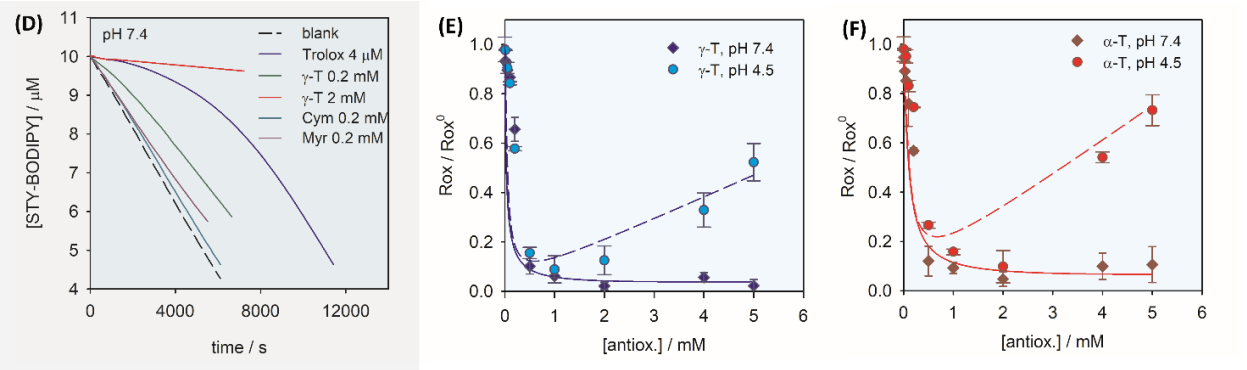

Figure 2.3, *STY-BODIPY consumption traces (D) and relative oxidation rates Rox/Rox^0 (E, F) as function of the concentration of the terpenes during the autoxidation of: THF (3.1 M) in Buffered water initiated by AAPH (D-F)*

In the systems 2, the pH dependence was also investigated, by considering the physiologic pH 7.4 and a more acidic pH 4.5 (Figure 2.3 E and F), relevant for cellular compartments like lysosomes, that could ensure a partial protonation of superoxide to HOO•.[100] At pH 7.4, we found that the relative oxidation rates increased with rising γ-T and α-T concentrations, then remained stable once the antioxidant concentration reached 1 mM. In contrast, at pH 4.5, higher antioxidant concentrations induced a pro-oxidative effect. This behavior may be attributed to the elevated abundance of HOO• at low pH, combined with its pK_a of 4.8, which facilitates further reaction with ArH_2, ultimately promoting oxidation. Furthermore, the inability of $O_2^{\bullet -}$ to propagate the oxidative chain was also verified by studying the peroxidation of the γ-T analogue 1,4-CHD in acetonitrile in the presence of

bases of variable strength. The reaction was initiated by the decomposition of AIBN and its rate was determined by measuring the O_2 uptake (Figure 2.4A, B). The pK_a of each base in MeCN and water were shown in Table 2.1.

Table 2.1 The pKa of different base in MeCN and Water

Base	pK_a MeCN	Reference	pK_a Water	Reference
pyridine	12.53	[127]	5.25	[127]
Tert-octylamine	≈ 18	[128]	10.7	[129]
piperidine	19.35	[128]	11.3	[130]
2,2,6,6-tetramethylpiperidine	19.7	[131]	11.8	[130]
Tetrabutylammonium hydroxide	> 23	[132]	> 13	[133]

We can know that pyridine had the smallest pK_a 12.53 [127] and O_2 consumption rate was reduced proportionally to the base strength in agreement with the mechanism reported in Figure 2.4C. The base can covert HOO• to O_2•- and plenty of O_2•- could prevent the further oxidation of 1,4-CHD.

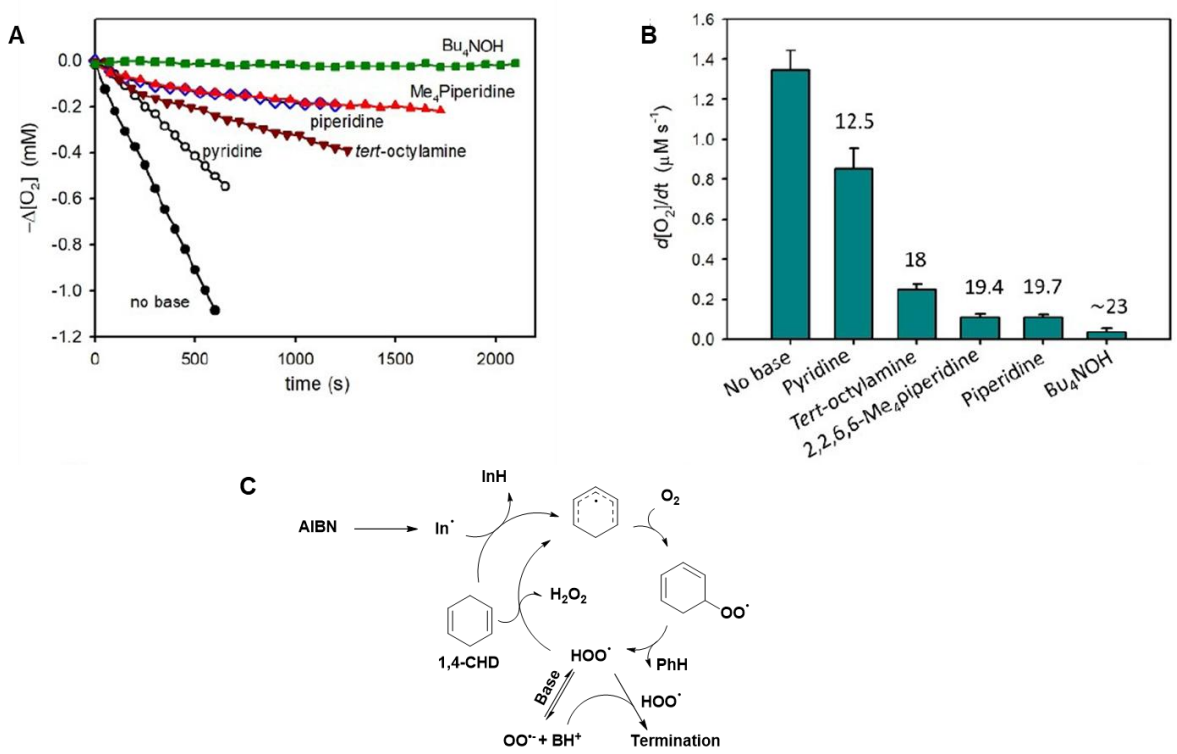

***Figure 2.4**, A, B. Oxygen consumption (A) and rates of O2 consumption (B) recorded during the autoxidation of 1,4-CHD (0.26 M) in MeCN initiated by AIBN (25 mM) at 30°C in the presence of bases (0.1 mM), whose protonated form has the pKa reported in graph B. C. Mechanism of the effect of bases (B) on 1,4-CHD autoxidation, where In* is the initiating radical formed by decomposition of AIBN*

2.3.1.3 Autoxidation of MeLH in a micellar system in buffered water

This part of work was conducted in micelles with buffered water. Micelle is an aggregate (or supramolecular assembly) of surfactant amphipathic lipid molecules dispersed in a liquid, forming a colloidal suspension (also known as associated colloidal system). A typical micelle in water forms an aggregate, with the hydrophilic "head" regions in contact with surrounding solvent, sequestering the hydrophobic single-tail regions in the micelle center,[134] see figure 2.5J.

Firstly, we explored pro-aromatic terpenes γ-T and α-T, along with their negative controls Cym and Myr, these antioxidant effect in the autoxidation of MeLH in Triton X-100 micelles at two different pH values, 7.4 and 4.5, representative of the pH of cytoplasm and

of lysosomes at 37°C, respectively, whose membrane damage is correlated to ferroptosis. The generation of radicals was provided by the water-soluble initiator AAPH and α-TOH as the reference antioxidant. The peroxidation rate was followed by measuring by UV-vis spectroscopy the disappearance of the oxidation probe STY-BODIPY. γ-T and α-T showed an antioxidant effect at all concentrations, evident already in the micromolar concentration range. At pH 4.5, γ-T and α-T inhibited the autoxidation at all concentrations, differently from experiments in water / THF, where the antioxidant effect is gradually lost when increasing the concentration of γ-T and α-T. The reference Cym and Myr did not provide significant changes to the STY-BODIPY consumption rate.

The comparison of the antioxidant activities of γ-T and at pH 4.5 and 7.4 demonstrates that although it is known that HOO· is a more active H-atom abstracting radical than $O2\cdot^{-}$, [135], [136] the deprotonation of HOO· (pKa =4.69) is not essential for the "slingshot" mechanism. Reasonably, HOO· has limited ability to propagate the radical chain within the lipophilic micelle core, and it decays in the water phase. As expected, 1,4-CHD showed also an antioxidant effect against the peroxidation of MeLH in Triton X-100 micelles, although smaller than γ-T.

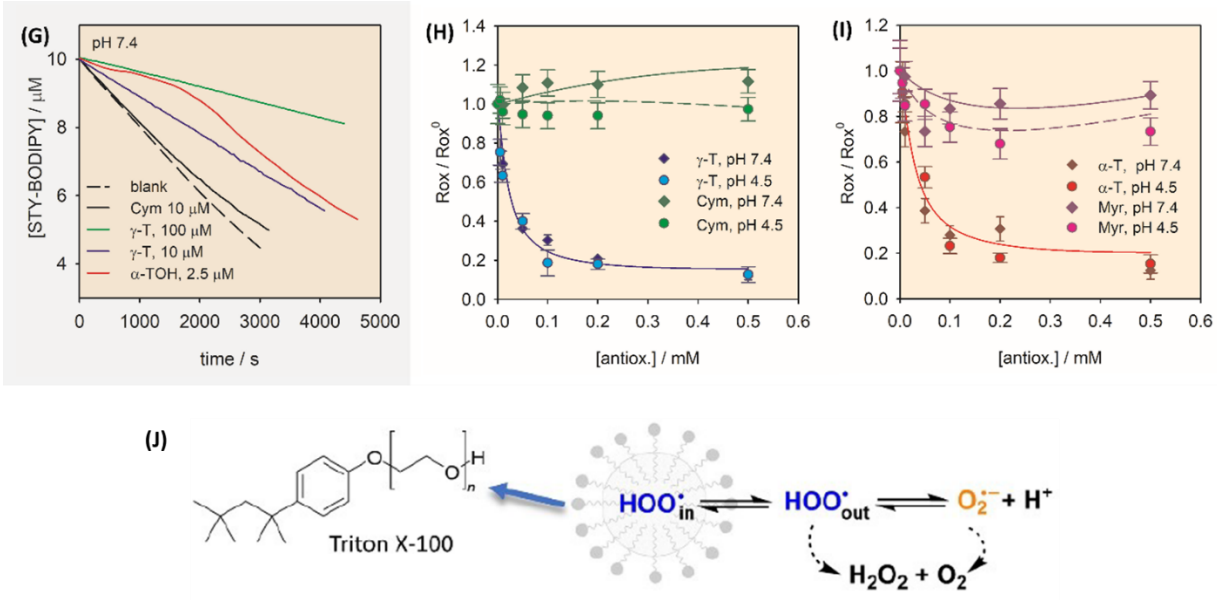

Figure 2.5, *STY-BODIPY consumption traces (G) and relative oxidation rates Rox/Rox^0 (E, F) as function of the concentration of the terpenes during the autoxidation of: MeLH (2.7 mM) in*

Triton X-100 micelles (8.0 mM), in Buffered water initiated by AAPH (G-I), (J): Effect of pH on HOO· exportation from the micelle to the water

2.3.1.4 Autoxidation of liposomes of egg-yolk phosphatidylcholine in PBS buffer

Liposome is a small, spherical artificial vesicle composed of at least one lipid bilayer. Owing to their tunable hydrophobic/hydrophilic balance, biocompatibility, particle size, and other physicochemical properties, liposomes serve as versatile carriers for the delivery of pharmaceutical agents and nutrients, including applications such as lipid nanoparticles in mRNA and DNA vaccines.[137] Liposomes are typically composed of phospholipids[138], most commonly phosphatidylcholine, in combination with cholesterol to modulate membrane fluidity and stability. Other lipids, such as those derived from egg phospholipids or phosphatidylethanolamine, may also be incorporated, provided they are compatible with the lipid bilayer structure.[137]

The last oxidation model consisted of monolamellar liposomes of egg-yolk phosphatidylcholine (PC) of 100 nm diameter, prepared by extrusion in phosphate buffer at pH 7.4. The O_2 concentration in the sample was determined by a fiber-optical oxygen sensor (FireSting O_2 fiber optic O_2-meter from PyroScience) of dissolved O_2. The instrument was shown in figure 2.6. The antioxidant activity can be determined by the equation (10, 12).

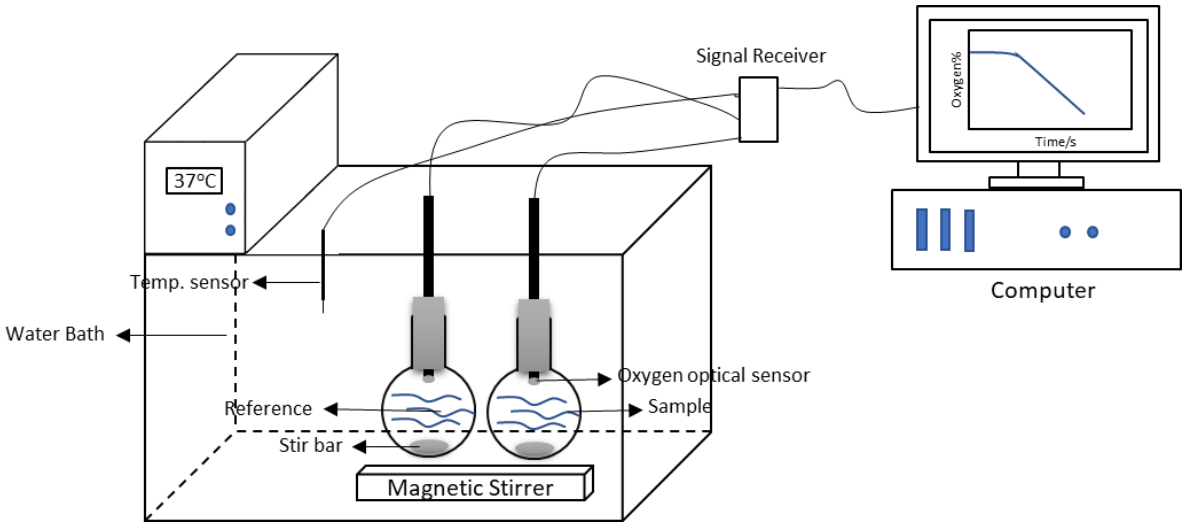

Figure 2.6, *Oxygen uptake apparatus for autoxidation kinetics*

The reaction was initiated by using 1,2-bis((2-methyldecan-2-yl)oxy)diazene (DTUN), a highly lipophilic azoinitiator that generates alkoxyl radicals (RO•). Because of their higher reactivity and smaller selectivity respect peroxyl ones, initiator-derived RO• mostly attack PC fatty acids, generating alkyl radicals on the lipid chains. This approach reduces the possibility of artifacts due to the direct reaction of the antioxidant with the radicals derived from the initiator.[123] In Figure 2.7A, it is shown that, in the presence of γ-T and α-T, the O_2 consumption during PC autoxidation was inhibited to a similar extent as α-tocopherol used at approximately 2 to 4 times smaller concentration, while only minor effects were found in the case of Cym and Myr. In Figure 2.7B, we measured different concentrations of γ-T, α-T, and negative control groups Myr and Cym, and compared them to the standard control α-TOH. We found that even when the concentration of Myr and Cym doubled, their consumption rates did not change significantly, and even slightly accelerated. However, when the concentration of γ-T and α-T doubled, the consumption rates significantly decreased, and the effect of 100 μM γ-T was better than that of 50 μM α-TOH. This is surprising because, interestingly, in chlorobenzene, an apolar organic solvent, α-TOH has a rate constant of reaction with LOO· of $3.2\times106\ M^{-1}\ s^{-1}$,[139] i. e. about 1000 times larger than that of γ-T in the same solvent.

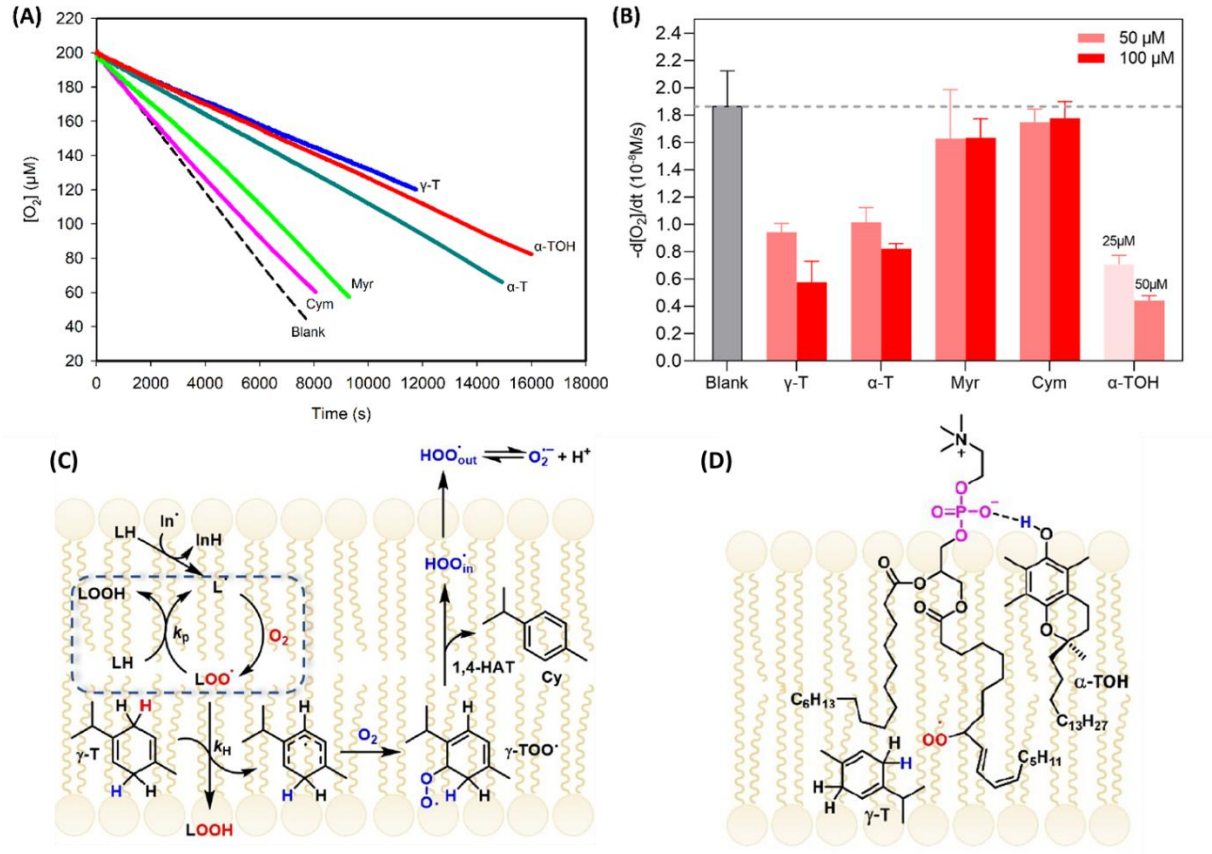

Figure 2.7, *A) Example of O_2 consumption profiles during the autoxidation of PC (5 mM) liposomes initiated by DTUN (0.4 mM) at 37 °C, presence of 100 μM of γ-T, α-T, Cym and Myr (100 μM) and α-TOH (25 μM). (B) O2 consumption rates of PC at different concentrations of the investigated compounds. C) "Slingshot" mechanism explaining the removal of lipophilic peroxyl radicals (LOO·) from the membrane by γ-T. D) Different localization in PCL bilayer of α-TOH and γ-T.*

Figure 2.7C showed the slingshot mechanism of γ-T reacting with lipophilic peroxyl radicals from the lipids and form aromatic product Cym producing HOO•. Figure 2.7D shows the locations of α-TOH and γ-T in the liposome, which is closely related to their mechanism of action. The hydrogen bonds in α-TOH may be constrained by the phosphate group, resulting in reduced activity.

2.3.2 Mechanism studies

To elucidate the role of antioxidants in inhibiting autoxidation, we performed three complementary experiments designed to investigate the possible mechanisms in different systems. 1) **$O_2^{\bullet-}$ trapping**, A fluorescent probe reactive toward $O_2^{\bullet-}$ was used to detect its presence and monitor its production; 2) **Effect of lipophilicity**, A series of 1,4-CHD derivatives with different lipid and water solubilities were synthesized to assess whether solubility influences the reaction mechanism; 3) **Detection of aromatic components**, The formation of aromatic compounds was analyzed to identify CHD derivatives; for instance, Cym formation occurs via a "slingshot" mechanism similar to that of γ-T.

1.4.2.1 $O_2^{\bullet-}$ trapping

The formation of superoxide by γ-T and α-T was ascertained by using the colorimetric probe iodonitrotetrazolium chloride, that upon reduction by $O_2^{\bullet-}$, forms a purple formazan dye with an absorption maximum at 502 nm (Figure 2.8B). [140] A standard experiment was performed using INT, xanthine, and xanthine oxidase (XO) to generate a reference curve, with the maximum absorbance observed at approximately 502 nm in Figure 2.8A.[141] We incubated egg yolk PC with DTUN as initiator, in the presence of γ-T and α-T, at 37 °C for 20 h. Preliminary experiments showed that there is not direct reaction between INT and the terpinene derivatives in the absence of the radical initiator [basal: PC (5 mM) and INT (0.25 mM)]. The addition of γ-T and α-T caused an increase in the reduction of the dye, demonstrating the formation of $O_2^{\bullet-}$. The difference between γ-T and α-T at 1 mM could be explained by considering that at such relatively high concentration the terpinenes react directly with the initiating alkoxyl radicals generated by DTUN (see Figure 2.8C). Alkoxyl radicals are expected to behave differently to alkylperoxyl radicals regarding the preference between H-atom transfer (leading to aromatization and $O_2^{\bullet-}$ formation) and radical addition (leading to oxygenated products).[142] Unexpectedly, the results reported in Figure 2.8D, show that in the control (i.e. in the absence of the terpinenes) there is a small but noticeable increase in the absorption at 502 nm, that arises from the occurrence of a certain degree of $O_2^{\bullet-}$ production during LP in liposomes. This might be due to fragmentation of the

alkylperoxyl radicals (LOO• → L_{-H} + HO_2• → O_2•$^-$ + H^+)[143] or by the chemistry of lipid alkoxyl radicals (LO•) originating from addition/fragmentation pathways.

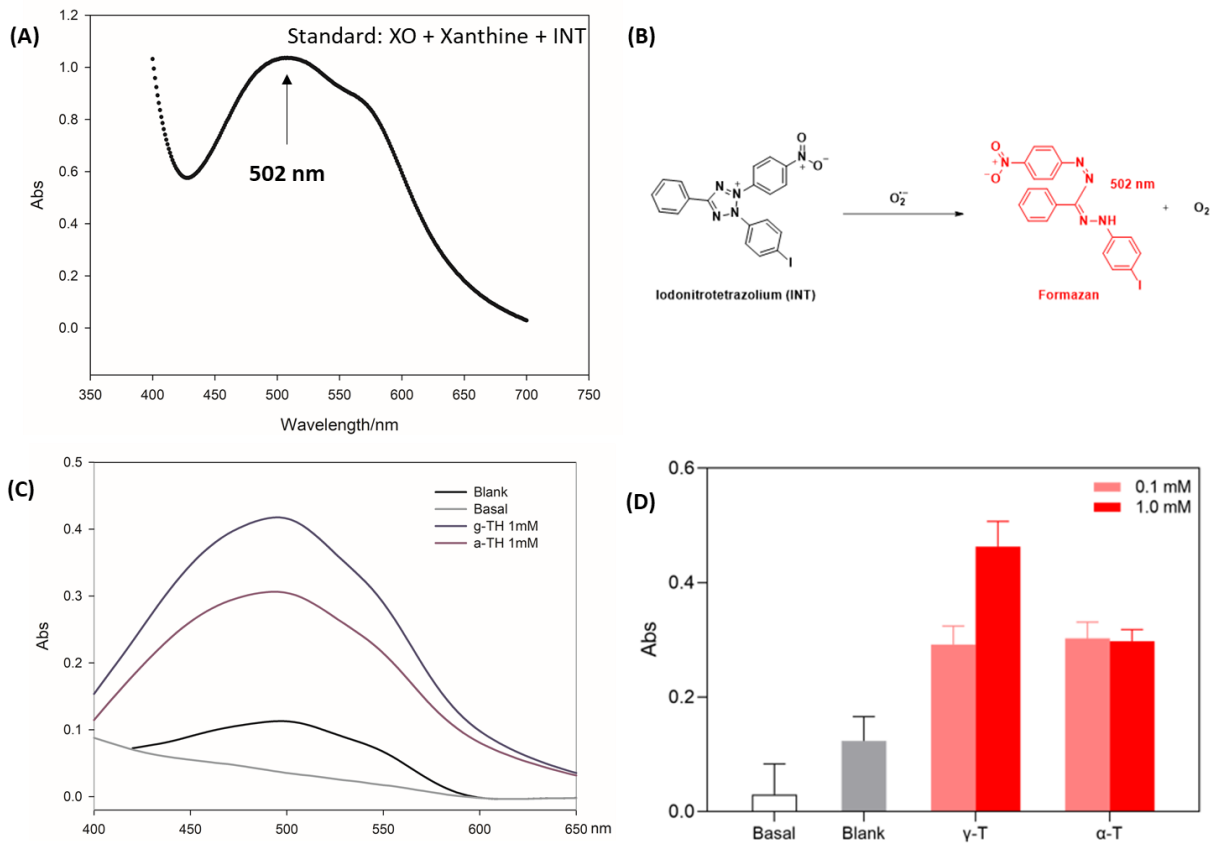

Figure 2.8, *A) Standard Experiment of INT (0.25 mM) with O_2•$^-$ (generate by Xanthine 0.5 mM and XO 0.25U/mL). B) Reaction of the INT probe with superoxide (wavelength 502 nm). C, D) Absorption increase at 502 nm measured by mixing INT (0.25 mM) with PC (5 mM) liposomes in the presence of DTUN (0.4 mM) at 37°C and incubating for 20 hours. The condition of Basal is PC (5 mM) and INT (0.25 mM)*

2.3.2.1 Effect of lipophilicity

To better understand the role of antioxidant partition in the inhibition of the autoxidation of phospholipids in membranes, some 1,4-cyclohexadienes and DTUN having clearly distinct affinity for the lipidic phase were synthetized. 1,4-cyclohexadienes derivatives were straightforwardly obtained by a Birch-like reduction of the respective aromatic precursors by using Li at 0°C.[144] DTUN was synthetized according to the report of Derek A. Pratt[123] see *Section 2.7*.

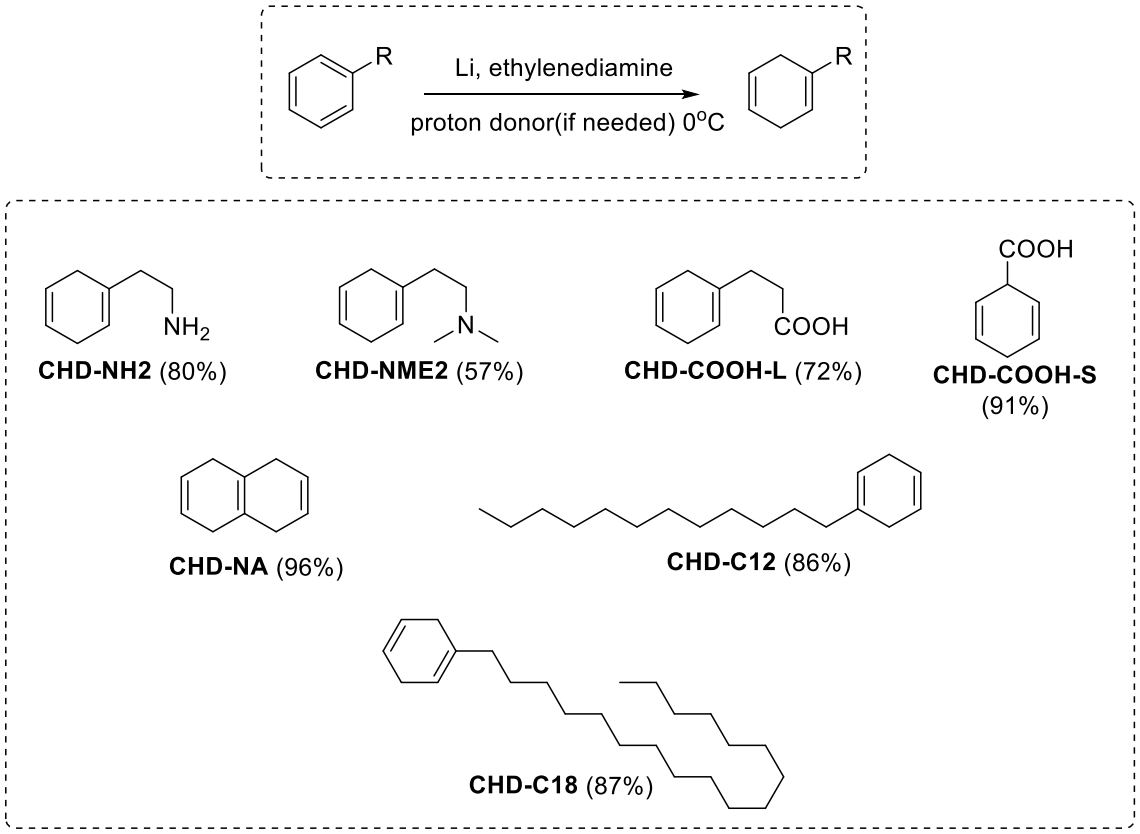

Scheme 2.2, *Synthesis procedure of the pro-aromatic derivatives*

We chose compounds CHD-COOH-L, CHD-NH2, CHD-NA and CHD-C12 which showed the distinct affinity for the lipidic phase to perform the experiments of lipophilicity effect in liposomes in Figure 2.9A. As shown, CHD-COOH-L and CHD-NH_2 are both hydrophilic CHD derivatives and therefore exhibit similar antioxidant properties. In contrast, CHD-NA and CHD-C12 are lipophilic derivatives, and their antioxidant behaviors are comparable to that of γ-T. While the 1,4-CHD moieties of the synthesized molecules are expected to be similar to γ-T in their reactivity toward ROO•, as deduced by the very similar bond dissociation enthalpy (BDE) values of their bis-allylic CH bonds (see Figure 2.9B), respectively, 74.5 kcal/mol (γ-T) and 74.7 kcal/mol (CHD-C12), yet they show very different antioxidant activity in PC liposomes, as the CHD-C12 provides the expected inhibition while CHD-COOH has a much weaker effect.

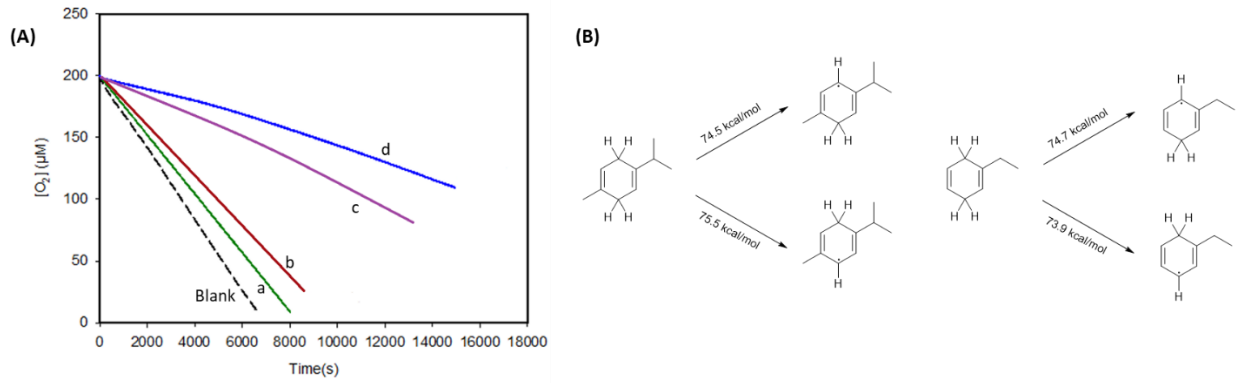

Figure 2.9, *A) O_2 consumption during the autoxidation of PC (5 mM) liposomes initiated by DTUN (0.4 mM) at 37 °C, in the presence of 100 µM of CHD-COOH-L (a), 100 µM of CHD-NH2 (b), 100 µM of CHD-NA (c) or 100 µM of CHD-C12 (d); B) Bond Dissociation Enthalpies calculated at the CBS-QB3 level, for the bis-allylic positions of γ-T and the reactive portion of CHD-C12 and CHD-COOH-L.*

2.3.2.2 Detection of aromatic components

Similarly, we investigated the formation of aromatic compounds by employing HPLC analysis to determine whether γ-T undergoes conversion to Cym. An HPLC method was developed to enable the baseline separation and independent quantification of γ-T and Cym. In the autoxidation, 1 mM γ-T was dissolved in THF, and the PBS buffer (pH = 7.4) with AAPH used as the radical initiator. Experiment details in *section 2.7*. Samples were collected at defined time intervals, and the concentrations of γ-T and Cym were measured to assess whether the consumption of γ-T corresponded stoichiometrically to the formation of Cym. The results were shown in figure 2.10A. Initially, the concentration of γ-T was approximately 1 mM. After 14 hours of reaction, γ-T levels began to decrease, coinciding with the first detectable formation of Cym. By 36 hours, the concentration of Cym had reached ~0.6 mM, while γ-T had declined to ~0.4 mM. These data strongly support the occurrence of an intra-1,4-HAT within γ-T, leading to its progressive conversion into the aromatic product Cym throughout the reaction. In Figure 2.10B, under the same experimental conditions, α-T was already partially converted into Cym at time 0. After 14 hours of reaction, the concentration of α-T decreased from 0.85 mM to 0.15 mM, while the

concentration of Cym increased by only 0.16 mM. With further reaction time, α-T was completely consumed, yet the amount of Cym rose to just 0.35 mM. These results indicate that the transformation of α-T cannot be explained solely by hydrogen atom transfer (HAT) reactions, but must also involve addition pathways.

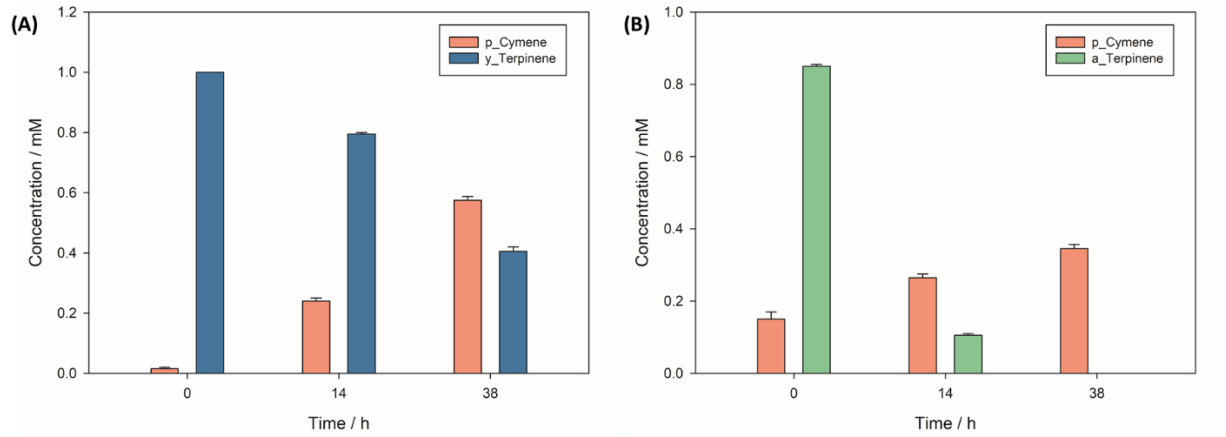

Figure 2.10, *A, B) The Conversion rate of γ-T, a-T and Cym during the autoxidation of THF (3.1 M) initiated by AAPH (1 mM) in PBS 7.4 at 37°C;*

2.3.3 Biologic studies

The part of work presented were carried out in collaboration with Dr. Luca Pincigher, who performed the biologic experiments and analyses, while I contributed to data interpretation. To investigate the protective effects of natural terpenes and synthetic cyclohexadienes in a biological system, lipid peroxidation was induced in the human hepatoma cell line HepG2 ,a widely used in vitro model for lipid peroxidation studies[145,146] by using RSL3 (Ras-selective lethal 3), which is a selective inhibitor of glutathione peroxidase 4 (GPx4). [147] Inhibition of GPx4 leads to the accumulation of lipid hydroperoxides, which react with Fe^{2+} to generate new radicals (see Scheme 2.3), thereby amplifying lipid peroxidation and ultimately triggering ferroptotic cell death. As a positive control for ferroptosis inhibition we used Ferrostatin-1 (Fer-1), an aromatic amine that prevents lipid hydroperoxide accumulation mainly by trapping chain propagating LOO•.[148] Preliminary experiments showed that none of the investigated molecules, nor the aromatic derivative that is formed

upon aromatization like Cym, were toxic to cells at the concentrations employed in the assays (Figure A 2.2).

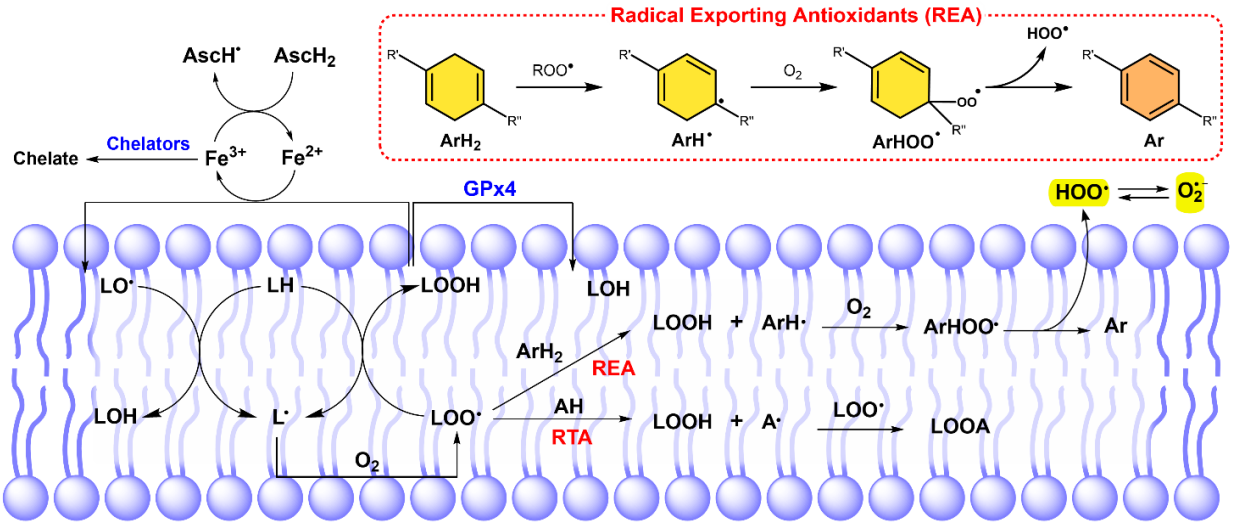

Scheme 2.3, *Mechanism of lipid peroxidation with possible antioxidant mechanisms: preventive (chelators, GPx4, in blue) and chain breaking (in red). RTA: radical-trapping antioxidants; REA: radical-exporting antioxidants; ArH2: pro-aromatic species;*

Treatment of HepG2 cells with 350nM RSL3 for four hours resulted in a reduction in cell viability of over 50%, as determined by the crystal violet assay (Figure 2.11A). Co-treatment with a-T and g-T provided almost complete, dose-dependent protection. By contrast, treatment with Cym and Myr provided significantly weaker protection against RSL3-induced lipid peroxidation. Finally, co-treatment with 500 nM Fer-1 completely restored cell viability. (Figure 2.11A).

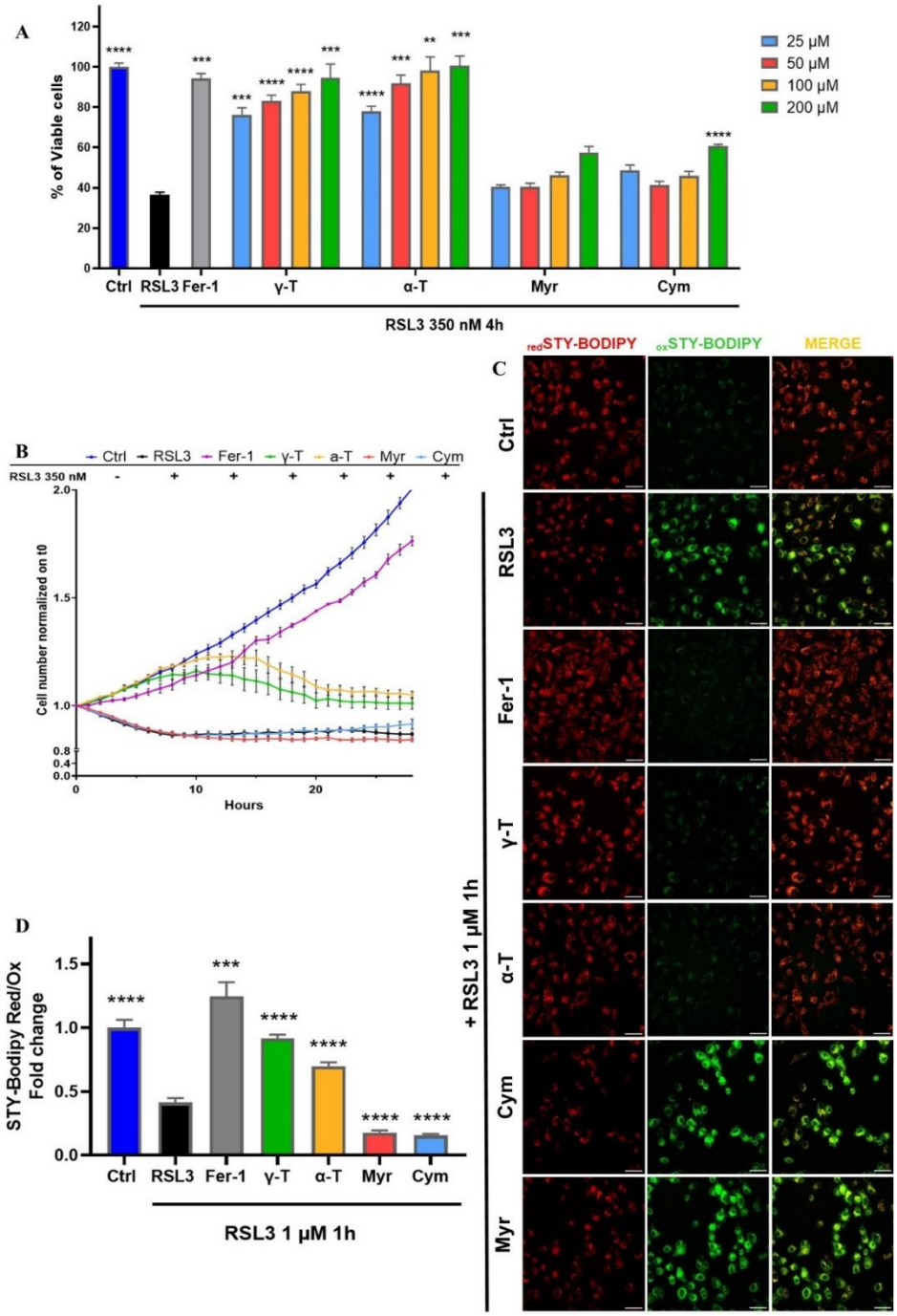

Figure 2.11, *Protective effects of natural terpenoids against RSL3-induced lipid peroxidation in HepG2 cells.* ***(A)*** *Cell viability assessed by Crystal Violet assay after treatment with γ-T, α-T, Cym, or Myr (25–200 µM) for 4 hours, followed by 350 nM RSL3. Fer-1 (500 nM) was used as a positive control. Data are mean ± SEM (n = 6, one-way ANOVA, **p < 0.01; ***p < 0.001; ****p < 0.0001 vs. RSL3).* ***(B)*** *Cell proliferation analyzed using the IncuCyte Live-Cell Assay. Cells were treated with 100 µM γ-T, α-T, Cym, and Myr in the presence of 350 nM RSL3. Data*

are mean ± SEM (n = 4 independent experiments). ***(C)*** *Representative confocal images of HepG2 cells treated with 100 μM γ-T, α-T, Cym, Myr, or 400 nM Fer-1 in the presence of 1 mM RSL3, followed by STY-BODIPY staining. Scale bar = 30 mm.* ***(D)*** *Quantification of fluorescence intensity ratio (reduced/oxidized STY-BODIPY) from confocal images. Data are mean ± SEM (n = 4, one-way ANOVA, ***p < 0.001; ****p < 0.0001 vs. RSL3).*

To assess the persistence of the compounds' protective effects, HepG2 cells were treated with RSL3 in the presence or absence of natural terpenes, and cell proliferation was monitored for 28 hours using a real-time imaging system. As shown in Figure 2.11B, RSL3 treatment completely suppressed cell proliferation, whereas co-treatment with α-T and γ-T was able to maintain the cell proliferation rate at a level similar to that of the control group for up to 18 hours. In contrast, co-treatment with Myr and Cym failed to protect cells from RSL3-induced lipid peroxidation. Finally, cells co-treated with the specific ferroptosis inhibitor Fer-1 maintained a proliferation rate comparable to that of control cells for up to 28 hours. Representative images of cell morphology recorded during the experiment (Figure A 2.3) showed that co-treatment with both α-T and γ-T preserved cell structure after 12 hours. However, membrane integrity was lost after 24 hours, consistent with the absence of cell proliferation observed beyond 18 hours.

To investigate lipid membrane peroxidation in depth, we stained HepG2 cells with the oxidisable fluorescent dye STY-BODIPY, [149] and detected the fluorescence emission of the reduced and oxidised probe by confocal microscopy analysis. The probe localizes to cell membranes, and its oxidation serves as an indicator of ongoing lipid peroxidation. Specifically, probe oxidation changes the emission peak from ~590 nm to ~510 nm, shifting the fluorescence from red to green emission. HepG2 cells stained with STY-BODIPY were treated with different natural terpenes, then exposed to RSL3 for one hour (Figure 2.11C). Consistent with previous results, RSL3-treated cells exhibited a significant increase in green fluorescence compared to the control group (Figure 2.11D). In the presence of both γ-T and α-T, however, the STY-BODIPY was predominantly found in its reduced state. Interestingly, Cym and Myr increased probe oxidation. As expected, co-treatment with Fer-1 was able to maintain the probe in a predominantly reduced state.

The same set of experiments were performed using the synthetic compounds CHD-C_{12} and CHD-COOH, and the results are shown in Figure 2.12.

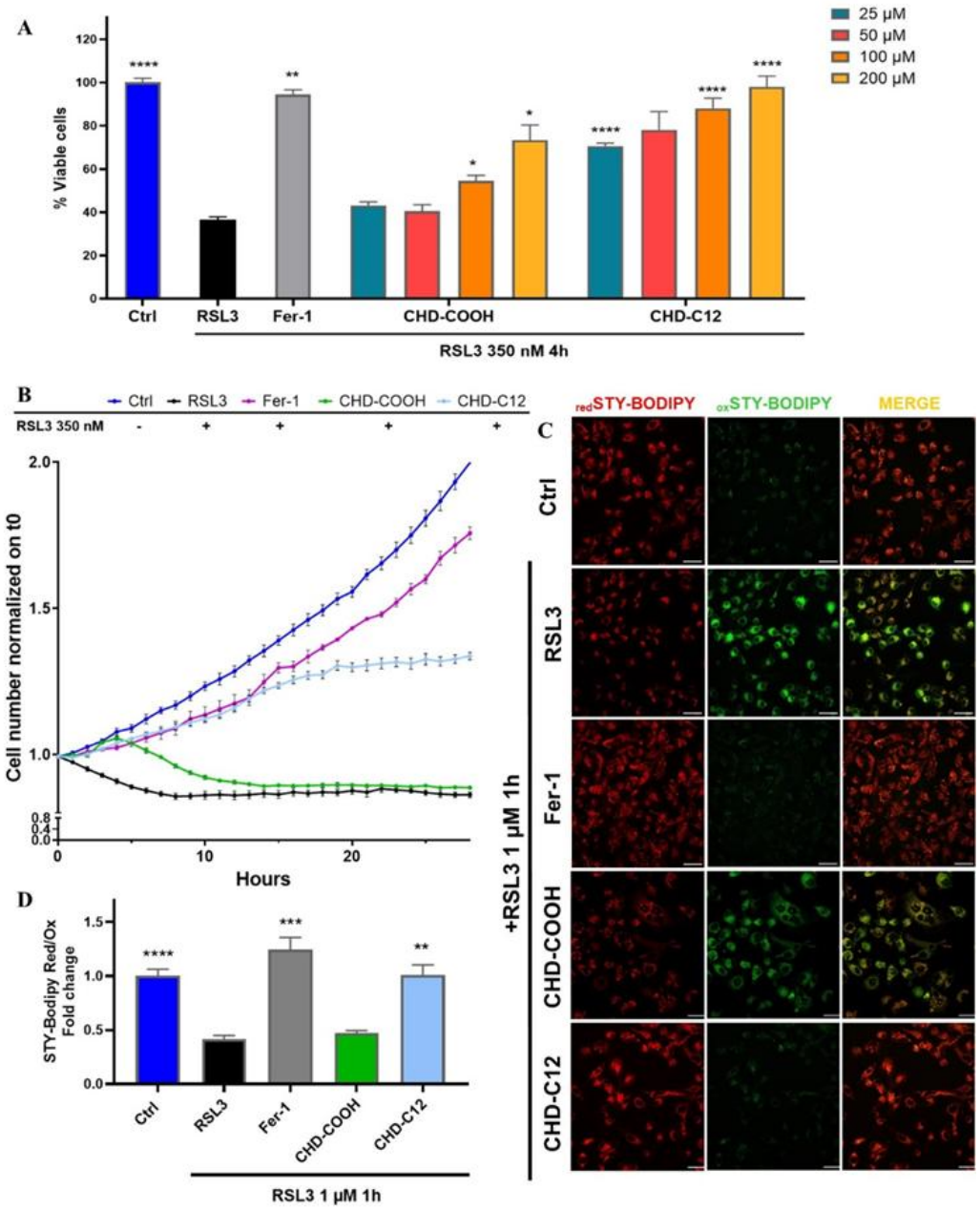

Figure 2.12, *Protective effects of synthetic 1,4-cyclohexadienes against RSL3-induced lipid peroxidation in HepG2 cells. (A) Cell viability assessed by Crystal Violet assay after treatment with CHD-C_{12} and CHD-COOH (25–200 µM) for 4 hours, followed by 350 nM RSL3. Fer-1 (500 nM) was used as a positive control. Data are mean ± SEM (n = 6, one-way ANOVA, **p < 0.01; ***p < 0.001; ****p < 0.0001 vs. RSL3). (B) Cell proliferation analyzed using the IncuCyte*

*Live-Cell Assay. Cells were treated with 100 μM CHD-C12 and CHD-COOH in the presence of 350 nM RSL3. Data are mean ± SEM (n = 4 independent experiments). (C) Representative confocal images of HepG2 cells treated with 100 μM CHD-C12 and CHD-COOH, or 400 nM Fer-1 in the presence of 1 μM RSL3, followed by STY-BODIPY staining. Scale bar = 30 μm. (D) Quantification of fluorescence intensity ratio (reduced/oxidized STY-BODIPY) from confocal images. Data are mean ± SEM (n = 4, one-way ANOVA, ***p < 0.001; ****p < 0.0001 vs. RSL3).*

In the crystal violet assay, CHD-C_{12} and, to a lesser extent, CHD-COOH were able to rescue HepG2 cell viability from RSL3-induced LP (Figure 2.12A). Regarding the duration of the antioxidant effect, proliferation experiments reported in Figure 2.12B showed that CHD-C_{12} had a much longer duration than its natural counterpart, γ-T. In fact, CHD-C_{12} was able to maintain cell viability for up to 42 hours and to preserve morphology, similar to Fer-1 (see also Figures A 2.3 and A 2.4). Furthermore, CHD-C_{12} was effective in preserving lipid redox status in the presence of RSL3 induction (Figures 2.12C, D). In contrast, CHD-COOH was unable to rescue the cell proliferation rate or protect the lipid membrane from RSL3-induced peroxidation.

2.4 Discussions

Lipid peroxidation (LP) has emerged as a critical biochemical process implicated in the pathogenesis of various degenerative diseases and organ injuries. Consequently, there is an urgent need for a deeper understanding of its underlying chemical mechanisms and the development of a broader spectrum of peroxidation inhibitors. Current research predominantly focuses on phenol-, quinone-, and diarylamine-based scaffolds[150]. However, with few notable exceptions[151], the discovery and advancement of novel compounds operating through alternative mechanisms of LP inhibition have been relatively neglected. In this study, we present a series of natural and synthetic pro-aromatic compounds as inhibitors of LP, emphasizing their structural attributes, mechanistic strengths, and inherent limitations. Furthermore, we demonstrate that these compounds serve as "mechanistic probes," providing critical insights into the dynamics of radical

species involved in LP. Notably, we explore their role in hydroperoxyl radical (HOO•) formation and elucidate the significance of the "radical exporting" mechanism in mitigating LP.

Pro-aromatic cyclohexadienes, such as γ-T and α-T, are highly effective in preventing lipid peroxidation (LP) under various conditions. In contrast, control compounds that are either non-cyclic (e.g., myrcene, Myr) or fully aromatic (e.g., p-cymene, Cym) show no significant inhibitory effect. The protective action of pro-aromatic compounds (ArH_2) is explained by the instability of the corresponding peroxyl radicals (ArHOO•, nomenclature in Scheme 2.3). These intermediates are extremely short-lived and decompose before they can react with polyunsaturated fatty acids (MeLH), yielding instead the aromatic species (Ar) and HOO•.

The decomposition of ArHOO• is intrinsically fast because it drives aromatization. For γ-T, the decomposition rate constant has been measured as high as $5 \times 10^4\ s^{-1}\ M^{-1}$[117], which is about three orders of magnitude greater than the pseudo-first-order rate constant for the hypothetical reaction of ArHOO• with MeLH (estimated as k_p[MeLH] = 62 $M^{-1}s^{-1} \times 0.8$ M = 49 s^{-1}, based on the known propagation rate constant, k_p, of MeLH: [22]

MeLH + MeLOO• ⟶ MeL• + MeLOOH

A similar situation is observed with other oxidizable substrates, such as THF, whose propagation rate constant is even lower (k_p = 4.3 $M^{-1}s^{-1}$)[22] In the organic solvent of low polarity like chlorobenzene, a bimodal behaviour is observed, as LP inhibition occurs only at low concentrations, while at higher concentrations a pro-oxidant effect prevails (Figure 2.1 A-C and Figure A 2.1 A-B). This result is because the HOO• radicals react efficiently with α-T or γ-T (i.e red arrows in Scheme 2.4A), thus the autoxidation of terpinenes prevails when large concentrations of them are used.

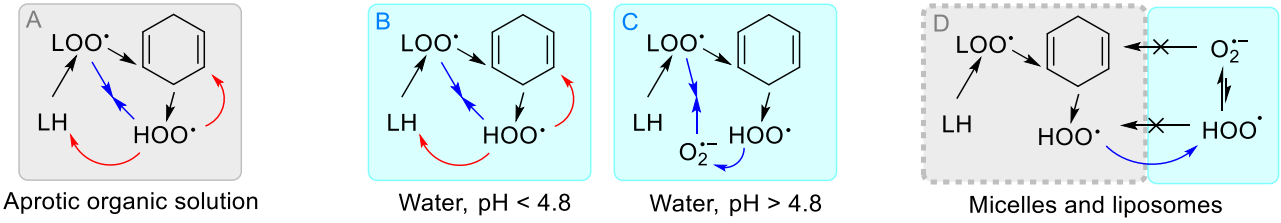

Aprotic organic solution | Water, pH < 4.8 | Water, pH > 4.8 | Micelles and liposomes

***Scheme 2.4**. Interactions among the crucial species during lipid peroxidation in the presence of pro-aromatic derivatives. A) In aprotic organic solution, HOO• can propagate the radical chain, although inhibition may arise from the reaction with LOO•. B) in water at pH < 4.8. that is deprotonation of HOO•, the situation is similar to A. C) in water at pH > 4.8, HOO• deprotonates to O2•−, that is unable to propagate the radical chain and can quench LOO•. D) in micelles and liposomes, HOO• diffuse to the water phase, and whatever the pH, it is physically unable to propagate the radical chain.*

In the water/THF system at pH 7.4, γ-T and α-T behave as antioxidant at all concentrations. This is the hallmark of HOO• deprotonation to $O_2^{\bullet-}$ that, being a poor oxidizer,[135] has little ability of propagating the autoxidation, while it is effective in chain termination by reacting with ROO• radicals. On the contrary, in the water/THF system at pH 4.5, γ-T and α-T show again a bimodal effect on LP, because HOO• at this pH is mostly protonated, and thus is able to propagate the oxidation by reacting with the terpenes (see Scheme 2.4B, C).

The autoxidation of MeLH in micelles at pH 7.4 is slowed down by γ-T and α-T at all concentrations, while Cym and Myr have little effect. As this is a biphasic system where the LP occurs in the lipophilic micellar core, this result implies that the reaction of HOO• with MeLH is insufficiently fast to compete with its diffusion out of the lipid phase.[100] Interestingly, experiments in micelles at pH 4.5 didn't show the bimodal antioxidant/prooxidant effect found in the water/THF system at the same pH value. However, this result can be explained by the difficulty for the highly hydrophilic HOO• radical to reach the hydrophobic phase to react with MeLH or the terpenes, as shown in Scheme 2.4D).

The experiment in egg yolk liposomes represents the ultimate proof of the relevance of pro-aromatic compounds as inhibitors of LP in membranes. Herein, the comparison with the physiological antioxidant a-tocopherol (a-TOH) provides the estimation of their effectiveness as inhibitors, that can be estimated as being about twice as smaller than a-TOH. The crucial role of HOO•/O_2•− in the radical exporting mechanism is also supported by its reaction with the INT probe. In addition, the experiments performed by using the

synthetic derivatives CHD-C12 and CHD-COOH clearly demonstrate the importance of the partition of the pro-aromatic derivatives into the bilayer in order to achieve LP inhibition.

In addition to γ-T, alcohol compounds and methyl linoleate (ML) can also generate hydroperoxyl radicals (HOO•) through hydrogen atom transfer (HAT) reactions[]. To evaluate the ability of γ-T, alcohols, and ML to produce HOO•, the reaction barriers for their interactions with ROO• and their subsequent intramolecular HAT reactions were calculated at the CBS-QB3 level of theory. The results are summarized in Scheme 2.5. Generally, a lower Gibbs free energy change (ΔG) indicates a more thermodynamically favorable reaction pathway.

In reaction A, γ-T reacts with ROO•, yielding ΔG values of 14.8 kcal/mol and 11.3 kcal/mol for the first and second steps, respectively. In reaction B, the α-C–H bonds of primary and secondary alcohols are abstracted by radicals to form stabilized alkyl radicals, with a ΔG of 20.4 kcal/mol. Upon subsequent reaction with molecular oxygen, an intra-HAT process occurs, generating HOO• with a ΔG of 11.7 kcal/mol. This energy barrier is comparable to that observed for γ-T, suggesting that alcohols possess a similar capability for HOO• production, although the initial step requires a significantly higher activation energy than that of γ-T.

In reaction C, the bis-allylic structure of ML allows the CH_2 group at the bis-allylic position to be preferentially attacked by ROO•, with a ΔG of 19.9 kcal/mol for this step. The following intramolecular HAT reaction, however, proceeds with a much higher ΔG of 26.3 kcal/mol, indicating that this process is considerably less favorable than reactions A and B. Overall, these computational results demonstrate that γ-T exhibits a greater tendency to generate HOO• compared with the other compounds examined, primarily due to its lower energy barrier in the intramolecular HAT step. The relatively low barrier in the initial ROO• reaction further indicates that γ-T readily participates in radical scavenging processes, consistent with its antioxidant nature. These theoretical findings are in strong agreement with the experimental data, confirming that γ-T not only acts as an effective antioxidant but also facilitates HOO• formation.

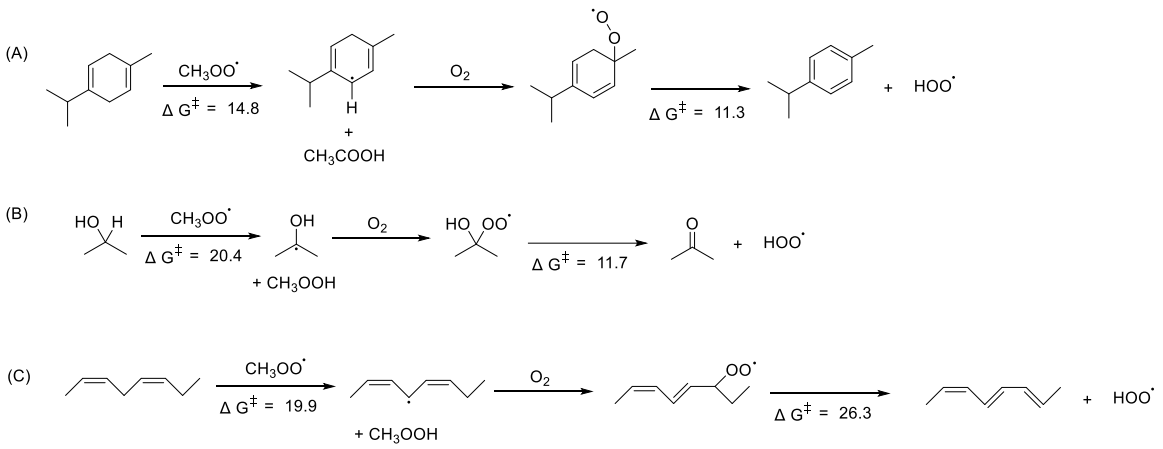

Scheme 2.5. *Proposed mechanism for hydrogen atom transfer (HAT) reaction to produce HOO• corresponding transition states calculated at the CBS-QB3 level. A) HAT pathway for γ-T; B) HAT pathway for alcohol; C) HAT pathway for methyl linoleate.*

In the experiments aimed at detecting aromatic products, it was observed that within the entire self-oxidation system, γ-T predominantly undergoes intra-1,4-hydrogen atom transfer (HAT), typically leading to the formation of Cym, as shown in Figure 2.3. In addition, the non-conjugated double bonds present in γ-T could, in principle, participate in addition reactions. However, no decrease in the total Cym content was detected experimentally, with the combined concentration of Cym and γ-T remaining around 1 mM. To further explore this behavior, we calculated the activation energies for both the HAT and addition (ADD) pathways of γ-T and α-T at the CBS-QB3 level[152] (Figure 2.13 and 2.14). CBS-QB3 is a composite quantum chemical method developed by John Pople's group, designed to give highly accurate thermochemical data (e.g., reaction energies, enthalpies, ionization potentials, barrier heights) at a relatively moderate computational cost. The HAT pathway showed an energy barrier of 14.9 kcal/mol, whereas the ADD pathway required a higher barrier, exceeding it by 3.7 kcal/mol. Moreover, the products of the HAT reaction were found to be significantly more stable than those of the ADD pathway, with relative energies of –11.5 kcal/mol and +6.2 kcal/mol, respectively. These findings strongly support the conclusion that γ-T preferentially undergoes intra-HAT reactions, in agreement with the experimental observations.[100]

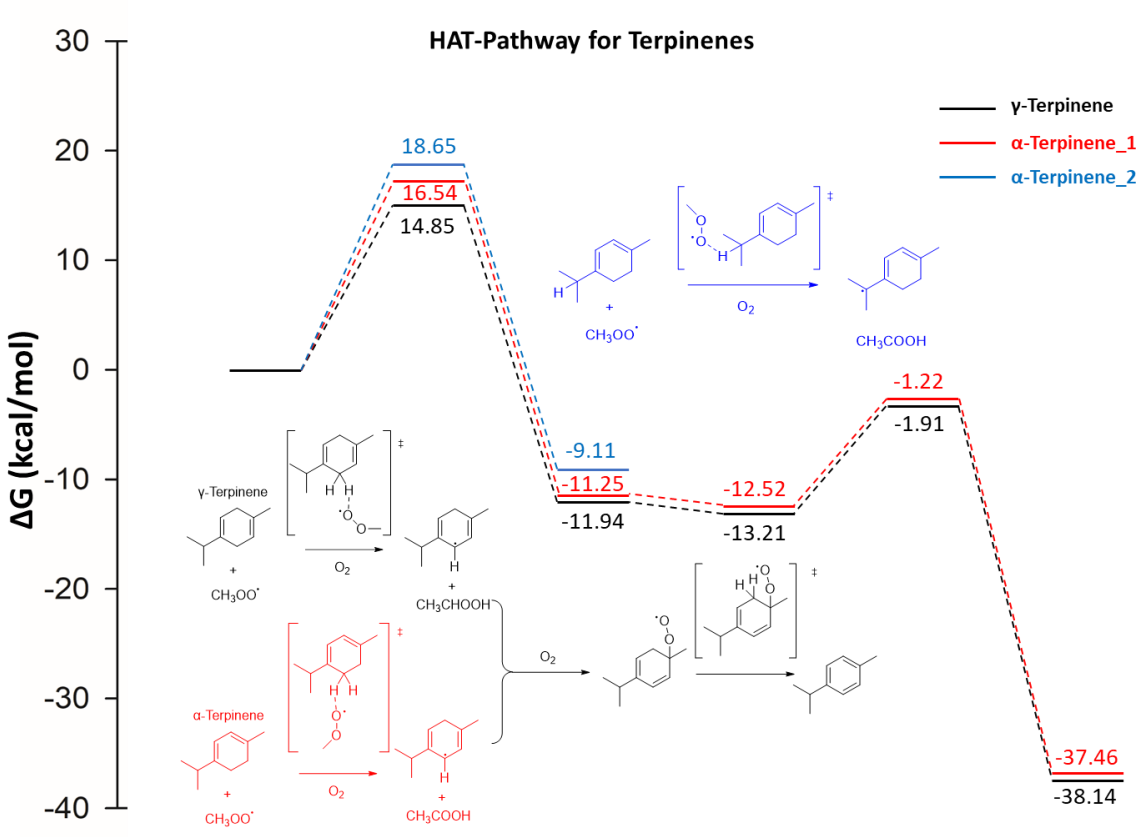

Figure 2.13, *Transition states calculated at the CBS-QB3 level, for HAT pathway of γ-T and α-T.*

Furthermore, the experimental results for α-T revealed that it does not predominantly produce Cym via HAT reactions; instead, a substantial fraction of α-T undergoes addition (ADD) reactions, leading to structures resembling epoxide derivatives. DFT calculations further support this outcome, showing that the energy barrier for the HAT pathway in α-T is 16.5 kcal/mol, whereas the ADD pathway requires only 12.0 kcal/mol. Furthermore, as illustrated in Figure 2.13, the ROO• radical can also abstract a hydrogen atom from the methyl group of α-T; however, the calculated energy barrier for this transition state is 18.6 kcal/mol, which is considerably higher than that for hydrogen abstraction from the 1,3-CHD ring. This indicates that ROO• preferentially abstracts hydrogen from the CHD ring rather than from the methyl group. This lower barrier indicates a stronger propensity of α-T to undergo addition reactions. Overall, these computational insights are in good agreement with the experimental observations.

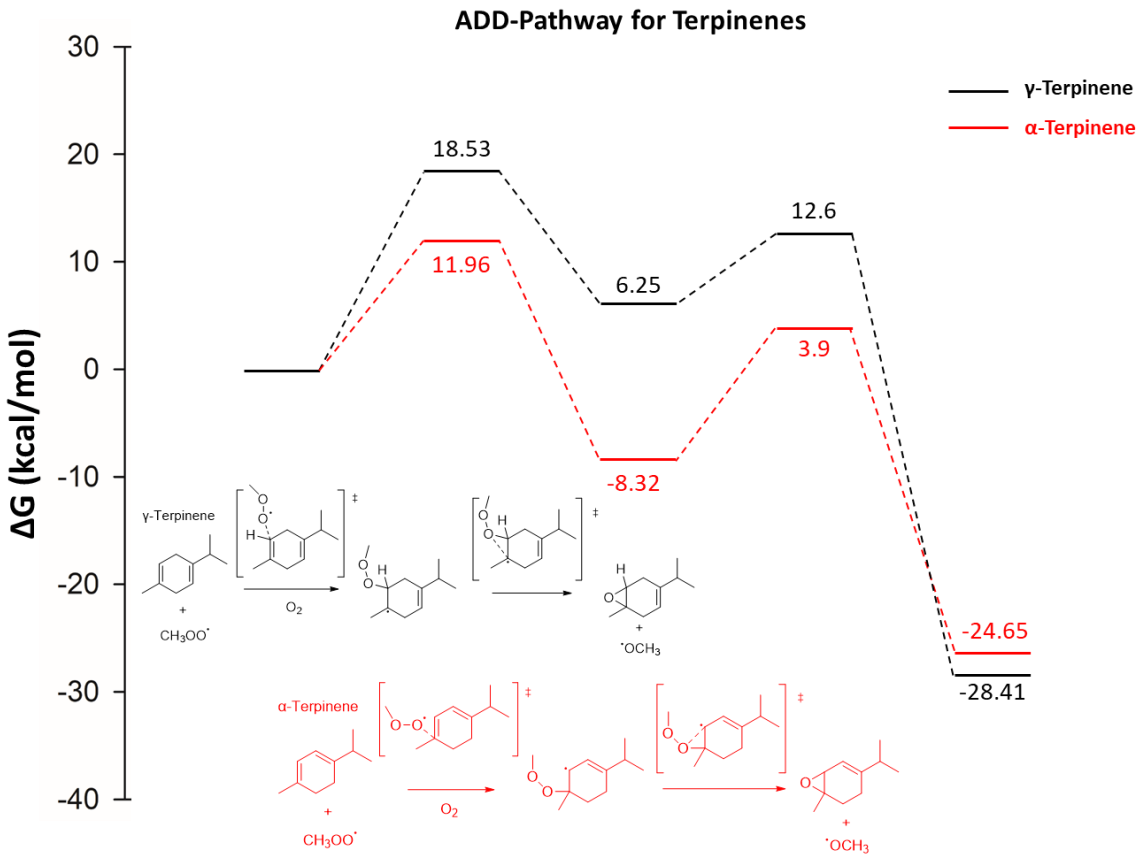

Figure 2.14, *Transition states calculated at the CBS-QB3 level, for ADD pathway of γ-T and α-T.*

As shown in Figure 2.10, α-T can react via two different mechanisms. According to the HPLC results, approximately 70% of α-T did not form Cym but instead produced other products. To have a complete overview of the reaction, as illustrated in Figure 2.15, we compared the two reaction pathways of α-T in different solvents using DFT calculations. First, the optimized geometries obtained at the CBS-QB3 level in the gas phase were selected. Single-point energy calculations were then performed in both the gas phase and solvent phases using the lower-level B3LYP/6-311+G(d,p) method. The free energy difference between the gas and solvent phases (ΔG_{solv}) was calculated according to Equation 13[153] and this ΔG_{solv} was subsequently added to the CBS-QB3 Gibbs free energy to obtain the final G_{solv} of CBS values based on Equation 14[153].

$$\Delta G_{solv} \approx G_{DFT}^{solv} - G_{DFT}^{gas} \quad (13)$$

$$G_{CBS}^{solv} = \Delta G_{solv} + G_{CBS}^{gas} \quad (14)$$

Comparison of the calculated energy barriers of α-T in different solvents revealed similar trends for both mechanisms. In aqueous solution, both pathways exhibited the lowest barriers, with ΔG values of 14.4 kcal/mol for the HAT (hydrogen atom transfer) pathway and 11.1 kcal/mol for the ADD (addition) pathway. In contrast, the highest barriers were obtained in PhCl (chlorobenzene). The energy barrier differences between the solvent and gas phases were 1.9 kcal/mol for the HAT pathway and 0.9 kcal/mol for the ADD pathway in water, whereas in PhCl, these differences were 1.1 kcal/mol and 2.7 kcal/mol, respectively. On the other hand, the energy decrease from PhCl to water was almost identical, -3.2 kcal/mol for HAT vs -3.5 kcal/mol for ADD.

These results indicate that solvation has minimal effect on HAT and ADD patways.

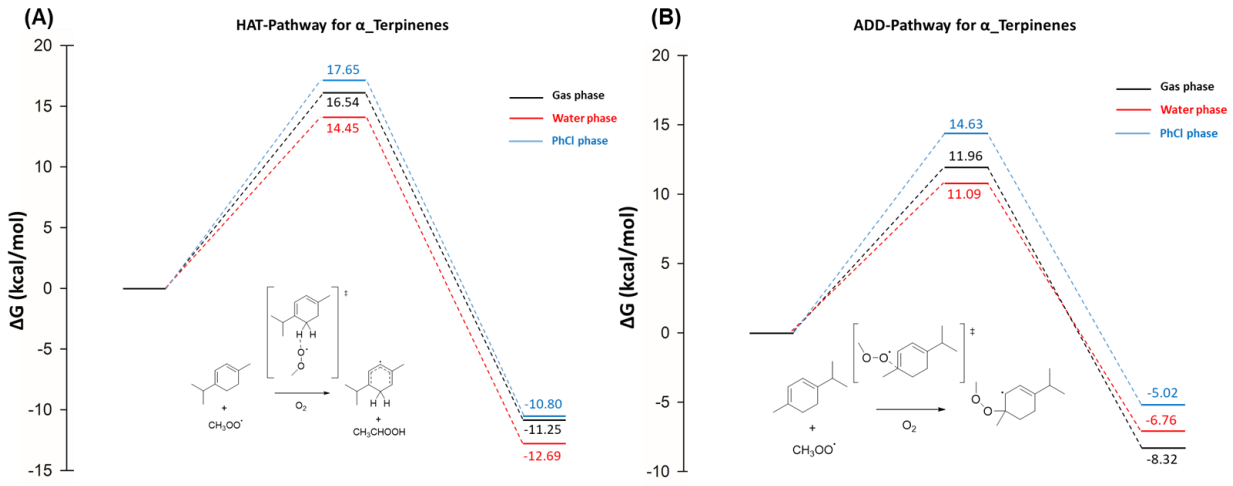

Figure 2.15, *The comparison of Transition states for α-T in gas phase, water phase and Chlorobenzene phase. A) HAT pathway for α-T; B) ADD pathway for α-T.*

The observed results can be interpreted within the framework of co-oxidation kinetics (Scheme 2.6, Eq. 15, and Table 2.2) [154, 155]. In this model, RH represents the main

oxidizable substrate (e.g., MeLH or THF), while EH denotes the co-oxidizing species. Inhibition occurs when the peroxyl radicals derived from the co-oxidant (EOO•) display termination rate constants greater than those of the primary substrate (i.e., k_6 and $k_7 > k_5$), and/or possess a reduced capacity to propagate the radical chain (i.e., k_3 and $k_4 < k_2$).

$$Rox = \frac{\{k_2k_4[RH]^2 + 2k_1k_4[RH][EH] + k_1k_3[EH]^2\}R_i^{1/2}}{\{k_5k_4^2[RH]^2 + k_7k_1k_4[RH][EH] + k_6k_1^2[EH]^2\}^{1/2}} \quad (15)$$

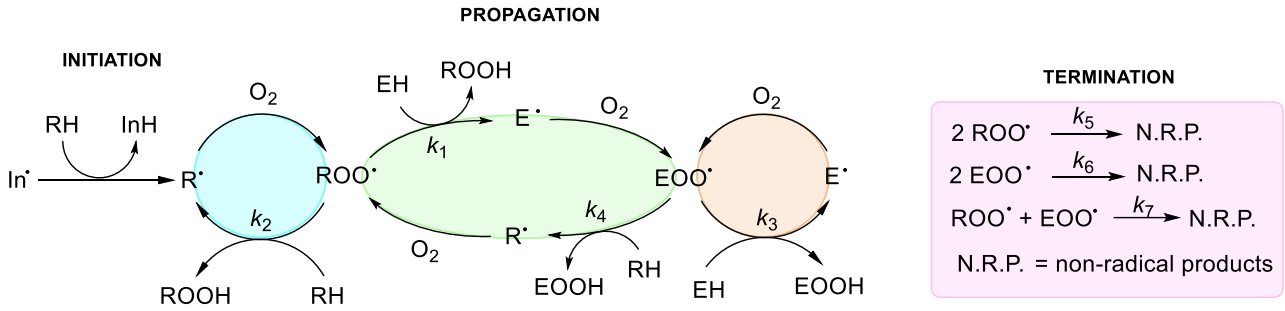

Scheme 2.6, *Mechanism of the co-oxidation of two oxidizable substrates, RH and EH. If EH is pro-aromatic, then EOO• = HOO• and EOOH = H_2O_2*

Table 2.2 Rate constants ($M^{-1}s^{-1}$) obtained from co-oxidation analysis of γ-T, apparent inhibition constant (k_{inh}') of γ-T, and inhibition constant (k_{inh}) for reference antioxidants.

entry	Reaction conditions	k_1	k_3	k_4	k_{inh}'	k_{inh} (reference)
1	MeLH / PhCl[a]	$9.7x10^2$	$1.1x10^3$	$1.3x10^2$	43±4	$(7.7±0.7)x10^5$ (a-TOH)[b]
2	MeLH / Mic pH 7.4[c]	$1.0x10^3$	0.13	15	$(9.2±0.5)x10^2$	$2.2x10^4$ (a-TOH) [156]
3	MeLH / Mic pH 4.5[c]	$9.3x10^2$	0.10	15	$(8.3±0.5)x10^2$	-
4	THF / H2O pH 7.4[d]	$7.5x10^2$	5.5	$3.2x10^{-3}$	$(1.6±0.2)x10^3$	$2.0x10^5$ (PMHC) [157]

5	THF/H2O pH 4.5[d]	$8.1x10^2$	$7.7x10^2$	$1.3x10^{-2}$	$(2.3\pm0.2)x10^2$	-
	PC liposomes				$(1.3\pm0.2)x10^3$	$4.3x10^3$ (a-TOH) [158]

[a] k_2=62 $M^{-1}s^{-1}$; k_5=1.0 x 10^7 $M^{-1}s^{-1}$,[159] k_6 = 6.3 x 10^8 $M^{-1}s^{-1}$ [160] b) Measured in this work. c) k_2=36 $M^{-1}s^{-1}$; k_5=1.2 x 10^3 $M^{-1}s^{-1}$,[156] d) k_2=4.8 $M^{-1}s^{-1}$; k_5=6.6 x10^7 $M^{-1}s^{-1}$ [157] k_6 (pH 7.4) = 1.1 x 10^6 $M^{-1}s^{-1}$, k_6 (pH 4.5) = 3.0 x 10^7 $M^{-1}s^{-1}$.[161]

These requirements are fulfilled in the case of the pro-aromatic compounds investigated herein, because, in these molecules, EOO• radicals are very short lived and fragment to HOO• ones before undergoing other reactions (see above). In turn, HOO• are characterized under most conditions by high termination constants and/or low propagating activity, especially in water solvents where they are deprotonated to $O_2^{\bullet-}$.

The co-oxidation model (see Figure A 2.1)[154, 155] provided a satisfactory fit to the experimental data in all cases, as indicated by the solid lines in Figure 2.1, 2.3 and 2.5. To elucidate the origin of the inhibitory effect observed for pro-aromatic compounds, selected kinetic parameters obtained from the model for γ-T are reported in Table 2.2. Given the presence of STY-BODIPY as an additional oxidizable species in some experiments, and the uncertainty associated with several variables, these parameters should be regarded as semi-quantitative estimates.

In Table 2.2, the values derived from the co-oxidation model are compared to the apparent inhibition rate constants (k_{inh}'), calculated using Equation 16. This equation, commonly employed in autoxidation studies, relates the rate of oxidation in the presence of antioxidant (R_{in}) to the rate of initiation (R_i), the propagation rate constant (k_p), and the antioxidant concentration. However, it does not account for possible side reactions involving peroxidation of the antioxidant itself:

$$R_{in} = \frac{k_p[Substrate]R_i}{2\,k'_{inh}[Antioxidant]} \qquad (16)$$

Here, R_{in} represents the rate of substrate oxidation in the presence of antioxidant (either −d[O_2]/dt or −d[STY-BODIPY]/dt), k_p is the propagation rate constant of the oxidizable

substrate (MeLH, STY-BODIPY, or phosphatidylcholine), and R_i is the rate of radical initiation by the azoinitiators.

The rate constant k_1, describing the reaction of γ-T with ROO•, falls within the range reported for similar compounds[162, 163] and remains relatively stable across different experimental systems. This is consistent with previous findings that ROO• reactivity with C–H bonds of hydrocarbons is largely insensitive to solvent polarity.[164] In contrast, the rate constants for reactions involving HOO• − specifically, its reactions with γ-T (k_3) and with the oxidizable substrate (k_4) − showed substantial variation between homogeneous organic and aqueous or micellar systems. These differences reflect the influence of acid–base equilibrium and phase partitioning on the reactivity of this radical.

In micellar autoxidation of MeLH, k_3 and k_4 were small at both pH 7.4 and 4.5 (entries 2 and 3), indicating that the low reactivity of HOO• is primarily governed by its localization in the aqueous phase, rather than its protonation state. In the homogeneous THF/H_2O system (entries 4 and 5), lowering the pH from 7.4 to 4.5 led to an increase in both k_3 and k_4, consistent with enhanced H-atom transfer (HAT) reactivity upon protonation of $O_2^{\bullet-}$ to HOO•. Comparison of k_{inh}' and k_1 values offers additional mechanistic insight into γ-T's behavior. In organic solution (entry 1) and acidic aqueous media, k_{inh}' is much smaller than k_1, consistent with competing peroxidation of γ-T, which reduces its effective antioxidant capacity. In contrast, in neutral aqueous buffer and in Triton X-100 micelles, $k_{inh}' \approx k_1$, as expected under conditions where neither HOO• nor $O_2^{\bullet-}$ can sustain efficient chain propagation.

Finally, the efficacy of pro-aromatic compounds can be conveniently evaluated by comparing their apparent inhibition rate constants (k_{inh}') to that of a-tocopherol or structurally related chromanol derivatives (k_{inh}(ref)) (see Table 2.2). While γ-T is approximately 10^4-fold less effective than a-TOH in apolar organic solvents (entry 1), its relative efficacy increases markedly in aqueous and micellar systems, reaching values comparable to a-TOH in liposomal membranes. This trend reflects the kinetic solvent effect (KSE) on k_{inh}(ref), which is known to be significantly reduced in protic and amphiphilic environments due to hydrogen bonding between α-TOH and solvent molecules or the

phosphate headgroups of phospholipids (see Scheme 2.7A).[123] Since liposomes are a well-established model of biological membranes, these results provide a compelling mechanistic rationale for the observed protective effects of pro-aromatic terpenes against lipid peroxidation in cellular systems. They also offer strong evidence for the potential biological relevance of mono- and sesquiterpenoid antioxidants that operate via a pro-aromatic mechanism (see Scheme 2.7C).

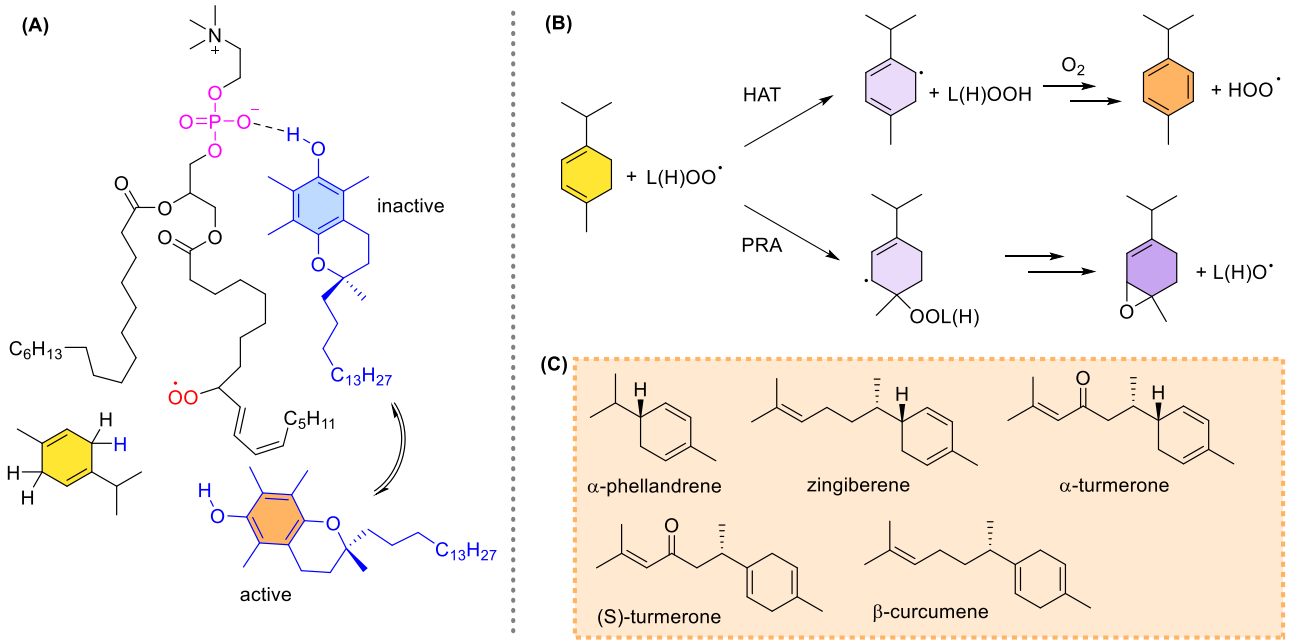

Scheme 2.7*. A) H-bond effects on a-tocopherol in membranes; B) competition between H-atom transfer (HAT) and Peroxyl Radical Addition (PRA) in the reaction of a-terpinene with peroxyl radicals; C) main pro-aromatic terpenes present in nature.*

The present study reveals comparable antioxidant behavior between α-T and γ-T. Notably, α-T features a conjugated 1,3-cyclohexadiene moiety, a structural motif also found in naturally occurring terpenes such as a-turmerone, a-phellandrene, and zingiberene (Scheme 2.7 C).[165] In nonpolar solvents such as chlorobenzene, a-T exhibits relatively modest inhibition efficiency (Figure 2.1 C), which may be attributed to competition between two oxidation pathways: hydrogen atom transfer (HAT) and peroxyl radical addition (PRA) (Scheme 2.7 B). While HAT leads to antioxidant regeneration via

hydroperoxide formation and subsequent aromatization, PRA yields a variety of oxygenated products, including alkyl hydroperoxides and epoxides, without aromatization. Moreover, PRA can generate reactive alkoxyl (RO• or LO•) radicals, potentially propagating further oxidative damage, as previously reported.[166] Although literature data suggest that in a-T HAT is faster than PRA - e.g., $k_{PRA} \approx 300\ M^{-1}\ s^{-1}$ versus $k_{HAT} \approx 1000\ M^{-1}\ s^{-1}$ for MeLOO• in benzene at 37 °C [162] – the relatively small difference in rate constants implies that both pathways may compete under certain conditions. Interestingly, the difference in antioxidant performance between α-T and γ-T observed in chlorobenzene diminishes in aqueous and micellar systems, but reappears − albeit to a lesser extent − in liposomal membranes. This behavior underscores the influence of solvent polarity and interfacial effects on the relative contributions of HAT and PRA mechanisms. Together, these findings highlight the antioxidant potential of natural 1,3-cyclohexadienes, while also cautioning against the possible pro-oxidant consequences of PRA-derived reactive intermediates, which may have implications for safety and biological activity.

In the HepG2 cell model, α-T, γ-T and the synthetic derivative CHD-C12 were found to protect cellular membranes and sustain cell viability in the presence of RSL3, a known inducer of lipid peroxidation (LP) and ferroptotic cell death. Real-time, continuous monitoring of cell proliferation revealed that α-T and γ-T conferred protection against RSL3-induced toxicity for approximately 18 hours, after which a decline in proliferation was observed, culminating in cell death as evidenced by marked morphological changes (see Figure A 2.3). In contrast, CHD-C12 displayed prolonged protective activity, maintaining cell viability for at least 42 hours − comparable to the ferroptosis inhibitor ferrostatin-1 (Figure 2.12).

Although the basis for this extended protection remains uncertain, it is plausible that the C12 aliphatic chain of CHD-C12 reduces its intracellular redistribution or metabolic degradation by anchoring the molecule within the plasma membrane. In support of this hypothesis, the structurally related compound CHD-COOH showed minimal protective activity in all assays, likely due to the presence of a carboxylic acid group that limits membrane partitioning. This observation is consistent with results obtained in liposomal

systems, reinforcing the relevance of egg yolk unilamellar liposomes as a predictive model for antioxidant behavior in biological membranes. The antioxidant behavior observed for pro-aromatic terpenes in HepG2 cell model supports the idea that the generation of superoxide is not detrimental under physiological conditions. This is likely due to two key factors: first, the amount of $O_2^{\bullet-}$ generated through this pathway is minimal compared to established cellular sources (e.g., mitochondria, NADPH oxidases); second, superoxide is efficiently detoxified by cellular antioxidant defenses, including superoxide dismutase.[167]

2.5 Conclusion

We have shown that the antioxidant activity of lipophilic pro-aromatic derivatives arises from their ability to intercept peroxyl radicals within the membrane and convert them into hydrophilic hydroxyperoxyl radicals through a series of studies. These polar radical species can diffuse into the aqueous phase, where they are deprotonated to form the less reactive superoxide anion. This breaks the radical chain in the membrane and, from the cell viability data, we can speculate that the superoxide anion is efficiently detoxified by superoxide dismutase (mitochondrial and cytosolic SODs). In this study, lipophilic pro-aromatic molecules function as "radical-trapping" antioxidants via the unconventional "radical export" mechanism. The chemistry proposed here also helps explain previously reported antioxidant effects of γ-T in red blood cells[168] and in low-density lipoproteins.[97] Notably, the ability of pro-aromatic compounds to inhibit membrane lipid peroxidation supports further investigation into their antioxidant effects, for example by modifying their lipophilicity with suitable substituents, or by modulating the reactivity of the pro-aromatic moiety. While additional studies are required to confirm and extend our preliminary findings, particularly regarding the relatively short duration of protection of α-T and γ-T in cell models, the compound's high lipophilicity and low molecular weight suggest good bioavailability and the potential to cross the blood-brain barrier, a critical property for compounds targeting the central nervous system.[169] These results may also help clarify the neuroprotective properties of certain essential oils containing γ-T, such as those from

bergamot and coriander, that show activity even when administered by inhalation.[170, 171] This supports the pharmacological relevance of aromatic plant extracts used in traditional medicine. Moreover, the reactivity principles described here could apply to other readily oxidizable compounds capable of forming hydroperoxyl radicals, including reduced Coenzyme Q and vitamin K, both of which are under active investigation for their roles in regulating lipid peroxidation.[172, 173]

2.6 Experimental Section

2.6.1 Materials

All solvents (H_2O, chlorobenzene, DMSO) were of the highest grade commercially available (≥99.9% HPLC grade, Sigma-Aldrich) and used as received. γ-Terpinene (γ-T; >97%, Sigma-Aldrich), was percolated on alumina and silica before each experiment to remove impurities and traces of stabilizer, and its purity checked by 1HNMR. Chemicals were purchased from Sigma-Aldrich and TCI, and were used without any additional purification: 2,2'-azobis(2-amidinopropane) dihydrochloride (AAPH; 97%, Sigma-Aldrich), Triton X-100 (t-octylphenoxypolyethoxyethanol, for molecular biology, Sigma-Aldrich), methyl linoleate (MeLH; 98%, TCI), L-α-phosphatidylcholine (from egg yolk, Type XI-E, 100 mg/mL in chloroform, ≥99%, solution, Sigma-Aldrich), (±)-6-hydroxy-2,5,7,8-tetramethylchromane-2-carboxylic acid (Trolox; 97%, Sigma-Aldrich), α-tocopherol (95.5%, Sigma-Aldrich), 2,2,5,7,8-pentamethyl-6-chromanol (PMHC; 97%, Sigma-Aldrich), iodonitrotetrazolium chloride (INT, 97%, Sigma-Aldrich). Azobisisobutyronitrile (AIBN) was recrystallised from methanol before use.

PBS Buffer (pH= 7.4): 0.1 M buffer solution at pH 7.4 was prepared in a 50-mL flask using 101 mg $Na_2HPO_4•7H_2O$, 17 mg $NaH_2PO_4•H_2O$ and 438 mg NaCl, bringing to volume with MilliQ water.

Acetic Buffer (pH= 4.5): 0.1 M buffer solution at pH 4.5 was prepared in a 500 mL volumetric flask by weighing 2.93 g of CH_3COONa and adding 1.62 ml of neat CH_3COOH,

bringing to volume with MilliQ water. Adjust pH to 4.5 ± 0.1 with 100 mM sodium acetate or 100 mM acetic acid.

UV–visible measurements were performed using a Cary 1E (Varian) spectrometer coupled to Cary Temperature Control (Varian).

The concentration of O_2 was measured using an optical oxygen meter FireStingO_2 (PyroScience GmbH).

2.6.2 Synthesis section

2.6.2.1 The synthesized procedure of DTUN [123]

Synthesis of 2-Methyldecan-2-ol

1-Bromooctane (19.3 g, 100 mmol, 1 eq) was added dropwise to magnesium turnings (3.04 g, 125 mmol, 1.25 eq, activated dry with iodine) suspended in anhydrous THF (100 mL) under N_2 atmosphere at a rate that maintained a gentle reflux. Upon completion of the reaction, the solution was transferred via cannula to a dry round bottom flask under N_2, cooled thoroughly in an ice bath, and acetone (7.0 mL, 95 mmol, 0.95 eq, dried overnight on 3A sieves) was added dropwise over about 30 min. The mixture was allowed to warm to room temperature over 3 h, then recooled on ice, quenched with 6 mL acetic acid and concentrated in vacuo. The residue was vigorously stirred with 100 mL 3:1 chloroform: isopropanol and 100 mL water for 10 min before extracting the aqueous layer 2x 50 mL 3:1 chloroform: isopropanol. The combined organics were washed 3x 100mL 10% aqueous sodium chloride, 1x 100 mL brine, dried over Na_2SO_4, filtered and concentrated to dryness. The residual oil was distilled with a short path fractionating distillation apparatus collecting the middle fraction of distillate to afford 2-methyldecan-2-ol (13.95 g, 81%) as a colorless oil. Spectra were in agreement with literature values. (Dryzhakov et al., 2015)[174].

Synthesis of 2-Iodo-2-methyldecane

An oven dried 25 mL round-bottom flask and stir bar were cooled under N_2 atmosphere, wrapped completely in foil, charged with concentrated HI (6.7 mL, ca. 2 eq) and then cooled in an ice bath. Lithium iodide (3.36g, 25 mmol, 1 eq) was added in portions (caution:

exotherm/fumes with powdered LiI; beads are preferred). A solution of 2-methyldecan-2-ol (4.31 g, 25 mmol, 1 eq.) in methylene chloride (5 mL) was added slowly by syringe with vigorous stirring under nitrogen atmosphere. The ice bath was then removed and the biphasic mixture stirred for about 10 minutes, at which point the alcohol was completely consumed by ^{1}H-NMR. The mixture was carefully transferred to separatory funnel and the bottom aqueous layer cautiously extracted twice with methylene chloride (10 mL). The combined organic layers were washed once with 1:1 brine:water containing drops of sodium bisulfite solution until the mixture was mostly colourless. The organic extracts were fully protected from light while drying over Na_2SO_4, filtering and concentrating on a rotary evaporator followed by hivac (flask backfilled with nitrogen) to yield the title compound as a pale oil (6.63 g, 94%). The product was pure by ^{1}H-NMR without distillation and was stored at -20°C in a foil-wrapped vial, ideally backfilled with nitrogen. ^{1}H-NMR (300 MHz, $CDCl_3$) δ 1.92 (m, 6H), 1.65-1.22 (m, 14H), 0.88 (t, J = 6.9 Hz, 3H). ^{13}C-NMR (75 MHz, $CDCl_3$) δ 53.27, 50.72, 38.20, 32.02, 29.65, 29.57, 29.43, 28.63, 22.81, 14.27. HRMS: m/z Calc: $C_{11}H_{23}$ (ESI: M-I)$^{+}$ 155.1800 Found: 155.1817.

Synthesis of Di-tert-undecyl Hyponitrite (DTUN)

An oven dried 25 mL round-bottom flask and stir bar were cooled under N_2 atmosphere and charged with 2-iodo-2-methyldecane (1.44 g, 6 mmol) followed by degassed anhydrous methylene chloride (10 mL). The flask was completely wrapped in aluminum foil to exclude light and then cooled thoroughly in an ice bath. Freshly dried silver hyponitrite (1.24 g, 4.5 mmol) was added in three portions over 5 min with vigorous stirring. The ice bath was then removed and NMR analysis indicated consumption of the tertiary iodide usually within 10-20 min. The reaction mixture was then re-cooled in an ice bath and diluted with cold pentane (10 mL) before filtering over celite. The filtrate was concentrated on a rotary evaporator without heating followed by hivac for about 5 min while on ice. The residual oil was crystallized overnight from methanol (ca. 20 mL, N2 purged) on dry ice. The majority of supernatant was then removed by syringe, discarded, and the solid washed with three portions of cold methanol in the same manner. The solid was allowed to thaw into a small volume of methanol (ca. 5 mL) until a solution formed.

The product was promptly isolated thereafter while being kept cold on ice at all times. The solution was extracted with three portions of cold pentane (5 mL), the combined pentane extracts washed once with 1:1 methanol: water, dried over Na_2SO_4, filtered, concentrated on a rotary evaporator without heating followed by high vacuum to yield DTUN (270 mg, 24%) as a colorless wax. The product when free from residual solvent is solid on ice and rapidly melts when allowed to warm to ambient temperature. The solid was aliquoted by Pasteur pipette into tared vials and the vials were stored at -78°C. ^{1}H-NMR (600 MHz, $CDCl_3$) δ 1.65 (m, 2H), 1.34 (s, 6H), 1.34-1.24 (m, 12H), 0.88 (t, J = 6.6 Hz, 3H). ^{13}C-NMR (151 MHz, $CDCl_3$) δ 83.42, 40.63, 32.03, 30.16, 29.69, 29.42, 25.94, 24.02, 22.82, 14.27. HRMS: m/z Calc: $C_{11}H_{23}$ (EI: $M^-C_{11}H_{23}N_2O_2)^+$ 155.1794 Found: 155.1787.

2.6.2.2 The synthesized procedure of STY-BODIPY.

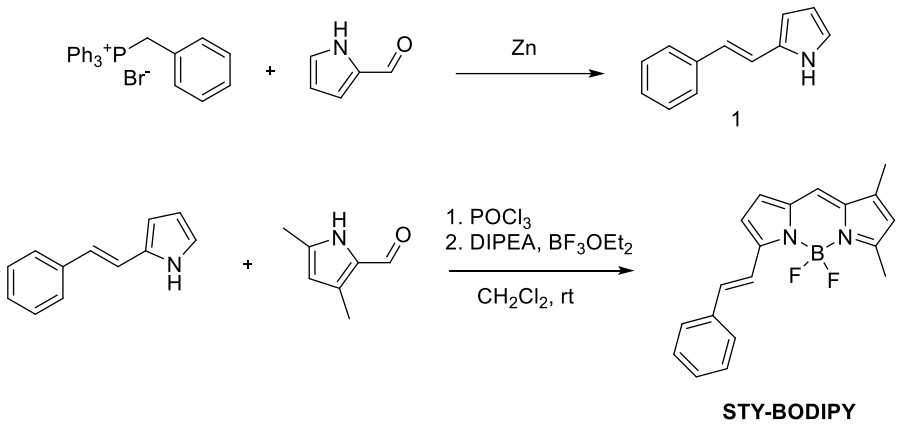

Synthesis of Compound 1

A solid mixture of pyrrole-2-carboxaldehyde (1.0 g, 10.5 mmol), zinc dust (0.69 g, 10.5 mmol), and benzyl triphenylphosphonium bromide (4.3 or 4.5 g, 10.5 mmol) was heated to 100 °C under an inert atmosphere and stirred overnight. The mixture was allowed to cool before it was diluted with $CHCl_3$ (25 mL) and filtered. The filtrate was washed once with water and once with brine before drying with $MgSO_4$. Following filtration and concentration under reduced pressure, the product was purified by column chromatography on silica gel using a gradient of 20–30% $CHCl_3$ in hexanes.

Synthesis of STY-BODIPY

The product styryl-substituted pyrrole (0.53 or 0.46 g, 2.7 mmol) was then combined with 3,5-dimethylpyrrole-2-carboxaldehyde (0.34 g, 2.7 mmol) in dry CH_2Cl_2 (135 mL) under an inert atmosphere. $POCl_3$ (0.27 mL, 2.9 mmol) was then added dropwise over several minutes, and the reaction was stirred overnight in the dark at room temperature. Diisopropylethylamine (2.0 mL, 11.5 mmol) was then added slowly, and the reaction was stirred for another 10 min, followed by dropwise addition of BF_3–OEt_2 (1.4 mL, 11.2 mmol). The reaction was stirred at room temperature until complete (∼1 h, as judged by TLC), poured into a separatory funnel, and washed twice with water and then a small amount of brine. The organic phase was dried with $MgSO_4$ and filtered and the solvent evaporated. Column chromatography (100% CH_2Cl_2) removed the major impurities. A second column (60% CH_2Cl_2 in hexanes) afforded pure product. ^{1}H-NMR (600 MHz, DMSO-d_6) δ = 7.69 (s, 1H), 7.62 - 7.56 (m, 3H), 7.45 (d, J = 17.5 Hz, 3H), 7.40 - 7.34 (m, 1H), 7.21 (d, J = 4.3 Hz, 1H), 7.15 (d, J = 4.3 Hz, 1H), 6.34 (s, 1H), 2.52 (d, J = 1.8 Hz, 3H), 2.28 (s, 3H). ^{13}C-NMR (151 MHz, DMSO-d6) δ = 159.3, 152.7, 144.1, 136.6, 136.2, 135.3, 135.1, 129.6, 129.5, 127.4, 124.3, 120.8, 118.8, 116.2, 15.1, 11.5.

Due to the oxidizability of STY-BODIPY, 2.0 mM stock solutions of each compound were prepared in DMSO (depending on whether they are for use in organic or aqueous solutions) and stored under nitrogen, frozen at −20°C. When stored in this manner, there was minimal background oxidation of the either compound over several months.

2.6.2.3 Synthesis of CHD-derivatives

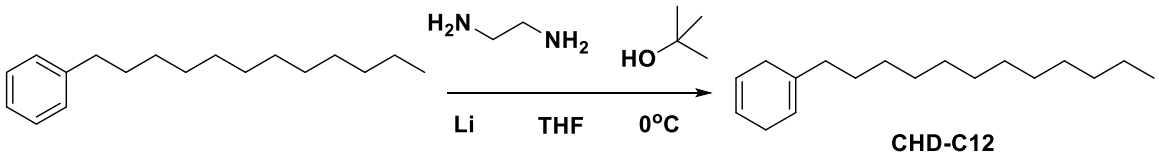

Reduction of 1-dodecylcyclohexa-1,4-diene: A single-neck, 100-mL round-bottom flask was equipped with a magnetic stir bar and a septum equipped with a needle connected to a bubbler as a gas outlet. Dodecylbenzene (1.00 g, 4.06 mmol), THF (30 mL), ethylenediamine (1.63 mL, 24.3 mmol, 6.0 equiv), and t-BuOH (0.58 mL, 6.1 mmol, 1.5 equiv) were added to the flask, and the resulting solution was stirred while cooling to 0 °C. Lithium (84 mg, 12.2 mmol, 3.0 equiv) was added to the solution. The reaction mixture

was stirred at 0 °C (external temperature) until TLC analysis showed the reaction to be complete (25 min). Saturated aqueous NH_4Cl (40 mL) was added to reaction mixture (CAUTION: Evolution of hydrogen gas), and the resulting mixture was stirred until the remaining lithium was quenched. The resulting mixture was concentrated under reduced pressure with a rotary evaporator and the water bath at 25 °C until most THF was removed. The resulting mixture was poured to a 125-mL separatory funnel, and the product was extracted with Et_2O (30 mL × 3). The organic extracts were combined, dried over Na_2SO_4, filtered through cotton, and concentrated under reduced pressure. The oil was determined to be pure by ^1H NMR spectroscopy to give 1-dodecylcyclohexa-1,4-diene (866 mg, 86% yield) as a colorless oil.

Data for 1-dodecylcyclohexa-1,4-diene; ^1H NMR (600 MHz, $CDCl_3$, 294K) δ 5.63 (m, 2 H), 5.32 (m, 1 H), 2.61 (m, 2 H), 2.51 (m, 2 H), 1.87 (m, 2 H), 1.23 (s, 20 H), 0.81 (t, 2H, *J* = 6 Hz); ^{13}C NMR (151 MHz, $CDCl_3$, 294K) δ135.3, 124.5, 124.3, 118.0, 37.6, 31.9, 29.7, 29.6, 29.4, 28.9, 27.4, 26.8, 22.7, 14.1.

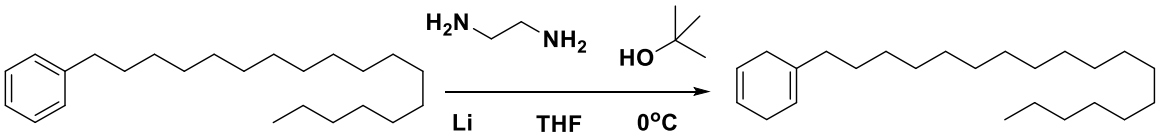

CHD-C18

Reduction of 1-octadecylcyclohexa-1,4-diene: A single-neck, 100-mL round-bottom flask was equipped with a magnetic stir bar and a septum equipped with a needle connected to a bubbler as a gas outlet. Octadecylbenzene (1.00 g, 3.02 mmol), THF (30 mL), ethylenediamine (1.09 g, 18.2 mmol, 6.0 equiv), and t-BuOH (0.34 g, 4.5 mmol, 1.5 equiv) were added to the flask, and the resulting solution was stirred while cooling to 0 °C. Lithium (63 mg, 9.1 mmol, 3.0 equiv) was added to the solution. The reaction mixture was stirred at 0 °C (external temperature) until TLC analysis showed the reaction to be complete (30 min). Saturated aqueous NH_4Cl (40 mL) was added to reaction mixture (CAUTION: Evolution of hydrogen gas), and the resulting mixture was stirred until the remaining lithium was quenched. The resulting mixture was concentrated under reduced pressure with a rotary evaporator and the water bath at 25 °C until most THF was removed. The resulting mixture was poured to a 125-mL separatory funnel, and the product was extracted with

Et_2O (30 mL × 3). The organic extracts were combined, dried over Na_2SO_4, filtered through cotton, and concentrated under reduced pressure. The oil was determined to be pure by ^1H NMR spectroscopy to give 1-octadecylcyclohexa-1,4-diene (872 mg, 87% yield) as a white solid.

Data for 1-octadecylcyclohexa-1,4-diene; ^1H NMR (600 MHz, $CDCl_3$, 294K) δ 5.71 (m, 2 H), 5.41 (m, 1 H), 2.68 (m, 2 H), 2.58 (m, 2 H), 1.96 (m, 2 H), 1.19 (s, 32 H), 0.88 (t, 2H, *J* = 6 Hz); ^{13}C NMR (151 MHz, CDCl3, 294K) δ135.3, 124.5, 124.3, 118.0, 37.6, 31.9, 29.7, 29.6, 29.4, 28.9, 28.3, 27.7, 27.4 26.8, 23.1, 22.7, 14.1.

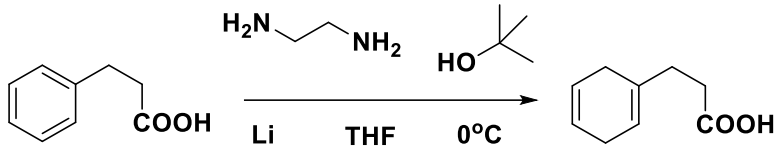

Reduction of hydrocinnamic acid to 3-(1,4-cyclohexadien-1- yl)propanoic acid: A single-neck, 100-mL round-bottom flask was equipped with a magnetic stir bar and a septum equipped with a needle connected to a bubbler as a gas outlet. Hydrocinnamic acid (1.00 g, 6.66 mmol), THF (22 mL), ethylenediamine (4.45 mL, 66.6 mmol, 10 equiv) and t-BuOH (1.27 mL, 13.3 mmol, 2.0 equiv) were added to the flask, and the resulting solution was stirred while cooling to 0 °C. Lithium (231 mg, 33.3 mmol, 5.0 equiv) was added to the solution. The reaction mixture was stirred at 0 °C (external temperature) until TLC analysis showed the reaction to be complete (30 min). Saturated aqueous NH_4Cl (40 mL) was added to reaction mixture (CAUTION: Evolution of hydrogen gas), and the resulting mixture was stirred until the remaining lithium was quenched. The resulting mixture was cooled with an ice bath and acidified with concentrated HCl until pH = 2. The resulting mixture was concentrated under reduced pressure with a rotary evaporator until most THF was removed. The resulting mixture was poured to a 125-mL separatory funnel, and the product was extracted with Et_2O (30 mL × 3). The organic extracts were combined, dried over Na_2SO_4, filtered through cotton, and concentrated under reduced pressure. The oil was determined to be pure by ^1H NMR spectroscopy to give 1-dodecylcyclohexa-1,4-diene (730 mg, 72% yield) as a white solid.

Data for 3-(1,4-cyclohexadien-1-yl)propanoic acid: ^{1}H NMR (600 MHz, $CDCl_3$, 294K) δ 5.70 (br s, 2 H), 5.46 (br s, 1 H), 2.71–2.56 (m, 4 H), 2.55–2.42 (m, 2H), 2.30 (t, 2 H, J = 7.6 Hz); ^{13}C NMR (151 MHz, $CDCl_3$, 294K) δ 179.4, 133.0, 124.2, 123.8, 119.2, 32.1, 29.0, 26.7.

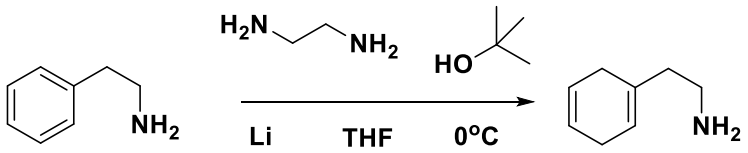

Reduction of benzylamine to 2-(1,4-cyclohexadien-1-yl)ethan-1- amine: A single-neck, 100-mL round-bottom flask was equipped with a magnetic stir bar and a septum equipped with a needle connected to a bubbler as a gas outlet. Phenethylamine (1.00 g, 8.21 mmol), THF (27 mL), ethylenediamine (3.29 mL, 49.3 mmol, 6.0 equiv), and t-BuOH (1.18 mL, 12.3 mmol, 1.5 equiv) were added to the flask, and the resulting solution was stirred while cooling to 0 °C. Lithium (171 mg, 24.6 mmol, 3.0 equiv) was added to the solution. The reaction mixture was stirred at 0 °C (external temperature) until TLC analysis showed the reaction to be complete (20 min). Saturated aqueous NH_4Cl (40 mL) was added to reaction mixture (CAUTION: Evolution of hydrogen gas), and the resulting mixture was stirred until the remaining lithium was quenched. The resulting mixture was concentrated under reduced pressure with a rotary evaporator and the water bath at 25 °C until most THF was removed. The resulting mixture was poured to a 125-mL separatory funnel, and the product was extracted with Et_2O (30 mL × 3). The organic extracts were combined, dried over Na2SO4, filtered through cotton, and concentrated under reduced pressure. The oil was determined to be pure by ^{1}H NMR spectroscopy to give 2-(1,4-cyclohexadien-1-yl)ethan-1-amine (815 mg, 80% yield) as a light yellow oil.

Data for 2-(1,4-cyclohexadien-1-yl)ethan-1-amine: Rf = 0.53 (10% MeOH in CH_2Cl_2, I_2); ^{1}H NMR (400 MHz, $CDCl_3$, 294K) δ 5.70 (app t, 2 H, *J* = 11.9 Hz), 5.48 (app s, 1 H), 2.77 (t, 2 H, *J* = 6.8), 2.74–2.66 (m, 2 H), 2.58 (app t, 2 H, *J* = 8.7 Hz), 2.11 (t, 2 H, *J* = 6.8 Hz), 1.28 (br s, 2H); ^{13}C NMR (100 MHz, $CDCl_3$, 294K) δ 132.4, 124.3, 124.2, 120.4, 41.6, 39.6, 28.7, 26.8.

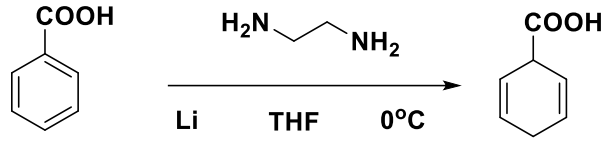

Reduction of benzoic acid to 1,4-dihydrobenzoic acid: A single-neck, 500-mL round-bottom flask was equipped with a magnetic stir bar and a septum equipped with a needle connected to a bubbler as a gas outlet. Benzoic acid (1.00 g, 8.2 mmol), THF (25 mL), and ethylenediamine (3.3 mL, 49.2 mmol, 6.0 equiv) were added to the flask, and the resulting mixture was cooled to 0 °C while stirring. Lithium (170 mg, 24.6 mmol, 3.0 equiv) was added to the solution. The reaction mixture was stirred at 0 °C (external temperature) until TLC analysis showed the reaction to be complete (25 min). Cold water (20 mL) was added to the reaction mixture (CAUTION: Evolution of hydrogen gas), and the resulting mixture was stirred until the remaining lithium was quenched. The resulting mixture was cooled with an ice bath and acidified with concentrated HCl until pH = 2. The mixture was concentrated under reduced pressure with a rotary evaporator until most THF was removed. The resulting mixture was poured to a 125-mL separatory funnel, and the product was extracted with Et_2O (30 mL × 3). The organic extracts were combined, dried over Na2SO4, filtered through cotton, and concentrated under reduced pressure to give 1,4-dihydrobenzoic acid as a pale-yellow oil (0.92 g, 91% yield).

Data for 1,4-dihydrobenzoic acid: ^{1}H NMR (600 MHz, $CDCl_3$, 294K) δ 5.75 (app t, 2 H, *J* = 11.9 Hz), 5.68 (app t, 2 H, *J* = 11.9 Hz), 3.65-3.60 (m, 1H), 2.60–2.49 (m, 2 H); ^{13}C NMR (150 MHz, $CDCl_3$, 294K) δ 178.8, 126.9, 121.5, 41.5, 25.8.

Reduction of 2-(cyclohexa-1,4-dien-1-yl)-N,N-dimethylethan-1-amine

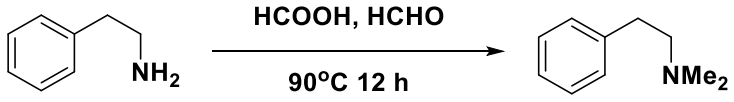

An oven dried 100 mL round-bottom flask was charged with formic acid (0.95 mL, 5.0 equiv.) and 2-phenylethan-1-amine (605.9 mg, 5 mmol) slowly. To this resulting clear solution, formaldehyde (37% solution) (1.23 mL, 3.0 equiv.) was added and placed in a preheated oil bath at 90 °C. A vigorous evolution of carbon dioxide was observed after 2–3 minutes, then the flask is removed from the bath until the gas evolution subsides (15–20

minutes), then it was again placed into the oil bath and heated at 90 °C for 12 hours. The reaction mixture was cooled to room temperature, 4(N) HCl (6.0 mL) is added and the solution is evaporated to dryness under reduced pressure. The syrupy residue was dissolved in water (10 mL), extracted with hexane (30 mL × 2). The aqueous part was basified with 18(N) aq. NaOH (20 mL) and extracted with DCM (50 mL × 2), washed with brine (50 mL) and dried over anhydrous Na_2SO_4. The organic extract was concentrated under reduced pressure and chromatographic separation with silica gel (DCM as eluent) gave 597.0 mg (80%) of *N,N-dimethyl-2-phenylethan-1-amine* as light yellow oil.

Data for N,N-dimethyl-2-phenylethan-1-amine: ^{1}H NMR (600 MHz, $CDCl_3$, 294K) δ 7.29-7.24 (m, 2 H), 7.19-7.15 (m, 3 H), 2.78-2.74 (m, 2H), 2.54-2.50 (m, 2H), 2.29 (s, 6 H).

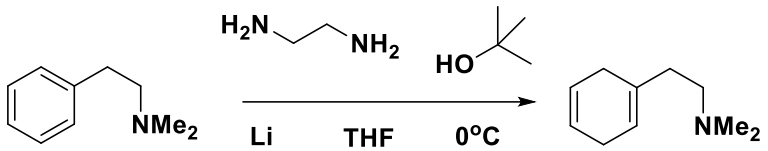

Reduction of benzylamine to 2-(1,4-cyclohexadien-1-yl)ethan-1- amine: A single-neck, 100-mL round-bottom flask was equipped with a magnetic stir bar and a septum equipped with a needle connected to a bubbler as a gas outlet. N,N-dimethyl-2-phenylethan-1-amine (0.2 g, 1.3 mmol), THF (5 mL), ethylenediamine (0.54 mL, 8.0 mmol, 6.0 equiv), and t-BuOH (0.19 mL, 2.0 mmol, 1.5 equiv) were added to the flask, and the resulting solution was stirred while cooling to 0 °C. Lithium (28 mg, 4.0 mmol, 3.0 equiv) was added to the solution. The reaction mixture was stirred at 0 °C (external temperature) until TLC analysis showed the reaction to be complete (25 min). Saturated aqueous NH_4Cl (40 mL) was added to reaction mixture (CAUTION: Evolution of hydrogen gas), and the resulting mixture was stirred until the remaining lithium was quenched. The resulting mixture was concentrated under reduced pressure with a rotary evaporator and the water bath at 25 °C until most THF was removed. The resulting mixture was poured to a 100-mL separatory funnel, and the product was extracted with Et_2O (15 mL × 3). The organic extracts were combined, dried over Na_2SO_4, filtered through cotton, and concentrated under reduced pressure. The oil was determined to be pure by ^{1}H NMR spectroscopy to give 2-(cyclohexa-1,4-dien-1-yl)-N,N-dimethylethan-1-amine (115 mg, 57% yield) as a light yellow oil.

Data for 2-(cyclohexa-1,4-dien-1-yl)-N,N-dimethylethan-1-amine: ^{1}H NMR (400 MHz, $CDCl_3$, 294K) δ, 5.68 (m, 2 H), 5.44 (m, 2 H), 2.68-2.65 (m, 2 H), 2.62–2.57 (m, 2 H), 2.38–2.31 (m, 2 H), 2.28 (s, 6 H), 2.22–2.14 (m, 2 H); ^{13}C NMR (100 MHz, $CDCl_3$, 294K) δ 133.2, 124.2, 119.3, 58.0, 45.4, 35.7, 29.1, 26.8.

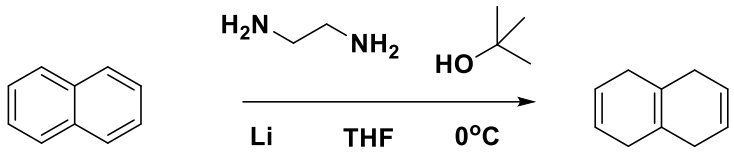

Reduction of naphthalene to 1,4,5,8-tetrahydronaphthalene: A single neck, 100-mL round-bottom flask was equipped with a magnetic stir bar and a septum equipped with a needle connected to a bubbler as a gas outlet. Naphthalene (1.00 g, 7.80 mmol), THF (26 mL), ethylenediamine (5.21 mL, 78.0 mmol, 10 equiv), and t-BuOH (2.24 mL, 23.4 mmol, 3.0 equiv) were added to the flask, and the resulting solution was stirred while cooling to 0 °C. Lithium (271 mg, 39.0 mol, 5.0 equiv) was added to the solution. The reaction mixture was stirred at 0 °C (external temperature) until TLC analysis showed the reaction to be complete (33 min). Saturated aqueous NH_4Cl (40 mL) was added to reaction mixture (CAUTION: Evolution of hydrogen gas), and the resulting solution was stirred until the remaining lithium was quenched. The resulting mixture was concentrated under reduced pressure with a rotary evaporator until most THF was removed. The resulting mixture was poured to a 125-mL separatory funnel, and the product was extracted with Et_2O (30 mL × 3). The organic extracts were combined, dried over Na_2SO_4, filtered through cotton, and concentrated under reduced pressure. The resulting residue was purified by flash column chromatography (SiO_2, 5 to 10% EtOAc in cyclohexane) to give 1,4,5,8-tetrahydronaphthalene (966 mg, 96% yield) as a colorless solid. Data for 1,4,5,8-tetrahydronaphthalene: 1H NMR (400 MHz, $CDCl_3$, 294K) δ 5.73 (s, 4 H), 2.54 (s, 8 H).

2.6.3 Procedures of Kinetic studies

2.6.3.1 Autoxidation kinetics in Chlorobenzene

Autoxidation experiments were performed by measuring the oxygen consumption in a two-channel gas uptake apparatus, immersed in a thermostatted bath, based on Validyne DP15 pressure transducer developed in our laboratory.[46]

All the autoxidation experiments were initiated by the thermal decomposition of AIBN at 30 °C, in chlorobenzene (PhCl). In a typical experiment, an air-saturated solution of the oxidizable substrate methyl linoleate (25%, 0.77 M) containing AIBN (0.05 M) in PhCl is equilibrated at 30 °C with an identical reference solution containing an excess of 2,2,5,7,8-pentamethyl-6-hydroxychromane (PMHC, 125 mM) so to block any radical chain in the reference during the experiment. After reaching a constant O_2 consumption, a stock solution of antioxidant (in PhCl) is injected in the sample flask. The rate of initiation Ri (3.2±0.3 x 10-9 $M^{-1}s^{-1}$) was measured in preliminary experiments from the length of the inhibition period (t) of PMHC, used as reference antioxidant, by equation 17, wherein 2 is the number of radicals trapped by each molecule of PMHC:

$$R_i = 2[PMHC]/t \quad (17)$$

2.6.3.2 Autoxidation kinetics in Chlorobenzene with Bases

Autoxidation experiments were performed by using the pervious procedures. Basically, the autoxidation experiments were initiated by the thermal decomposition of AIBN at 30 °C, in acetonitrile (MeCN). In a typical experiment, an air-saturated solution of the oxidizable substrate 1,4-cyclohexadiene (0.26 M) containing AIBN (0.025 M) in MeCN is equilibrated at 30 ◦C with an identical reference solution containing an excess of 2,2,5,7,8-pentamethyl-6-hydroxychromane (PMHC, 125 mM) so to block any radical chain in the reference during the experiment. After reaching a constant O_2 consumption, a stock solution of base in MeCN is injected in the sample flask. Final concentration 0.1 mM.

2.6.3.3 Autoxidation kinetics in water/THF

Purified THF (0.625 mL) was loaded into a 3 mL cuvette along with 1.8 mL of H_2O. The cuvette was placed into the thermostated sample holder of a Cary 3500 UV−vis

spectrophotometer and allowed to equilibrate to 37 °C. A small aliquot (12.5 μL) of a 2.0 mM solution of the STY-BODIPY probe in DMSO was added, followed by 50 μL of 0.05 M solution of AAPH in H_2O, and the solution was thoroughly mixed. The absorbance at 562 nm was monitored for 10−20 min to ensure that the reaction was proceeding at a constant rate, after which 10 μL of a certain quantity solution of the test antioxidant was added. The solution was thoroughly mixed, and the absorbance readings were resumed.

2.6.3.4 Autoxidation kinetics in micelles.

Micellar suspension of MeLH preparation. In a scintillation vial, 22 μL of methyl linoleate (MeLH) and 10 mL of 17.6 mM Triton X-100, were mixed by a vortex stirrer for 3 min. Next, 10 mL of phosphate buffer solution 0.1 M (pH 4.5 or pH 7.4) was added, and the mixture was stirred again for 3 min. The final concentration of MeLH and Triton X-100 in the micellar system was 3.3 mM for lipid and 8.8 mM for surfactant.[175]

Inhibited Co-autoxidation of MeLH in micellar system. A 3 mL quartz cuvette was loaded with 1.8 mL of micellar suspension of MeLH, 10 μL of 2 mM STY-BODIPY (λ=562 nm, ε=94000 $M^{-1}cm^{-1}$) in DMSO and 200 μL of 100 mM AAPH in phosphate buffer solution. The solution was thoroughly mixed. The cuvette was placed into the thermostatted sample holder of a UV−vis spectrophotometer and allowed to equilibrate to 37 °C. The absorbance at 562 nm was monitored for 10−20 min to ensure that the reaction was proceeding at a constant rate, after which a small aliquot (2 μL, 4 μL or 10 μL) of a 1 mM in DMSO solution of the test antioxidant was added.

2.6.3.5 Autoxidation of Egg-Yolk phosphatidylcholine liposomes

Egg-Yolk PC Liposomes Preparation. 150 μL of a solution 100 mg/mL in chloroform of egg yolk phosphatidylcholine was added in a round-bottom flask and the solvent was then evaporated under argon and the lipids were vacuum-dried 1h to yield a thin film. The lipid film was hydrated with 1 mL of a 10 mM phosphate buffered-saline (PBS) solution containing 150 mM NaCl (pH 7.4), yielding a 20 mM lipid suspension. The lipid suspension was then extruded 21 times using a mini extruder equipped with a

polycarbonate membrane with 100 nm pores.[175] The diameter was measured by Dynamic Light Scattering (DLS) at 37°C.

Inhibited Autoxidation of Egg-Yolk PC Liposomes. To a 1 mL graduated flask were added 250 μL of liposome suspension 20 mM in PBS, 30 μL of 100 mM AAPH in PBS solution and made up to the mark with PBS solution and mixed. Next, 600-1000 μL of the mixture was transferred to a vial and used to measure O_2 consumption during autoxidation using a Fire Sting O_2 optical oxygen meter (PyroScience GmbH) at 37 °C. The rate of O_2 consumption was monitored for 10-15 minutes until it was ensured that the reaction was proceeding at a constant rate, after which 10 μL of a 600 μM solution in DMSO of the test antioxidant was added.

2.6.3.6 Inhibited Autoxidation of Egg-PC Liposomes with INT on UV-vis

In a closed vessel with a total volume of 3 mL, 1 mL of a 5 mM liposome solution (prepared in 10 mM PBS buffer, pH 7.4; the liposome formation from egg phosphatidylcholine (PC) was described elsewhere) was combined with 12.5 μL of a 20 mM INT solution in DMSO (final concentration 250 μM). A blank and 22 μL of a 20 mM DTUN solution in ethanol (final concentration 0.4 mM) were also added, followed by an aliquot of terpinene stock solution in acetonitrile (final concentrations 100 μM and 1 mM). The mixture was thoroughly vortexed for 60 seconds. A small stir bar was placed in each sample, and all samples were incubated at 37 °C for 20 hours. Subsequently, each sample was transferred to a 1.5 mL cuvette, and the absorbance changes were recorded in the range of 700 nm to 400 nm. The standard reduction experiment of INT by superoxide was carried out by using the Xanthine/Xanthine oxidase method as previously described.[141]

2.6.3.7 The detection of aromatic component convention by HPLC

The formation of aromatic products was monitored by high-performance liquid chromatography (HPLC). A method was developed to achieve baseline separation between γ-terpinene (γ-T) and its potential aromatic derivative, p-cymene (Cym). Calibration curves

for both compounds were established using authentic standards, enabling quantitative analysis.

HPLC analyses were run on Agilent HPLC 1260, The LC system consists of a quaternary pump, autosampler, thermostated column compartment, and DAD detector. A volume of 5 µL of each sample was injected by the autosampler, chromatographic separation were conduct with Xbridge C18 100 mm * 3 mm, 3.5 µm. The mobile phases consisted of A: water, B: acetonitrile. The LC gradient was as follows: 0–30 min solvent A from 70%–10%; B from 30 % to 90 %; the flow was varied linearly 0.5 mL/min. The column was operating at a constant temperature of 40 °C.

In the experiment, γ-T (1 mM) and a-T (1 mM) was incubated in THF (3.1 M) with AAPH (1 mM) as a radical initiator in PBS buffer 7.4, and aliquots were collected at predetermined time intervals. These samples were analyzed by HPLC, allowing the concentration changes of γ-T and Cym to be followed over time.

2.6.3.8 Crystal Violet Proliferation assay

In order to evaluate the vitality of the cells after RSL3 treatment, a Crystal Violet assay according to reference [6] with few modifications, was performed. 2.5×103 HepG2 cells/wells were plated in 96-well plates in complete DMEM High Glucose media and allowed to adhere 24 h. The cells were then treated with γ-T, α-T, Cym, Myr, CHD-COOH, CHD-C12 in a range of concentration from 25 to 200 µM followed by 350 nM RSL3 for 4 hours. Ferrostatin-1 (500 nM) was used in the same conditions as a positive control. After 4 h cells were washed 2 times with 1× PBS, fixed in 3.7% paraformaldehyde for 20 min at room temperature (RT). Then cells were stained with 1 mg/ml of crystal violet solution (Sigma Aldrich) in deionized water for 10 min. The plate was then washed 5 times with tap water and air-dried at RT for at least 24 h. Then 200 µL of 100% of methanol was added to each well and gently shaken on the rotator for 20 min to dissolve the crystal violet. The absorbance of each well was measured at a wavelength of 570 nm with a plate reader (Perkin Elmer, Victor Nivo).

2.6.3.9 Live Cell proliferation assay

Cell proliferation across the different treatment conditions was monitored in real time for 42 hours using the IncuCyte® Live-Cell Analysis System (Sartorius, Göttingen, Germany) to continuously monitor and quantify cell proliferation, capturing images and calculating cell confluence at regular intervals (1 hours).

Live cell proliferation assay was assessed as described by Diquiguiovanni et al.[7] 2.5×103 HepG2 cells/wells were plated in 96-well plates in complete DMEM High Glucose media and allowed to adhere 24 h. The cells were then treated with 100 μM of γ-T, α-T, Cym, Myr, CHD-COOH, CHD-C12 or 500 nM Ferrostatin-1 and 350 nM of RSL3. Real-time proliferation was assessed for 42 hours using the IncuCyte® S3 Live Cell Analysis System (Roche Applied Sciences, Indianapolis, IN, USA). Data were analyzed by Graph Pad Prizm.

Cell proliferation across the different treatment conditions was monitored in real time for 96 hours using the IncuCyte® Live-Cell Analysis System (Sartorius, Göttingen, Germany) to continuously monitor and quantify cell proliferation, capturing images and calculating cell confluence at regular intervals (6/8 hours). Data were collected using the IncuCyte 2022B Rev2 GUI software, and post-acquisition analysis of proliferation data was conducted using GraphPad Prism v8.0 (GraphPad Software Inc., CA, USA).

2.6.3.10 Lipid peroxidation assay

The determination of lipid peroxidation induced by RSL3 treatment in HepG2 cells was performed using the lipid peroxidation sensor dye STY-BODIPY® according to the method described by Pratt et al.[8] Cells were seeded onto an 8-well chambered coverslip (μ-Slide 8 Well, (Ibidi, Germany) according to the manufacturer's instructions and incubated overnight to allow adhesion. The cells were then treated with 100 μM of γ-T, α-T, Cym, Myr, CHD-COOH, CHD-C12 D or 500 nM Ferrostatin-1. The cells were co-incubated with 1 μM STY-BODIPY and exposed to 1 μM of RSL3 dissolved in complete medium for 1 h. After this time, the cells were washed with HBSS and images were captured using a Nikon C1si confocal microscope (Nikon, Tokyo, Japan). Green and red fluorescence intensities were quantified using standard ImageJ software tools (NIH)

2.6.3.11 Theoretical calculations

Calculations were carried out by using gas phase enthalpy corrected energies using the CBS-QB3 complete basis set method[176] as implemented in the Gaussian 16 suite of programs.[177]

2.7 Appendix

2.7.1 Analysis of the results by the co-oxidation model

The oxidation of methyl linoleate or THF in the presence of terpenes can be described by the reactions 1-7, where RH is the main oxidizable substrate and EH is the terpene. The radical EOO• can represent either an alkylperoxyl or HOO• depending on the nature of EH. At the steady state, the rate of peroxidation (Rox) is given by equation 2.

Equation 2:[155]

$$Rox = \frac{\{k_2k_4[RH]^2 + 2k_1k_4[RH][EH] + k_1k_3[EH]^2\}R_i^{1/2}}{\{k_5k_4^2[RH]^2 + k_7k_1k_4[RH][EH] + k_6k_1^2[EH]^2\}^{1/2}}$$

The rate of initiation by the azoinitiators (R_i) is known, being measured under each condition by using a reference antioxidant (see Experimental Section). As we used well characterized oxidizable substrates, the rate constants describing the RH autoxidation (k_2 and k_5) are known from the literature (see the footer of Table 1), while the remaining rate constants k_1, k_3, k_4, k_6 and k_7 were fitted to the experimental data or taken from literature when possible. As shown by the lines in the result parts, the co-oxidation model was successful in describing the behavior of all terpenes under all experimental settings, despite the different experimental approaches used to measure the oxidation rates.

The nonlinear numeric fitting was performed by using the software LabPlot Version 2.11.1 freely available at https://labplot.org. The results of the fitting procedure to obtain the values reported in Table 2.2 are reported below.

2.7.1.1 Methyl linoleate gamma-terpinene in Chlorobenzene

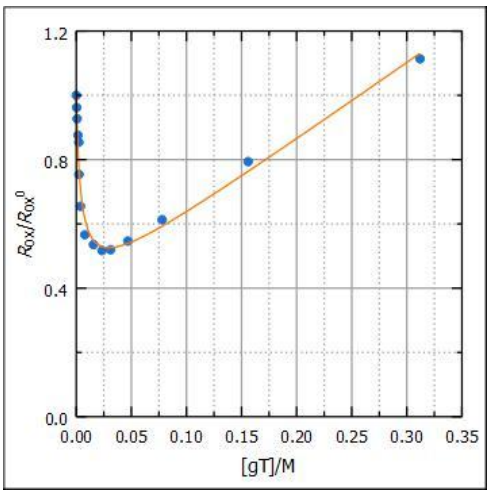

Rate constant	$M^{-1}s^{-1}$	Error $M^{-1}s^{-1}$	Error %
K4	61	Lit	
K7	127	11	9%
K5	968	205	21%
K6	1118	98	9%
K8	1e7	Lit	
K9	4e8	NA	
K10	1e9	NA	

[MeLH]=0.73 M; R_i=3e-9 Ms^{-1};
Coefficient of determination (R^2) 0.969609

2.7.1.2 THF, water pH 7.4, gamma-terpinene BODIPY

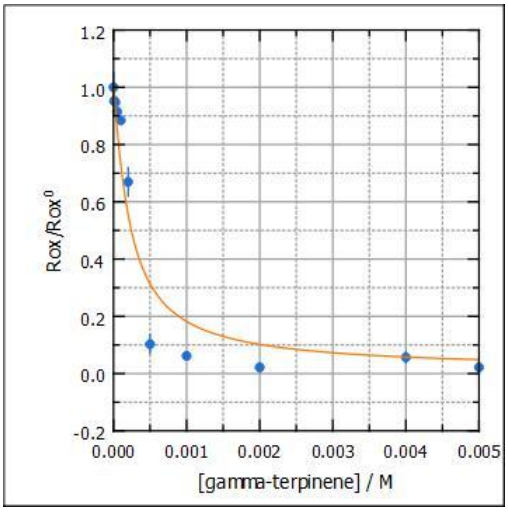

[THF] = 3.1 M; R_i=2.6e-9
Coefficient of determination (R^2) 0.946412

Rate constant	$M^{-1}s^{-1}$	Error $M^{-1}s^{-1}$	Error %
K4	4.1	Lit	
K7	3.2e-3	1e-3	30%
K5	750	NA	
K6	5.5	NA	
K8	6e7	Lit	
K9	1e7	NA	
K10	5e5	Lit	

2.7.1.3 THF, water pH 4.5, gamma-terpinene BODIPY

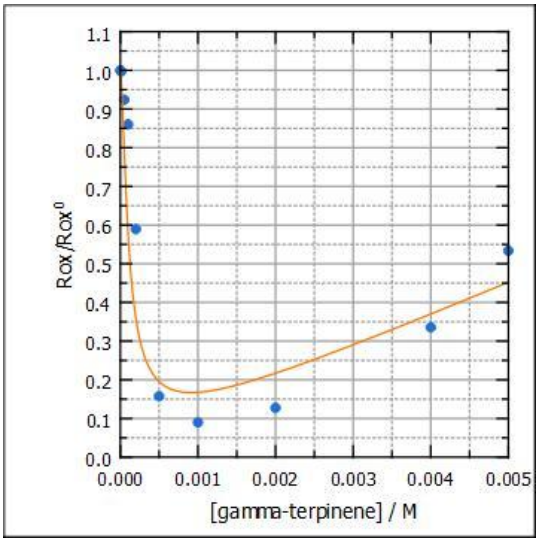

Rate constant	$M^{-1}s^{-1}$	Error $M^{-1}s^{-1}$	Error %
K4	4.1	Lit	
K7	0.013	0.003	52
K5	810	NA	
K6	770	130	20
K8	6e7	Lit	
K9	1e7	NA	
K10	3e7	lit	

[THF] = 3.1 M; R_i=2.6e-9
Coefficient of determination (R^2) 0.860

2.7.1.4 Methyl linoleate gamma-terpinene micelles pH 7.4

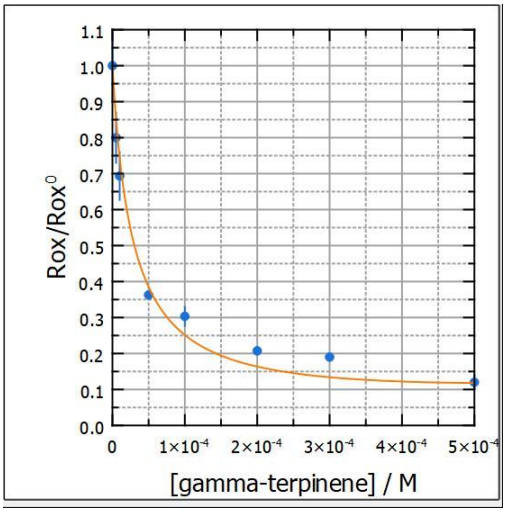

Rate constant	$M^{-1}s^{-1}$	Error $M^{-1}s^{-1}$	Error %
K4	36	Lit	
K7	15	na	
K5	1017	Na	
K6	0.13	na	
K8	1200	Lit	
K9	5.0e3	NA	
K10	3.0e4	NA	

[MeLH]=0.003 M; R_i=3e-9 Ms^{-1};
Coefficient of determination (R^2) 0.986

2.7.1.5 Methyl linoleate gamma-terpinene micelles pH 4.5

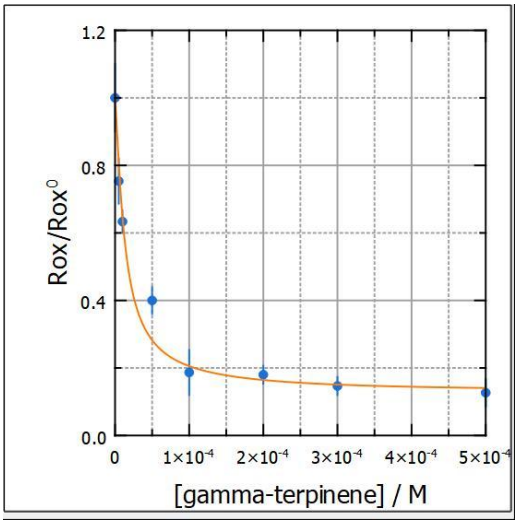

Rate constant	$M^{-1}s^{-1}$	Error $M^{-1}s^{-1}$	Error %
K4	36	Lit	
K7	15	na	
K5	930	Na	
K6	0.10	na	
K8	1200	Lit	
K9	5.4e3	NA	
K10	4.9e4	NA	

[MeLH]=0.003 M; Ri=3e-9 Ms-1;
Coefficient of determination (R^2) 0.915

2.7.2 Additional Schemes and Figures

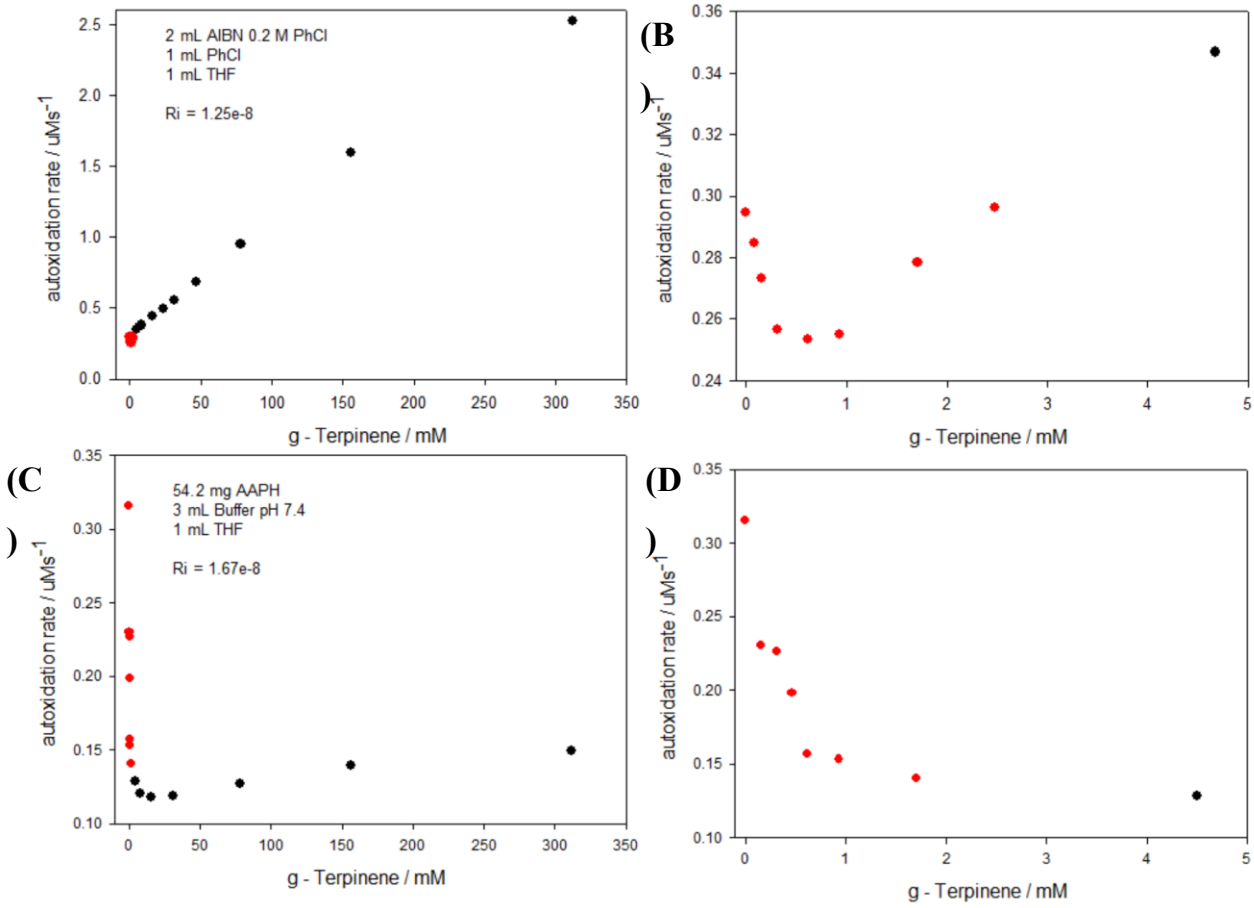

Figure A 2.1. *O_2 consumption rate measured by differential pressure oximetry during the autoxidation of THF in chlorobenzene at 30°C (A-B) or in buffered water (B-C)with increasing amounts of gamma-terpinene. Plot B and D represent an enlarged view of plots A and C, respectively, in the low millimolar range.*

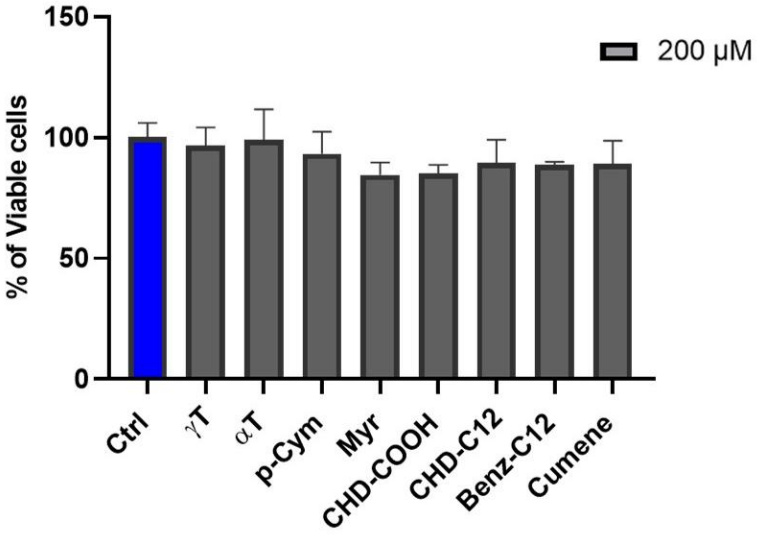

Figure A 2.2*. Evaluation of viability in HepG2 cells treated with natural terpenoids and their oxidized derivatives. HepG2 cells were incubated for 24 hours with 200 µM of γ-T, α-T, Cym, Myr, CHD-COOH, CHD-C12, Benz-C12, or Cumene. Cell viability was assessed using the Crystal Violet assay. None of the tested compounds or their oxidized derivatives showed toxicity at the concentration of 200 µM.*

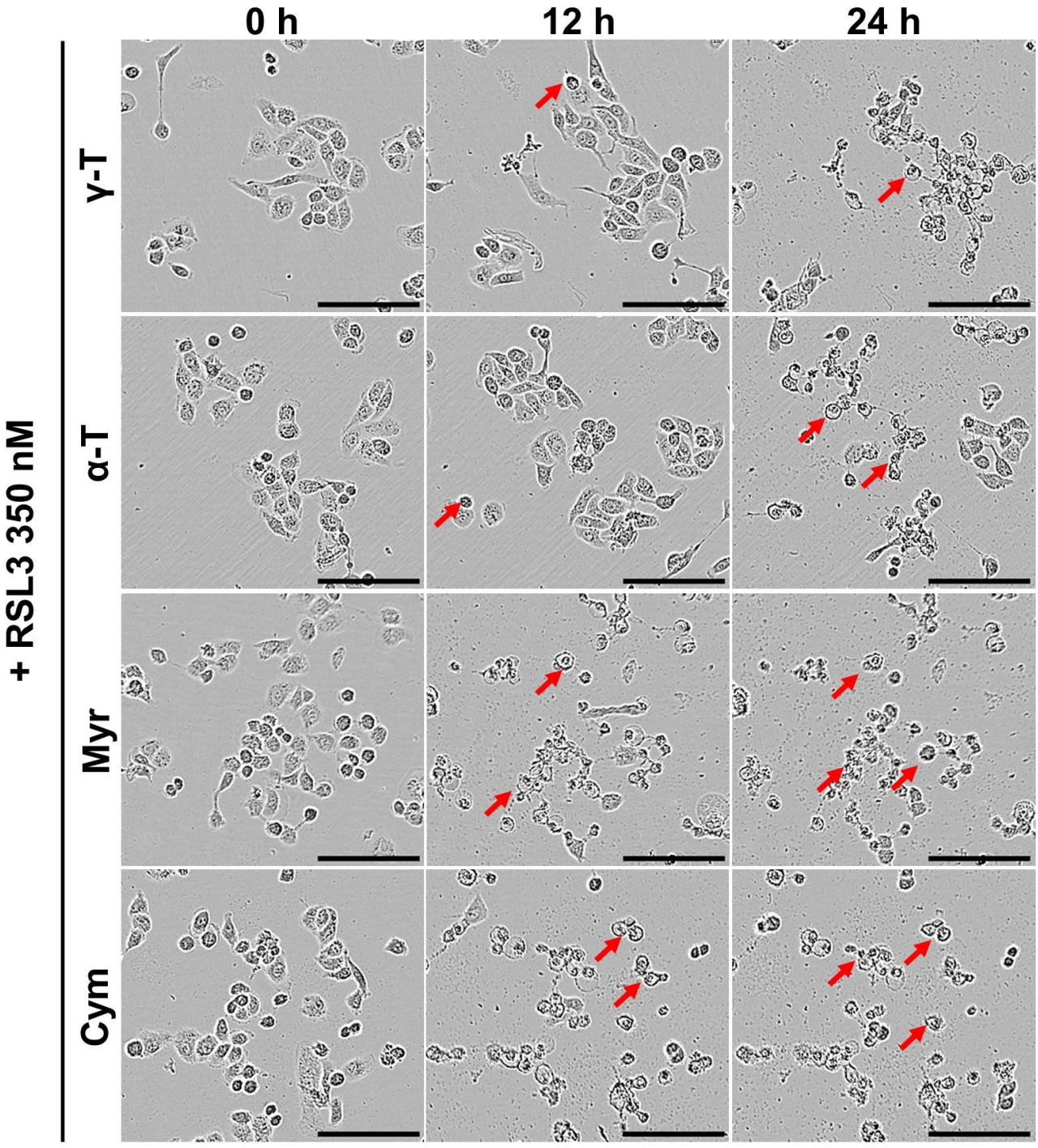
0 h
12 h
24 h
γ-T
α-T
Myr
Cym
+ RSL3 350 nM

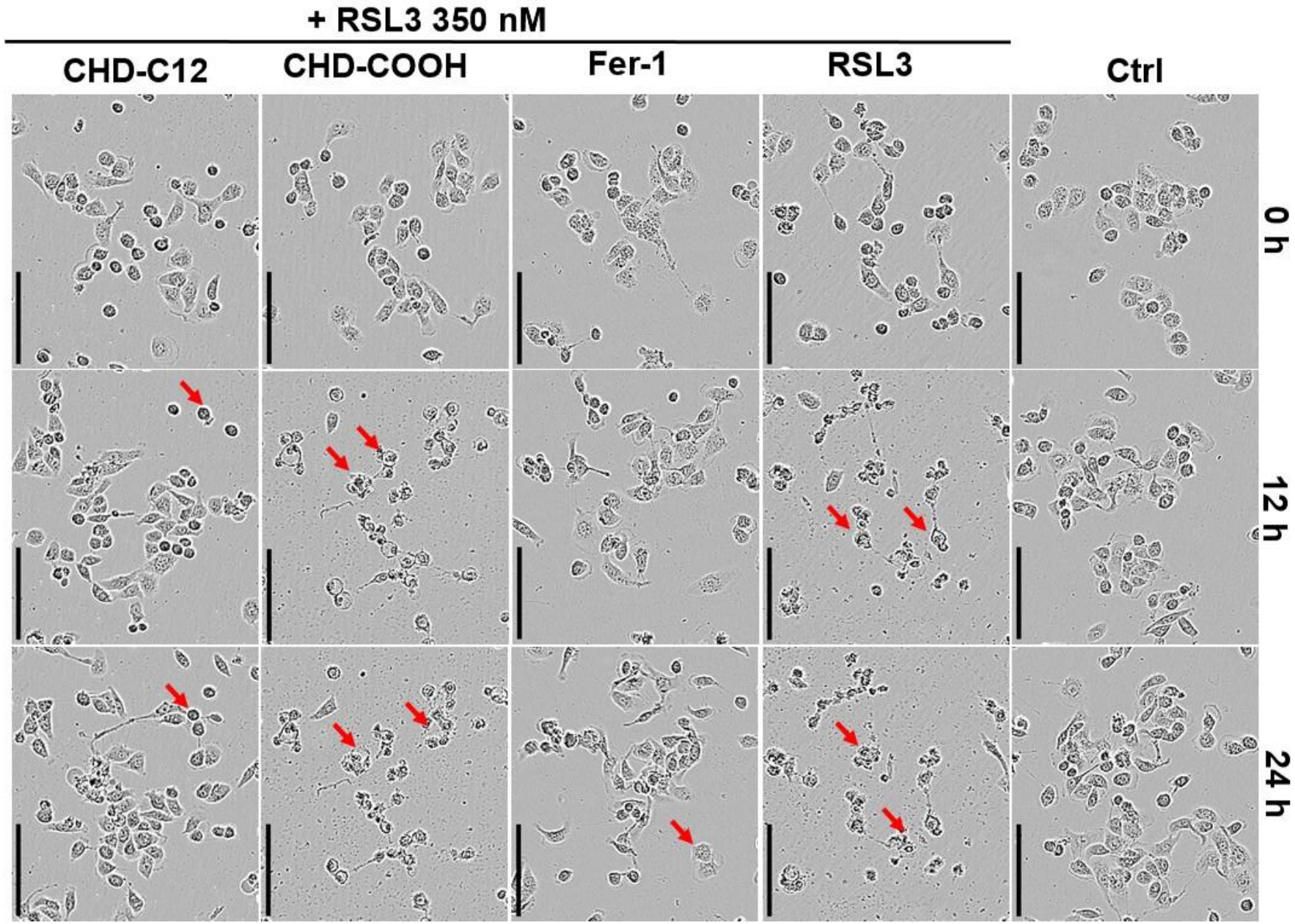
+ RSL3 350 nM
CHD-C12
CHD-COOH
Fer-1
RSL3
Ctrl
0 h
12 h
24 h

Figure A 2.3. *Representative images from cell proliferation analysis using the IncuCyte Live-Cell Assay. HepG2 cells were treated with 100 µM of γ-T, α-T, Cym, Myr, CHD-COOH, and CHD-C12, in the presence of 350 nM RSL3. Images were captured at 0h, 12h, and 24h. Fer-1 (500 nM) served as the positive control. Red arrows indicate cells exhibiting morphological impairment due to lipid peroxidation of the membranes. Scale bar = 300 µm.*

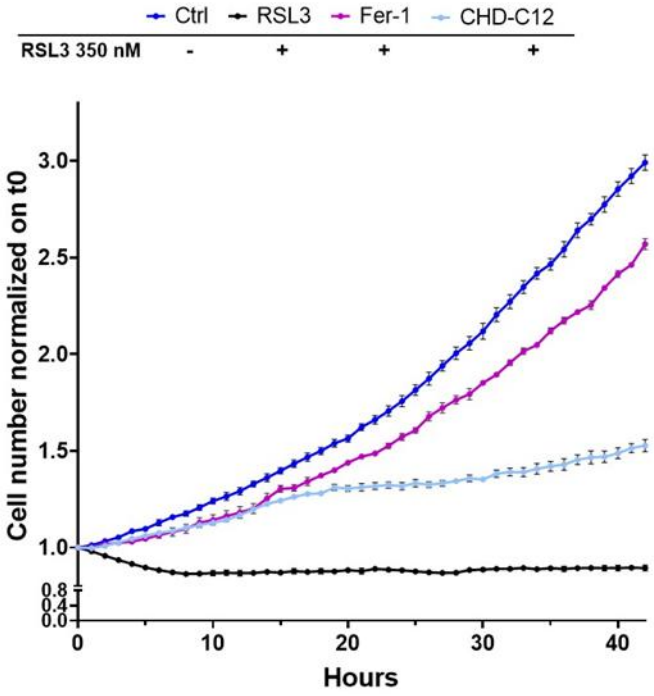

Figure A 2.4. *Cell proliferation analyzed using the IncuCyte Live-Cell Assay for 42 hours. Cells were treated with 100 µM CHD-C12 or Ferrostatin 1 (Fer-1) in the presence of 350 nM RSL3. Data are mean ± SEM (n = 4 independent experiments).*

2.7.3 DFT Calculation

Thermochemical method: CBS-QB3

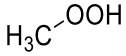

CBS-QB3 Enthalpy= -190.589781 CBS-QB3 Free Energy= -190.619411

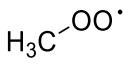

CBS-QB3 Enthalpy= -189.954722 CBS-QB3 Free Energy= -189.985248

CBS-QB3 Enthalpy= -114.870540 CBS-QB3 Free Energy= -114.897465

CBS-QB3 Enthalpy= -150.161249 CBS-QB3 Free Energy= -150.184522

CBS-QB3 Enthalpy= -150.737293 CBS-QB3 Free Energy= -150.763274

CBS-QB3 Enthalpy= -0.497457 CBS-QB3 Free Energy= -0.510472

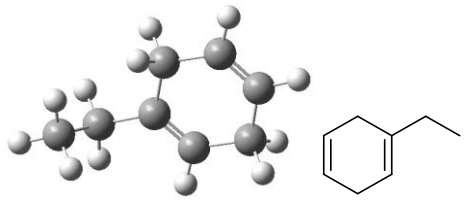

CBS-QB3 Enthalpy= -311.388418 CBS-QB3 Free Energy= -311.430464

```
0 1
C 2.32583200 0.23507000 0.18918500
C 1.54927500 1.30186000 0.01105100
C 1.80214500 -1.17342700 0.16983300
C 0.32201400 -1.24908800 -0.08902900
C -0.47549700 -0.19133000 -0.26414400
C 0.06570100 1.22078500 -0.22379600
H 2.34246900 -1.75927400 -0.58876400
H -0.10878600 -2.24704900 -0.13792000
H -0.18912200 1.73178100 -1.16528700
H 1.98679800 2.29648700 0.03508300
H 3.39140200 0.36539500 0.35764500
H -0.45617300 1.80033500 0.55108600
H 2.04099100 -1.67135700 1.12173900
C -1.95644800 -0.34538300 -0.52548700
H -2.17720300 -1.40163800 -0.70728100
H -2.21466400 0.19000700 -1.44916200
C -2.85687900 0.16882200 0.61183500
H -3.91142200 0.00840700 0.37057800
H -2.64023400 -0.35583200 1.54652200
H -2.72091400 1.23888300 0.78907300
```

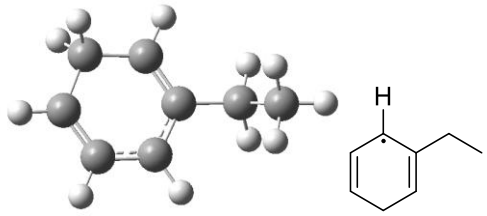

CBS-QB3 Enthalpy= -310.771975 CBS-QB3 Free Energy= -310.814107

```
0 2
C -2.31211600 -0.25430800 0.20709700
C -1.49687700 -1.33046200 0.01040600
C -1.78269200 1.14730200 0.16418500
C -0.31032200 1.22532400 -0.11565600
C 0.47413800 0.12260800 -0.30192300
C -0.11291700 -1.17606800 -0.24256100
H -2.34009000 1.73766900 -0.58511400
H 0.13352500 2.21538300 -0.16916200
H -1.91554400 -2.33157400 0.04470000
H -3.37074500 -0.39388700 0.39862100
H 0.50516800 -2.05233100 -0.40250700
H -2.01228600 1.66520100 1.11319500
C 1.96229700 0.25163500 -0.55368100
H 2.19166500 1.28414600 -0.83360600
H 2.23657500 -0.37186000 -1.41259600
C 2.82070500 -0.15149600 0.65675400
H 3.88609100 -0.05345000 0.42917800
H 2.59772900 0.48177700 1.51982200
H 2.63461100 -1.18828300 0.94974500
```

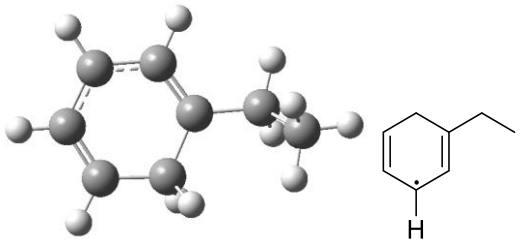

CBS-QB3 Enthalpy= -310.773215 CBS-QB3 Free Energy= -310.815471

```
0 2
C -2.35355400 -0.10184100 0.20955100
C -1.62253400 -1.23741600 0.02523000
C -1.74416300 1.17656300 0.16258500
C -0.35267600 1.28297000 -0.07972000
C 0.44744800 0.18915100 -0.26966800
C -0.14502800 -1.19806100 -0.23374900
H 0.09506500 2.27241100 -0.12022500
H 0.08522600 -1.71553400 -1.18396400
H -2.10114700 -2.21053200 0.06185500
H -3.42066700 -0.17412700 0.39411300
H 0.37860000 -1.81265400 0.51929000
H -2.33881000 2.07004400 0.30743200
C 1.92496100 0.31267400 -0.52997300
H 2.16579000 1.36009700 -0.73640500
H 2.18001800 -0.25070700 -1.43853600
C 2.81543400 -0.18958400 0.62360300
H 3.87302800 -0.06580800 0.37457700
H 2.61508600 0.36946700 1.54153400
H 2.64848300 -1.24939600 0.83318000
```

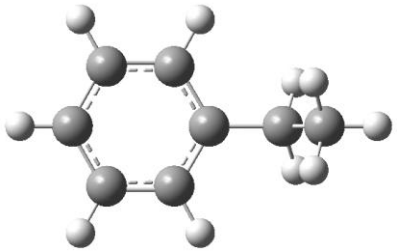

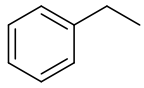

CBS-QB3 Enthalpy= -310.238028 CBS-QB3 Free Energy= -310.278465

```
0 1
C -2.32423400 0.00012800 0.23787400
C -1.63624900 -1.20385800 0.09596000
C -1.63603200 1.20400900 0.09580100
C -0.27065300 1.20074000 -0.18408600
C 0.43398300 -0.00013600 -0.32638400
C -0.27082900 -1.20085000 -0.18392100
H 0.25510500 2.14388200 -0.29885800
H -2.16354500 -2.14613700 0.19812400
H -3.38703300 0.00026500 0.45221900
C 1.92386900 -0.00024700 -0.59122800
H 2.18555900 0.87670800 -1.19209800
H 2.18554800 -0.87761900 -1.19147900
C 2.76397000 0.00018200 0.69808000
H 3.83316400 0.00029000 0.46716700
H 2.54824700 0.88282400 1.30631700
H 2.54849300 -0.88225100 1.30670800
H 0.25472500 -2.14412200 -0.29853400
H -2.16322200 2.14635900 0.19785300
```

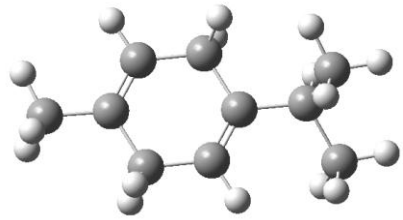

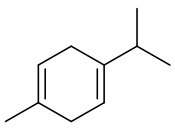

Gamma-terpinene

CBS-QB3 Enthalpy= -389.845652 CBS-QB3 Free Energy= -389.894526

```
0 1
C -2.22960800 0.01210100 0.02066300
C -1.61590500 1.15465900 -0.29288400
C -1.44411600 -1.25130700 0.26796100
C 0.04596500 -1.09442900 0.13330700
C 0.66512300 0.04923700 -0.16986400
C -0.12740800 1.31150100 -0.42998500
H -1.68605200 -1.63913000 1.26995500
H 0.62802900 -1.99566500 0.30041700
H 0.21555500 2.11333400 0.23958100
H -2.21265000 2.04769100 -0.46662300
H 0.11230200 1.68005900 -1.43980500
H -1.79654300 -2.03734600 -0.41822100
C 2.17755900 0.18945500 -0.28128400
H 2.36621900 0.81656100 -1.16448100
C 2.92677100 -1.13187800 -0.49497300
H 3.98930200 -0.93791500 -0.66677700
```

H 2.85395000 -1.78331700 0.38116300
H 2.53831000 -1.67932700 -1.35745900
C 2.76081700 0.93785700 0.93673300
H 3.83326700 1.11074800 0.80577700
H 2.28601200 1.90980600 1.08971700
H 2.62077600 0.34871500 1.84815300
C -3.72479500 -0.09968000 0.14802500
H -4.01059100 -0.43331000 1.15281400
H -4.21860200 0.85477000 -0.04654500
H -4.12570400 -0.84076900 -0.55385800

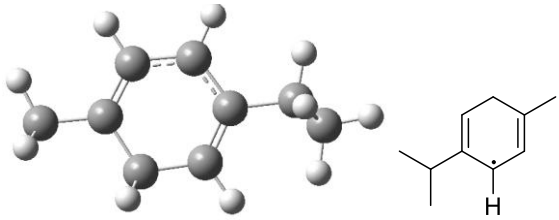

CBS-QB3 Enthalpy= -389.229067 CBS-QB3 Free Energy= -389.279390

0 2
C 1.59327800 1.22662100 0.00010000
C 0.18213300 1.35195300 0.00011500
C -0.65557700 0.20597200 0.00004300
C -0.08074100 -1.03625300 -0.00004900
C 1.40372800 -1.24988800 -0.00009100
C 2.22005000 0.01440400 0.00000800
C -2.17122200 0.38728000 0.00005400
C -2.82216700 -0.18963200 -1.26926600
C 3.71145200 -0.13394000 -0.00002600
C -2.82221500 -0.19000800 1.26917600
H -0.26536700 2.33944400 0.00019100
H -0.70184800 -1.92663900 -0.00010100
H 1.69538500 -1.87397800 -0.86575600
H 1.69541400 -1.87414300 0.86544200
H 2.19559200 2.13107500 0.00016700
H 4.05571500 -0.69509200 -0.87855800
H 4.21407200 0.83545000 0.00013600
H 4.05572800 -0.69539800 0.87830300
H -2.35942200 1.46703500 0.00021200
H -3.89670500 0.01715200 1.28187100
H -2.69107700 -1.27471600 1.32247200
H -2.38110500 0.24345200 2.17032500
H -3.89665800 0.01752100 -1.28193900
H -2.38102700 0.24410100 -2.17026900
H -2.69101100 -1.27432300 -1.32287900

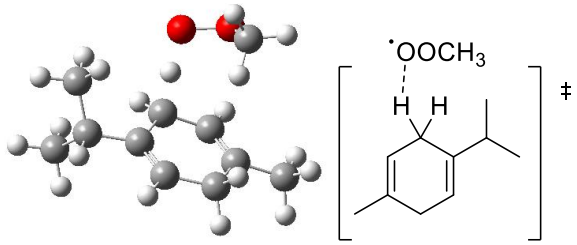

CBS-QB3 Enthalpy= -579.794272 CBS-QB3 Free Energy= -579.856113

0 2
C 1.02009600 -0.67630100 -1.12961600
C 1.65250900 -1.45321700 -0.23025300
C 0.97751900 -1.81945500 1.06536500

C -0.46200500 -1.40473500 1.15619900
C -1.07924200 -0.63385800 0.24412400
C -0.31133900 -0.10325700 -0.90470000
C 3.03380400 -1.99779900 -0.45425600
C -2.55277300 -0.28343900 0.37493700
C -3.39730400 -0.95911100 -0.72257300
C -2.79646400 1.23634900 0.39936400
O 0.24434300 2.38470100 -0.48468100
O 1.62700400 2.39790900 -0.40652600
C 2.01855200 2.36519600 0.96657700
H -0.08140500 1.12283000 -0.66880000
H 1.52313200 -0.41682400 -2.05631500
H 1.06361000 -2.90474900 1.23101400
H -1.02179400 -1.77292000 2.01223500
H 3.71643600 -1.67994100 0.34341300
H 3.44843200 -1.66445300 -1.40728600
H 3.03290900 -3.09433000 -0.44468000
H 1.54785400 -1.38219800 1.90454100
H -2.88613900 -0.68844900 1.33736200
H -2.21188000 1.72072400 1.18431200
H -2.52134500 1.70488700 -0.54959200
H -3.85487600 1.44676900 0.57874000
H -3.13875500 -0.58477000 -1.71742700
H -3.25235200 -2.04242000 -0.72186600
H -4.46072200 -0.75792200 -0.56343000
H -0.89271600 0.03252700 -1.82019300
H 3.10862500 2.42415600 0.95844200
H 1.59618100 3.22049900 1.50015500
H 1.69391100 1.43347000 1.43803200

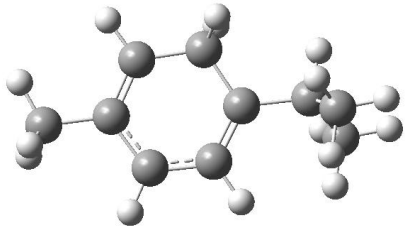

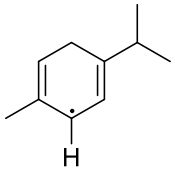

CBS-QB3 Enthalpy= -389.227877 CBS-QB3 Free Energy= -389.277435

0 2
C -2.23523800 -0.07438500 0.01244000
C -1.67297500 1.17495000 -0.15250800
C -1.37893100 -1.21423400 0.14177200
C 0.02989200 -1.06914300 0.09695100
C 0.64754000 0.15683100 -0.06755700
C -0.18997400 1.40259800 -0.19871800
H 0.63774500 -1.96479400 0.19614900
H 0.10347000 2.12411800 0.58727300
H -2.31210000 2.04782900 -0.25477900
H 0.08194900 1.92893400 -1.13243000
H -1.81369700 -2.19950000 0.27209500
C 2.15699100 0.33028400 -0.09066900
H 2.35526100 1.37412400 -0.36445700
C 2.84353100 -0.55490900 -1.14682600
H 3.91789800 -0.34965400 -1.18168800
H 2.71674900 -1.61713800 -0.91905300
H 2.42997700 -0.37611100 -2.14273900
C 2.77474800 0.10313300 1.30440800
H 3.84955800 0.31018900 1.29212600

H 2.31330700 0.75194600 2.05382200
H 2.63382500 -0.93209300 1.62862700
C -3.73284700 -0.27258300 0.05883100
H -4.04165900 -0.71190000 1.01309800
H -4.26456600 0.67287300 -0.06531300
H -4.06413800 -0.95406700 -0.73148300

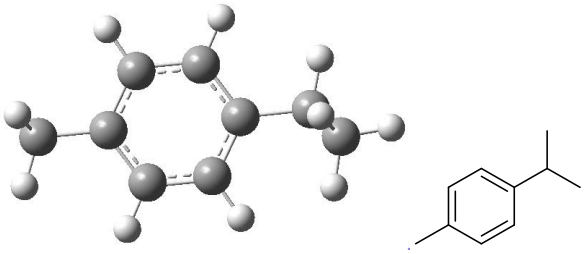

CBS-QB3 Enthalpy= -388.694364 CBS-QB3 Free Energy= -388.740209

0 1
C -2.20555400 -0.07006500 0.00004200
C -1.60525900 1.19305000 -0.00131400
C -1.36429800 -1.18645000 0.00102500
C 0.02241900 -1.04779000 0.00068000
C 0.62425900 0.21484200 -0.00066200
C -0.21922600 1.33082600 -0.00165600
H 0.63799900 -1.94149400 0.00146100
H -2.22868700 2.08236800 -0.00214100
C 2.13716000 0.38156100 -0.00070100
H 2.33643400 1.45946900 -0.00274300
C 2.78202500 -0.20761400 -1.26849900
H 3.85974800 -0.01795400 -1.27706700
H 2.63485300 -1.29050100 -1.32204900
H 2.35122500 0.23215800 -2.17164300
C 2.78109700 -0.20268900 1.26991000
H 3.85886200 -0.01326300 1.27846800
H 2.34976100 0.24075400 2.17099500
H 2.63353700 -1.28532000 1.32758300
C -3.70871500 -0.21552800 0.00050100
H -4.15379500 0.25772700 0.88140800
H -4.15427100 0.25697900 -0.88056200
H -4.00591400 -1.26628800 0.00103700
H 0.21596600 2.32575900 -0.00276800
H -1.79915900 -2.18124700 0.00206000

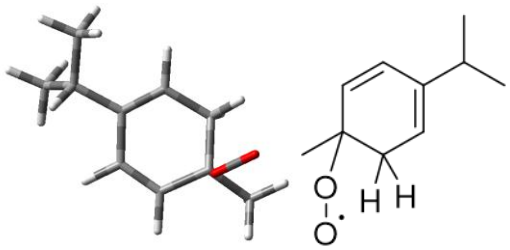

CBS-QB3 Enthalpy= -539.412830 CBS-QB3 Free Energy= -539.465929

0 2
C 2.34290300 -0.14724700 0.19891700
C 1.69602900 -0.84171400 -0.91899200
C 0.37250300 -0.81091500 -1.12386100
C -0.54076200 -0.01265000 -0.24335200

C 0.06747000 0.33043400 1.11211300
C 1.56732500 0.40620800 1.14210800
C -1.97142100 -0.60476900 -0.19042700
C -2.97005400 0.24480600 0.60750500
O -0.68341400 1.29266100 -1.07834000
O -0.95637400 2.37296700 -0.39632400
C 3.84760000 -0.10301200 0.23261600
C -1.96617200 -2.05524000 0.32180400
H -0.06856100 -1.31156500 -1.97923700
H -0.36426900 1.28280400 1.43125200
H 2.01630700 0.90662300 1.99496300
H 2.32999700 -1.39384100 -1.60729600
H 4.27157300 -1.11336900 0.23993100
H 4.24668900 0.40422300 -0.65242800
H 4.21084600 0.42389000 1.11666900
H -2.30598100 -0.62267600 -1.23530800
H -3.97296500 -0.17923800 0.50767600

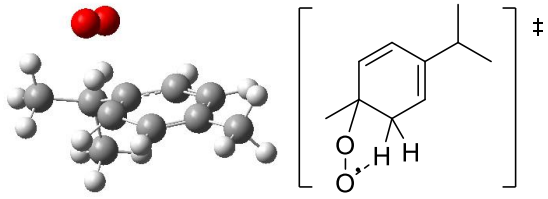

CBS-QB3 Enthalpy= -539.395929 CBS-QB3 Free Energy= -539.449326

0 2
C 0.08797700 0.29908500 1.04225300
C 1.54787200 0.17120700 1.18166600
C 2.34090400 -0.24447600 0.16174300
C 1.70467100 -0.66601500 -1.05648300
C 0.34478700 -0.69063800 -1.20064300
C -0.52531500 -0.24184900 -0.17150500
C 3.84401300 -0.30194700 0.26841800
C -1.97856200 -0.68353500 -0.20455400
C -2.92485800 0.13186900 0.68676600
C -2.06810700 -2.18488200 0.15346500
O -0.94825800 1.77167600 -1.03889700
O -0.61160000 2.56887300 -0.11965900
H -0.09213300 -1.06890600 -2.11936300
H -0.11014300 1.45963900 0.89542000
H 1.98878400 0.48346500 2.12339200
H 2.33071300 -1.00747000 -1.87546800
H 4.21753800 -1.31151800 0.06877500
H 4.31558200 0.36630800 -0.45949000
H 4.18314700 -0.00650600 1.26291500
H -2.31297600 -0.56978800 -1.24214400
H -3.95331800 -0.20656600 0.53640700
H -2.69616000 0.00074100 1.74883700
H -2.88069300 1.19553600 0.45493400
H -3.10286100 -2.53012600 0.07397000
H -1.45308100 -2.79666300 -0.51025600
H -1.73294300 -2.36271100 1.17997700
H -0.46289500 0.09725900 1.96379300

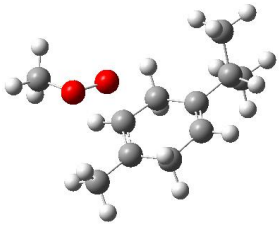

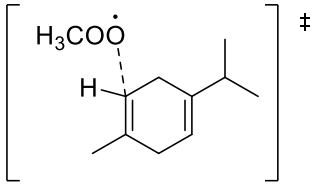

CBS-QB3 Enthalpy= -579.789404 CBS-QB3 Free Energy= -579.850239

```
0 2
C 1.10416500 1.41555900 -0.82022200
C 1.52560000 0.37818000 -0.09568500
C 0.61974500 -0.28273400 0.91829200
C -0.81880700 0.16629700 0.85654100
C -1.17915100 1.37152600 0.26201200
C -0.26834900 2.02059700 -0.73529400
C 2.93052500 -0.17870900 -0.26221900
C 3.74201100 -0.13187600 1.04601000
C -2.56607400 1.91357400 0.39323400
C 2.92370400 -1.60247300 -0.85165900
O -1.37448900 -1.13849300 -0.40796400
O -2.74273000 -1.08841900 -0.68752200
C -3.43106100 -1.95725600 0.20517600
H 0.99921200 -0.09425900 1.93238000
H -1.44165900 -0.18212000 1.67493300
H -0.74786300 1.98454800 -1.72818300
H 1.78165200 1.86874200 -1.54032200
H -2.57595900 3.00841400 0.37525300
H -3.05123900 1.57635100 1.31220800
H -3.18302900 1.56507200 -0.44705400
H -0.19153200 3.09633900 -0.51157200
H 3.43761900 0.47032400 -0.98527400
H 3.76467100 0.87911600 1.46191500
H 3.32427400 -0.80088200 1.80436600
H 4.77418000 -0.44679400 0.86688800
H 2.48385500 -2.32535000 -0.15855600
H 2.35132200 -1.63970900 -1.78142800
H 3.94525200 -1.93199000 -1.06373800
H 0.64162400 -1.37128500 0.79611000
H -4.47688400 -1.92977100 -0.10888400
H -3.04257000 -2.97636800 0.12609900
H -3.34900700 -1.61118300 1.24163100
```

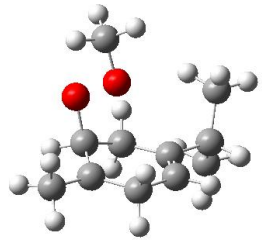

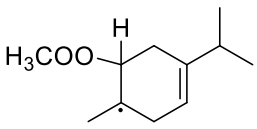

CBS-QB3 Enthalpy= -579.808495 CBS-QB3 Free Energy= -579.869823

```
0 2
C 0.51662000 -0.28412200 -1.10755200
C -1.01748700 -0.32796400 -1.07276000
C -1.58652000 -1.29378700 -0.08958200
C -0.86012000 -1.59003600 1.18213100
C 0.57412500 -1.14322000 1.21821000
```

```
C 1.20676600 -0.53246800 0.21591300
O -1.59947000 1.00024400 -0.94337100
O -1.25757100 1.50255000 0.39561500
C -1.90546300 2.75370300 0.47833200
C -3.02697600 -1.67189700 -0.19458000
C 2.65211000 -0.08235200 0.35594000
C 3.56790700 -0.69315800 -0.72092900
C 2.77555100 1.45360800 0.37390200
H 0.86013600 -1.03591200 -1.83040900
H -1.38914900 -0.56480500 -2.07785100
H -1.39874500 -1.11465500 2.02281300
H 1.10716900 -1.32522600 2.14875300
H -3.21468800 -2.66331600 0.23221100
H -3.37524800 -1.67149900 -1.23160600
H -3.66831100 -0.96524600 0.35550100
H -0.92094900 -2.66902000 1.40181300
H 3.00039000 -0.44759600 1.32893200
H 3.50170000 -1.78463700 -0.72360100
H 3.30714300 -0.33626300 -1.72183400
H 4.61084400 -0.41840300 -0.53770000
H 2.47564600 1.89432100 -0.58130700
H 2.14481500 1.88658400 1.15345900
H 3.81133300 1.75220700 0.56241700
H 0.80686200 0.68475000 -1.52412600
H -1.65354400 3.13355400 1.47102400
H -1.53616900 3.44551400 -0.28670800
H -2.99198500 2.64747200 0.38611000
```

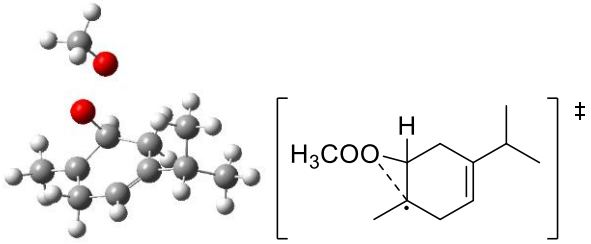

CBS-QB3 Enthalpy= -579.797878 CBS-QB3 Free Energy= -579.859696

```
0 2
C -1.22432500 -0.63737600 -0.14095100
C -0.44538100 -0.14690200 1.05938000
C 1.06865100 -0.23041500 0.89626400
C 1.59126000 -1.37288500 0.10418800
C 0.74490900 -1.97062200 -0.96893800
C -0.67208900 -1.46924900 -1.02603900
O 1.59834900 0.63254600 -0.07280300
O 1.33116900 2.26435600 0.48034900
C 1.84725500 3.02546800 -0.56606600
C 2.98516300 -1.85787500 0.30104400
C -2.65437300 -0.15023500 -0.30841600
C -2.70029000 1.33869700 -0.70365100
C -3.51575900 -0.41543400 0.93958800
H -0.73310200 -0.72495500 1.94796100
H 1.57323000 -0.10529200 1.86320900
H 1.23378500 -1.81730200 -1.94400400
H -1.26118100 -1.81684500 -1.87118800
H 2.98200600 -2.82517700 0.82558400
H 3.57069500 -1.15537500 0.89533200
H 3.49690300 -2.01952800 -0.65363600
H 0.75173100 -3.06695100 -0.83899000
H -3.08905700 -0.72175200 -1.13672400
H -3.50016600 -1.47364300 1.21517100
```

H -3.16643400 0.16346100 1.79953400
H -4.55533000 -0.13067200 0.75360600
H -2.27163700 1.97712200 0.07364700
H -2.13849400 1.51475300 -1.62383600
H -3.73390700 1.65954700 -0.86536300
H -0.68483100 0.89649700 1.27868100
H 1.70817800 4.07356400 -0.26414000
H 2.92084000 2.85296200 -0.72281900
H 1.31049900 2.86532600 -1.51080800

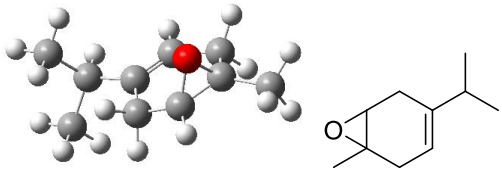

CBS-QB3 Enthalpy= -464.977878 CBS-QB3 Free Energy= -465.027580

0 1
C -0.85031900 0.31816400 -0.05539100
C -0.26184800 -1.00030800 -0.50758200
C 1.23183000 -1.12016000 -0.32401800
C 2.07959100 0.04310800 -0.02255700
C 1.42543600 1.40073000 0.14519900
C -0.07619600 1.36997600 0.21986500
O 1.73623100 -0.91053100 1.00441300
C 3.54106100 0.05141700 -0.40602100
C -2.36359300 0.40740200 0.07538700
C -2.89621400 -0.45254200 1.23801900
C -3.09081900 0.06368600 -1.23768700
H -0.48629600 -1.15929600 -1.57108600
H 1.69153100 -1.96572000 -0.83617300
H 1.83181400 1.87098000 1.05084600
H -0.55036500 2.29879600 0.52920000
H 3.68901500 0.51365100 -1.38666700
H 3.93330900 -0.96663400 -0.43562100
H 4.12362000 0.61879100 0.32675400
H 1.73997100 2.04643800 -0.68681500
H -2.59383600 1.45202800 0.31347200
H -2.72982500 0.68239100 -2.06386400
H -2.95059100 -0.98564100 -1.51423800
H -4.16661500 0.23262000 -1.13456200
H -2.74683200 -1.52065000 1.05481600
H -2.39471100 -0.19904800 2.17497200
H -3.97029300 -0.29158100 1.37036500
H -0.74332100 -1.83171000 0.02202100

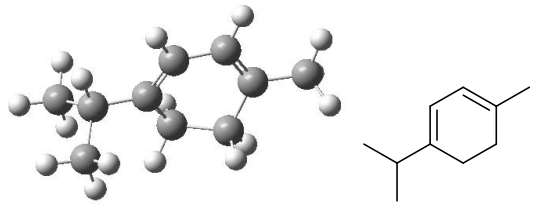

CBS-QB3 Enthalpy= -389.847568 CBS-QB3 Free Energy= -389.895623

0 1
C 1.60682700 1.22608700 0.03297400
C 0.15440800 1.34169700 0.16281200
C -0.66509800 0.29160300 -0.01659600

C -0.03914700 -1.03140300 -0.41977800
C 1.36932800 -1.21260400 0.16286700
C 2.22090700 0.03185600 0.01468300
C -2.17125100 0.40896600 0.08875500
C -2.87519700 0.00824500 -1.22222900
C 3.71013000 -0.13688900 -0.05059400
C -2.73356500 -0.39472000 1.27811300
H -0.26094000 2.31878400 0.39447600
H -0.67008700 -1.87455500 -0.12527400
H 1.85815100 -2.07064800 -0.30977300
H 1.30025400 -1.45499300 1.23537700
H 2.19217600 2.13992400 -0.01670700
H 4.00783800 -0.71478700 -0.93375200
H 4.22499200 0.82572600 -0.08385700
H 4.08006100 -0.69136300 0.82152700
H -2.39472500 1.46601200 0.27463400
H -3.81393000 -0.24476500 1.36644400
H -2.56009900 -1.46816800 1.15599500
H -2.26869300 -0.08301100 2.21660200
H -3.95504600 0.16310100 -1.14063100
H -2.50984400 0.60276400 -2.06361900
H -2.71175400 -1.04740000 -1.45894900
H 0.01758600 -1.06364600 -1.51852500

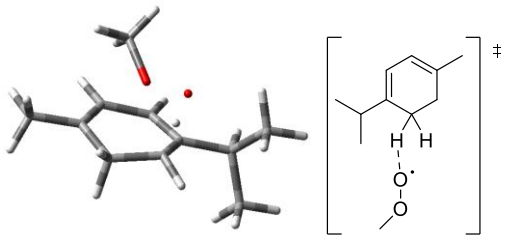

CBS-QB3 Enthalpy= -579.795282 CBS-QB3 Free Energy= -579.854513

0 2
C 0.63097400 -1.38436600 -1.14734700
C 1.21662000 -0.54972100 -0.22902100
C 0.39824400 -0.03361300 0.86296000
C -0.85680400 -0.81745800 1.23280200
C -1.48381200 -1.56535600 0.08342000
C -0.74097400 -1.82367100 -1.02332000
C 2.65621900 -0.09105000 -0.39003200
C 3.55810400 -0.63984100 0.73552400
C -2.88660400 -2.06733200 0.26729300
C 2.77195100 1.44368800 -0.48785300
H 1.20533100 -1.72542400 -2.00559800
H 0.95927000 0.30073100 1.73956500
H -1.59260700 -0.14052400 1.68902200
H -0.61753000 -1.55287600 2.02491600
H -1.17119300 -2.40395200 -1.83705500
H -3.58707200 -1.23679300 0.42691600
H -3.22859000 -2.64556000 -0.59598300
H -2.95895800 -2.70708700 1.15807200
H 3.02031300 -0.51292000 -1.33633300
H 4.60120000 -0.35356000 0.56024500
H 3.26600700 -0.24018000 1.71315700
H 3.50938000 -1.73252400 0.78836500
H 3.81291400 1.73193400 -0.67184900
H 2.15654600 1.83931700 -1.30143600
H 2.44962600 1.93208400 0.43795500
H -0.04092900 1.09504000 0.46505400

```
O -0.53713300 2.28856100 0.21861700
O -1.91767300 2.22170000 0.44739100
C -2.57666900 1.95892500 -0.79107700
H -3.64627800 2.00540400 -0.56488000
H -2.31226400 2.72071300 -1.53133400
H -2.31020800 0.96285200 -1.16696200
```

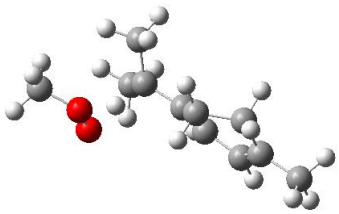

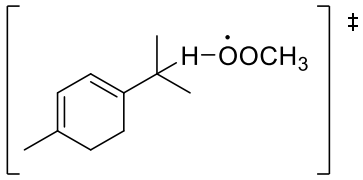

CBS-QB3 Enthalpy= -579.788711 CBS-QB3 Free Energy= -579.851153

```
0 2
C 2.66453700 0.67567900 -0.78409600
C 1.35140100 1.24883300 -0.55298300
C 0.38905500 0.59292000 0.15308700
C 0.69944000 -0.82571000 0.58650500
C 2.18173900 -1.01735100 0.92834300
C 3.09632900 -0.41226300 -0.11310600
C -0.97344300 1.10961200 0.30513100
C -1.63645700 0.90646600 1.66646500
C 4.46831900 -0.99287800 -0.27500700
C -1.23328500 2.47513900 -0.32285900
O -2.23912400 -0.59003000 -1.18915100
O -2.81448200 -1.56336500 -0.37349600
C -4.20524200 -1.28537700 -0.23504200
H 1.14748600 2.23104000 -0.96727800
H 0.07830500 -1.13976100 1.42776500
H 2.39528400 -2.08278300 1.05989000
H 2.40895400 -0.54076800 1.89563300
H 3.32304300 1.17276700 -1.49058000
H 4.41918000 -2.03516200 -0.61232700
H 5.06610400 -0.42891800 -0.99397700
H 5.00369300 -1.00307500 0.68303800
H -1.64448700 0.28418100 -0.43115300
H -2.28683100 2.74810800 -0.23530300
H -0.64828700 3.25970000 0.17396000
H -0.97672100 2.48438200 -1.38415700
H -2.71765500 1.05388300 1.59896400
H -1.46199600 -0.09156400 2.07202500
H -1.25401700 1.63957400 2.38832700
H 0.42190300 -1.47810700 -0.25172500
H -4.60695400 -2.10376100 0.36608800
H -4.36314000 -0.33096500 0.27812700
H -4.68936900 -1.26203200 -1.21477800
```

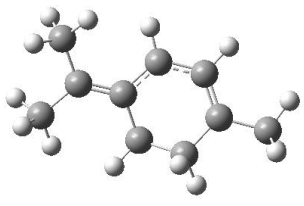

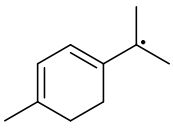

CBS-QB3 Enthalpy= -389.226273 CBS-QB3 Free Energy= -389.275986

```
0 2
C 2.20919700 0.09218700 0.02746800
C 1.46415300 1.22186400 -0.18208000
C 0.05082500 1.23099100 -0.13653800
C -0.72384800 0.03484700 -0.09283000
C 0.08273200 -1.24535200 -0.29005500
C 1.47604500 -1.18240000 0.35595300
C -2.09462600 0.02991200 0.02616400
C -2.90542000 1.28354000 0.24066800
C 3.70628900 0.08567000 0.04741100
C -2.94139500 -1.21196500 -0.07349700
H -0.44805800 2.19027500 -0.18006000
H -0.44636200 -2.11481800 0.10009300
H 2.06166800 -2.05467600 0.04558200
H 1.37913900 -1.25892000 1.45090700
H 1.97564900 2.16676100 -0.34703700
H 4.11368000 -0.59792800 -0.70869100
H 4.11899700 1.07989600 -0.13794200
H 4.08868000 -0.26533500 1.01543700
H -3.39178300 1.60571500 -0.69011400
H -3.71056800 1.09306300 0.95907500
H -2.32048900 2.12024700 0.62008300
H -3.76431500 -1.05007800 -0.78087800
H -2.39639100 -2.09442800 -0.40399500
H -3.41249800 -1.44667800 0.89081700
H 0.20893300 -1.40886100 -1.36924900
```

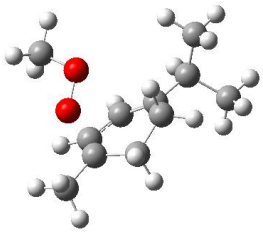

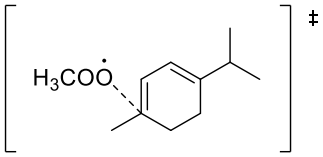

CBS-QB3 Enthalpy= -579.802743 CBS-QB3 Free Energy= -579.861804

```
0 2
C -0.67036000 -0.56577700 -1.06265600
C 0.54733800 -1.49826200 -0.98916300
C 1.50491800 -1.14191700 0.12532900
C 0.94347700 -0.68957700 1.31086900
C -0.42498600 -0.28551900 1.38475900
C -1.24085700 -0.22921200 0.29567300
C 2.84722900 -1.81379800 0.10864600
C -2.67658100 0.23455100 0.40644200
C -3.67408300 -0.90793100 0.12367500
C -2.96392900 1.44757800 -0.50011900
O 2.27964400 0.57619100 -0.70130200
O 1.49405000 1.70398400 -0.57959400
C 2.02801000 2.53639800 0.44684800
H -0.81944100 0.00892800 2.35381200
H -1.43481300 -1.01253700 -1.70546300
H 1.07588400 -1.50100600 -1.94449300
H 0.21202700 -2.53112500 -0.80601500
H 1.56482400 -0.61458000 2.19744700
H 3.39703000 -1.54359500 -0.79653300
H 3.44750700 -1.53135200 0.97507000
H 2.72430800 -2.90367000 0.11112900
H -2.83132600 0.55225800 1.44414800
H -4.70119100 -0.56115300 0.27103500
```

H -3.59221900 -1.26672800 -0.90630400
H -3.50244300 -1.75552500 0.79170500
H -3.98195300 1.81218000 -0.33581900
H -2.27011700 2.26643100 -0.29484200
H -2.87244900 1.18729300 -1.55832500
H -0.37157200 0.37349000 -1.54208400
H 1.41894800 3.44286700 0.44014200
H 1.95406200 2.03844200 1.41825400
H 3.07231500 2.77877200 0.23248600

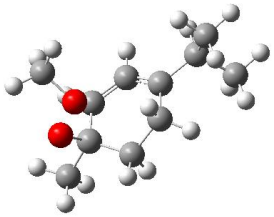

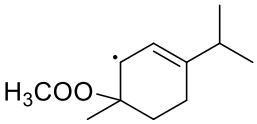

CBS-QB3 Enthalpy= -579.835755 CBS-QB3 Free Energy= -579.894124

0 2
C -1.59075500 -0.84430900 0.00853200
C -0.90075000 -0.57545700 -1.29654000
C 0.45073300 -0.27940700 -1.37349600
C 1.28402000 -0.14709600 -0.26834000
C 0.68961000 -0.29141800 1.10735900
C -0.57267300 -1.16893900 1.11683900
C 2.74975700 0.18646500 -0.42770900
C 3.65717400 -0.99792700 -0.03096400
C -2.62489800 -1.96978300 -0.12555000
O -2.45966600 0.26999800 0.39092600
O -1.67184600 1.48219800 0.56029900
C -2.21422600 2.43820600 -0.33302700
C 3.14671800 1.45788900 0.34873400
H 0.88550100 -0.12959000 -2.35973400
H 1.42402300 -0.71218200 1.80294700
H -1.08016800 -1.10060300 2.08270700
H -0.26939000 -2.21312700 0.98189400
H -1.50383900 -0.61457600 -2.19789400
H -3.13185000 -2.13709500 0.82761700
H -3.37468600 -1.70736200 -0.87492000
H -2.13153400 -2.89408200 -0.43205600
H 2.92172600 0.38303500 -1.49266000
H 4.70830200 -0.75125100 -0.20889800
H 3.55133100 -1.24506200 1.02940600
H 3.41495300 -1.89148900 -0.61160300
H 4.19371300 1.71128100 0.15825300
H 2.53122200 2.31075200 0.05122200
H 3.03086800 1.31957700 1.42748500
H 0.43901600 0.70438300 1.49021300
H -1.65960700 3.35712500 -0.12618900
H -2.06711000 2.14239200 -1.37658300
H -3.27863100 2.60095900 -0.13603000

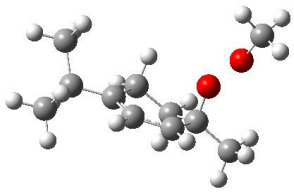

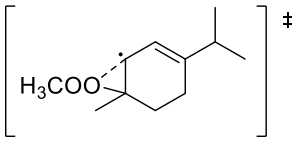

CBS-QB3 Enthalpy= -579.814908 CBS-QB3 Free Energy= -579.874644

0 2
C 0.42773900 -0.70747400 -1.27704500
C 1.29681800 -0.95290100 -0.03914200
C 0.48157000 -1.19109000 1.18694300
C -0.86816500 -0.79576100 1.27008200
C -1.51389300 -0.14094500 0.25331800
C -0.73627800 0.24581800 -0.97569300
C 2.43288000 -1.93854200 -0.28455100
O 1.71193500 0.22828400 0.58759500
O 2.83603100 1.10822400 -0.58652300
C 3.53921000 1.94680200 0.26768400
C -2.96558800 0.26006300 0.38173000
C -3.16063200 1.78036200 0.21756400
C -3.85881300 -0.51887500 -0.60671500
H -1.40700500 -1.00670800 2.18985400
H -1.39520600 0.32561200 -1.84501500
H 1.05590300 -0.28841700 -2.06550200
H 0.04159900 -1.67070000 -1.62934000
H 0.97702200 -1.63834900 2.03926700
H 3.11864600 -1.51716400 -1.02116100
H 2.98961700 -2.10636600 0.64035100
H 2.05644400 -2.89795100 -0.65095400
H -3.28715700 -0.00907700 1.39424100
H -4.90929100 -0.25718700 -0.45128200
H -3.60976800 -0.28344100 -1.64508000
H -3.75404900 -1.59782800 -0.46915700
H -4.20837000 2.04637700 0.38280200
H -2.55169100 2.33721600 0.93395100
H -2.88822600 2.11279900 -0.78777900
H -0.32041200 1.24731600 -0.80761600
H 4.21069400 2.53477000 -0.37839700
H 2.88937300 2.65196300 0.80491700
H 4.15905900 1.40032300 0.99227200

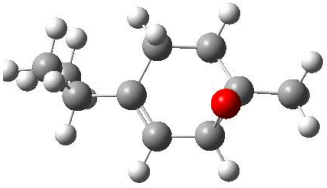

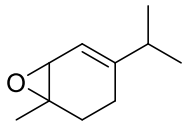

CBS-QB3 Enthalpy= -464.977786 CBS-QB3 Free Energy= -465.026963

0 1
C 1.12048400 1.31028100 0.29810500
C 2.06274900 0.15845600 -0.00151000
C 1.43525800 -1.08297500 -0.49405800
C -0.03428600 -1.13737100 -0.68125200
C -0.85526400 -0.24446900 -0.11360000
C -0.26836100 0.84070900 0.76674300
C 3.47804900 0.52070300 -0.38424500
O 1.93761000 -0.97514500 0.87004400
C -2.35987500 -0.31827800 -0.29244300
C -3.09159000 -0.46626700 1.05484400
C -2.90669900 0.88333800 -1.08712900
H -0.43229600 -1.93793400 -1.29833700
H -0.93964800 1.70225300 0.81908400
H 1.56424400 1.96259700 1.05806300
H 1.02202600 1.90924900 -0.61562200
H 2.03078100 -1.75058100 -1.11200700
H 3.96909600 1.05382600 0.43598500
H 4.05883100 -0.37770800 -0.60047400
H 3.49277600 1.16909200 -1.26548800

```
H -2.56523400 -1.21985100 -0.88085700
H -3.98225400 0.77264200 -1.25354100
H -2.75396700 1.82568200 -0.55273700
H -2.41926400 0.96503700 -2.06187000
H -4.16695100 -0.58688100 0.89475800
H -2.73022300 -1.33826300 1.60572800
H -2.94957500 0.41484500 1.68760200
H -0.18201400 0.45239200 1.78663400
```

Theoretical level: B3LYP/6-311+G(d,p)

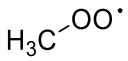

SP of gas: -190.278515

SP of water: -190.285613

SP of PhCl: -190.284999

SP of gas: -190.918919

SP of water: -190.927936

SP of PhCl: -190.924427

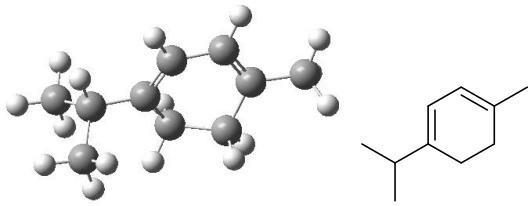

SP of gas: -390.790779

SP of water: -390.789482

SP of PhCl: -390.801885

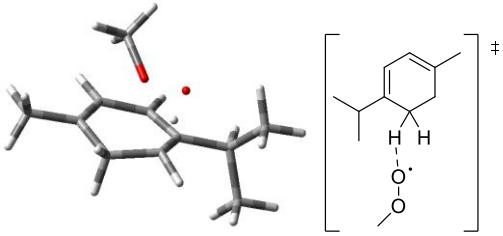

SP of gas: -581.052753

SP of water: -581.061886

SP of PhCl: -581.068575

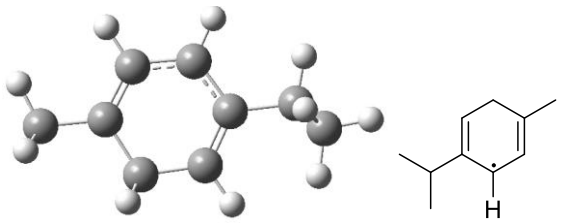

SP of gas: -390.161732

SP of water: -390.160811

SP of PhCl: -390.173095

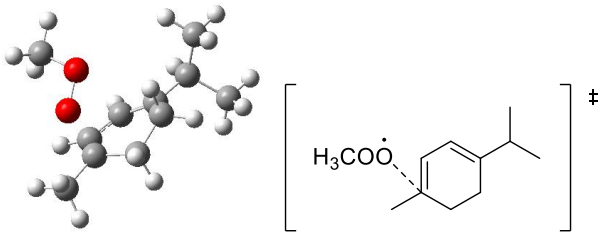

SP of gas: -581.062549

SP of water: -581.069737

SP of PhCl: -581.075887

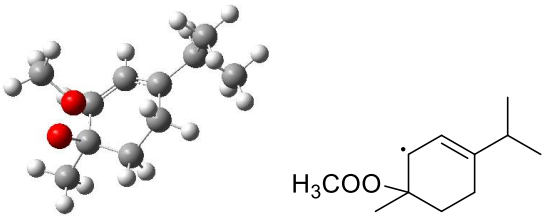

SP of gas: -581.086689

SP of water: -581.090007

SP of PhCl: -581.099024

2.7.4 NMR Spectra

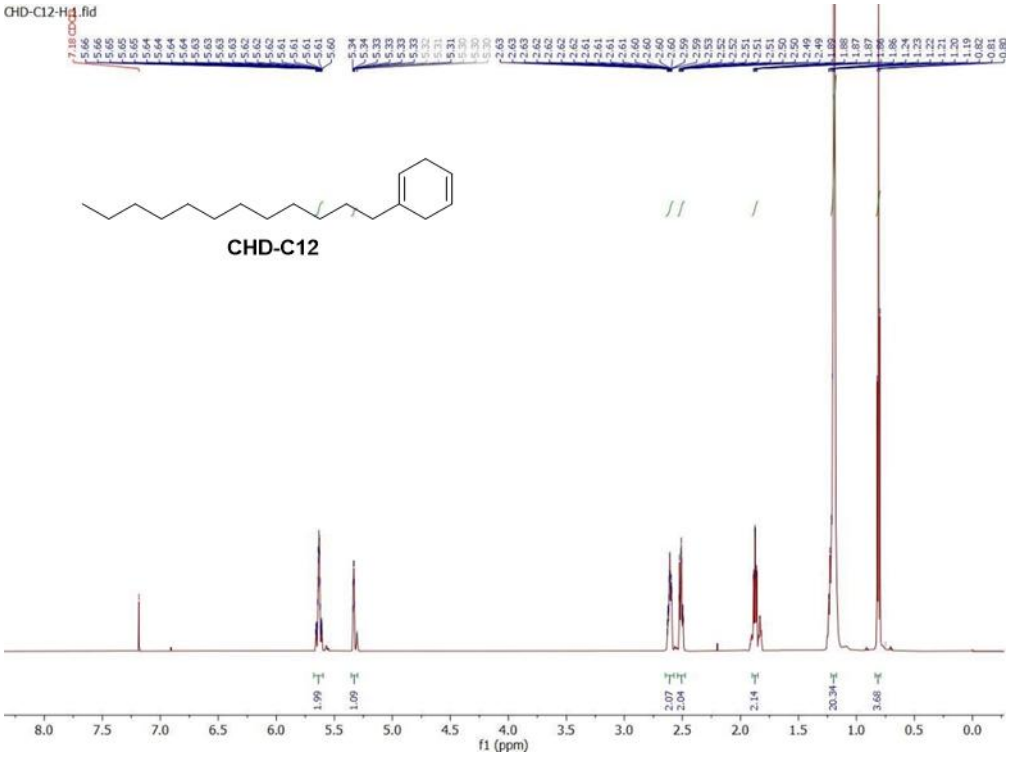

***Figure A 2.5**. 1H-NMR spectra of CHD-C12*

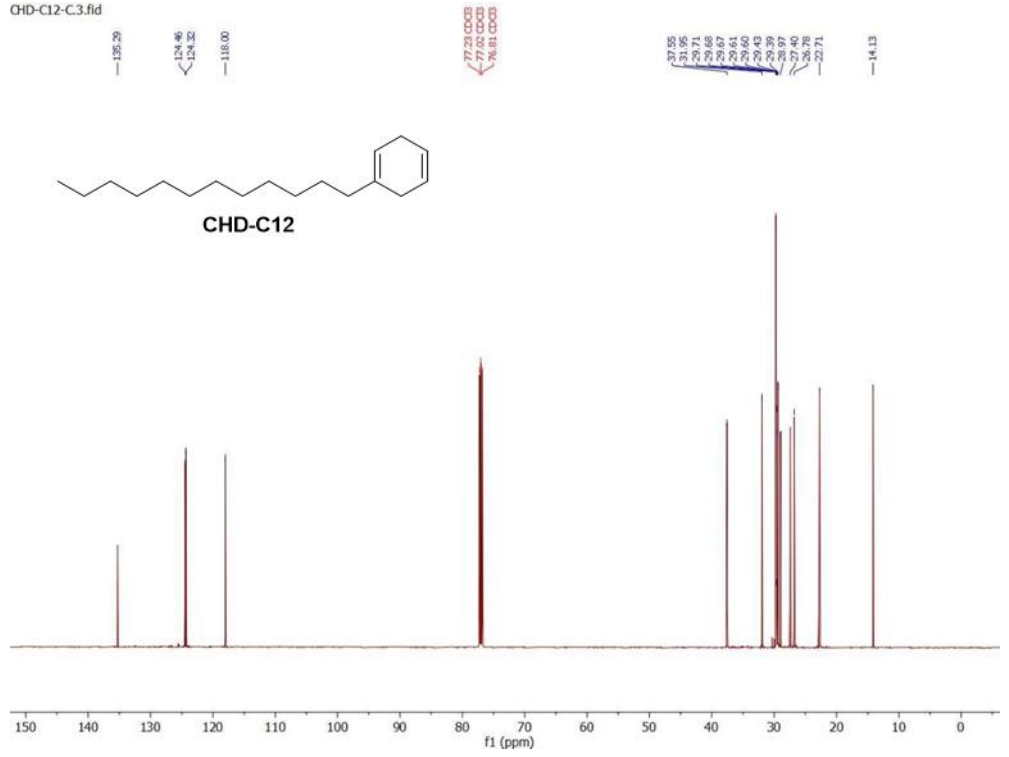

***Figure A 2.6.** ^{13}C-NMR spectra of CHD-C12*

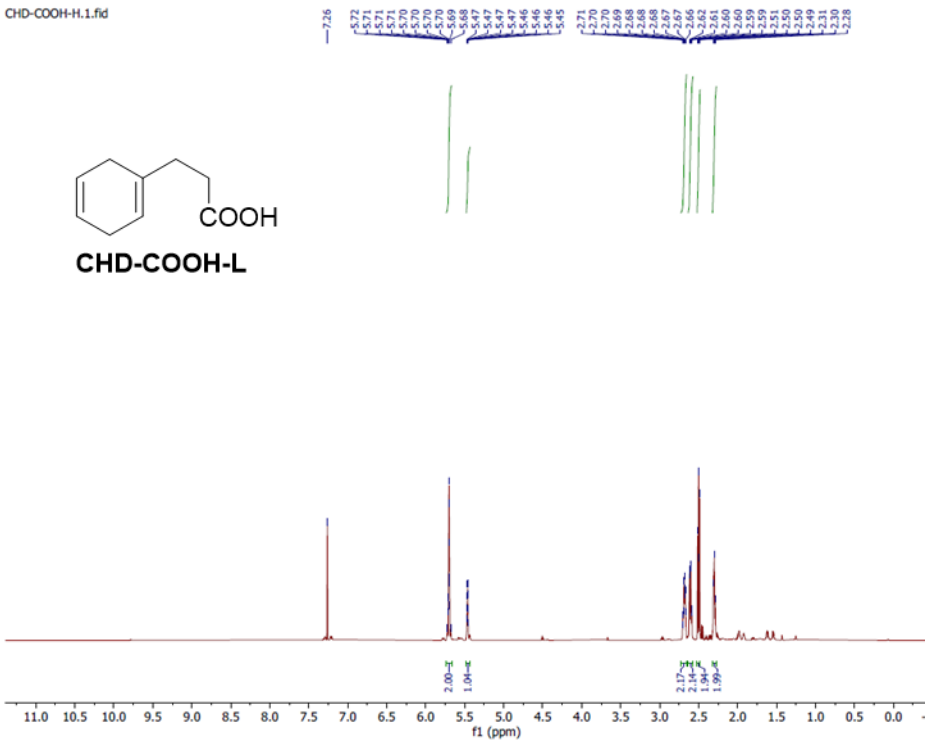

Figure A 2.7. *^{1}H-NMR spectra of CHD-COOH-L*

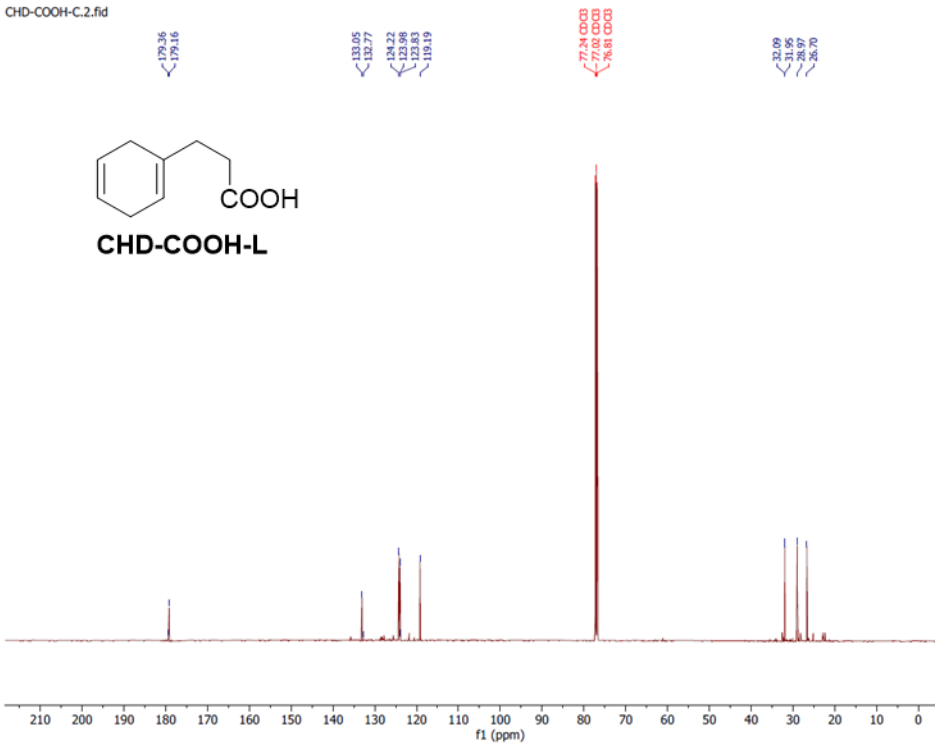

Figure A 2.8. *^{13}C-NMR spectra of CHD-COOH-L*

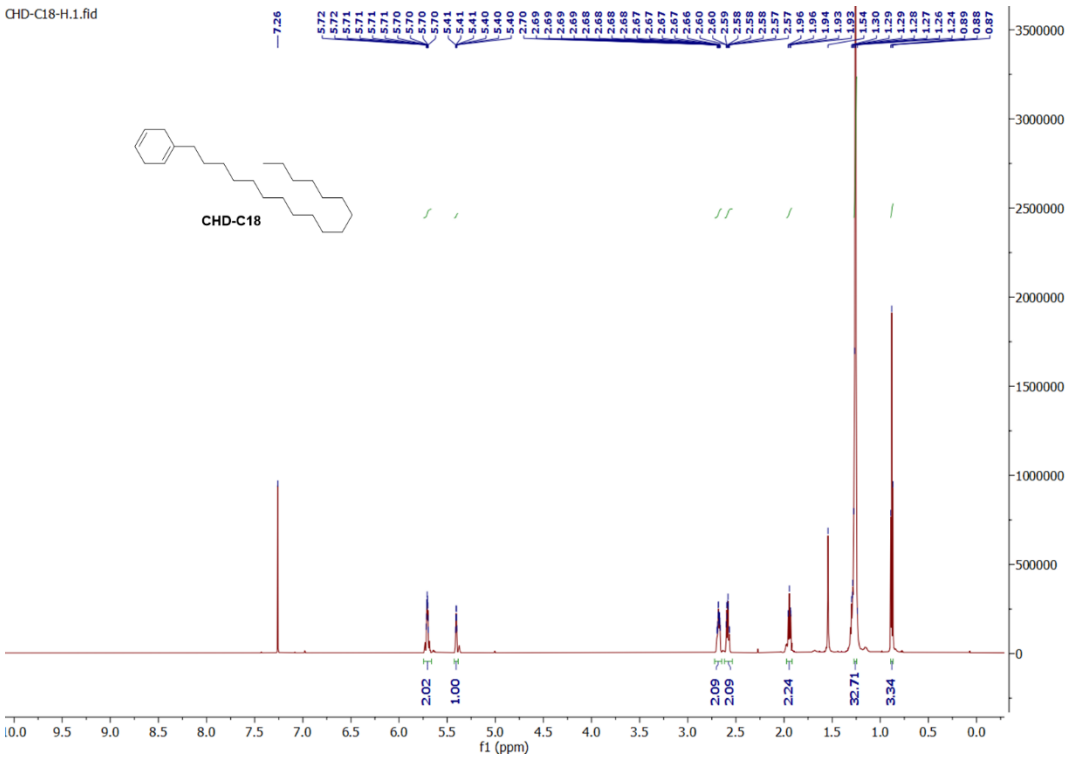

Figure A 2.9. *^{1}H-NMR spectra of CHD-C18*

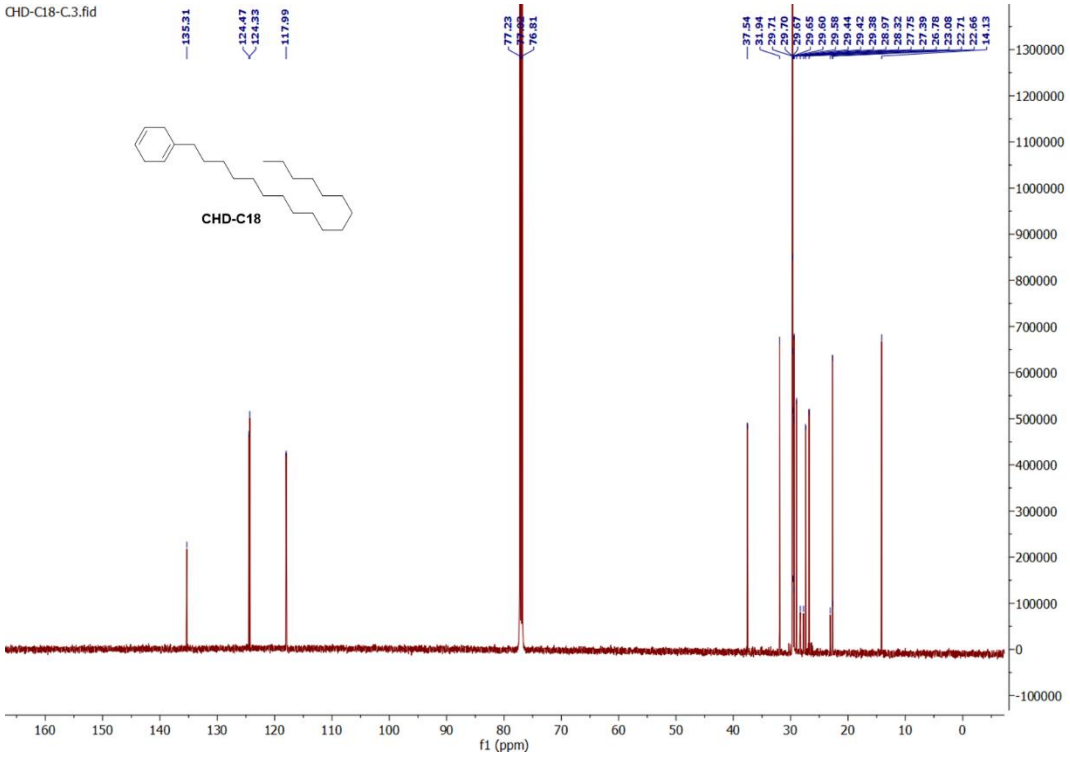

Figure A 2.10. *^{13}C-NMR spectra of CHD-C18*

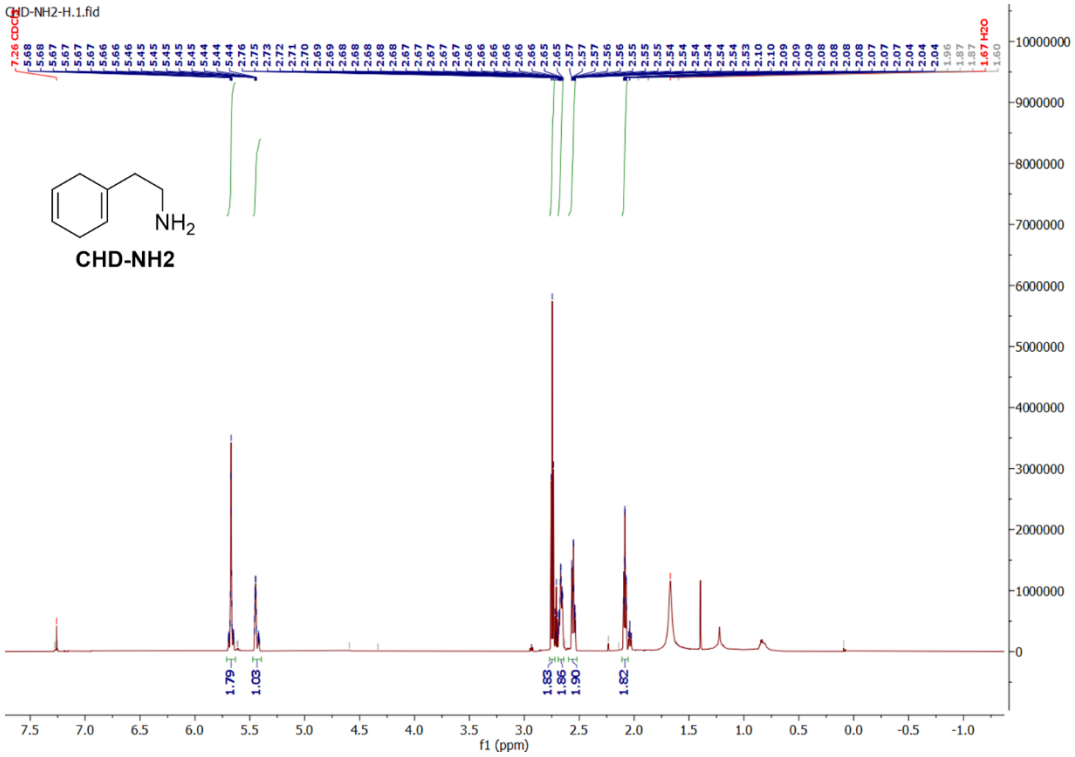

Figure A 2.11. *^{1}H-NMR spectra of CHD-NH2*

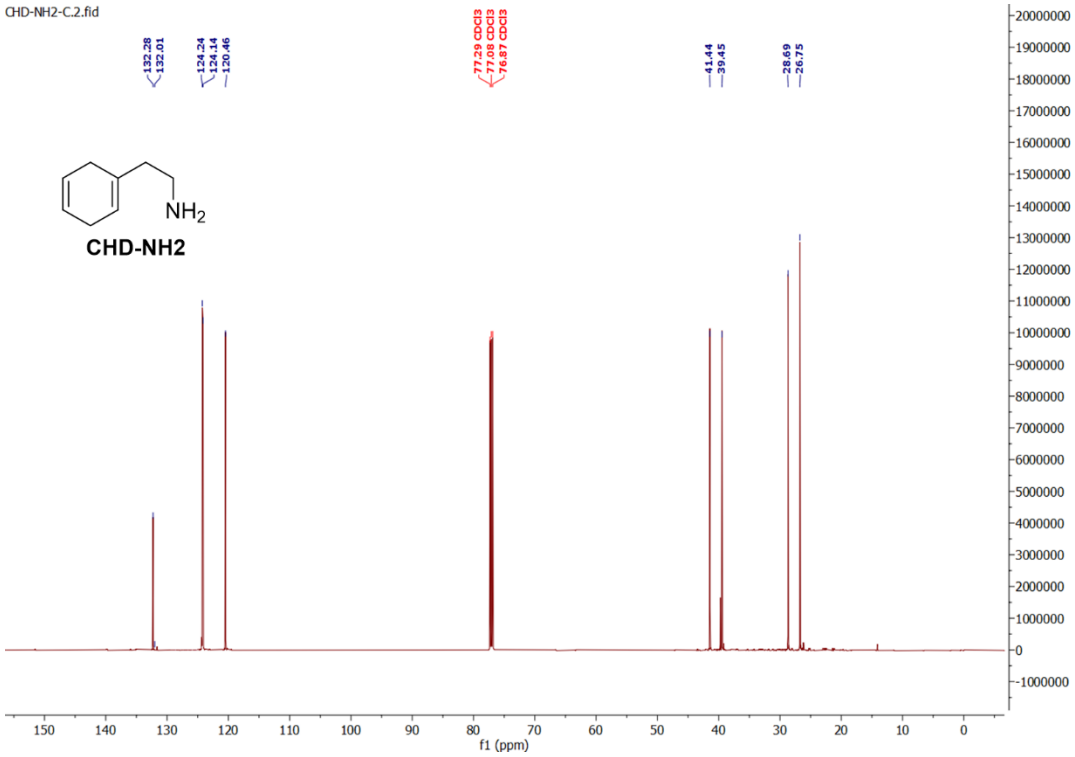

Figure A 2.12. *^{13}C-NMR spectra of CHD-NH2*

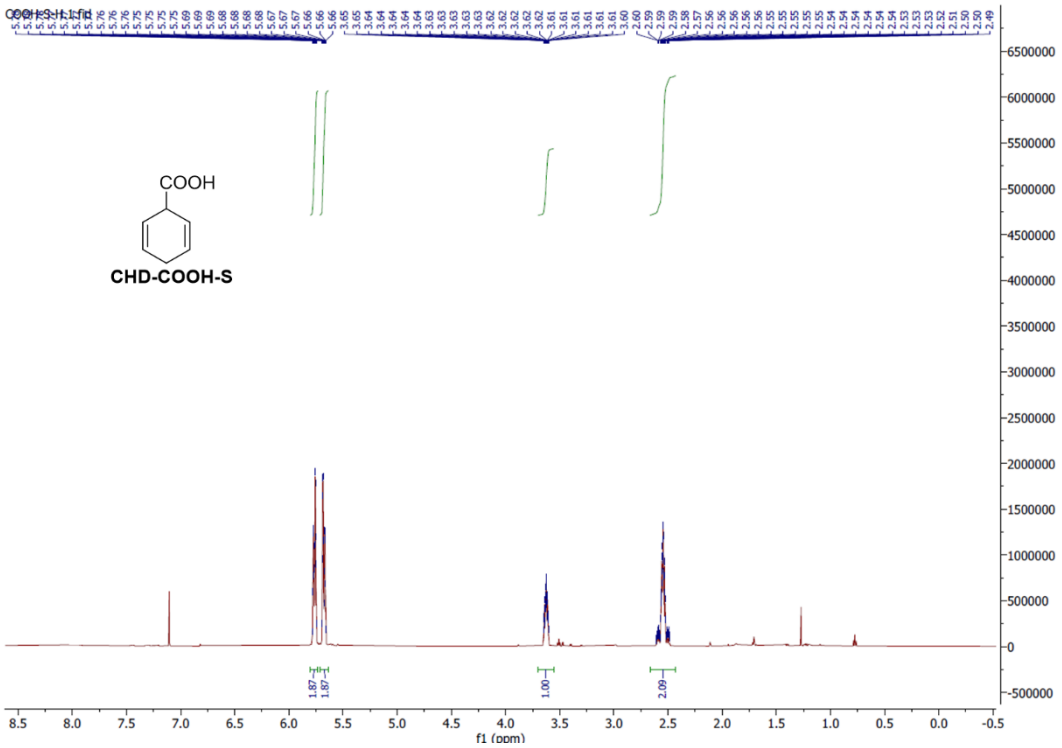

Figure A 2.13. *^{1}H-NMR spectra of CHD-COOH-S*

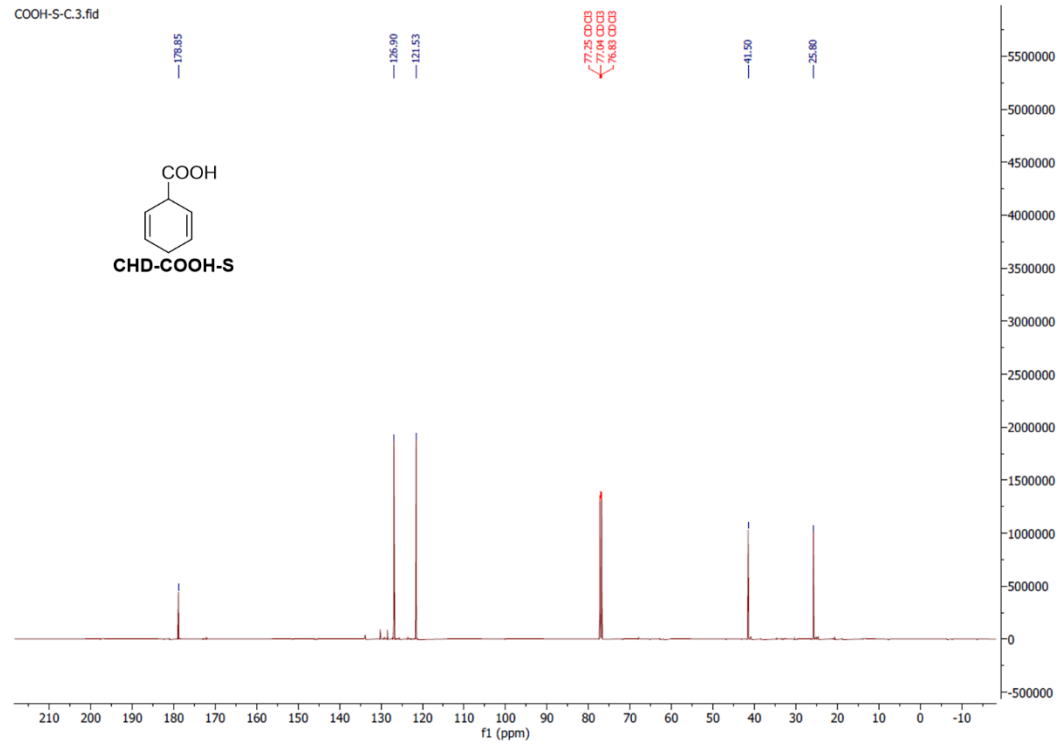

Figure A 2.14. *^{13}C-NMR spectra of CHD-COOH-S*

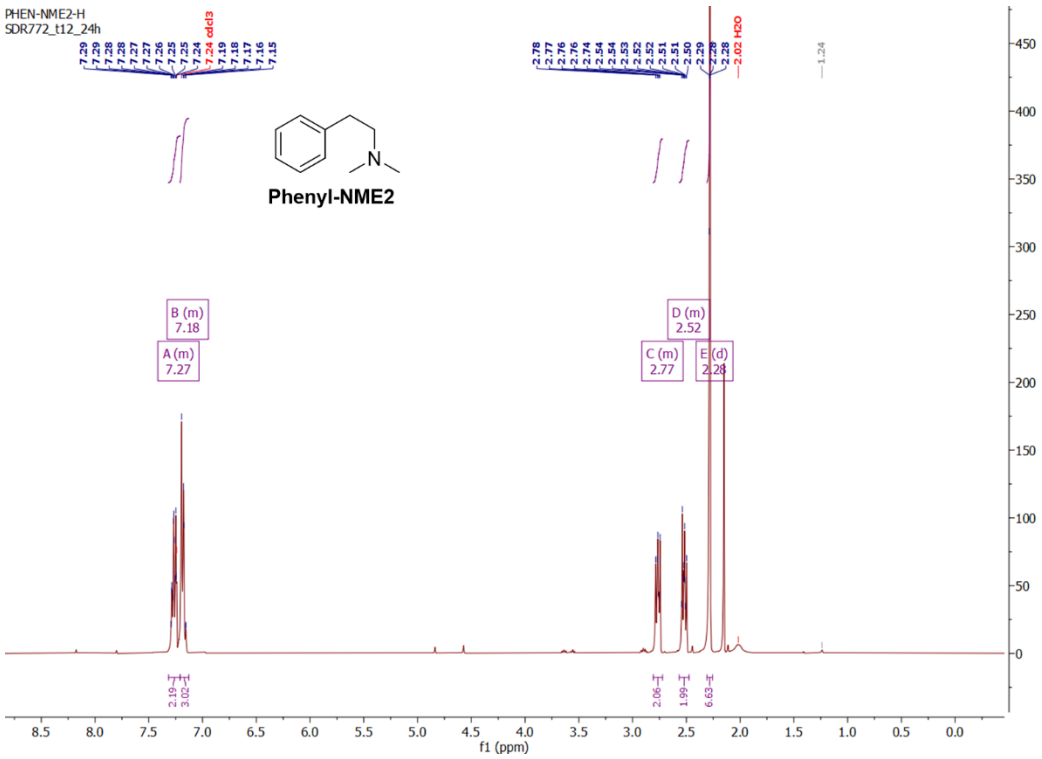

Figure A 2.15. *[1]H-NMR spectra of Phenyl_NME2*

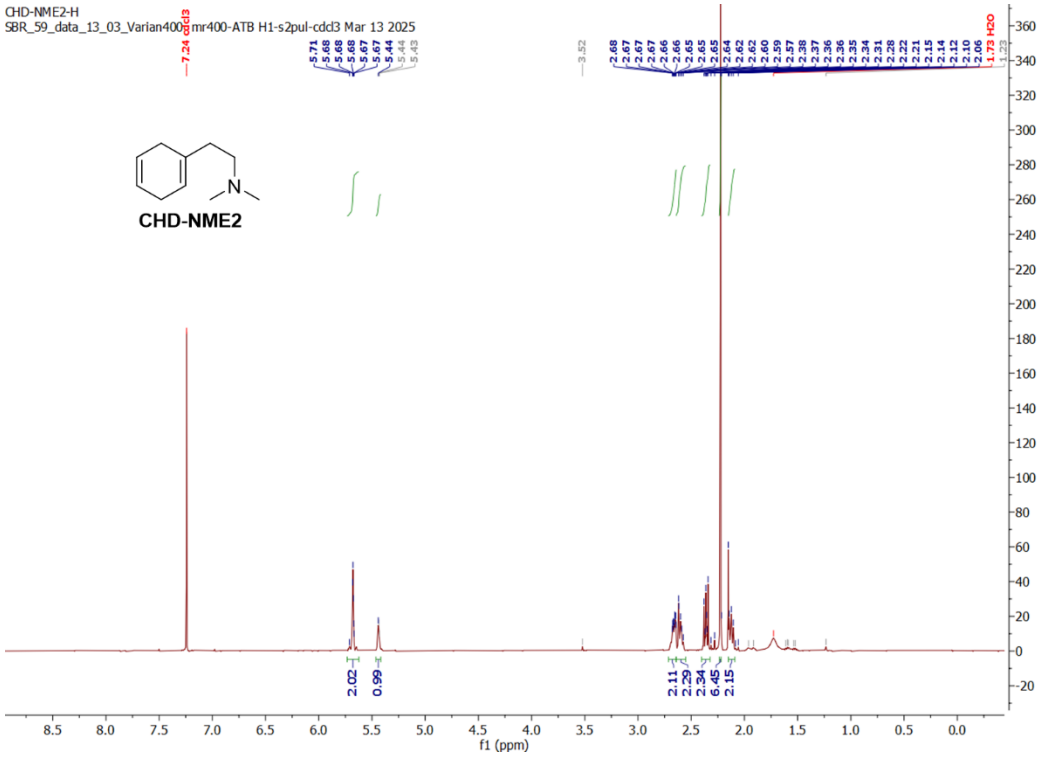

Figure A 2.16. *[1]H-NMR spectra of CHD_NME2*

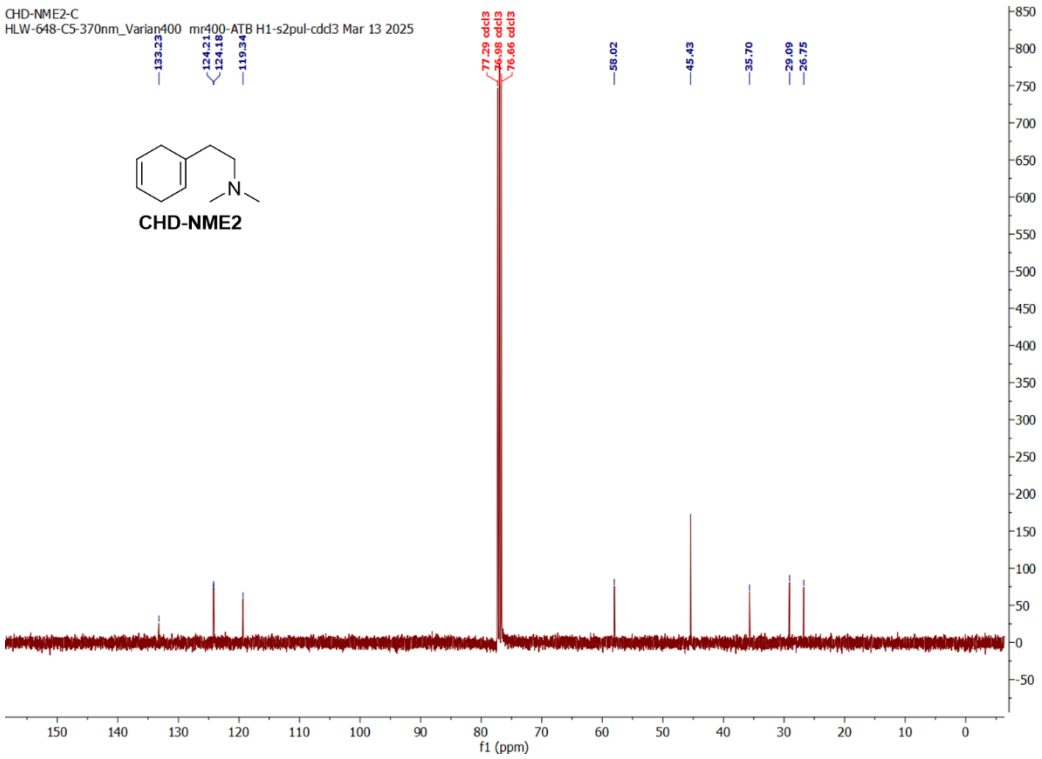

Figure A 2.17. *^{13}C-NMR spectra of CHD_NME2*

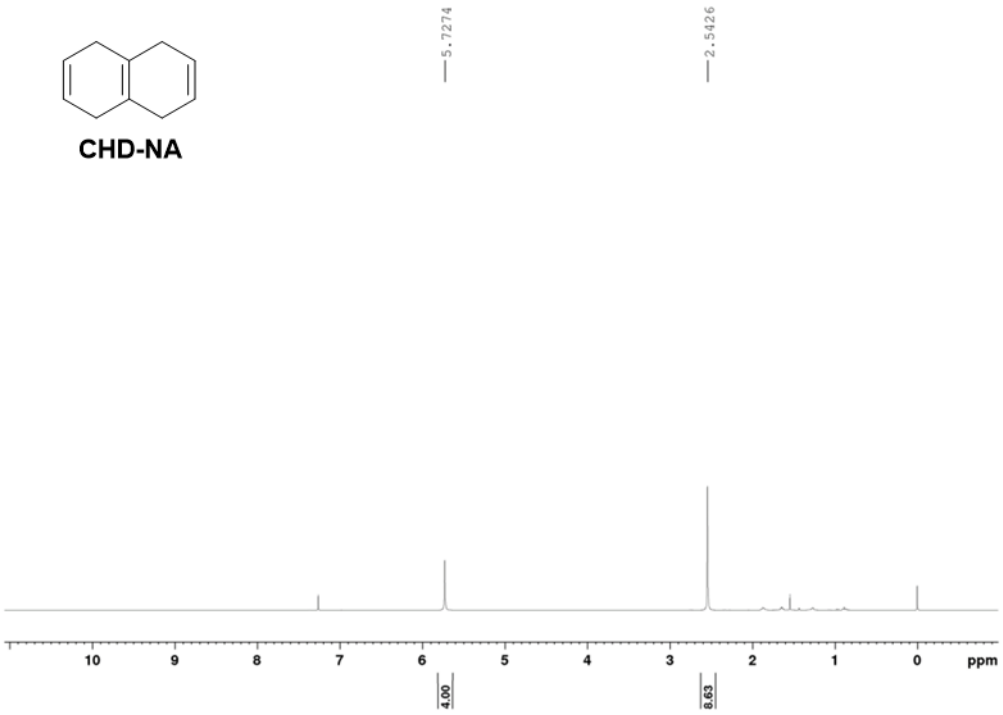

Figure A 2.18. *^{1}H-NMR spectra of CHD_NA*

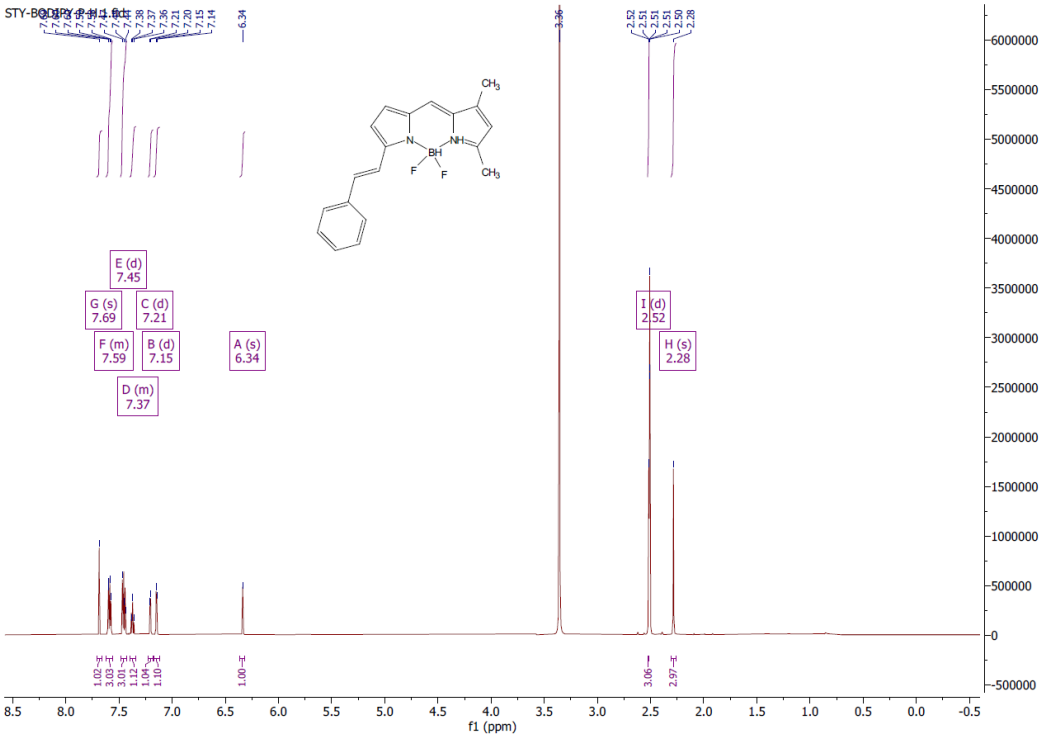

Figure A 2.19. *^{1}H-NMR spectra of STY-BODIPY*

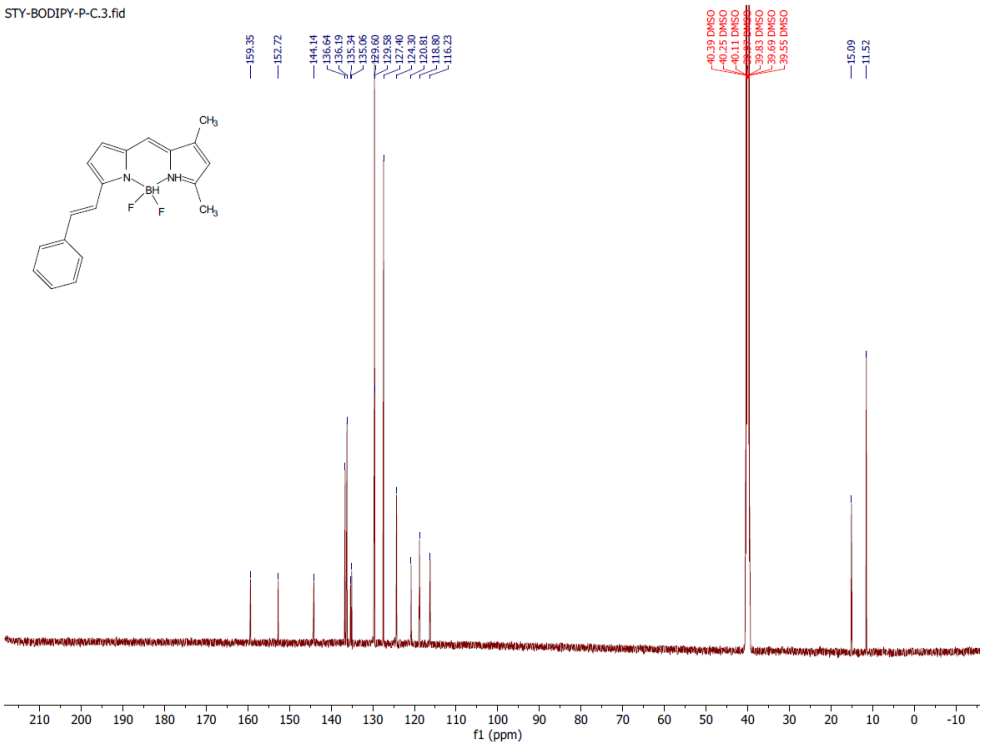

Figure A 2.20. *^{13}C-NMR spectra of STY-BODIPY*

Part II

Unexpected Effect of Free Fatty acid on Lipid Peroxidation

3 Main Work of Part 2

3.1 Preface

In this chapter, the focus was on free fatty acids (FFAs), such as palmitic acid, a 16-carbon saturated fatty acid that is one of the most common in animals, plants, and microorganisms. These fatty acids are known to accelerate lipid peroxidation in edible oils, a phenomenon reported in previous studies but whose mechanism has never been explained. For instance, N. Frega et al. (1999) demonstrated that FFAs act as strong prooxidants and are particularly susceptible to thermo-oxidative degradation in certain vegetable oils. The intensity of this effect was found to depend on the concentration of FFAs. In the present work, using edible oil as the matrix, we investigated the potential mechanisms underlying this phenomenon at 130 °C, as well as the influence of FFAs on lipid peroxidation in the presence of antioxidants. Furthermore, we examined the effects of selected oxidation by-products on lipid peroxidation.

3.2 Research objectives

FFAs are generally known to promote lipid oxidation; however, limited studies have investigated how different types of fatty acids influence the degree of lipid oxidation. Free fatty acids significantly contribute to lipid oxidation in oils. The hypothesis advanced so far include boosting the pro-oxidant effects of transition metals and accelerating the breakdown of lipid hydroperoxides[83]. Additionally, free fatty acids reduce the oil's surface tension, which allows more oxygen to diffuse into the oil, further speeding up oxidation[178]. Commercial edible oils typically contain trace amounts of FFAs (0.05–0.70%). The presence of natural antioxidants in edible oils, such as α-tocopherol, can significantly impact oxidation processes[179]. These antioxidants interrupt termination reactions between peroxyl radicals, effectively delaying the progression of lipid oxidation and extending the shelf life of the oils. Nevertheless, the specific effects of FFAs on the oxidative stability of oils containing antioxidants remain largely unexplored. Given this gap in the literature, it is essential to investigate both the mechanisms and the extent to which various types of FFAs influence lipid oxidation in antioxidant-rich systems. Therefore, the objective of this study is to elucidate the impact of FFA type on lipid oxidation in the presence of different antioxidant compounds. This study is also the first to comprehensively investigate the underlying mechanisms of peroxidation acceleration by FFA in oils. Moreover, it provides a clearer understanding of the relationship between unsaturation levels, oxygen concentration, and the extent of oxidative inhibition.

3.3 Results

3.3.1 Free Fatty acid Effect in different oleic content oils

In order to investigate the effect FFA in a controlled and reproducible system, sunflower oil was purified by chromatographic column to remove its natural antioxidants (stripped High linolenic sunflower oil, SHLS). When placed at 130 °C under stirring, SHLS oxidized without a lag phase, whereas in the presence of a radical trapping antioxidant (RTA), the start of autoxidation was delayed for a certain amount of time, referred to as the induction

period (IP). After this period, the rate of oxygen consumption usually was similar to that in the absence of antioxidants. The lowest rate of oxygen consumption observed during the delayed phase (known as the inhibited rate, R_{inh}) and the length of the induction period were used to evaluate how effective the antioxidants were. Figure 3.1 shows the autooxidation curve (a), while curves b, c, and d are for the antioxidants butylated hydroxytoluene (BHT), Propyl gallate (PG), and tert-Butylhydroquinone (TBHQ), respectively.

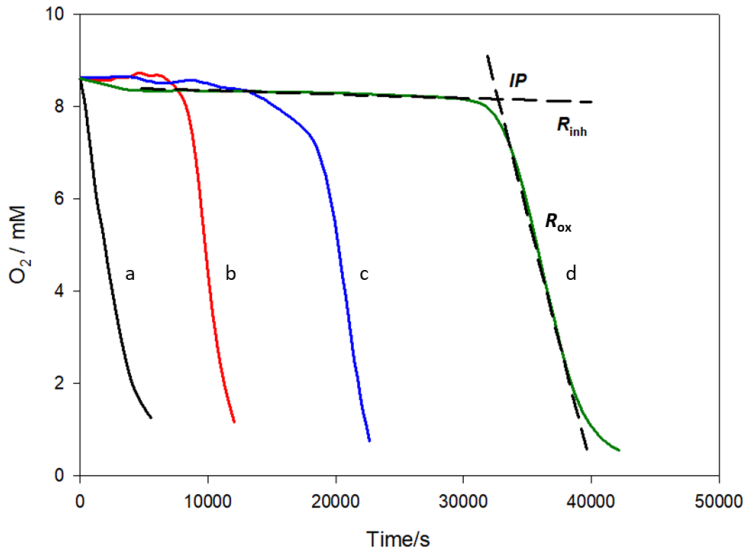

$$\text{initiator} \xrightarrow{R_i} R^\bullet$$

$$R^\bullet + O_2 \rightarrow ROO^\bullet$$

$$ROO^\bullet + RH \xrightarrow{k_p} R^\bullet + ROOH$$

$$2ROO^\bullet \xrightarrow{k_t} \text{nonradical products}$$

$$ROO^\bullet + AH \xrightarrow{k_{inh}} ROOH + A^\bullet$$

$$A^\bullet + ROO^\bullet \rightarrow \text{nonradical products}$$

***Figure 3.1**, O_2 consumption during the oxidation of SHLS at 130°C without antioxidant (a) or with 0.1% w/w of BHT (4.1 mM) (b), in the presence of 0.1% w/w PG (5.3 mM) (c) and in the presence of 0.1% w/w TBHQ (5.4 mM) (d). Right side: kinetic scheme of oil autoxidation.*

The kinetics of SHLS co-autoxidation were described in a previous work, we demonstrated that TBHQ at 130 °C is a good antioxidant with a stoichiometry of radical trapping of 2, following the general scheme reported in Figure 3.1.[180]

We measured the value of the initiation rate (R_i) of different oils and their blends using equation 17.[46]

$$R_i = \frac{n[AH]}{\tau} \qquad (17)$$

$$-Rinh = \frac{k_p[RH]R_i}{nk_{inh}[AH]} \quad (18)$$

In this equation, R_i represents the rate of initiation (that is the formation of new radicals in the system), n represents the stoichiometric factor, [AH] represents the concentration of a reference antioxidant (in our case TBHQ), τ represents the inhibition period. Equation 18 shows the slope of O_2 consumption during the inhibited period (R_{inh}), where k_p represents the rate constant of propagation, k_{inh} the rate constant of inhibition and [RH] represents the concentration of substrate.

In order to investigate the fatty acid effect, we chose Palmitic Acid (PA) because PA is most common saturated fatty acid present in oils, especially in the palm oil, and it has no unsaturation, therefore its amount did not change the overall concentration of oxidizable groups. In order to obtain constant conditions, the fully saturated, short chain triglyceride triacetin (glycerol triacetate) was used to dilute the samples so that the amount of oxidizable oil is set to 0.2 g, and the total weight is kept constant to 0.4 g (see section *3.7*). First, the effect of PA on the oxidation of commercial high-linoleic sunflower oil (HLS) and high oleic sunflower oil (HOS), having a linoleate content of 53% and 6% respectively (See Table 3.1 entry 1 and 2), was investigated (see Fig. 3.2 A, B). The plots can be analysed and quantified by measuring the essential factors that characterize the oil oxidation. The inhibited (R_{inh}) and noninhibited (R_{ox}) O_2 consumption rates (in nmol/s and μmol/s) and the length of the induction periods (τ, in seconds) (in Table A 3.1). In this experiment, the same amount of oil (50 %) was used to ensure the concentration of the oxidizable groups was constant. Normally, commercial sunflower oil contains about 500 ppm of the natural antioxidant α-tocopherol (α-TOH), that provides an IP of about 12 ks and 40 ks in HLS and HOS respectively as shown by the lines a that represents the control experiment without palmitic acid. With the increase of the percentage of PA, the inhibition period became progressively shorter. When the content of palmitic acid reaches 50% (line e), a very short inhibition period is observed in both HLS and HOS. However, in the HLS, the inhibition period decreased from 12ks to 5ks when the concentration of palmitic acid reached 50%. In contrast, in the HOS, the inhibition period decreased from 40ks to 4ks,

representing approximately 10% of the period observed in the absence of palmitic acid. As we can infer by comparing the results of HLS and HOS, HOS exhibited a prolonged inhibition period due to the smaller ability of oleic acid to generate radicals in the initiation step than linoleic acid. With the increase in palmitic acid (PA) content, the antioxidant inhibition period of both oils was significantly shortened (Fig. 3.2 C, D), suggesting that the presence of saturated fatty acids like PA can promote or facilitate the oxidation of unsaturated fatty acids such as oleic and linoleic acid.

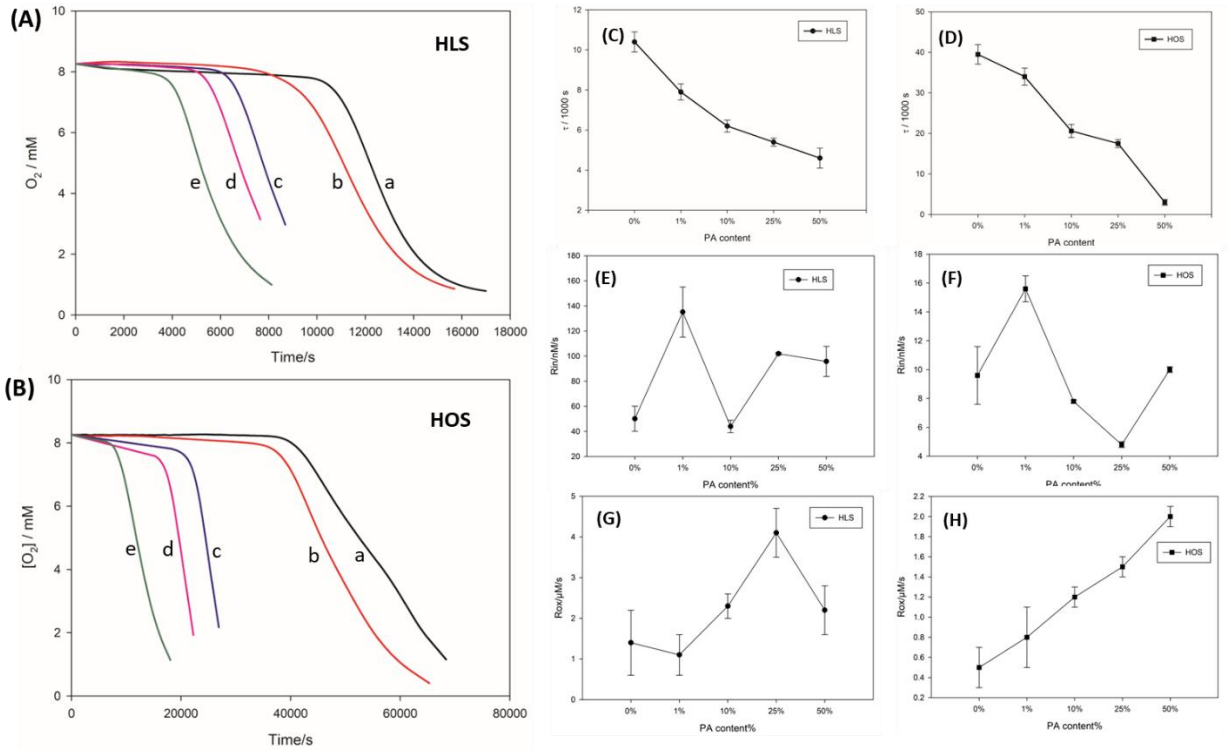

***Figure 3.2**, Panel A: oxygen consumption during the oxidation of High linoleic sunflower oil (HLS, 0.2 g) at 130 °C; diluted with Glyceryl Triacetate (GT) (a); HLS 0.2 g, GT 0.2 g, PA 4 mg (b); HLS 0.2 g, GT 0.16 g, PA 40 mg (c); HLS 0.2 g, GT 0.1 g, PA 0.1 g (d); HLS 0.2 g, PA 0.2 g (e). Panel B: oxygen consumption during the oxidation of High oleic sunflower oil (HOS, 0.2 g) at 130 °C; with GT, 0.2 g (a); HOS 0.2 g, GT 0.2 g, PA 4 mg (b); HOS 0.2 g, GT 0.16 g, PA 40 mg (c); HOS 0.2 g, GT 0.1 g, PA 0.1 g (d); HOS 0.2 g, PA 0.2 g (e). Panels C (HLS) and D (HOS) represent the relationship between different concentrations of PA and IP, Panels E (HLS) and F (HOS) represent the relationship between different concentrations of PA and Rin, Panels*

g (HLS) and h (HOS) represent the relationship between different concentrations of PA and Rox respectively.

In Figure 3.2, Panels E and F, we measured the hydroperoxide (ROOH) content in HLS and HOS. Hydroperoxides are important intermediates in lipid peroxidation (LP) and can also act as pro-oxidants, thereby serving as indicators of the LP reaction.[82] At the beginning of the reaction, ROOH was either absent or present only at negligible levels. As the reaction proceeded, the ROOH content gradually increased with time. Notably, the sample containing 10% PA exhibited a significantly higher ROOH content compared to the sample without PA. This effect can be attributed to the increased presence of free fatty acids (FFA), which behave as pro-oxidants and thereby accelerate the LP reaction.

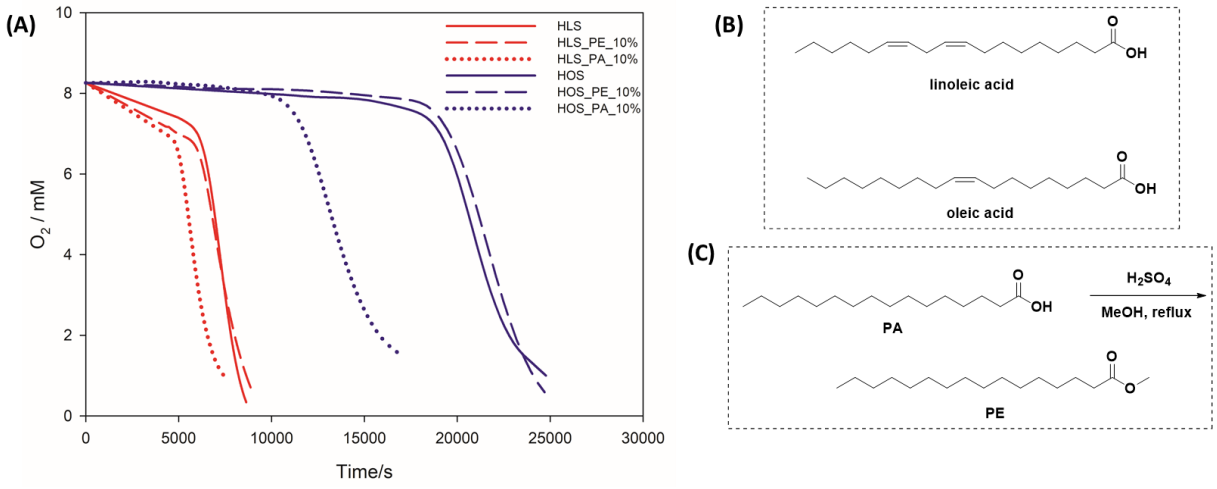

***Figure 3.3**, (A): oxygen consumption during the oxidation of HLS and HOS in the presence of 10% of PA and PE at 130 °C; (B). The chemical structure of Linoleic acid and oleic acid; (C); Synthetic route of PE.*

To assess whether the pro-oxidative effect arises exclusively from free fatty acids, we synthesized the methyl ester derivative of PA (PE ester) and examined its influence on oxidation kinetics at the same concentration (Fig. 3.3; Table A 3.3). The results show that the inhibition period (τ) and the initial oxidation rate (R_{inh}) of HLS and HOS were not substantially altered by the addition of PE. Specifically, τ values of HLS and HOS were 6

ks and 20 ks, respectively, and remained nearly unchanged after PE addition (5.7 ks and 21 ks). In contrast, when the same amount of PA was added, τ decreased by 0.7 ks in HLS and 3 ks in HOS.

3.3.2 Antioxidant activity in the presence of FFAs

To better understand the interaction between antioxidant activity and FFAs, it is essential to first examine the relationship between oxygen concentration, the degree of unsaturation, and the initiation rate (R_i). Therefore, we first studied the relationships with the different polyunsaturated content oils under the same concentration of TBHQ (1.2 mM) (the result is shown in Fig. 3.4 A). Various proportions of stripped HLS, HOS, and $PhCl_2$ (used as inert solvent) were employed to simulate different levels of unsaturated fatty acids within the oil matrix. Stripped HLS (SHLS) and HOS (SHOS) were obtained by alumina column purification as detailed in the Experimental section. As illustrated in the figure 3.4 C and D, an increase in the proportion of unsaturated fatty acids resulted in a progressive and linear shortening of the IP of TBHQ, which was used to calculate the R_i change by equation 17. In Fig. 3.4 D, the influence of oxygen concentration on R_i was further explored. By introducing nitrogen to adjust the oxygen levels within the system, it was observed that a reduction in oxygen concentration led to a corresponding linear decrease in R_i. In addition, COPASI software[181] was employed to simulate the autoxidation kinetics of HLS in the presence of 0.1% TBHQ at 130 °C (Fig. 3.4 B). The initiation step was modeled as the reaction: triglycerides + O_2 → R• + HOO•, with a rate constant of $k = 4.2 \times 10^{-4}$ $M^{-1}s^{-1}$. The initial concentrations were set at 1.03 M for triglycerides and 1.0 mM for dissolved O_2.

These results support the view that the initiation in this system is due only to the reaction of O_2 with linoleate moieties. There is no significant auto-acceleration (see for instance line a in figure 2) so under these conditions (purified oil, relatively high linoleic concentration, no added acid) the contribution of hydroperoxides decomposition to R_i appears negligible.

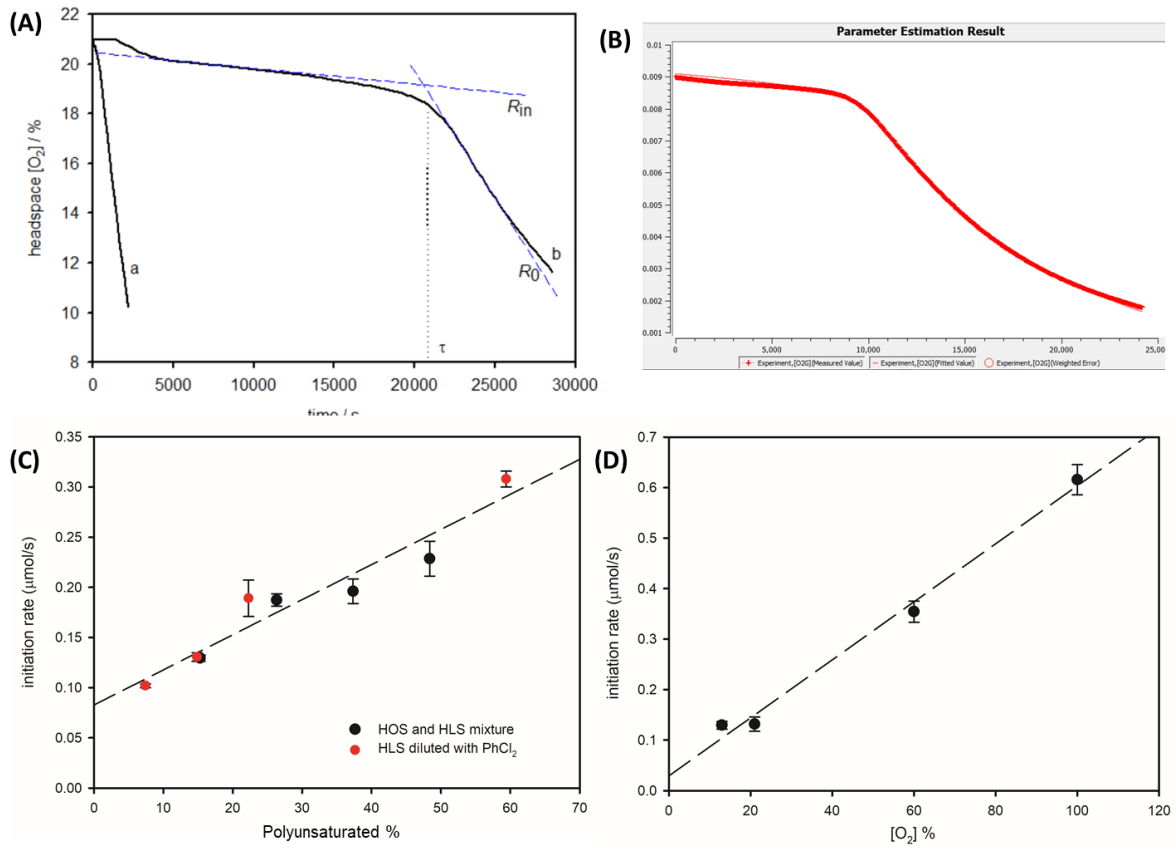

***Figure 3.4**, (**A**): O_2 consumption during the autoxidation of SHLS at 130 °C without antioxidants (a) or in the presence of 0.1 % (w/w) TBHQ (b); (**B**) Numerical fitting (by Copasi software) of the autoxidation kinetic of SHLS at 130 °C inhibited by TBHQ 0.1%; (**C**) Initiation rate (Ri) at 130 °C as a function of the concentration of linoleate residues. The different concentrations of linoleate were obtained either by dilution of SHLS with $PhCl_2$, or by mixing with SHOS; (**D**): Initiation rate (R_i) at 130 °C as a function of the concentration of O_2 in the headspace of HLS (25%, w/w in $PhCl_2$).*

Although the previous results of different contents of oleic acid had shown that PA had an obvious effect on commercial oil in the presence of RTA, like tocopherol, other RTAs can be investigated through the same method; the results were shown in Fig. 3.5A. In this section, SHLS was used to avoid the influences of tocopherol present in the non-purified oil. As expected, oxidation of SHLS did not show any inhibition period. Three RTAs were tested in the presence of PA, and the comparison was shown in Fig. 3.5C. When 10% of

PA was added, the antioxidant ability was obviously decreased, and the inhibition period of TBHQ and PG had a very significant decrease of about 2.9 and 3.4 times, respectively. However, the reduction of BHT was not very obvious, only from 8.5 k to 6.1 k. Another phenomenon that should also be noticed is that R_{in} increased significantly when PA was added (that is, the antioxidant efficiency decreased), for example, R_{in} of PG increased from 27 nM/s to 290 nM/s. We also investigated the changes in the initiation rate (R_i) with and without the addition of PA. These proved that the presence of a large amount of saturated fatty acids not only reduces the inhibition time, but also accelerates oxidation (In Table A 3.4 entry 2 and 8). In addition, different concentrations of PA were also tested, results are shown in Table A 3.4 (entry 11-14). In the Figure A 3.2 Upon the addition of 50% PA, the IP of TBHQ decreased drastically from 16.2 ks to 0, indicating a complete loss of oxidative stability and besides, the rate of oxidation (R_{ox}) increased significantly, rising from 1.8 μM/s to 5.6 μM/s (See Table A 3.4 entry 13 and 14).

To evaluate whether the pro-oxidative effect is shared by other types of acids, cinnamic acid (CA) was selected as a comparative compound for further investigation. (Fig. 3.5 B) CA is a naturally occurring aromatic carboxylic acid, widely distributed in plants, and it serves as a key intermediate in the biosynthesis of lignins, flavonoids, and other phenolic compounds.[182] Experimental results indicated that, under identical conditions and with the same concentration of CA added, the antioxidant protection time was markedly diminished. Notably, the presence of 10% CA resulted in the complete loss of antioxidant efficacy for both TBHQ and PG (In fig. 3.5 B line c' and d'). In a separate set of experiments, it was substituted with HLS, which exhibited a significantly reduced inhibition time even in the absence of added antioxidants. (see Fig, A 3.1) These findings suggest that CA, as a carboxylic acid, exhibits a pro-oxidant effect larger than that of PA, reasonably because its smaller molecular weight makes its molar concentration bigger.

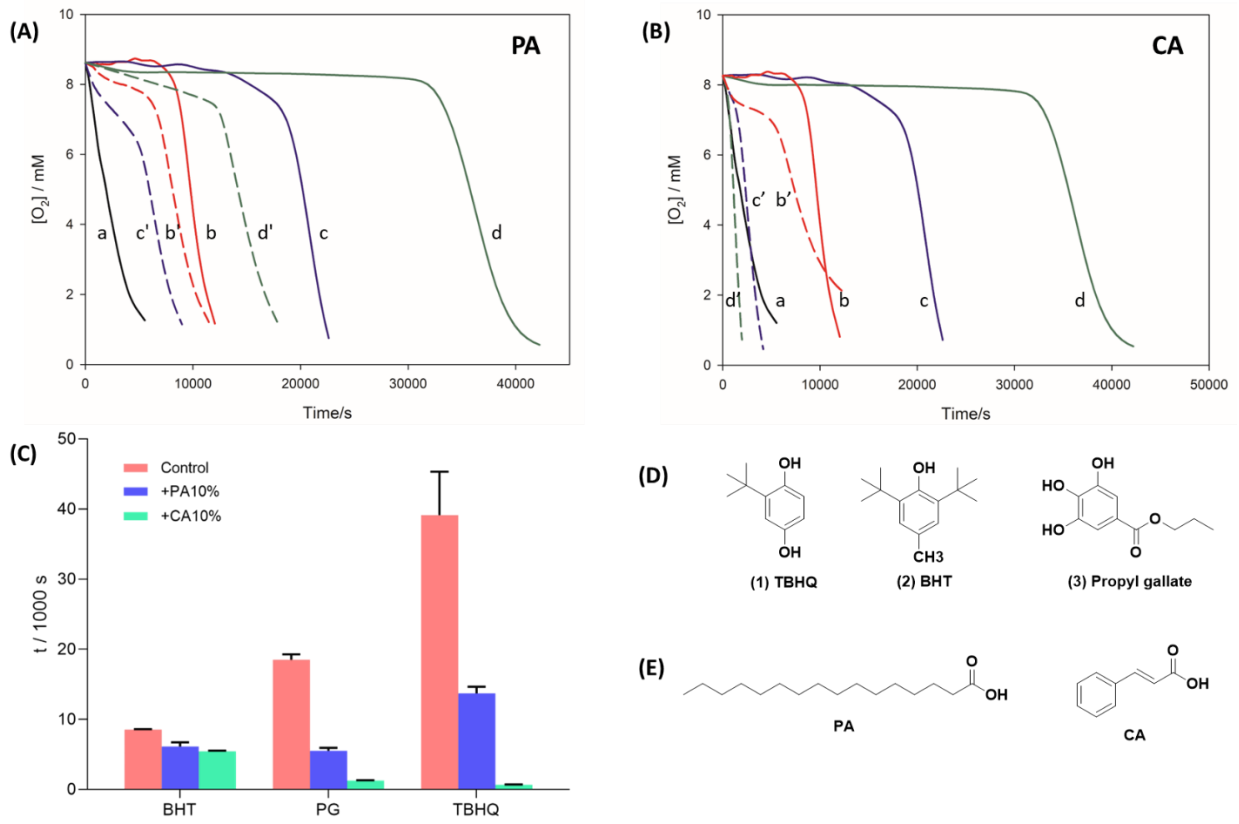

***Figure 3.5**, (**A**): O_2 consumption during the autoxidation of SHLS at 130 °C without antioxidants (a), in the presence of 0.1 % (w/w) BHT (b) and 10% of PA (w/w) (b'); in the presence of 0.1 % (w/w) PG (c) and 10% of PA (w/w) (c'); in the presence of 0.1 % (w/w) TBHQ (d) and 10% of PA (w/w) (d') (**B**) Same condition as Panel (A), replace PA into CA; (**C**) effect of the different acids on IP (τ) (PA: 0.43 M and CA: 0.75 M); (**D**): The chemical structures of antioxidants; (**D**): The chemical structures of Free acids.*

3.3.3 Mechanism studies

Our experimental results demonstrate that FFAs can accelerate fat oxidation and markedly diminish the protective effects of antioxidants. In literature, it was proposed that acids may act by increasing the decomposition of peroxides but no proof was given. Moreover, there is no information about the role of other minor oxidation products like epoxides. To better understand the underlying mechanism of this phenomenon, we examined it from the following three perspectives. (1) Examining the changes in R_i, *R*in, and IP upon the addition of a defined amount of peroxide; (2) Monitoring the variations in R_i, Rin, and IP after the

addition of epoxides; and (3) Inferring the composition of the reaction products through ^{1}H-NMR and IR analysis.

3.3.3.1 FFA effect in the presence of peroxides

Hydroperoxides (ROOH) are the primary products formed during autoxidation, and their concentration is commonly used as an indicator of the extent of oxidation. Similarly, since a certain amount of ROOH is produced during the oxidation of oils, we hypothesized that the addition of acidic compounds would accelerate the decomposition of ROOH and thus speed up the overall oxidation process. To verify this hypothesis, we oxidised a sample of SHLS to enrich it with ROOH (OX-SHLS), and we added it to HLS at the beginning of the reaction, with or without PA (Fig. 3.6 A/C). OX_HLS was obtained by reacting SHLS at 130 °C for 2 and the peroxide level was measured as 94 μM/g (see Fig A 3.2) The results showed that before adding hydroperoxide or acid, the IP of HLS was around 6ks, while after adding 2% oxidized OX-SHLS, their IP decreased to approximately 5 ks, which was similar to the one with 10% PA. When 2% OX-SHLS and 10% PA were added together, the results showed a marked decrease in both IP and *R*in (line d).

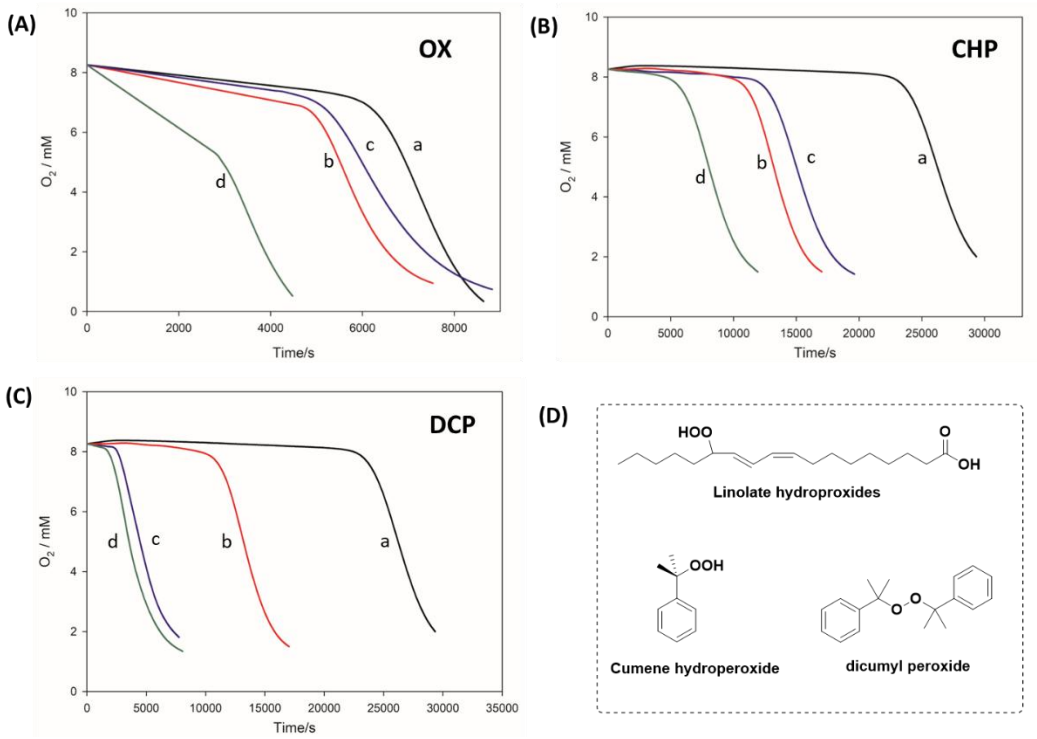

***Figure 3.6**, (**A**): O_2 consumption during the autoxidation of neat HLS at 130 °C (a), in the presence of 10 % (w/w) PA (b), in the presence of 2% of OX_SSO (w/w) (c), 10% (w/w) PA and 2% of OX_SHLS (w/w); (**B**) O_2 consumption during the autoxidation of HOS at 130 °C (a), in the presence of 10 % (w/w) PA (b), in the presence of 0.4% of CHP (w/w), (24 mM) (c), 10% (w/w) PA and 0.4% of CHP (w/w), (24 mM); (**C**): O_2 consumption during the autoxidation of HOS at 130 °C (a), in the presence of 10 % (w/w) PA (b), in the presence of 0.4% of DCP (w/w), (14 mM); (c), 10% (w/w) PA and 0.4% of DCP (w/w), (14 mM); (**D**): The chemical structures of peroxides.*

In addition, Cumene Hydroperoxide (CHP) was selected as another representative ROOH to investigate its potential mechanism. CHP is an organic hydroperoxide commonly employed as a model compound in oxidation studies. In biological systems, CHP can initiate lipid peroxidation in membranes through metal ion catalysis or via interaction with heme proteins such as cytochrome P450, which is abundant in liver microsomes[183]. In our experiments, CHP displayed an effect like that of OX-SHLS, with addition of PA providing a synergic acceleration of the oxidation (Fig. 3.6 B).

We also examined dicumyl peroxide (DCP), a synthetic organic peroxide widely used as a radical initiator and cross-linking agent in polymer chemistry. DCP undergoes thermal decomposition to generate cumyloxy radicals[184]. As shown in Fig. 3.6 C, the addition of 0.4% DCP had a pronounced effect, markedly reducing the inhibition period of HOS (line c). However, the addition of 10% PA had little effect, as can be seen comparing lines c and d. We infer that upon heating, DCP decomposes into highly reactive cumyloxy radicals, but free acids have little influence on this process.

3.3.3.2 FFA effect in the presence of Epoxides

Epoxides, secondary products of lipid peroxidation (LP), contain a strained three-membered oxirane ring that makes them highly reactive and prone to further transformation into diols, aldehydes, and other oxygenated compounds. In this study, methyl oleate epoxide (ME) was obtained by oxidizing methyl oleate (Fig. 3.7 C), and its interaction with free fatty acids (FFAs) was investigated. As shown in Figures 3.7 A and 3.7 B, lines a and c represent the matrix alone and 1% ME, respectively, where no significant changes in inhibition time or curve shape were observed upon the addition of ME alone. In contrast, the addition of palmitic acid (PA), as shown in line d, resulted in a marked shortening of the IP, that was greater in the presence of ME. Moreover, the effect of ME + PA was similar in the two oils HLS and HOS, with varying degrees of unsaturation.

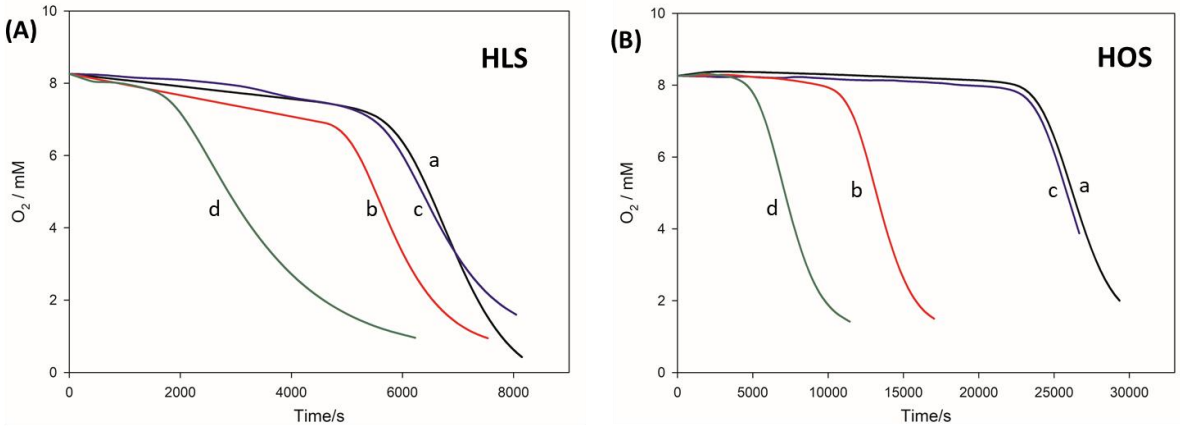

***Figure 3.7**, (**A**): O_2 consumption during the autoxidation of HLS at 130 °C (a), in the presence of 10 % (w/w) PA (b), in the presence of 1% of ME (w/w) (c), 10% (w/w) PA and 1% of ME (w/w) (d); (**B**) O_2 consumption during the autoxidation of HOS at 130 °C (a), in the presence of 10 % (w/w) PA (b), in the presence of 1% of ME (w/w) (c), 10% (w/w) PA and 1% of ME (w/w) (d).*

3.3.3.3 Composition analysis

Previous studies have reported the applicability of ^{1}H-NMR in detecting peroxides and in characterizing the composition of oils, such as castor oil[81]. In the present study, we employed ^{1}H-NMR to investigate the chemical composition of our samples. Figure 3.8 shows the ^{1}H-NMR spectrum of HOS, where the peak at $\delta = 2.75$ ppm corresponds to the bis-allylic CH_2 group of linoleic acid, while the peak at $\delta = 5.32$ ppm corresponds to the vinylic hydrogen on the double bond. These signals indicate that the linoleic acid content is approximately 6%. All the components containing double bonds account for about 91%[185].

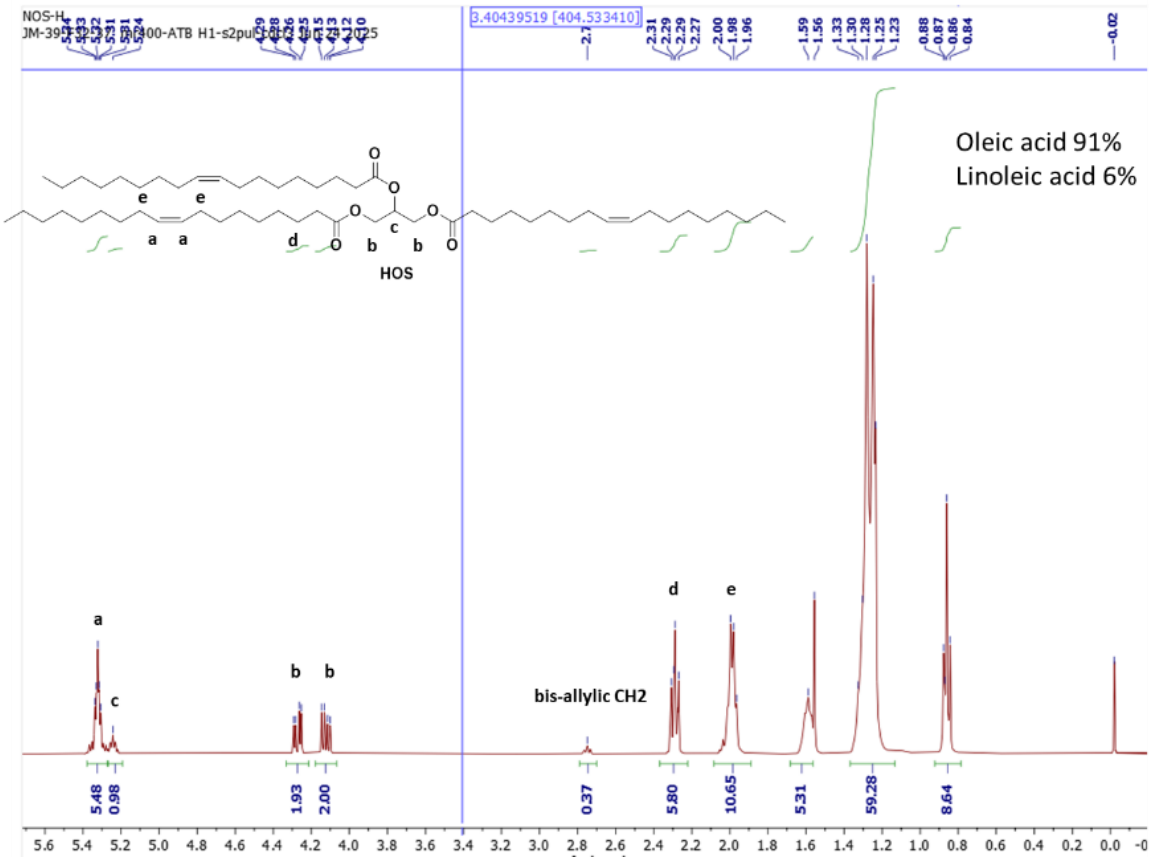

***Figure 3.8**, [1]H-NMR reference spectra of HOS*

To evaluate the extent of oxidation in the samples, we measured the variations in the integrals of bis-allylic CH_2 groups and vinyl hydrogens associated with double bonds at the beginning and at the end of the reaction, after complete consumption of headspace O_2. From these values, we calculated the content of oleic and linoleic residues (see Table 3.1). These experiments were performed on HOS samples to investigate the involvement of oleic acid in the oxidation process. In the presence of heating, with or without 10% PA, noticeable changes were observed in the bis-allylic CH_2 (2.8 ppm) and vinylic H (5.3 ppm) signals, corresponding to a decrease of linoleic and – to a smaller extent – of oleic acid (Table 3.1).

Table 3.1 H-NMR Integration of two types of H for different samples

Sample	Fatty acid	Content (%)	Decrease %[1]

HOS	Oleic	84±1	-
	Linoleic	6±0.5	-
HOS_heat[2]	Oleic	75±2	17
	Linoleic	4±0.3	33
HOS_10%PA without heating[3]	Oleic	83±1	-
	Linoleic	6±0.5	-
HOS_10%PA[4]	Oleic	75±1	13
	Linoleic	4±1	33
HOS_0.4%CHP[5]	Oleic	57±3	34
	Linoleic	3±0.5	50
HOS_0.4%CHP_10%PA[5]	Oleic	56±2	35
	Linoleic	3±0.5	50
HOS_0.4%DCP[5]	Oleic	58±1	30
	Linoleic	3±1	50
HOS_0.4%DCP_10%PA[5]	Oleic	60±2	31
	Linoleic	3±1	50

1): Decrease % is defined as the content decrease after oxidation divided for the content before oxidation. 2): HOS at 130 °C (Reaction time: 25ks), 3): HOS in the presence of 10% PA w/w. 4): HOS at 130 °C in the presence of 10% PA w/w (Reaction time: 13ks), 5): The condition same likes Figure 3.6 B and C.

We were surprised noticing that the difference between linoleic (approx. 33%) and the much less oxidizable oleic acid (approx. 15%) is relatively small, as the latter was oxidized about one half less respect the former.

After the addition of CHP and DCP, the unsaturation in the HOS_Heat sample decreased further up to 50% for linoleic and approx. 30% for oleic, although the end-point of the reaction is similar to the other conditions – that is complete consumption of headspace O_2. This may be explained as effect of polymerization events triggered by CHP and DCP decomposition in the absence of O_2. Moreover, after the addition of CHP and DCP, a new peak appeared at $\delta = 2.1$ ppm, which is probably due to the formation of polymerization with formation of new C-C bonds (Fig. A 3.2).

3.3.3.4 Stability of antioxidants

The stabilization of antioxidants at 130°C was investigated to understand the role of phenol degradation on the duration of the inhibited period. BHT, PG and TBHQ were dissolved in triacetin, which has no unsaturation, and were placed in the same reactor used in the peroxidation experiments. Then, their concentrations were measured by HPLC analysis for a time similar to the duration of their inhibition period in peroxidation experiments.

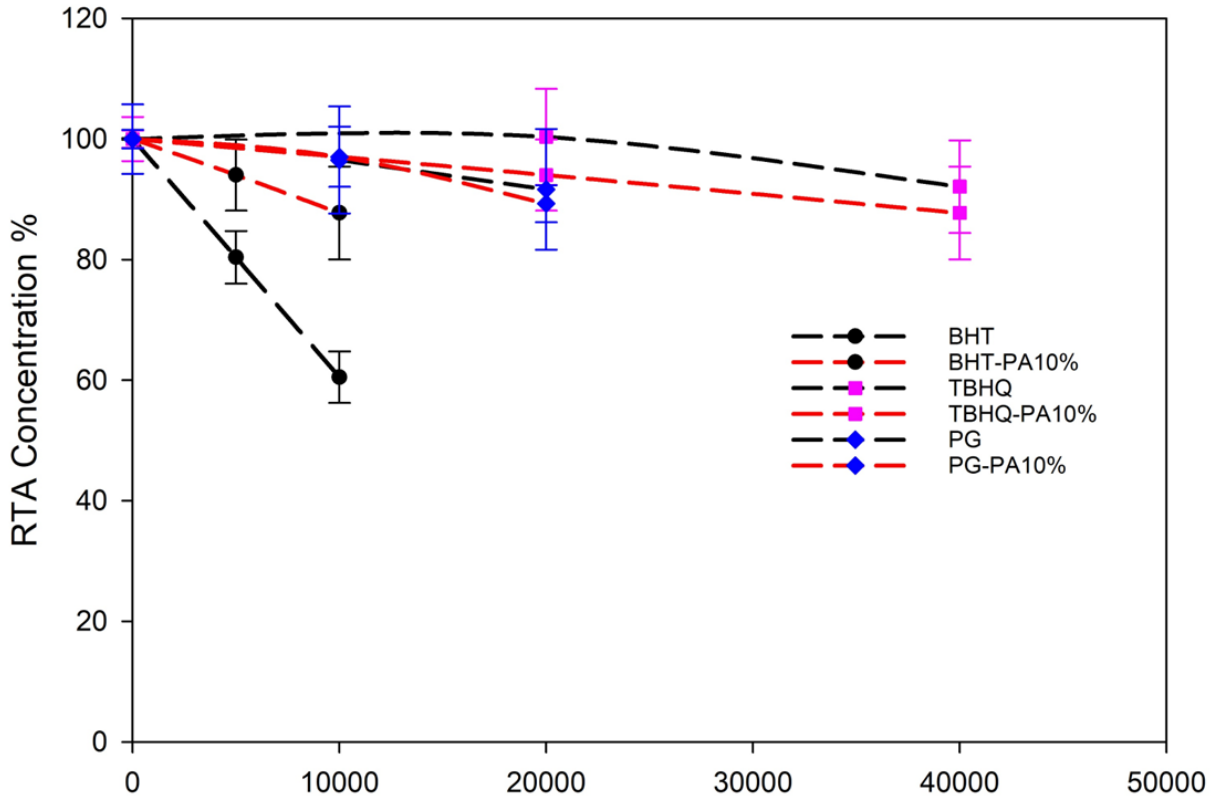

Figure 3.9 *Stability at 130 °C of selected phenols in triacetin under air. All the initial concentration is 0.5% w/w (BHT: 20.5 mM, PG: 26.5 mM and TBHQ: 27 mM).*

As shown in Figure 3.9, TBHQ and PG exhibited stable behavior, while the concentration of BHT decreased to 60% after 10 ks. With the addition of PA, their stability remained relatively high, while BHT was protected from decomposition. At the end of the reaction, TBHQ and PG showed decreases of 8% and 9%, respectively, while the addition of 10%

PA slightly increased their degradation to 12% and 11%. Therefore, the effect of PA on degradation can be considered negligible. The behavior of BHT differed from that of the other antioxidants, as upon addition of 10% PA, its degradation rate decreased significantly—from 40% to 17% after 10 ks. BHT is known to undergo degradation at high temperature under O_2. Although the mechanism is unclear, the high persistency of BHT radical may lead to its reaction with O_2 leading to BHT autoxidation. In this regard, the protective effect of PA might be due to the inhibition (i.e. by H-bonding effect) of this process.

3.4 Discussion

In the experiments, increasing PA concentrations (from 0% to 50%) progressively reduced IP in both HLS and HOS, with a more dramatic effect in HOS (from ~40 ks to ~4 ks) despite its inherent stability due to higher monounsaturated oleic acid content ($k_p \approx 1$ $M^{-1}s^{-1}$ vs. ~60 $M^{-1}s^{-1}$ for linoleate)[186]. ROOH measurements (Fig. 3.2E, F) showed elevated levels in PA-treated samples, confirming FFAs as pro-oxidants that amplify LP intermediates, which can further decompose into reactive species.[187]

The pro-oxidant activity is evidently linked to the carboxylic acid group, as methyl palmitate (PE) elicited negligible changes in IP or Rin (Fig. 3.3 A; Table A 3.4), suggesting esterification neutralizes this effect.

Overall, the results presented in this study highlight the significant pro-oxidant role of FFAs, such as PA and CA, in accelerating lipid peroxidation (LP) in sunflower oils with varying oleic acid content. LP is a radical-mediated chain reaction that degrades unsaturated fatty acids in lipids, leading to rancidity, reduced nutritional value, and potential health risks in food systems. It proceeds through three main stages: initiation, propagation and termination. In initiation, radicals are generated in the system by various processes, like the homolytic decomposition of peroxides or the hydrogen abstraction from allylic positions in polyunsaturated fatty acids (PUFAs) by O_2 to form HOO• and R•. In propagation, peroxyl radical (ROO•) are formed via reaction of R• with O_2, and ROO•

abstract an H-atom from bisallylic positions, with formation of hydroperoxide (ROOH) and new R•. In termination, radicals recombine. Antioxidants, including radical-trapping agents (RTAs) like tocopherols, butylated hydroxytoluene (BHT), propyl gallate (PG), and tert-butylhydroquinone (TBHQ), extend the induction period (IP) by scavenging ROO•, thereby inhibiting propagation.

Our findings demonstrate that FFAs disrupt this protective mechanism, shortening IP and elevating inhibited (R_{inh}) oxidation rates, as quantified by oxygen consumption kinetics (Fig. 3.3, 3.4, 3.5; Table A 3.3 and 3.4).

If considering the reaction mechanism described above, the FFA effect could derive from two distinct mechanisms: 1) acceleration of initiation, for instance by increasing ROOH decomposition; 2) antioxidant depletion, by inducing the degradation of antioxidants without significantly affecting the initiation step.

The study of the inhibited autoxidation of HLS or HOS cannot fully disentangle between these two mechanisms, because the depletion of the antioxidant can be caused by both mechanisms. However, if considering all findings together, some mechanistic insights can be derived.

1) A direct effect of FFA on antioxidants can be excluded because antioxidant stability under O_2 at 130 °C in an inert solvent with or without PA don't show any decomposition effect of FFA.
2) In HLS and HOS oxidation experiments, FFA (PA and CA) not only drastically reduce IP, but they also increase the oxidation rate in the absence of antioxidants Rox (see Figures 3.1 and 3.2).
3) The FFA effect is dependent on the nature of the antioxidants, as it decreases in the order TBHQ > PG > BHT, as shown in Fig 3.5. This may be due to the fact that BHT used alone is unstable and provides a small antioxidant effect (Fig. 3.9), while addition of FFA protects it from degradation.
4) When mixed to preformed hydroperoxides (CHP and OX-SHLS) FFA cause a larger decrease of IP, while in the case of peroxides (DCP) the effect is negligible, suggesting the involvement of hydroperoxides.

5) In the presence of epoxides, FFA have a larger effect,

All these observations can be reconciled by a mechanism which foresees the ability of FFA to increase the heterolytic decomposition of hydroperoxides.

We propose that under the condition considered herein, that are an organic media such as sunflower oil at relatively high temperature, FFA catalyze the formation of peroxyesters or hydroxy-peroxides from lipid-derived hydroperoxides and esters or epoxides, respectively (see Scheme 3.1). These reactions are well documented in organic chemistry, but their occurrence during oil oxidation is not demonstrated yet.

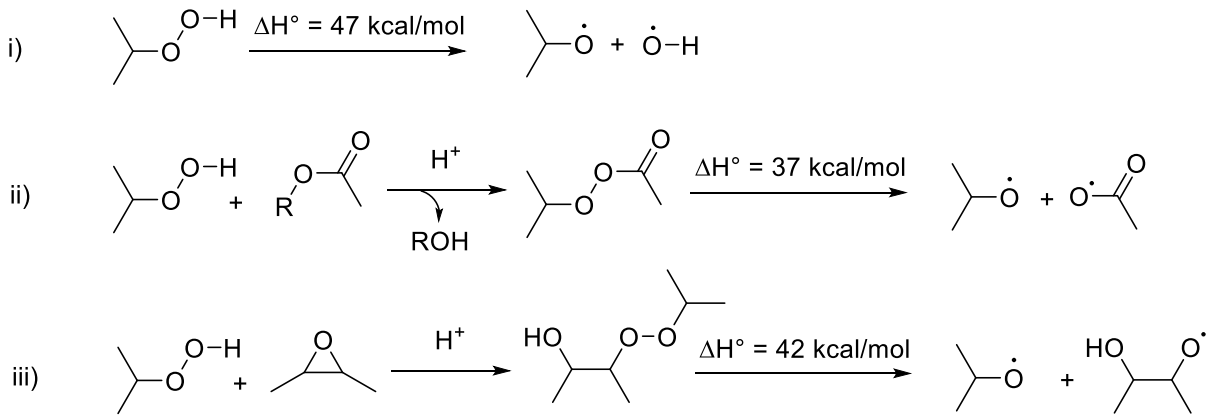

Scheme 3.1*, Possible Interaction Pathways Between FFAs and esters (ii) or epoxides (iii), with O-O BDE calculated at the CBS-QB3 level in the gas phase.*

Theoretical calculation at the CBS-QB3 level of the O-O bond dissociation enthalpy (BDE) shows that peroxyesters and hydroxy-peroxides have smaller BDE than lipid hydroperoxides, suggesting easier decomposition at high temperature.

3.5 Conclusion

This study conclusively demonstrates that free fatty acids (FFAs), such as palmitic acid (PA) and cinnamic acid (CA), act as potent pro-oxidants in accelerating lipid peroxidation (LP) in high linoleic sunflower oil (HLS) and high oleic sunflower oil (HOS), despite the latter's inherent oxidative stability due to its high monounsaturated oleic acid content. The

experimental results reveal that increasing FFA concentrations significantly shorten the induction period (IP), elevate inhibited (Rinh) oxygen consumption rates, and enhance the accumulation of hydroperoxides (ROOH), as evidenced by kinetic analyses and spectroscopic data from ^{1}H-NMR. The pro-oxidant effect is specifically attributed to the carboxylic acid group, as demonstrated by the negligible impact of PE, suggesting a mechanism involving acid-catalyzed decomposition of ROOH into reactive alkoxy (RO•) and hydroxyl (HO•) radicals in the presence of antioxidants. This effect is amplified in the presence of exogenous peroxides (e.g., CHP) and epoxides, which synergize with FFAs to further accelerate LP and facilitating antioxidant depletion.

Antioxidants like TBHQ, PG, and BHT mitigate LP by extending IP, but their efficacy is significantly diminished by FFAs, with polyphenolic RTAs (TBHQ, PG) showing greater susceptibility due to enhanced electron donation.

These findings have critical implications for the food industry, where FFAs accumulate during storage or high-temperature processing (e.g., baking or frying), undermining the oxidative stability of high-oleic oils and leading to rancidity, nutritional loss, and the formation of toxic LP products like malondialdehyde (MDA) and 4-hydroxynonenal (4-HNE). Our results show that strategies to enhance oil stability cannot rely on antioxidants, but should include refining to reduce FFA levels. From a health perspective, our results enlighten the role of acids in lowering the efficacy of antioxidants in apolar systems like membrane interior, that may be linked to oxidative stress-related diseases. Future studies are needed to fully clarify the effect of antioxidant structure on this process, as well as novel strategies to reduce the activity of free acids. For example, the possible activity of non-phenolic antioxidants like γ-terpinene will be investigated. Collectively, this work deepens the understanding of FFA-modulated LP, emphasizing the catalytic role of carboxylic acids in lipid degradation.

3.6 Experimental Section

3.6.1 Materials

High linoleic Sunflower oil (HLS) and high oleic Sunflower oil (HOS) were purchased from a local retail store and the Fatty acid composition was checked by H-NMR. Glyceryl Triacetate (GT) was purchased from Alfa Aesar (Germany). Palmitic acid (PA), Dicumyl Peroxide (DCP) and cinnamic acid (CA) were purchased from Thermo Scientific (USA). Cumene hydroperoxide (CHP) was purchased from FlukaTM (Germany). Butylated hydroxytoluene (BHT), propyl gallate (PG) and tert-Butylhydroquinone (TBHQ) was purchased from Sigma-Aldrich (Germany). Silica gel (100–200 mesh, 75–150 mL), activated charcoal (100–400 mesh), Ferrous sulfate ($FeSO_4*7H_2O$), Potassium thiocyanate (KSCN), hydrochloric acid, sulfuric acid and sodium hydroxide were purchased from Sigma-Aldrich (Germany). Aluminum oxide was purchased from Sigma-Aldrich (Switzerland). Tert-butyl hydroperoxide (t-BuOOH) 70% aqueous solution was purchased from Sigma-Aldrich (USA). Methanol (MeOH), n-hexane, water (H_2O) were purchased from Sigma-Aldrich (Germany).

3.6.2 Methods

3.6.2.1 General procedure for autoxidation experiment

Autoxidation experiments of sunflower oil were performed in a sealed system by using an oxygen-sensitive optical sensor (Pyroscience GmbH, Aachen, Germany), as previously reported[180]. In general, 0.2 g of oil, palmitic or cinnamic acids and the antioxidants were placed into a 5 mL round-bottom flask equipped with a magnetic stir bar. Triacetin was used to keep constant the total weigh to 0.4 g. The flask was connected to a compact, water-cooled condenser to maintain the temperature of the oxygen sensor below 40 °C, with the total internal volume of the setup being 14.5 mL. The oil sample was stirred vigorously and heated in a silicone bath at 130 °C. Prior to each experiment, the oxygen probe was calibrated in air. Oxygen consumption was determined based on the internal volume of the apparatus.

3.6.2.2 Preparation of Stripped High linoleic Sunflower oil

High linoleic sunflower oil (HLS) was purified using a method adapted from previous studies.[26,188] In short, 150 mL of the oil was mixed with 300 mL of cyclohexane and washed twice with 250 mL of 0.1 M sodium hydroxide at room temperature. The resulting organic phase was dried over anhydrous magnesium sulfate and then passed through a column packed with basic alumina and silica gel. Subsequently, three spoonfuls of activated charcoal were added to the organic solution. After filtration, the solvent was completely removed under high vacuum. Following this purification process, the SHLS exhibited immediate autoxidation without a lag phase. The degree of purification of stripped oil was determined through General procedure for autoxidation experiment 2.2.1. The results should not exhibit an antioxidant inhibition period.

3.6.2.3 The procedure of Autoxidation experiments in different unsaturated rate

Autoxidation experiments of sunflower oil was performed both in sealed system by using an oxygen-sensitive optical sensor (Pyroscience GmbH, Aachen, Germany), as previously reported[180]. Different unsaturated rate sunflower oil was conducted following the Table A 3.5. In general, 0.4 g of oil samples was placed in a 5 mL round bottom flask with a magnetic stir bar. The flask was connected to a compact, water-cooled condenser to maintain the temperature of the oxygen sensor below 40 °C, with the total internal volume of the setup being 14.5 mL. The oil sample was stirred vigorously and heated in a silicone bath at 130 °C. Prior to each experiment, the oxygen probe was calibrated in air. Oxygen consumption was determined based on the internal volume of the apparatus.

3.6.2.4 The procedure of Autoxidation experiments in different oxygen rate

Autoxidation experiments of sunflower oil was performed both in sealed system by using an oxygen-sensitive optical sensor (Pyroscience GmbH, Aachen, Germany), as previously reported[180]. Different oxygen rate was conducted following the Table A 3.6. The procedure was followed by section *3.6.2.3*.

3.6.2.5 Determination of hydroperoxide

The concentration of hydroperoxides was quantified using the ferric thiocyanate assay, employing tert-butyl hydroperoxide as the reference standard. Equal volumes (250 µL) of a 5 mM solution of ferrous sulfate heptahydrate ($FeSO_4 \cdot 7H_2O$) in 0.02 M hydrochloric acid and a 3% (w/v) solution of potassium thiocyanate (KSCN) in methanol were added to 1 mL of the test sample or standard, both prepared in methanol. Following a one-minute reaction period, the absorbance was measured at 520 nm.[189]

3.6.2.6 Statistical Analysis

The results are expressed as the average ± standard deviation (SD) from at least two independent kinetic measurements.

3.6.2.7 Stability of antioxidants analysis

The experimental procedure was conducted in accordance with Section 3.6.2.3. Selected antioxidants (0.5% w/w) were dissolved in triacetin (0.4 g), an oxidation-resistant triacylglycerol devoid of unsaturations, and subsequently introduced into the same reactor employed for the peroxidation experiments at 130 °C. The concentration of each antioxidant was quantified by HPLC at predetermined time intervals corresponding to the inhibition period characteristic of each compound.

3.6.2.8 Characterization method

^{1}H-NMR (400 MHz) and ^{13}C-NMR (100 MHz) spectra were performed by Bruke. FT-IR spectra were recorded on an Agilent Technologies Cary 630 FT-IR instrument over the range of 4000−400 cm^{-1}. HPLC were performed by Agilent 1260 infinity ii. Which mobile phase A and B is separately Water and ACN.

3.6.2.9 Kinetic analysis by COPASI software

See Appendix 3.7.1.

3.6.2.10 Synthesis section

The procedure to synthesis *methyl palmitate (PE)*

To a solution of palmitic acid (5.57g, 20 mmol) in methanol (50 ml), H_2SO_4 (concentrated 98% w/w, 1.5 mL) was added dropwise in a 250 ml round bottom flask and the mixture was refluxed for 5h. The mixture was cooled down and a saturated solution of $NaHCO_3$ was added to pH = 7. Then, the resulting aqueous solution was washed with dichloromethane (3 x 20 mL) and the organic phase was dried, evaporated under vacuum and the residue was used in the next step without purification. Colourless oil (5.13g, 88% yield).^{1}H-NMR, δ_H (ppm): 3.66 (s, 3H), 2.30 (t, J = 7.8 Hz, 2H); 1.62 (m, 2H), 1.28 (m, 24H), 0.88 (t, J = 7.8 Hz, 3H). ^{13}C-NMR, δ_C(ppm): 174.13, 51.4, 34.2-22.8, 14.1. MS(DIP) m/z: 270(M^+, 100%). HRMS required for $C_{17}H_{34}O_2$ requires: 270.2559; found: 270.2555.

The procedure to synthesis *methyl oleate epoxide (ME)*

Methyl cis-9,10-epoxyoctadecanoate. mCPBA (1.52 g, 8.8 mmol) was added in small portions to a solution of methyl cis-9-octadecenoate (methyl oleate) (2.00 g, 6.8 mmol) in DCM (50 ml) at 0 ºC under a N_2 atmosphere. The reaction mixture was stirred for 21 h at room temperature, cooled to 0 ºC, and then quenched with a 20 % $Na_2S_2O_3$ solution. The mixture was stirred for 2h, and then the organic products were extracted into DCM (3x30 ml). The combined organic layers were washed with a 15 % NaOH (3x30 ml) and water (3x30 ml). Drying over $MgSO_4$ and concentration under reduced pressure gave the ME (3.55 g, 84 %) as clear oil. ^{1}H NMR d ($CDCl_3$): 3.60 (3H, s), 2.83 (2H, m), 2.23 (2H, t, J = 7.3 Hz), 1.12-1.62 (26H, m), 0.81 (3H, t, J = 7.0 Hz).

3.7 Appendix

3.7.1 Kinetic analysis of COPASI software

The numerical modeling of some representative O_2 consumption traces were performedby using a kinetic simulation software (Copasi). [190] This software was used previously in other studies by us and by other research groups to analyze the autoxidation kinetics [191,192] We used the species and equation reported below table A 3.1 and table A 3.2 in addition to those describing the autoxidation of linoleic acid.

Table A 3.1 Species considered in numerical fitting of the autoxidation of High linoleic sunflower oil at 130 °C.

Chemical Name	Symbol used in equations	Initial concentration
R	Linoleic alkyl radical	0
ROO	Linoleic peroxyl radicals	0
RH	Linoleic Acid	1.03
ROOH	Linoleic polyperoxide or hydroperoxide	0
P	Non radical product	0
O2G	Dissolved O2 in Gas	0.0091
O2L	Dissolved O2 in Liquid	0.002
Q	1,4-di-tert-butyl ortho quinone	0
Q1	1,4-di-tert-butyl-1,4-benzoquinone	0
QH2	1,4-di-tert-butyl catechol	0.0024
QH	Radical from 1,4-di-tert-butyl catechol	0

Table A 3.2 Kinetic scheme of the autoxidation of High linoleic sunflower oil at 130°C.

N	Reaction Equations	Rate Constants ($m^{-1}s^{-1}$) or Fluxes	Notes and references
1	RH+O2L -> R+ROO	0.000127457	Initiation
2	R+O2L -> ROO	2e9	React with O2
3	ROO+RH -> R+ROOH	427.355	Propagation
4	2*ROOH -> P	1e8	Termination
5	ROO+QH2 -> QH+ROOH	120920	Inhibition 1
6	ROO+QH -> Q+ROOH	1e8	Inhibition 2
7	O2L = Q2G	k1 = 9e5, k2 = 2e5	equilibrium liq-gas
8	2*Q -> QH2+Q1	1e8	Inhibition 3

3.7.2 Additional Schemes and Figures

Table A 3.3 Descriptors of High Oleic (HOS) and High Linoleic (HLS) Sunflower Oil Autoxidation at 130 °C: Slope of O_2 Consumption during the Inhibited Period (Rin) or in the Absence of the Antioxidant (R_{ox}), and Duration of the Inhibited Period (τ)

Entry		Rin (nM/s)	R_{ox} (µM/s)	τ (1000 s)
1	HLS	171±18	6.2±0.2	6.1±0.1
2	HLS + PE 10%	158±19	4.8±0.2	5.7±0.3
3	HLS + PA 10%	200±84	5.6±0.1	5.0±0.4
4	HLS + CA 10%	678±90	4.6±0.1	2.0±0.1
5	HLS + ME 1%	298±50	2.4±0.3	5.7±0.1
6	HLS + OX_SSO 0.2%	330±100	5.3±0.6	5.0±0.4
7	HLS + PA 10% + OX_SSO 0.2%	520±80	6.4±0.2	3.0±0.4
8	HLS + ME 1% + PA 10%	1000±200	6.4±0.3	1.9±0.1
9	HLS 50% + GT 50%	50.1±10	1.4±0.8	10.4±0.5
10	HLS 50% + GT 49% + PA 1%	135.2±50	1.1±0.5	7.9±0.1

11	HLS 50% + GT 40% + PA 10%	44.0±5	2.3±0.3	6.2±0.3
12	HLS 50% + GT 25% + PA 25%	102±1	4.1±0.6	5.4±0.2
13	HLS 50% + PA 50%	95.8±12	2.2±0.6	4.6±0.5
14	HOS	24.2±0.7	1.5±0.1	19.7±0.3
15	HOS + PE 10%	21.5±0.9	1.5±0.2	21.0±0.5
16	HOS + PA 10%	53.4±0.6	1.6±0.1	11.1±0.3
17	HOS + ME 1%	10.3±2.1	1.4±0.1	21.5±0.1
15	HOS + CHP 0.4%	28.8±0.6	1.8±0.2	12.6±0.3
16	HOS + DCP 0.4%	87.5±1.5	2.2±0.3	2.5±0.1
17	HOS + CHP 0.4% + PA 10%	59.2±1	1.8±0.1	7.1±0.1
18	HOS + DCP 0.4% + PA 10%	56.3±1	2.0±0.4	2.9±0.8
19	HOS + ME 1% + PA 10%	17.3±4	1.6±0.1	5.2±0.1
20	HOS 50% + GT 50%	9.6±4	0.5±0.2	39.6±2.4
21	HOS 50% + GT 49% + PA 1%	15.6±0.9	0.8±0.3	34.1±2.1
22	HOS 50% + GT 40% + PA 10%	7.8±0.1	1.2±0.1	20.6±1.6
23	HOS 50% + GT 25% + PA 25%	4.8±0.2	1.5±0.1	17.6±1.0
24	HOS 50% + PA 50%	10.0±0.2	2.0±0.1	3.0±0.7

Table A 3.4 Descriptors of Strip Sunflower Oil Autoxidation at 130 °C: Slope of O_2 Consumption during the Inhibited Period (Rin) or in the Absence of the Antioxidant (R_{ox}), and Duration of the Inhibited Period (τ)

Entry		**R_{in} (nM/s)**	**R_{ox} (µM/s)**	**τ (1000 s)**
1	SHLS		2.5±0.4	
2	SHLS + BHT 0.1%	35.5±15	2.5±0.3	8.5±0.1
3	SHLS + TBHQ 0.1%	4.8±3	1.6±0.1	39.1±4.4
4	SHLS + PG 0.1%	26.7±0.1	2.0±0.5	18.5±0.5
5	SHLS + BHT 0.1% & PA 10%	153±43	2.4±0.7	6.1±0.4

6	SHLS + TBHQ 0.1% & PA 10%	33.8±7	1.2±0.3	13.7±0.7
7	SHLS + PG 0.1% & PA 10%	291±54	2.3±0.5	5.5±0.3
8	SHLS + BHT 0.1% & CA 10%	115±10	1.2±0.1	5.4±0.1
9	SHLS + TBHQ 0.1% & CA 10%		5.3±0.7	
10	SHLS + PG 0.1% & CA 10%		3.4±0.1	1.2±0.1
11	SHLS 50% + GT 50%		2.4±0.2	
12	SHLS 50% + GT 50% + TBHQ 0.1%	14.8±2	2.0±0.2	45.3±0.3
13	SHLS 50% + GT 40% + TBHQ 0.1% + PA 10%	44.4±10	1.8±0.2	16.2±0.2
14	SHLS 50% + TBHQ 0.1% + PA 50%		5.6±0.2	

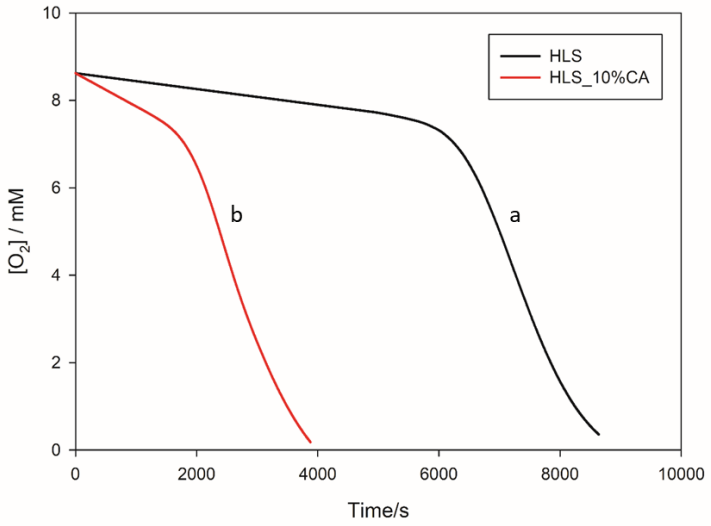

Figure A 3.1, *oxygen consumption during the oxidation of High Linoleic oil (HLS, 0.4 g) at 130 °C (a); HLS 0.4 g, CA 0.1% (w/w) (b).*

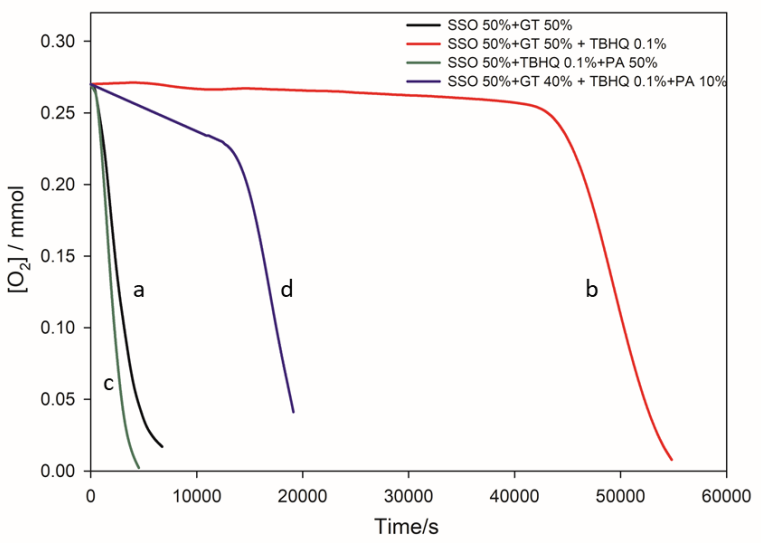

Figure A 3.2, *oxygen consumption during the oxidation of Stripped high linolenic sunflower oil (SHLS, 0.2 g) and GT (0.2 g) at 130 °C (a); SHLS 0.2 g, GT 0.2 g, TBHQ 0.1%(w/w) (b); SHLS 0.2 g, TBHQ 0.1%(w/w), PA 0.2 g (c); SHLS 0.2 g, GT 0.1 g, PA 0.1 g, TBHQ 0.1%(w/w) (d).*

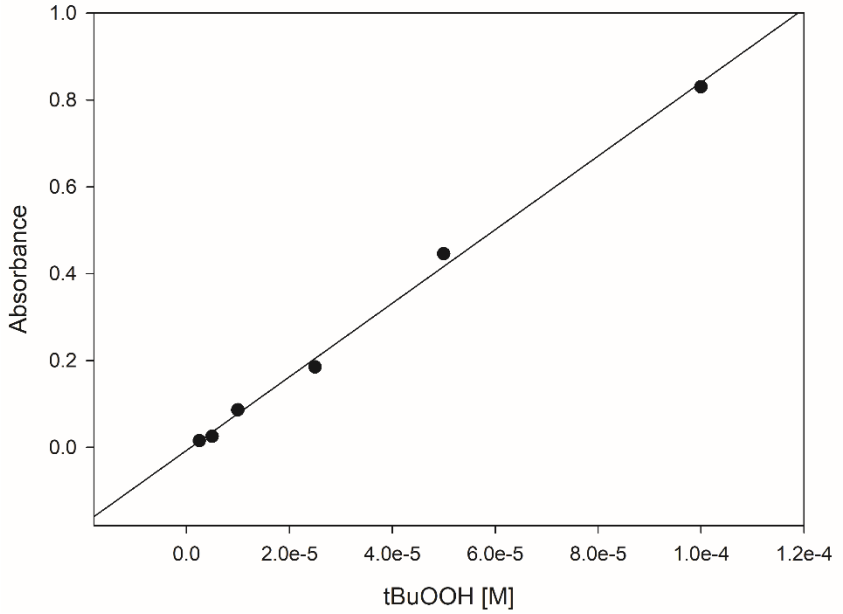

Figure A 3.3, *The standard relation of Absorbance and hydroperoxide. Which equation is Abs=8474.0091*[ROOH]-6.9744E-03.*

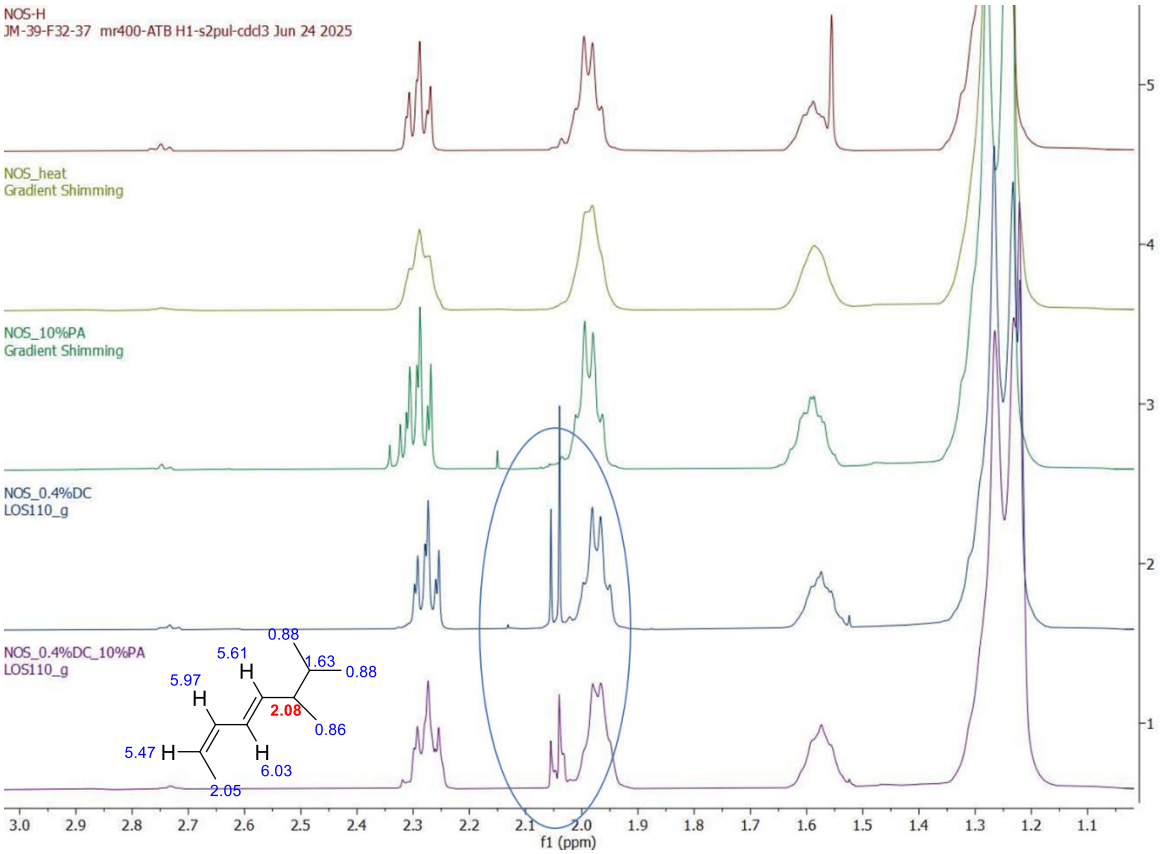

Figure A 3.4, *The comparison of all samples*

3.7.3 NMR Spectra

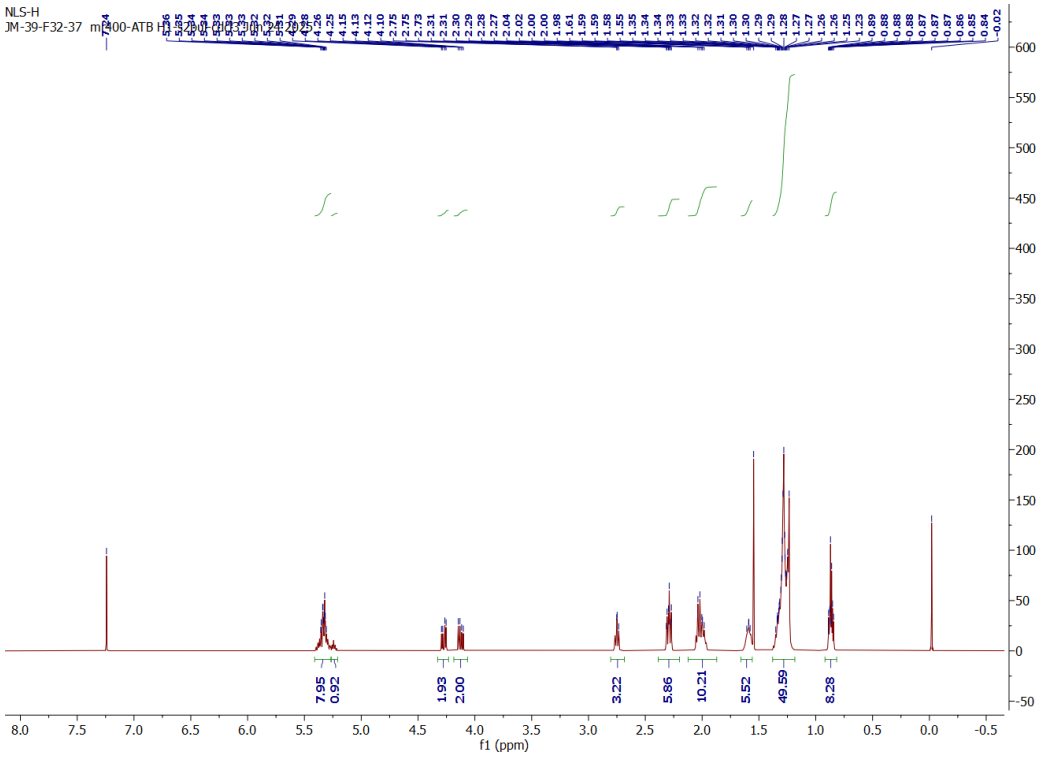

Figure A 3.5, *^{1}H-NMR spectra of HLS*

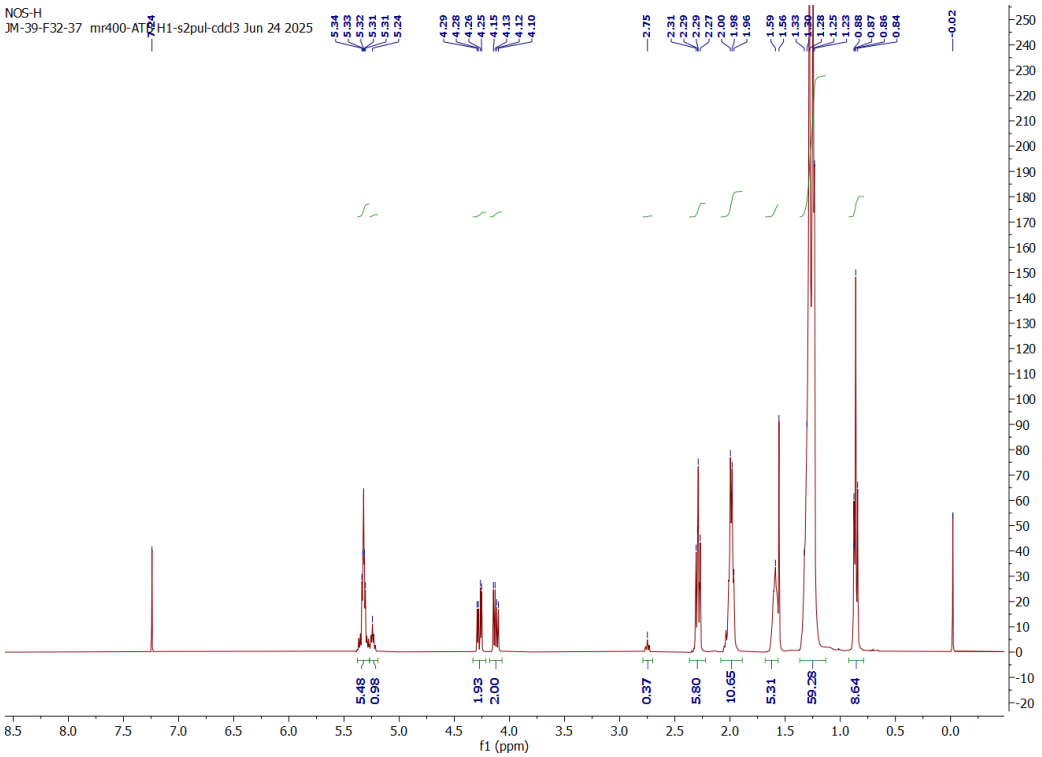

Figure A 3.6, *^{1}H-NMR spectra of HOS*

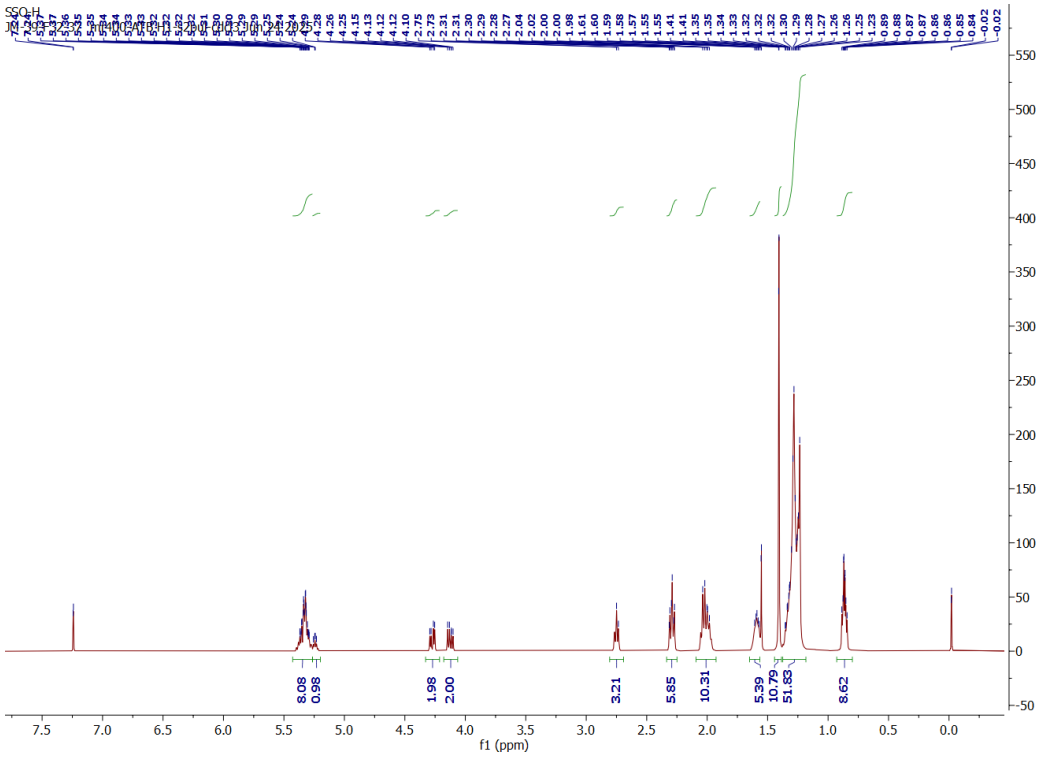

Figure A 3.7, *^{1}H-NMR spectra of SHLS*

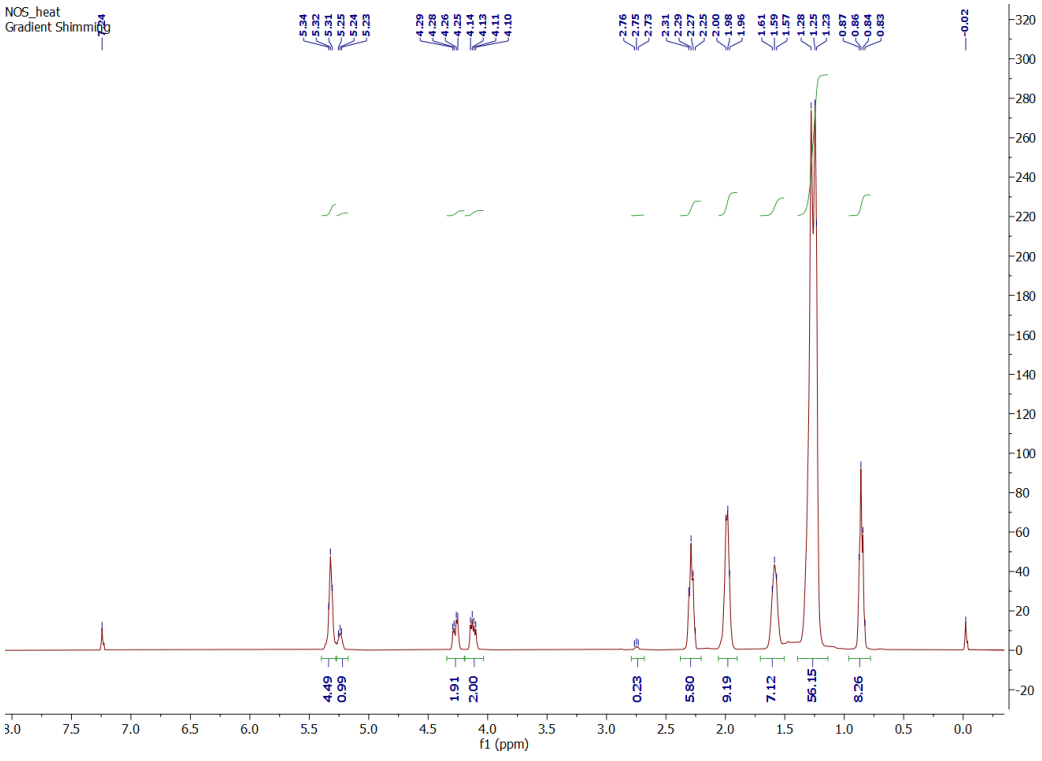

Figure A 3.8, *^{1}H-NMR spectra of HOS_heat*

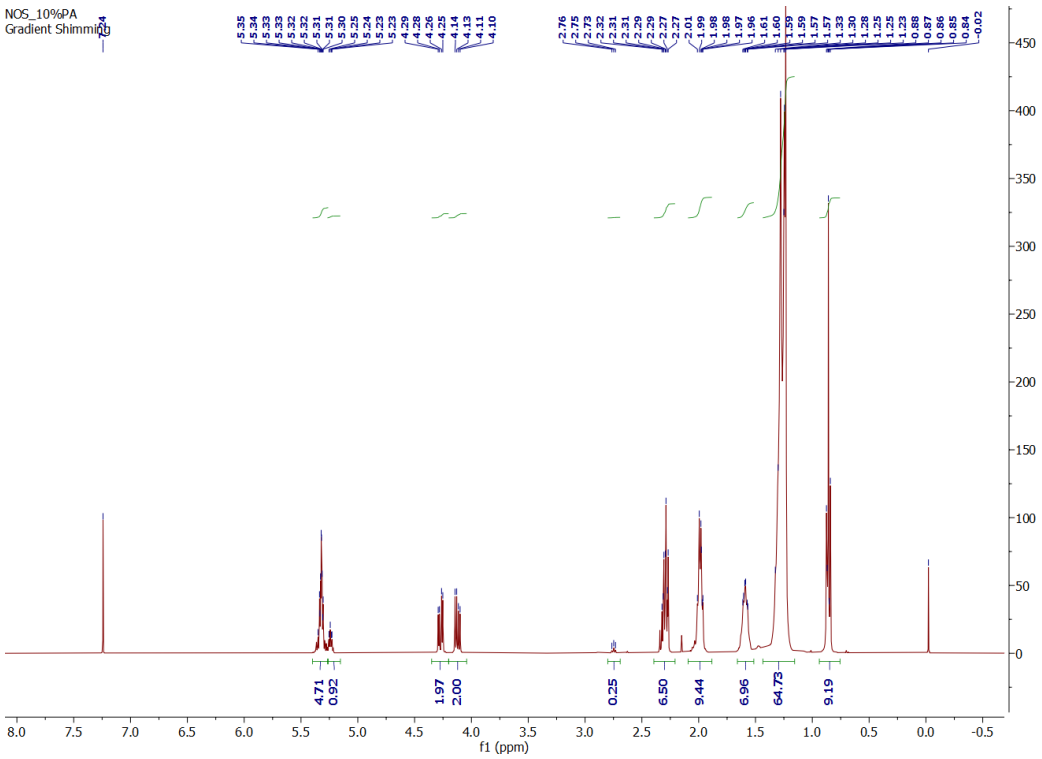

Figure A 3.9, *[1]H-NMR spectra of HOS_10%PA*

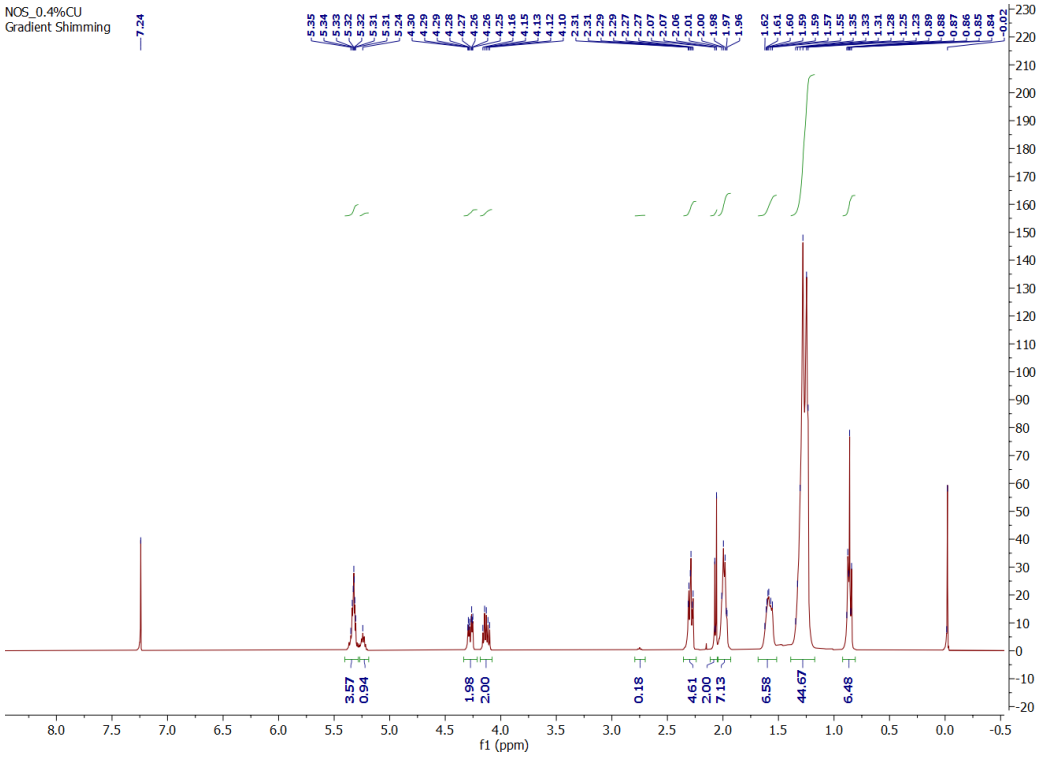

Figure A 3.10, *[1]H-NMR spectra of HOS_0.4%CHP*

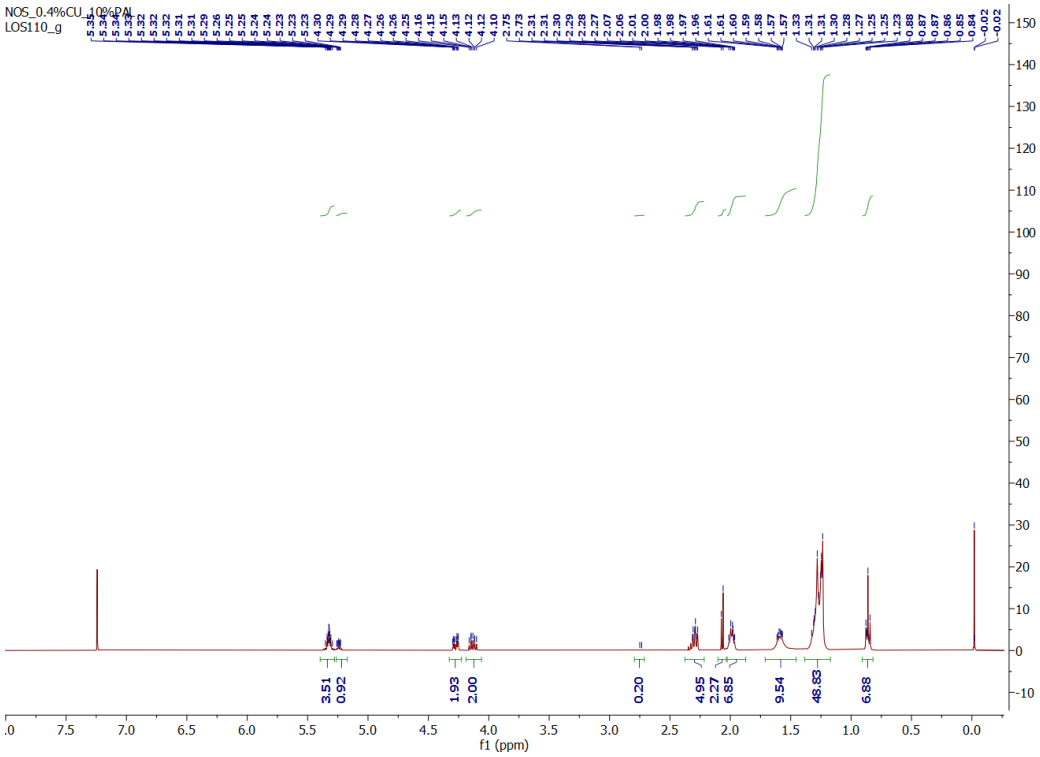

Figure A 3.11, *1H-NMR spectra of HOS_0.4%CHP_10%PA*

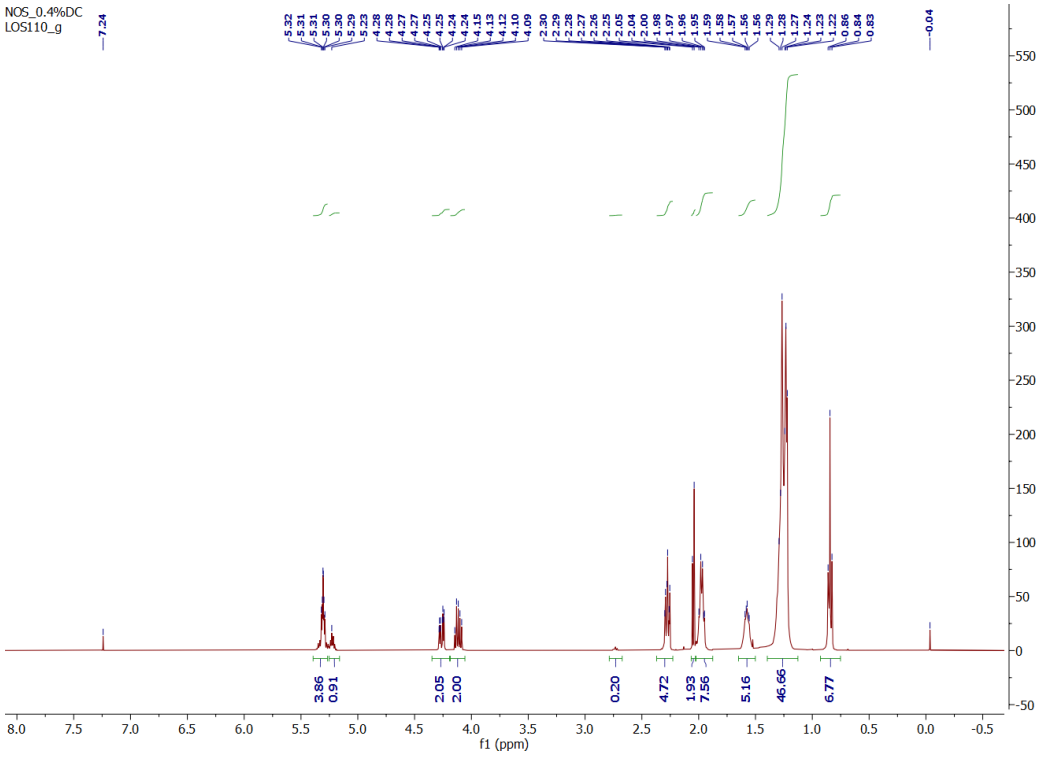

Figure A 3.12, *[1]H-NMR spectra of HOS_0.4%DCP*

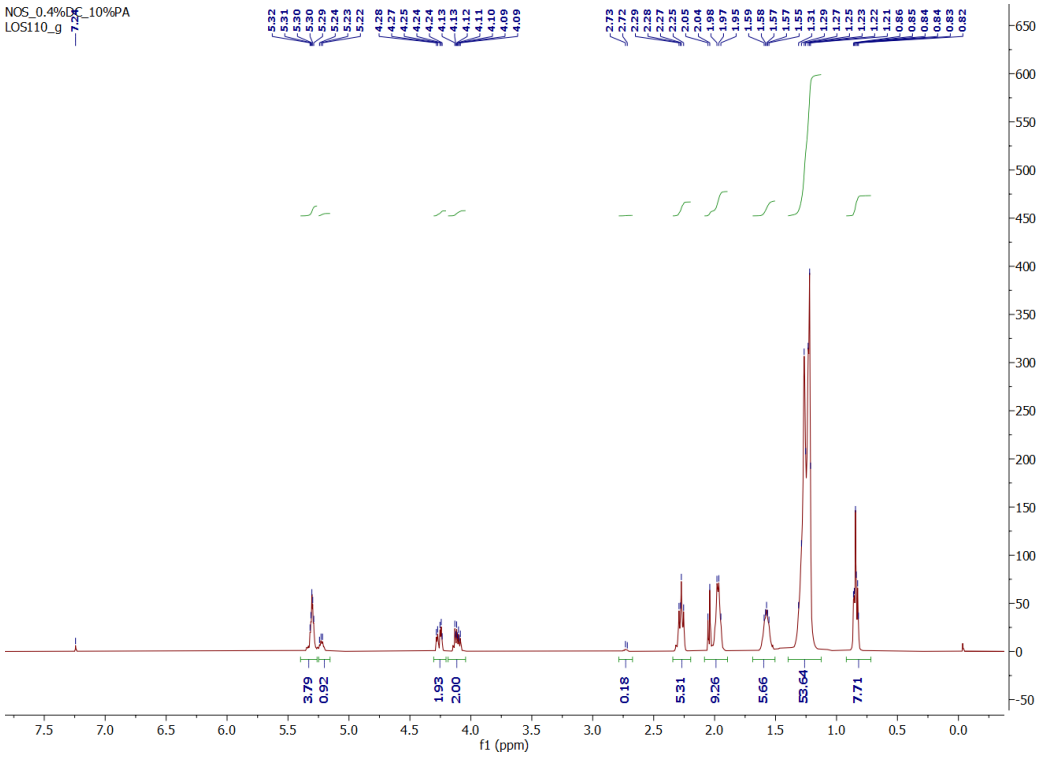

Figure A 3.13, *[1]H-NMR spectra of HOS_0.4%DCP_10%PA*

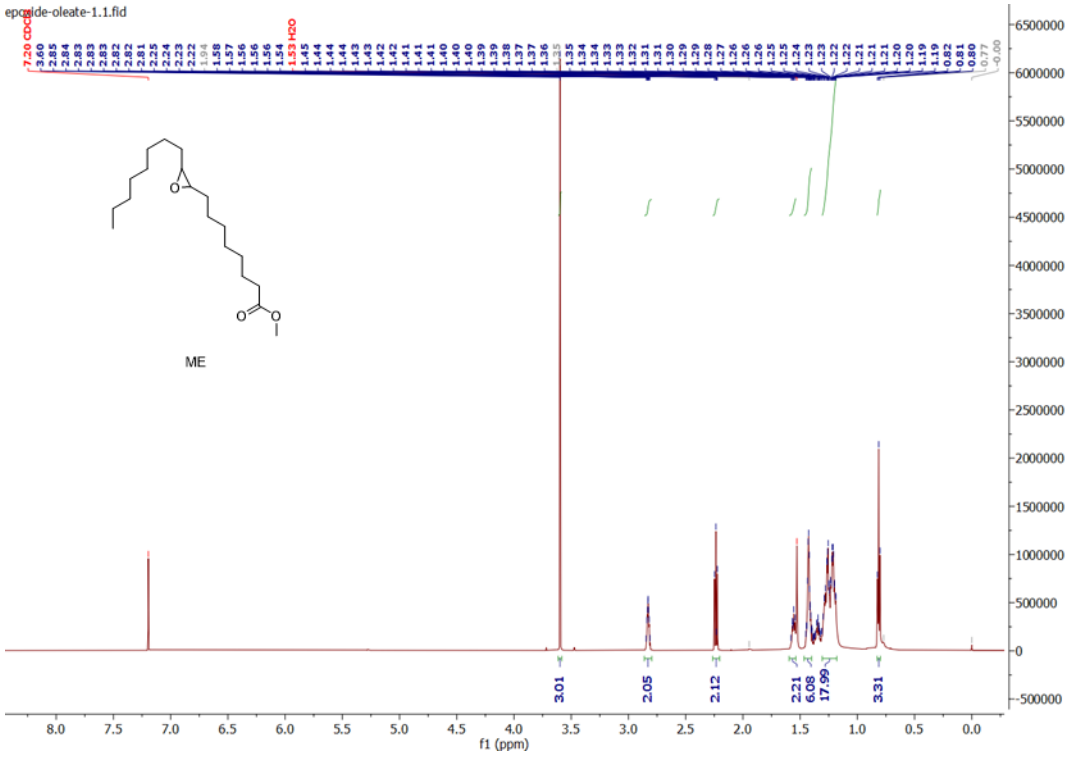

Figure A 3.14, *[1]H-NMR spectra of ME*

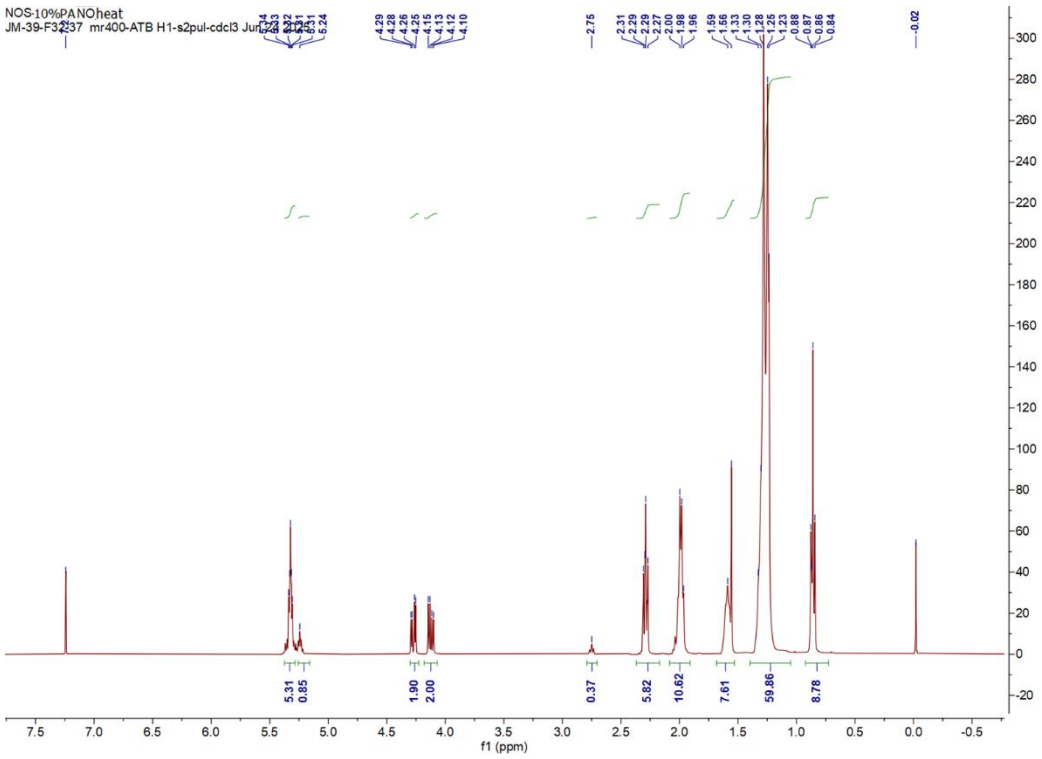

Figure A 3.15, *^{1}H-NMR spectra of HOS_10% PA without heating*

3.7.4 HPLC Spectra

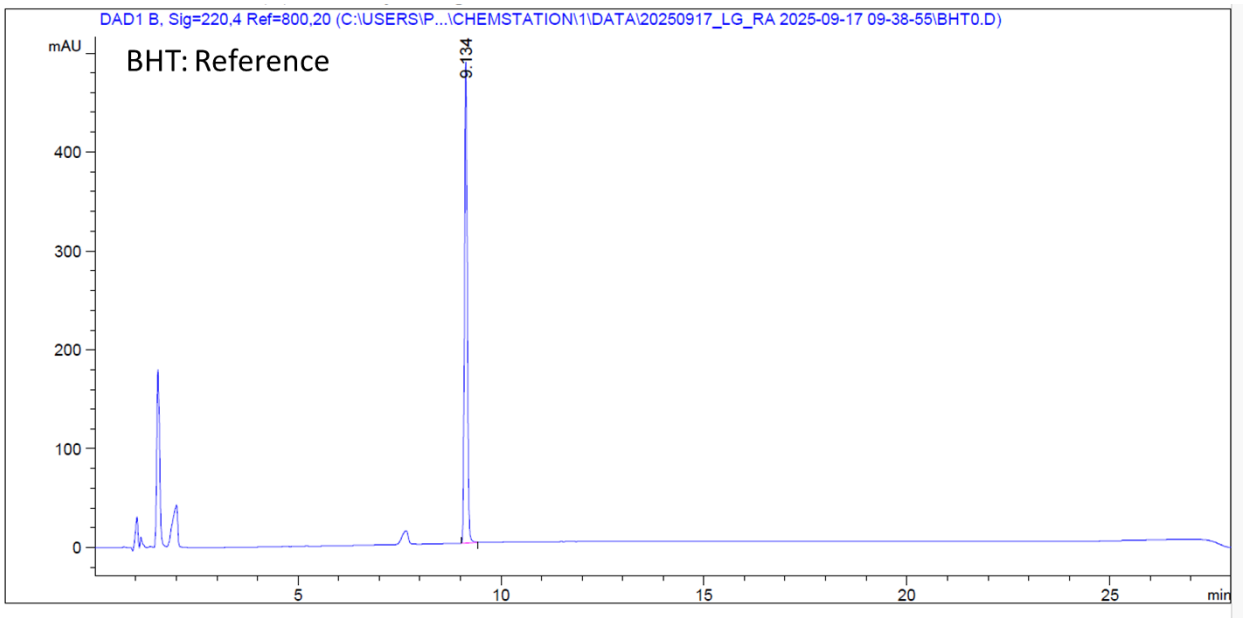

Figure A 3.16, *HPLC spectra of BHT reference*

Table A 3.5 HPLC result of BHT.

Sample Name	Condition	Area (mAU*s)
BHT0	BHT	*
BHT1	BHT (0.5% w/w) in GT_1	183.7350
BHT2	BHT (0.5% w/w) in GT_2	183.1608
BHT3	BHT (0.5% w/w) in GT_1 T=5 ks	155.4239
BHT4	BHT (0.5% w/w) in GT_2 T=5 ks	139.4491
BHT5	BHT (0.5% w/w) in GT_1 T=10 ks	103.3110
BHT6	BHT (0.5% w/w) in GT_2 T=10 ks	118.9725
BHT7	BHT (0.5% w/w) + PA (10% w/w) in GT_1	156.5651
BHT8	BHT (0.5% w/w) + PA (10% w/w) in GT_2	168.6854
BHT9	BHT (0.5% w/w) + PA (10% w/w) in GT_1 T=5 ks	143.8449
BHT10	BHT (0.5% w/w) + PA (10% w/w) in GT_2 T=5 ks	153.9117
BHT11	BHT (0.5% w/w) + PA (10% w/w) in GT_1 T=10 ks	138.8028
BHT12	BHT (0.5% w/w) + PA (10% w/w) in GT_2 T=10 ks	132.8538

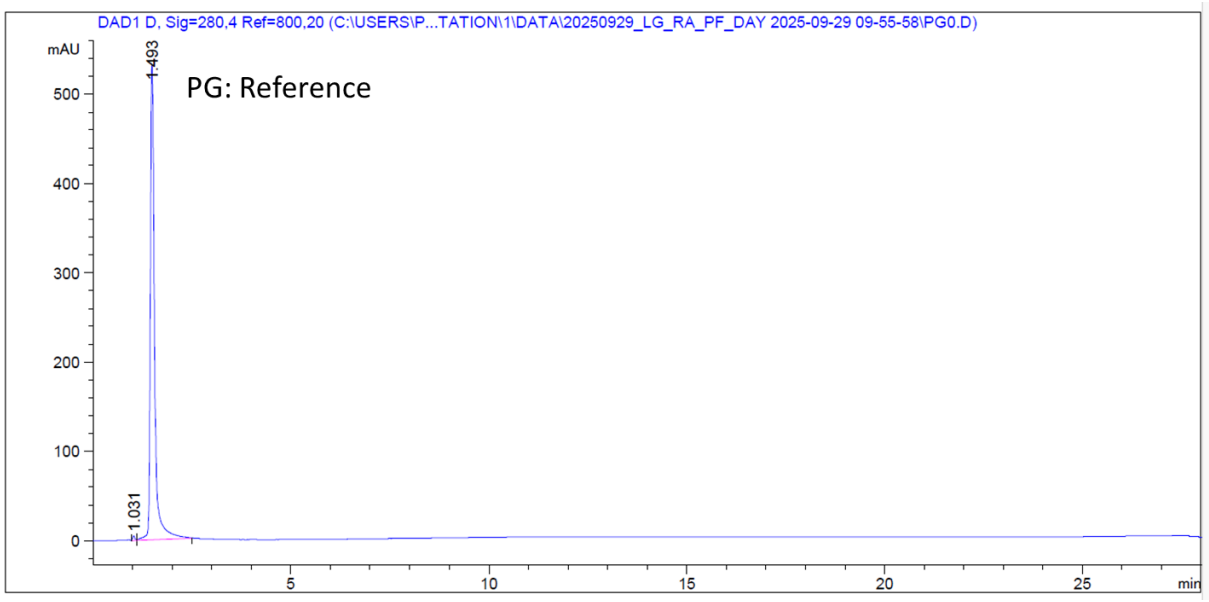

Figure A 3.17, *HPLC spectra of PG reference*

Table A 3.6 HPLC result of PG.

Sample Name	**Condition**	**Area (mAU*s)**
PG0	PG	*
PG1	PG (0.5% w/w) in GT_1	31.2303
PG2	PG (0.5% w/w) in GT_2	39.3609
PG3	PG (0.5% w/w) in GT_1 T=10 ks	27.7956
PG4	PG (0.5% w/w) in GT_2 T=10 ks	40.3464
PG5	PG (0.5% w/w) in GT_1 T=20 ks	39.4293
PG6	PG (0.5% w/w) in GT_2 T=20 ks	25.2752
PG7	PG (0.5% w/w) + PA (10% w/w) in GT_1	44.6125
PG8	PG (0.5% w/w) + PA (10% w/w) in GT_2	43.2496
PG9	PG (0.5% w/w) + PA (10% w/w) in GT_1 T=10 ks	45.0273
PG10	PG (0.5% w/w) + PA (10% w/w) in GT_2 T=10 ks	40.6436

PG11	PG (0.5% w/w) + PA (10% w/w) in GT_1 T=20 ks	40.5726
PG12	PG (0.5% w/w) + PA (10% w/w) in GT_2 T=20 ks	37.8735

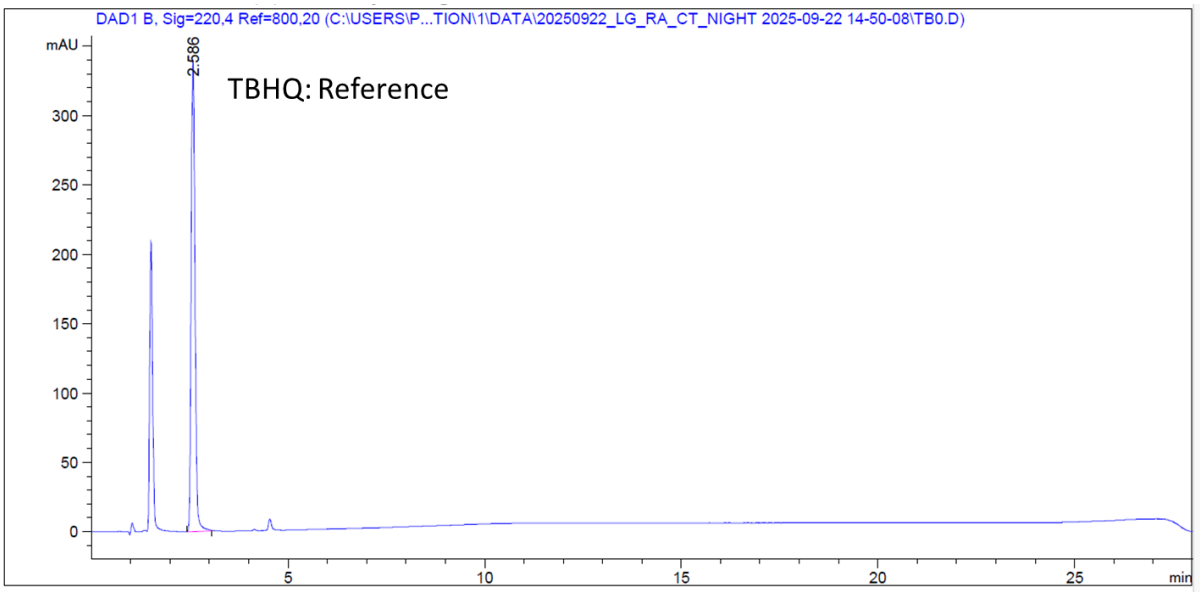

Figure A 3.28, *HPLC spectra of TBHQ reference*

Table A 3.7 HPLC result of TBHQ.

Sample Name	Condition	Area (mAU*s)
TB0	TBHQ	*
TB1	TBHQ (0.5% w/w) in GT_1	277.7754
TB2	TBHQ (0.5% w/w) in GT_2	298.8200
TB3	TBHQ (0.5% w/w) in GT_1 T=20 ks	251.9164
TB4	TBHQ (0.5% w/w) in GT_2 T=20 ks	326.7646
TB5	TBHQ (0.5% w/w) in GT_1 T=40 ks	243.4107
TB6	TBHQ (0.5% w/w) in GT_2 T=40 ks	287.6523
TB7	TBHQ (0.5% w/w) + PA (10% w/w) in GT_1	260.8119

TB8	TBHQ (0.5% w/w) + PA (10% w/w) in GT_2	268.1970
TB9	TBHQ (0.5% w/w) + PA (10% w/w) in GT_1 T=20 ks	230.5407
TB10	TBHQ (0.5% w/w) + PA (10% w/w) in GT_2 T=20 ks	261.7454
TB11	TBHQ (0.5% w/w) + PA (10% w/w) in GT_1 T=40 ks	252.4641
TB12	TBHQ (0.5% w/w) + PA (10% w/w) in GT_2 T=40 ks	211.7343

3.7.5 Theoretical Calculation at CBS-QB3 level

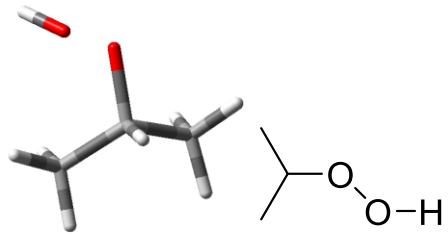

CBS-QB3 Enthalpy= -269.049876 CBS-QB3 Free Energy= -269.087204

0 1

C 0.41103800 0.01554400 -0.33459000

H 0.23491500 -0.04375800 -1.41509200

C 1.66487100 -0.77079400 0.02968100

H 2.53781400 -0.32514100 -0.45296400

H 1.82564300 -0.75985600 1.11093400

H 1.57579800 -1.80829600 -0.29700600

C 0.46016900 1.47514900 0.10410400

H 1.26272600 2.00672500 -0.41460700

H -0.48146600 1.97420100 -0.13019000

H 0.63934500 1.54466800 1.18125200

O -0.65136100 -0.69955200 0.31813600

O -1.91291700 -0.18495500 -0.19289100

H -2.29701900 0.16812200 0.62054900

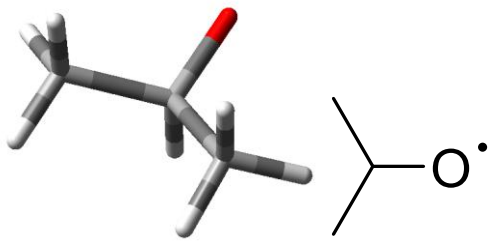

CBS-QB3 Enthalpy= -193.328524 CBS-QB3 Free Energy= -193.362666

0 2

C 0.00000000 0.12356000 0.29424600

H -0.00000100 0.26439200 1.39989700

C 1.28860800 -0.62695700 -0.07789900

H 1.32721300 -1.60962300 0.39956900

H 1.33497800 -0.77178400 -1.16081300

H 2.16150300 -0.04836900 0.22875300

C -1.28860500 -0.62696100 -0.07789900

H -1.32720800 -1.60962600 0.39957100

H -2.16150200 -0.04837500 0.22875100

H -1.33497400 -0.77179100 -1.16081200

O -0.00000300 1.42216500 -0.14570100

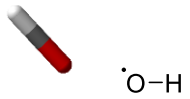

CBS-QB3 Enthalpy= -75.646408 CBS-QB3 Free Energy= -75.666640

0 2

O 0.00000000 0.00000000 0.10835600

H 0.00000000 0.00000000 -0.86685200

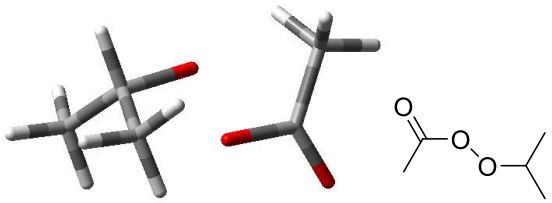

CBS-QB3 Enthalpy= -421.476087 CBS-QB3 Free Energy= -421.523290

0 1

C 1.77202400 -0.27156100 0.00039200

C 2.25585300 1.15178500 -0.00183900

H 1.88036200 1.68305400 0.87442200

H 3.34350100 1.13666400 -0.00163000

H 1.88066400 1.68021000 -0.87995100

O 2.45616500 -1.25581600 0.00224700

O 0.41504600 -0.48193000 0.00036900

O -0.33266900 0.78673800 -0.00206100

C -1.73133500 0.43837100 -0.00079100

H -2.16454000 1.44570000 -0.00279100

C -2.13284800 -0.28452900 1.28100800

H -3.21953700 -0.39534600 1.32359700

H -1.68347500 -1.27792300 1.32359400

H -1.80911200 0.28263300 2.15622100

C -2.13378700 -0.29001700 -1.27918500

H -3.22050400 -0.40105800 -1.32048500

H -1.81072600 0.27340900 -2.15705500

H -1.68440700 -1.28356800 -1.31786400

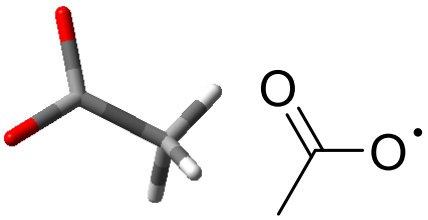

CBS-QB3 Enthalpy= -228.088540 CBS-QB3 Free Energy= -228.119740

0 2

C -0.10603500 0.00259300 -0.00000300

C 1.38755200 0.00867400 0.00000000

H 1.75230000 -0.51967800 0.88385500

H 1.75229800 -0.51982000 -0.88377100

H 1.76082700 1.03325400 -0.00008100

O -0.80256700 -1.04479700 0.00000100

O -0.81674900 1.03712800 0.00000100

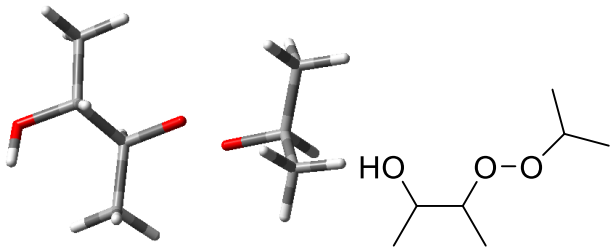

CBS-QB3 Enthalpy= -501.091964 CBS-QB3 Free Energy= -501.146355

0 1

C -2.12212700 1.83154700 0.07336800

H -2.40726200 1.96305600 -0.97397600

H -2.86353300 2.33746700 0.69479200

H -1.14554300 2.29004000 0.23210900

C -2.08075800 0.35082400 0.41439900

H -1.85176800 0.22653300 1.48290400

O -3.37592700 -0.17868300 0.12342600

H -3.46319900 -1.02939500 0.56257300

C -1.00233500 -0.41511200 -0.38518700

H -1.09634700 -0.14730600 -1.44430600

O 0.23691500 0.10085600 0.10230100

C -1.08040700 -1.92969600 -0.21969800

H -1.05603500 -2.20703700 0.83942100

H -1.99362900 -2.32131800 -0.67362800

H -0.22955300 -2.39724900 -0.71539400

O 1.25845500 -0.31217600 -0.87494100

C 2.54061800 -0.02638700 -0.30173800

H 3.19190100 -0.36170000 -1.11785600

C 2.74507200 1.47141100 -0.08219100

H 2.10025000 1.83827200 0.71806600

H 3.78404200 1.67517200 0.19137700

H 2.51226400 2.02261500 -0.99563900

C 2.81632200 -0.87016000 0.94112500

H 2.66391300 -1.92972400 0.72441600

H 3.84938800 -0.73056500 1.27129900

H 2.15125900 -0.58339100 1.75709000

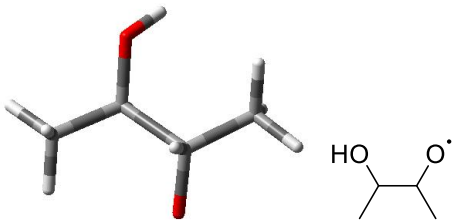

CBS-QB3 Enthalpy= -307.697445 CBS-QB3 Free Energy= -307.737661

0 2

C -1.81391000 -0.74300700 0.10097100

H -1.95919500 -0.67981700 1.18237300

H -2.73868500 -0.42732900 -0.38664300

H -1.59492600 -1.77769500 -0.16337200

C -0.67556500 0.16100700 -0.32642500

H -0.52682800 0.11966000 -1.41122000

O -0.96477700 1.47429900 0.09769800

H -0.44516200 2.09386200 -0.42320900

C 0.73021800 -0.31216800 0.32420100

H 0.51147800 -0.32527100 1.40750100

O 0.94643400 -1.54476800 -0.16769900

C 1.84370200 0.68951400 -0.00091100

H 1.95453100 0.80622900 -1.08326900

H 1.64655800 1.66250000 0.45735100

H 2.79230100 0.31952900 0.39347900

4 Reference

(1) Zhao, X.; Xiang, X.; Huang, J.; Ma, Y.; Sun, J.; Zhu, D. Studying the evaluation model of the nutritional quality of edible vegetable oil based on dietary nutrient reference intake. *ACS omega* **2021**, *6* (10), 6691-6698.

(2) Kappus, H. Lipid peroxidation: mechanisms, analysis, enzymology and biological relevance. *Oxidative stress* **1985**, 273-310.

(3) Gaschler, M. M.; Stockwell, B. R. Lipid peroxidation in cell death. *Biochemical and biophysical research communications* **2017**, *482* (3), 419-425.

(4) Dixon, S. J.; Lemberg, K. M.; Lamprecht, M. R.; Skouta, R.; Zaitsev, E. M.; Gleason, C. E.; Patel, D. N.; Bauer, A. J.; Cantley, A. M.; Yang, W. S. Ferroptosis: an iron-dependent form of nonapoptotic cell death. *cell* **2012**, *149* (5), 1060-1072.

(5) Chen, X.; Kang, R.; Kroemer, G.; Tang, D. Organelle-specific regulation of ferroptosis. *Cell Death & Differentiation* **2021**, *28* (10), 2843-2856.

(6) Jiang, X.; Stockwell, B. R.; Conrad, M. Ferroptosis: mechanisms, biology and role in disease. *Nature reviews Molecular cell biology* **2021**, *22* (4), 266-282.

(7) Dolma, S.; Lessnick, S. L.; Hahn, W. C.; Stockwell, B. R. Identification of genotype-selective antitumor agents using synthetic lethal chemical screening in engineered human tumor cells. *Cancer cell* **2003**, *3* (3), 285-296.

(8) Conrad, M.; Pratt, D. A. The chemical basis of ferroptosis. *Nature chemical biology* **2019**, *15* (12), 1137-1147.

(9) Li, W.; Liang, L.; Liu, S.; Yi, H.; Zhou, Y. FSP1: a key regulator of ferroptosis. *Trends in molecular medicine* **2023**, *29* (9), 753-764.

(10) Salas, J. n. J.; Sánchez, J.; Ramli, U. S.; Manaf, A. M.; Williams, M.; Harwood, J. L. Biochemistry of lipid metabolism in olive and other oil fruits. *Progress in lipid research* **2000**, *39* (2), 151-180.

(11) Vinnichek, L.; Pogorelova, E.; Dergunov, A. Oilseed market: Global trends. In *IOP conference series: Earth and environmental science*, 2019; IOP Publishing: Vol. 274, p 012030.

(12) Yang, R.; Zhang, L.; Li, P.; Yu, L.; Mao, J.; Wang, X.; Zhang, Q. A review of chemical composition and nutritional properties of minor vegetable oils in China. *Trends in food science & technology* **2018**, *74*, 26-32.

(13) Miras-Moreno, B.; Sabater-Jara, A. B.; Pedreño, M.; Almagro, L. Bioactivity of phytosterols and their production in plant in vitro cultures. *J. Agric. Food Chem* **2016**, *64* (38), 7049-7058.

(14) Shin, E.-C.; Huang, Y.-Z.; Pegg, R. B.; Phillips, R. D.; Eitenmiller, R. R. Commercial runner peanut cultivars in the United States: Tocopherol composition. *J. Agric. Food Chem* **2009**, *57* (21), 10289-10295.
(15) Alu'datt, M. H.; Rababah, T.; Alhamad, M. N.; Al-Mahasneh, M. A.; Almajwal, A.; Gammoh, S.; Ereifej, K.; Johargy, A.; Alli, I. A review of phenolic compounds in oil-bearing plants: Distribution, identification and occurrence of phenolic compounds. *Food Chem* **2017**, *218*, 99-106.
(16) Škorić, D.; Jocić, S.; Sakač, Z.; Lečić, N. Genetic possibilities for altering sunflower oil quality to obtain novel oils. *Canadian Journal of Physiology and Pharmacology* **2008**, *86* (4), 215-221.
(17) Ruiz Ruiz, J. C.; Ortiz Vazquez, E. D. L. L.; Segura Campos, M. R. Encapsulation of vegetable oils as source of omega-3 fatty acids for enriched functional foods. *Critical Reviews in Food Science and Nutrition* **2017**, *57* (7), 1423-1434.
(18) Orsavova, J.; Misurcova, L.; Vavra Ambrozova, J.; Vicha, R.; Mlcek, J. Fatty acids composition of vegetable oils and its contribution to dietary energy intake and dependence of cardiovascular mortality on dietary intake of fatty acids. *International journal of molecular sciences* **2015**, *16* (6), 12871-12890.
(19) Weisburger, J. H. Eat to live, not live to eat. *Nutrition* **2000**, *16* (9), 767-773.
(20) Simopoulos, A. P. Essential fatty acids in health and chronic disease. *The American journal of clinical nutrition* **1999**, *70* (3), 560S-569S.
(21) Abdullah, M.; Alwadai, N.; Al Huwayz, M.; Manzoor, S.; John, P.; Abid, A. G.; Ghouri, M. I.; Aman, S.; Al-Buriahi, M. S.; Ashiq, M. N. Effect of Ag content on the electrochemical performance of Ag2Te nanostructures synthesized by hydrothermal route for supercapacitor applications. *Energy & Fuels* **2023**, *37* (2), 1297-1309.
(22) Valgimigli, L. Lipid peroxidation and antioxidant protection. *Biomolecules* **2023**, *13* (9), 1291.
(23) Wang, P.-L.; Xie, L.-H.; Joseph, E. A.; Li, J.-R.; Su, X.-O.; Zhou, H.-C. Metal–organic frameworks for food safety. *Chem. Rev* **2019**, *119* (18), 10638-10690.
(24) Frankel, E. N. Secondary products of lipid oxidation. *Chemistry and physics of lipids* **1987**, *44* (2-4), 73-85.
(25) Girotti, A. W. Lipid hydroperoxide generation, turnover, and effector action in biological systems. *Journal of lipid research* **1998**, *39* (8), 1529-1542.
(26) Baschieri, A.; Pizzol, R.; Guo, Y.; Amorati, R.; Valgimigli, L. Calibration of squalene, p-cymene, and sunflower oil as standard oxidizable substrates for quantitative antioxidant testing. *Journal of agricultural and food chemistry* **2019**, *67* (24), 6902-6910.
(27) Porter, N. A. Mechanisms for the autoxidation of polyunsaturated lipids. *Accounts of Chemical Research* **1986**, *19* (9), 262-268.
(28) Russell, G. A. Deuterium-isotope effects in the autoxidation of aralkyl hydrocarbons. mechanism of the interaction of peroxy radicals1. *J Am Chem Soc* **1957**, *79* (14), 3871-3877.
(29) Amorati, R.; Foti, M. C. Mode of antioxidant action of essential oils. *Essential Oils in Food Processing: Chemistry, Safety and Applications* **2017**, 267-291.

(30) Zielinski, Z. A.; Pratt, D. A. Lipid peroxidation: kinetics, mechanisms, and products. *J. Org. Chem* **2017**, *82* (6), 2817-2825.
(31) Losada-Barreiro, S.; Paiva-Martins, F.; Bravo-Díaz, C. Analysis of the efficiency of antioxidants in inhibiting lipid oxidation in terms of characteristic kinetic parameters. *Antioxidants* **2024**, *13* (5), 593.
(32) Porter, N. A. A perspective on free radical autoxidation: the physical organic chemistry of polyunsaturated fatty acid and sterol peroxidation. *J. Org. Chem* **2013**, *78* (8), 3511-3524.
(33) Yin, H.; Gao, L.; Tai, H.-H.; Murphey, L. J.; Porter, N. A.; Morrow, J. D. Urinary prostaglandin F2α is generated from the isoprostane pathway and not the cyclooxygenase in humans. *Journal of Biological Chemistry* **2007**, *282* (1), 329-336.
(34) Caño-Ochoa, S. d.; Ruiz-Aracama, A.; Guillén, M. D. Individual and Joint Effect of Alpha-Tocopherol and Hydroxytyrosol Acetate on the Oxidation of Sunflower Oil Submitted to Oxidative Conditions: A Study by Proton Nuclear Magnetic Resonance. *Antioxidants* **2022**, *11* (6), 1156.
(35) Ten Klooster, S.; Takeuchi, M.; Schroën, K.; Tuinier, R.; Joosten, R.; Friedrich, H.; Berton-Carabin, C. Tiny, yet impactful: Detection and oxidative stability of very small oil droplets in surfactant-stabilized emulsions. *Journal of Colloid and Interface Science* **2023**, *652*, 1994-2004.
(36) Barani, M.; Bonetti, R.; Parker Jr, W. O. Thermal oxidation of model molecules to reveal vegetable oil polymerization studied by NMR spectroscopy and self‐diffusion. *Journal of the American Oil Chemists' Society* **2023**, *100* (7), 551-560.
(37) Flitsch, S.; Neu, P. M.; Schober, S.; Kienzl, N.; Ullmann, J. r.; Mittelbach, M. Quantitation of aging products formed in biodiesel during the rancimat accelerated oxidation test. *Energy & fuels* **2014**, *28* (9), 5849-5856.
(38) Howard, J.; Ingold, K. Absolute rate constants for hydrocarbon oxidation. XII. Rate constants for secondary peroxy radicals. *Canadian Journal of Chemistry* **1968**, *46* (16), 2661-2666.
(39) Spickett, C. M. The lipid peroxidation product 4-hydroxy-2-nonenal: advances in chemistry and analysis. *Redox biology* **2013**, *1* (1), 145-152.
(40) Esterbauer, H.; Schaur, R. J.; Zollner, H. Chemistry and biochemistry of 4-hydroxynonenal, malonaldehyde and related aldehydes. *Free radical Biology and medicine* **1991**, *11* (1), 81-128.
(41) Munteanu, I. G.; Apetrei, C. Analytical methods used in determining antioxidant activity: A review. *International journal of molecular sciences* **2021**, *22* (7), 3380.
(42) Demirci Çekiç, S.; Çetinkaya, A.; Avan, A. N.; Apak, R. a. Correlation of total antioxidant capacity with reactive oxygen species (ROS) consumption measured by oxidative conversion. *J. Agric. Food Chem* **2013**, *61* (22), 5260-5270.
(43) Sirivibulkovit, K.; Nouanthavong, S.; Sameenoi, Y. based DPPH assay for antioxidant activity analysis. *Analytical sciences* **2018**, *34* (7), 795-800.
(44) Hanthorn, J. J.; Haidasz, E.; Gebhardt, P.; Pratt, D. A. A versatile fluorescence approach to kinetic studies of hydrocarbon autoxidations and their inhibition by radical-trapping antioxidants. *Chemical Communications* **2012**, *48* (81), 10141-10143.

(45) Mengele, E.; Plashchina, I.; Kasaikina, O. Kinetics of lecithin oxidation in liposomal aqueous solutions. *Colloid journal* **2011**, *73* (6), 815-821.
(46) Amorati, R.; Baschieri, A.; Valgimigli, L. Measuring antioxidant activity in bioorganic samples by the differential oxygen uptake apparatus: Recent advances. *Journal of Chemistry* **2017**, *2017* (1), 6369358.
(47) Mollica, F.; Gelabert, I.; Amorati, R. Synergic antioxidant effects of the essential oil component γ-terpinene on high-temperature oil oxidation. *ACS Food Science & Technology* **2022**, *2* (1), 180-186.
(48) Valgimigli, L.; Pratt, D. A. Antioxidants in chemistry and biology. *Encyclopedia of radicals in chemistry, biology and materials* **2012**.
(49) Burton, G.; Ingold, K. Autoxidation of biological molecules. 1. Antioxidant activity of vitamin E and related chain-breaking phenolic antioxidants in vitro. *J Am Chem Soc* **1981**, *103* (21), 6472-6477.
(50) Valgimigli, L.; Amorati, R.; Petrucci, S.; Pedulli, G. F.; Hu, D.; Hanthorn, J. J.; Pratt, D. A. Unexpected acid catalysis in reactions of peroxyl radicals with phenols. *Angew. Chem* **2009**, *121* (44), 8498-8501.
(51) Amorati, R.; Valgimigli, L.; Pedulli, G. F.; Grabovskiy, S. A.; Kabal'nova, N. N.; Chatgilialoglu, C. Base-promoted reaction of 5-hydroxyuracil derivatives with peroxyl radicals. *Organic letters* **2010**, *12* (18), 4130-4133.
(52) Haidasz, E. A.; Meng, D.; Amorati, R.; Baschieri, A.; Ingold, K. U.; Valgimigli, L.; Pratt, D. A. Acid is key to the radical-trapping antioxidant activity of nitroxides. *J Am Chem Soc* **2016**, *138* (16), 5290-5298.
(53) Aksu, K.; Topal, F.; Gulcin, I.; Tümer, F.; Göksu, S. Acetylcholinesterase inhibitory and antioxidant activities of novel symmetric sulfamides derived from phenethylamines. *Archiv der Pharmazie* **2015**, *348* (6), 446-455.
(54) Sindhi, V.; Gupta, V.; Sharma, K.; Bhatnagar, S.; Kumari, R.; Dhaka, N. Potential applications of antioxidants–A review. *Journal of pharmacy research* **2013**, *7* (9), 828-835.
(55) Halliwell, B. Antioxidants in human health and disease. *Annual review of nutrition* **1996**, *16* (1), 33-50.
(56) Buttriss, J. L.; Hughes, J.; Kelly, C. N.; Stanner, S. Antioxidants in food: a summary of the review conducted for the Food Standards Agency. *Nutrition Bulletin* **2002**, *27* (4), 227-236.
(57) Permana, T.; Wiradjaja, N.; Sutanto, H.; Surya, V. S. A review on the potential of natural antioxidant sources to improve oxidative stability in edible oils. In *6th International Conference of Food, Agriculture, and Natural Resource (IC-FANRES 2021)*, 2022; Atlantis Press: pp 117-125.
(58) Niki, E. Antioxidants: basic principles, emerging concepts, and problems. *Biomed J* **2014**, *37* (3), 106-111.
(59) Podsędek, A. Natural antioxidants and antioxidant capacity of Brassica vegetables: A review. *LWT-Food science and Technology* **2007**, *40* (1), 1-11.
(60) Pokorný, J. Natural antioxidants for food use. *Trends in Food Science & Technology* **1991**, *2*, 223-227.

(61) Bendich, A.; Machlin, L.; Scandurra, O.; Burton, G.; Wayner, D. The antioxidant role of vitamin C. *Advances in Free Radical Biology & Medicine* **1986**, *2* (2), 419-444.
(62) Block, G.; Jensen, C.; Dietrich, M.; Norkus, E. P.; Hudes, M.; Packer, L. Plasma C-reactive protein concentrations in active and passive smokers: influence of antioxidant supplementation. *Journal of the American College of Nutrition* **2004**, *23* (2), 141-147.
(63) Block, J. P.; Scribner, R. A.; DeSalvo, K. B. Fast food, race/ethnicity, and income: a geographic analysis. *American journal of preventive medicine* **2004**, *27* (3), 211-217.
(64) Davey, M. W.; Montagu, M. V.; Inze, D.; Sanmartin, M.; Kanellis, A.; Smirnoff, N.; Benzie, I. J. J.; Strain, J. J.; Favell, D.; Fletcher, J. Plant L‐ascorbic acid: chemistry, function, metabolism, bioavailability and effects of processing. *Journal of the Science of Food and Agriculture* **2000**, *80* (7), 825-860.
(65) Aherne, S. A.; O'Brien, N. M. Dietary flavonols: chemistry, food content, and metabolism. *Nutrition* **2002**, *18* (1), 75-81.
(66) Holiman, P. C.; Hertog, M. G.; Katan, M. B. Analysis and health effects of flavonoids. *Food chemistry* **1996**, *57* (1), 43-46.
(67) Price, K. R.; Casuscelli, F.; Colquhoun, I. J.; Rhodes, M. J. Composition and content of flavonol glycosides in broccoli florets (Brassica olearacea) and their fate during cooking. *Journal of the Science of Food and Agriculture* **1998**, *77* (4), 468-472.
(68) Olsen, J. H.; Nielsen, A.; Schulgen, G. Residence near high voltage facilities and risk of cancer in children. *British medical journal* **1993**, *307* (6909), 891-895.
(69) Stahl, W.; Sies, H. Antioxidant activity of carotenoids. *Molecular aspects of medicine* **2003**, *24* (6), 345-351.
(70) Sies, H.; Stahl, W. Vitamins E and C, beta-carotene, and other carotenoids as antioxidants. *The American journal of clinical nutrition* **1995**, *62* (6), 1315S-1321S.
(71) Rice-Evans, C. A.; Sampson, J.; Bramley, P. M.; Holloway, D. E. Why do we expect carotenoids to be antioxidants in vivo? *Free radical research* **1997**, *26* (4), 381-398.
(72) Azzi, A. Tocopherols, tocotrienols and tocomonoenols: Many similar molecules but only one vitamin E. *Redox Biology* **2019**, *26*, 101259.
(73) Stampfer, M. J.; Rimm, E. B. Epidemiologic evidence for vitamin E in prevention of cardiovascular disease. *The American journal of clinical nutrition* **1995**, *62* (6), 1365S-1369S.
(74) Jiang, Q. Natural forms of vitamin E: metabolism, antioxidant, and anti-inflammatory activities and their role in disease prevention and therapy. *Free Radical Biology and Medicine* **2014**, *72*, 76-90.
(75) Ousji, O.; Sleno, L. Identification of in vitro metabolites of synthetic phenolic antioxidants BHT, BHA, and TBHQ by LC-HRMS/MS. *International journal of molecular sciences* **2020**, *21* (24), 9525.
(76) Sen, S.; Chakraborty, R. The role of antioxidants in human health. In *Oxidative stress: diagnostics, prevention, and therapy*, ACS Publications, 2011; pp 1-37.
(77) Hauso, Ø.; Martinsen, T. C.; Waldum, H. 5-Aminosalicylic acid, a specific drug for ulcerative colitis. *Scandinavian Journal of Gastroenterology* **2015**, *50* (8), 933-941.

(78) Taj, M.; Tirmizi, S.; Raheel, A.; Ali, H. M.; Qureshi, S.; Alshatir, H. Benzamide derivatives as potential candidates for anti-alzheimer, anti-fatigue, anti-urease and anti-oxidant activity. *Journal of the Chilean Chemical Society* **2017**, *62* (1), 3342-3344.
(79) Barteková, M.; Adameová, A.; Görbe, A.; Ferenczyová, K.; Pecháňová, O.; Lazou, A.; Dhalla, N. S.; Ferdinandy, P.; Giricz, Z. Natural and synthetic antioxidants targeting cardiac oxidative stress and redox signaling in cardiometabolic diseases. *Free Radical Biology and Medicine* **2021**, *169*, 446-477.
(80) Pilz, S.; März, W. Free fatty acids as a cardiovascular risk factor. *Clinical chemistry and laboratory medicine* **2008**, *46* (4), 429-434.
(81) Skiera, C.; Steliopoulos, P.; Kuballa, T.; Diehl, B.; Holzgrabe, U. Determination of free fatty acids in pharmaceutical lipids by 1H NMR and comparison with the classical acid value. *Journal of Pharmaceutical and Biomedical Analysis* **2014**, *93*, 43-50.
(82) Frega, N.; Mozzon, M.; Lercker, G. Effects of free fatty acids on oxidative stability of vegetable oil. *Journal of the American Oil Chemists' Society* **1999**, *76* (3), 325-329.
(83) Miyashita, K.; Takagi, T. Study on the oxidative rate and prooxidant activity of free fatty acids. *Journal of the American Oil Chemists' Society* **1986**, *63* (10), 1380-1384.
(84) Colakoglu, A. S. Oxidation kinetics of soybean oil in the presence of monoolein, stearic acid and iron. *Food Chemistry* **2007**, *101* (2), 724-728.
(85) Waraho, T.; McClements, D. J.; Decker, E. A. Impact of free fatty acid concentration and structure on lipid oxidation in oil-in-water emulsions. *Food chemistry* **2011**, *129* (3), 854-859.
(86) Choe, E.; Min, D. B. Mechanisms and factors for edible oil oxidation. *Comprehensive reviews in food science and food safety* **2006**, *5* (4), 169-186.
(87) Chaiyasit, W.; McClements, D. J.; Weiss, J.; Decker, E. A. Impact of surface-active compounds on physicochemical and oxidative properties of edible oil. *Journal of Agricultural and Food Chemistry* **2008**, *56* (2), 550-556.
(88) Lowry, R. R.; Tinsley, I. J. Rapid colorimetric determination of free fatty acids. *Journal of the American Oil Chemists Society* **1976**, *53* (7), 470-472.
(89) Mabou, F. D.; Yossa, I. B. N. TERPENES: Structural classification and biological activities. *IOSR J Pharm Biol Sci* **2021**, *16*, 25-40.
(90) Saito, A. Y.; Rodriguez, A. A. M.; Vega, D. S. M.; Sussmann, R. A.; Kimura, E. A.; Katzin, A. M. Antimalarial activity of the terpene nerolidol. *International journal of antimicrobial agents* **2016**, *48* (6), 641-646.
(91) Cox-Georgian, D.; Ramadoss, N.; Dona, C.; Basu, C. Therapeutic and medicinal uses of terpenes. In *Medicinal plants: from farm to pharmacy*, Springer, 2019; pp 333-359.
(92) Guppi, S. R.; O'Doherty, G. A. 1, 3-Cyclohexadiene. *Encyclopedia of Reagents for Organic Synthesis* **2001**.
(93) Basak, A.; Mandal, S.; Bag, S. S. Chelation-controlled Bergman cyclization: synthesis and reactivity of enediynyl ligands. *Chem. Rev* **2003**, *103* (10), 4077-4094.
(94) Amorati, R.; Foti, M. C.; Valgimigli, L. Antioxidant activity of essential oils. *J. Agric. Food Chem* **2013**, *61* (46), 10835-10847.

(95) Ahmed, A. F.; Attia, F. A.; Liu, Z.; Li, C.; Wei, J.; Kang, W. Antioxidant activity and total phenolic content of essential oils and extracts of sweet basil (Ocimum basilicum L.) plants. *Food Science and Human Wellness* **2019**, *8* (3), 299-305.
(96) Ruberto, G.; Baratta, M. T. Antioxidant activity of selected essential oil components in two lipid model systems. *Food Chem* **2000**, *69* (2), 167-174.
(97) Graßmann, J.; Schneider, D.; Weiser, D.; Elstner, E. F. Antioxidative effects of lemon oil and its components on copper induced oxidation of low density lipoprotein. *Arzneimittelforschung* **2001**, *51* (10), 799-805.
(98) Guo, Y.; Baschieri, A.; Mollica, F.; Valgimigli, L.; Cedrowski, J.; Litwinienko, G.; Amorati, R. Hydrogen Atom Transfer from HOO. to ortho-Quinones Explains the Antioxidant Activity of Polydopamine. *Angew. Chem. Int. Ed* **2021**, *60* (28), 15220-15224.
(99) Foti, M. C.; Ingold, K. Mechanism of inhibition of lipid peroxidation by γ-terpinene, an unusual and potentially useful hydrocarbon antioxidant. *J. Agric. Food Chem* **2003**, *51* (9), 2758-2765.
(100) Jin, Z.; Mollica, F.; Huang, Y.; Guernelli, S.; Baschieri, A.; Diquigiovanni, C.; Rizzardi, N.; Valenti, F.; Pincigher, L.; Bergamini, C. Pro-aromatic Natural Terpenes as Unusual "Slingshot" Antioxidants with Promising Ferroptosis Inhibition Activity. *Chem. Eur. J* **2024**, *30* (72), e202403320.
(101) Zimmerman, H. E. A mechanistic analysis of the Birch reduction. *Accounts of chemical research* **2012**, *45* (2), 164-170.
(102) Birch, A. J. 117. Reduction by dissolving metals. Part I. *Journal of the Chemical Society (Resumed)* **1944**, 430-436.
(103) Benkeser, R. A.; Arnold Jr, C.; Lambert, R. F.; Thomas, O. H. Reduction of organic compounds by lithium in low molecular weight amines. III. Reduction of aromatic compounds containing functional groups. *J Am Chem Soc* **1955**, *77* (22), 6042-6045.
(104) Garst, M. E.; Dolby, L. J.; Esfandiari, S.; Fedoruk, N. A.; Chamberlain, N. C.; Avey, A. A. Reductions with lithium in low molecular weight amines and ethylenediamine. *J. Org. Chem* **2000**, *65* (21), 7098-7104.
(105) Peters, B. K.; Rodriguez, K. X.; Reisberg, S. H.; Beil, S. B.; Hickey, D. P.; Kawamata, Y.; Collins, M.; Starr, J.; Chen, L.; Udyavara, S. Scalable and safe synthetic organic electroreduction inspired by Li-ion battery chemistry. *Science* **2019**, *363* (6429), 838-845.
(106) Semenza, G. L. Life with oxygen. *Science* **2007**, *318* (5847), 62-64.
(107) Kowaltowski, A. J.; Castilho, R. F.; Vercesi, A. E. Mitochondrial permeability transition and oxidative stress. *FEBS letters* **2001**, *495* (1-2), 12-15.
(108) Liu, P.; Wu, X.; Gong, B.; Lü, G.; Li, J.; Gao, H. Review of the mechanisms by which transcription factors and exogenous substances regulate ROS metabolism under abiotic stress. *Antioxidants* **2022**, *11* (11), 2106.
(109) Zorov, D. B.; Juhaszova, M.; Sollott, S. J. Mitochondrial reactive oxygen species (ROS) and ROS-induced ROS release. *Physiological reviews* **2014**, *94* (3), 909-950.

(110) Turrens, J. F. Mitochondrial formation of reactive oxygen species. *The Journal of physiology* **2003**, *552* (2), 335-344.
(111) Agarwal, R. G.; Coste, S. C.; Groff, B. D.; Heuer, A. M.; Noh, H.; Parada, G. A.; Wise, C. F.; Nichols, E. M.; Warren, J. J.; Mayer, J. M. Free energies of proton-coupled electron transfer reagents and their applications. *Chem. Rev* **2021**, *122* (1), 1-49.
(112) Das, A. B.; Nagy, P.; Abbott, H. F.; Winterbourn, C. C.; Kettle, A. J. Reactions of superoxide with the myoglobin tyrosyl radical. *Free Radical Biology and Medicine* **2010**, *48* (11), 1540-1547.
(113) Howard, J.; Ingold, K. Absolute rate constants for hydrocarbon autoxidation. V. The hydroperoxy radical in chain propagation and termination. *Canadian Journal of Chemistry* **1967**, *45* (8), 785-792.
(114) Cedrowski, J.; Litwinienko, G.; Baschieri, A.; Amorati, R. Hydroperoxyl Radicals (HOO.): Vitamin E Regeneration and H‐Bond Effects on the Hydrogen Atom Transfer. *Chem. Eur. J* **2016**, *22* (46), 16441-16445.
(115) Baschieri, A.; Jin, Z.; Amorati, R. Hydroperoxyl radical (HOO•) as a reducing agent: unexpected synergy with antioxidants. A review. *Free Radical Research* **2023**, *57* (2), 115-129.
(116) Roginsky, V.; Barsukova, T. Superoxide dismutase inhibits lipid peroxidation in micelles. *Chemistry and Physics of Lipids* **2001**, *111* (1), 87-91.
(117) Sortino, S.; Petralia, S.; Foti, M. C. Absolute rate constants and transient intermediates in the free-radical-induced peroxidation of-terpinene, an unusual hydrocarbon antioxidantDedicated to Professor Giuseppe Condorelli on the occasion of his 73rd birthday. **2003**.
(118) Vardanyan, R.; Denisov, E. Regeneration of inhibitors in oxidized 1, 3-cyclohexadiene. *Bulletin of the Academy of Sciences of the USSR, Division of chemical science* **1971**, *20* (12), 2681-2683.
(119) Chung, H. Y.; Baek, B. S.; Song, S. H.; Kim, M. S.; Huh, J. I.; Shim, K. H.; Kim, K. W.; Lee, K. H. Xanthine dehydrogenase/xanthine oxidase and oxidative stress. *Age* **1997**, *20* (3), 127-140.
(120) Vermot, A.; Petit-Härtlein, I.; Smith, S. M.; Fieschi, F. NADPH oxidases (NOX): an overview from discovery, molecular mechanisms to physiology and pathology. *Antioxidants* **2021**, *10* (6), 890.
(121) Huang, S.-W.; Hopia, A.; Schwarz, K.; Frankel, E. N.; German, J. B. Antioxidant activity of α-tocopherol and trolox in different lipid substrates: bulk oils vs oil-in-water emulsions. *J. Agric. Food Chem* **1996**, *44* (2), 444-452.
(122) Loshadkin, D.; Pliss, E.; Kasaikina, O. Features of methyl linoleate oxidation in Triton X-100 micellar buffer solutions. *Russian Journal of Applied Chemistry* **2020**, *93* (7), 1090-1095.
(123) Shah, R.; Farmer, L. A.; Zilka, O.; Van Kessel, A. T.; Pratt, D. A. Beyond DPPH: use of fluorescence-enabled inhibited autoxidation to predict oxidative cell death rescue. *Cell chemical biology* **2019**, *26* (11), 1594-1607. e1597.

(124) Amorati, R.; Baschieri, A.; Morroni, G.; Gambino, R.; Valgimigli, L. Peroxyl radical reactions in water solution: A gym for proton-coupled electron-transfer theories. *Chem. Eur. J* **2016**, *22* (23), 7924-7934.
(125) Konopko, A.; Litwinienko, G. Unexpected role of pH and microenvironment on the antioxidant and synergistic activity of resveratrol in model micellar and liposomal systems. *J. Org. Chem* **2021**, *87* (3), 1698-1709.
(126) Chen, M.; Ghelfi, M.; Poon, J.-F.; Jeon, N.; Boccalon, N.; Rubsamen, M.; Valentino, S.; Mehta, V.; Stamper, M.; Tariq, H. Antioxidant-independent activities of alpha-tocopherol. *Journal of Biological Chemistry* **2025**, *301* (4), 108327.
(127) Kaljurand, I.; Kütt, A.; Sooväli, L.; Rodima, T.; Mäemets, V.; Leito, I.; Koppel, I. A. Extension of the self-consistent spectrophotometric basicity scale in acetonitrile to a full span of 28 p K a units: unification of different basicity scales. *J. Org. Chem* **2005**, *70* (3), 1019-1028.
(128) Tshepelevitsh, S.; Kütt, A.; Lõkov, M.; Kaljurand, I.; Saame, J.; Heering, A.; Plieger, P. G.; Vianello, R.; Leito, I. On the basicity of organic bases in different media. *European journal of organic chemistry* **2019**, *2019* (40), 6735-6748.
(129) Droge, S.; Hermens, J.; Rabone, J.; Gutsell, S.; Hodges, G. Phospholipophilicity of C x H y N+ amines: chromatographic descriptors and molecular simulations for understanding partitioning into membranes. *Environmental Science: Processes & Impacts* **2016**, *18* (8), 1011-1023.
(130) Yang, D.; Zuccarello, G.; Mattes, B. R. Physical stabilization or chemical degradation of concentrated solutions of polyaniline emeraldine base containing secondary amine additives. *Macromolecules* **2002**, *35* (13), 5304-5313.
(131) Rossini, E.; Bochevarov, A. D.; Knapp, E. W. Empirical Conversion of p K a Values between Different Solvents and Interpretation of the Parameters: Application to Water, Acetonitrile, Dimethyl Sulfoxide, and Methanol. *ACS omega* **2018**, *3* (2), 1653-1662.
(132) Kaupmees, K.; Trummal, A.; Leito, I. Basicities of strong bases in water: A computational study. *Croatica chemica acta* **2014**, *87* (4), 385-395.
(133) Jin, S.; Sanii, R.; Song, B.-Q.; Zaworotko, M. J. Crystal Engineering of Ionic Cocrystals Sustained by the Phenol–Phenolate Supramolecular Heterosynthon. *Crystal Growth & Design* **2022**, *22* (7), 4582-4591.
(134) Cui, X.; Mao, S.; Liu, M.; Yuan, H.; Du, Y. Mechanism of surfactant micelle formation. *Langmuir* **2008**, *24* (19), 10771-10775.
(135) Sawyer, D. T.; Valentine, J. S. How super is superoxide? *Accounts of Chemical Research* **1981**, *14* (12), 393-400.
(136) Bowry, V. W.; Stocker, R. Tocopherol-mediated peroxidation. The prooxidant effect of vitamin E on the radical-initiated oxidation of human low-density lipoprotein. *J Am Chem Soc* **1993**, *115* (14), 6029-6044.
(137) Akbarzadeh, A.; Rezaei-Sadabady, R.; Davaran, S.; Joo, S. W.; Zarghami, N.; Hanifehpour, Y.; Samiei, M.; Kouhi, M.; Nejati-Koshki, K. Liposome: classification, preparation, and applications. *Nanoscale research letters* **2013**, *8* (1), 102.

(138) Mashaghi, S.; Jadidi, T.; Koenderink, G.; Mashaghi, A. Lipid nanotechnology. *International journal of molecular sciences* **2013**, *14* (2), 4242-4282.
(139) Burton, G. W.; Doba, T.; Gabe, E.; Hughes, L.; Lee, F.; Prasad, L.; Ingold, K. U. Autoxidation of biological molecules. 4. Maximizing the antioxidant activity of phenols. *J Am Chem Soc* **1985**, *107* (24), 7053-7065.
(140) Liu, Y.; Zhang, Y.; Liu, Q.; Wang, Q.; Lin, A.; Luo, J.; Du, Y.; Lin, Y.-W.; Wei, H. In vitro measurement of superoxide dismutase-like nanozyme activity: a comparative study. *Analyst* **2021**, *146* (6), 1872-1879.
(141) Podczasy, J. J.; Wei, R. Reduction of iodonitrotetrazolium violet by superoxide radicals. *Biochemical and biophysical research communications* **1988**, *150* (3), 1294-1301.
(142) Shelton, J. R.; Uzelmeier, C. W. Reactions of alkenes with di-tert-butyl peroxide and tert-butyl peroxypivalate. *J. Org. Chem* **1970**, *35* (5), 1576-1581.
(143) Tikhonov, I.; Pliss, E.; Borodin, L.; Sen', V. Effect of superoxide dismutase on the oxidation of methyl linoleate in micelles inhibited by nitroxyl radicals. *Russian Chemical Bulletin* **2016**, *65* (12), 2985-2987.
(144) Burrows, J.; Kamo, S.; Koide, K. Scalable Birch reduction with lithium and ethylenediamine in tetrahydrofuran. *Science* **2021**, *374* (6568), 741-746.
(145) Li, D.; Li, Y. The interaction between ferroptosis and lipid metabolism in cancer. *Signal transduction and targeted therapy* **2020**, *5* (1), 108.
(146) Lippmann, J.; Petri, K.; Fulda, S.; Liese, J. Redox modulation and induction of ferroptosis as a new therapeutic strategy in hepatocellular carcinoma. *Translational oncology* **2020**, *13* (8), 100785.
(147) Tang, D.; Chen, X.; Kang, R.; Kroemer, G. Ferroptosis: molecular mechanisms and health implications. *Cell research* **2021**, *31* (2), 107-125.
(148) Miotto, G.; Rossetto, M.; Di Paolo, M. L.; Orian, L.; Venerando, R.; Roveri, A.; Vučković, A.-M.; Travain, V. B.; Zaccarin, M.; Zennaro, L. Insight into the mechanism of ferroptosis inhibition by ferrostatin-1. *Redox biology* **2020**, *28*, 101328.
(149) Pedrera, L.; Prieto Clemente, L.; Dahlhaus, A.; Lotfipour Nasudivar, S.; Tishina, S.; Olmo González, D.; Stroh, J.; Yapici, F. I.; Singh, R. P.; Grotehans, N. Ferroptosis triggers mitochondrial fragmentation via Drp1 activation. *Cell Death & Disease* **2025**, *16* (1), 40.
(150) Scarpellini, C.; Klejborowska, G.; Lanthier, C.; Hassannia, B.; Vanden Berghe, T.; Augustyns, K. Beyond ferrostatin-1: a comprehensive review of ferroptosis inhibitors. *Trends in Pharmacological Sciences* **2023**, *44* (12), 902-916.
(151) Donohoe, M. N.; Upadhyay, A.; Pratt, D. A. Ligand-Based Radical Reactivity of Metal Thiosemicarbazones Prompts the Identification of Platinum (II)-Based Cytoprotectants. *J Am Chem Soc* **2024**, *146* (45), 31307-31320.
(152) Simmie, J. M.; Somers, K. P. Benchmarking compound methods (CBS-QB3, CBS-APNO, G3, G4, W1BD) against the active thermochemical tables: a litmus test for cost-effective molecular formation enthalpies. *J. Phys. Chem. A* **2015**, *119* (28), 7235-7246.
(153) Xu, L.; Coote, M. L. Methods to improve the calculations of solvation model density solvation free energies and associated aqueous p K a values: Comparison between

choosing an optimal theoretical level, solute cavity scaling, and using explicit solvent molecules. *The Journal of Physical Chemistry A* **2019**, *123* (34), 7430-7438.
(154) Baschieri, A.; Ajvazi, M. D.; Tonfack, J. L. F.; Valgimigli, L.; Amorati, R. Explaining the antioxidant activity of some common non-phenolic components of essential oils. *Food Chem* **2017**, *232*, 656-663.
(155) Howard, J.; Yamada, T. Absolute rate constants for hydrocarbon autoxidation. 31. Autoxidation of cumene in the presence of tertiary amines. *J Am Chem Soc* **1981**, *103* (24), 7102-7106.
(156) Konopko, A.; Litwinienko, G. Unexpected Role of pH and Microenvironment on the Antioxidant and Synergistic Activity of Resveratrol in Model Micellar and Liposomal Systems. *J. Org. Chem.* **2022**, *87* (3), 1698-1709. DOI: 10.1021/acs.joc.1c01801.
(157) Amorati, R.; Baschieri, A.; Morroni, G.; Gambino, R.; Valgimigli, L. Peroxyl Radical Reactions in Water Solution: A Gym for Proton-Coupled Electron-Transfer Theories. *Chem.-Eur. J.* **2016**, *22* (23), 7924-7934. DOI: 10.1002/chem.201504492.
(158) Shah, R.; Farmer, L. A.; Zilka, O.; Van Kessel, A. T. M.; Pratt, D. A. Beyond DPPH: Use of Fluorescence-Enabled Inhibited Autoxidation to Predict Oxidative Cell Death Rescue. *Cell Chem. Biol.* **2019**, *26* (11), 1594-1607. DOI: 10.1016/j.chembiol.2019.09.007.
(159) Xu, L. B.; Davis, T. A.; Porter, N. A. Rate Constants for Peroxidation of Polyunsaturated Fatty Acids and Sterols in Solution and in Liposomes. *J. Am. Chem. Soc.* **2009**, *131* (36), 13037-13044. DOI: 10.1021/ja9029076.
(160) Cedrowski, J.; Litwinienko, G.; Baschieri, A.; Amorati, R. Hydroperoxyl Radicals (HOO•): VitaminE Regeneration and H-Bond Effects on the Hydrogen Atom Transfer. *Chem.-Eur. J.* **2016**, *22* (46), 16441-16445. DOI: 10.1002/chem.201603722.
(161) Bielski, B. H.; Allen, A. O. Mechanism of the disproportionation of superoxide radicals. *J. Phys. Chem.* **1977**, *81* (11), 1048-1050.
(162) Do, Q.; Lee, D. D.; Dinh, A. N.; Seguin, R. P.; Zhang, R.; Xu, L. Development and application of a peroxyl radical clock approach for measuring both hydrogen-atom transfer and peroxyl radical addition rate constants. *J. Org. Chem* **2020**, *86* (1), 153-168.
(163) Roschek, B.; Tallman, K. A.; Rector, C. L.; Gillmore, J. G.; Pratt, D. A.; Punta, C.; Porter, N. A. Peroxyl radical clocks. *J. Org. Chem* **2006**, *71* (9), 3527-3532.
(164) Lucarini, M.; Pedulli, G. F.; Valgimigli, L. Do peroxyl radicals obey the principle that kinetic solvent effects on H-Atom abstraction are independent of the nature of the abstracting radical? *J. Org. Chem* **1998**, *63* (13), 4497-4499.
(165) Dosoky, N. S.; Setzer, W. N. Chemical composition and biological activities of essential oils of Curcuma species. *Nutrients* **2018**, *10* (9), 1196.
(166) Rudbäck, J.; Bergström, M. A.; Börje, A.; Nilsson, U.; Karlberg, A.-T. α-Terpinene, an antioxidant in tea tree oil, autoxidizes rapidly to skin allergens on air exposure. *Chemical Research in Toxicology* **2012**, *25* (3), 713-721.
(167) Halliwell, B. Understanding mechanisms of antioxidant action in health and disease. *Nature Reviews Molecular Cell Biology* **2024**, *25* (1), 13-33.

(168) Li, G.-X.; Liu, Z.-Q. Unusual antioxidant behavior of α-and γ-terpinene in protecting methyl linoleate, DNA, and erythrocyte. *J. Agric. Food Chem* **2009**, *57* (9), 3943-3948.
(169) Abbott, N. J.; Patabendige, A. A.; Dolman, D. E.; Yusof, S. R.; Begley, D. J. Structure and function of the blood–brain barrier. *Neurobiology of disease* **2010**, *37* (1), 13-25.
(170) Corasaniti, M.; Maiuolo, J.; Maida, S.; Fratto, V.; Navarra, M.; Russo, R.; Amantea, D.; Morrone, L. A.; Bagetta, G. Cell signaling pathways in the mechanisms of neuroprotection afforded by bergamot essential oil against NMDA‐induced cell death in vitro. *British journal of pharmacology* **2007**, *151* (4), 518-529.
(171) Cioanca, O.; Hritcu, L.; Mihasan, M.; Hancianu, M. Cognitive-enhancing and antioxidant activities of inhaled coriander volatile oil in amyloid β (1–42) rat model of Alzheimer's disease. *Physiology & behavior* **2013**, *120*, 193-202.
(172) Mao, C.; Liu, X.; Zhang, Y.; Lei, G.; Yan, Y.; Lee, H.; Koppula, P.; Wu, S.; Zhuang, L.; Fang, B. DHODH-mediated ferroptosis defence is a targetable vulnerability in cancer. *Nature* **2021**, *593* (7860), 586-590.
(173) Mishima, E.; Ito, J.; Wu, Z.; Nakamura, T.; Wahida, A.; Doll, S.; Tonnus, W.; Nepachalovich, P.; Eggenhofer, E.; Aldrovandi, M. A non-canonical vitamin K cycle is a potent ferroptosis suppressor. *Nature* **2022**, *608* (7924), 778-783.
(174) Dryzhakov, M.; Hellal, M.; Wolf, E.; Falk, F. C.; Moran, J. Nitro-assisted Brønsted acid catalysis: application to a challenging catalytic azidation. *J Am Chem Soc* **2015**, *137* (30), 9555-9558.
(175) Haidasz, E. A.; Van Kessel, A. T.; Pratt, D. A. A continuous visible light spectrophotometric approach to accurately determine the reactivity of radical-trapping antioxidants. *J. Org. Chem* **2016**, *81* (3), 737-744.
(176) Montgomery Jr, J. A.; Frisch, M. J.; Ochterski, J. W.; Petersson, G. A. A complete basis set model chemistry. VI. Use of density functional geometries and frequencies. *The Journal of chemical physics* **1999**, *110* (6), 2822-2827.
(177) Frisch, M.; Trucks, G.; Schlegel, H.; Scuseria, G.; Robb, M.; Cheeseman, J.; Scalmani, G.; Barone, V.; Petersson, G.; Nakatsuji, H. Gaussian 16, Revision C. 01. Gaussian, Inc., Wallingford CT. 2016. *There is no corresponding record for this reference* **2016**.
(178) Akoh, C. C. *Food lipids: chemistry, nutrition, and biotechnology*; CRC press, 2017.
(179) Fryer, M. The antioxidant effects of thylakoid vitamin E (α‐tocopherol). *Plant, Cell & Environment* **1992**, *15* (4), 381-392.
(180) Mollica, F.; Lucarini, M.; Passerini, C.; Carati, C.; Pavoni, S.; Bonoldi, L.; Amorati, R. Effect of antioxidants on high-temperature stability of renewable bio-oils revealed by an innovative method for the determination of kinetic parameters of oxidative reactions. *Antioxidants* **2020**, *9* (5), 399.
(181) Asma, U.; Bertotti, M. L.; Zamai, S.; Arnold, M.; Amorati, R.; Scampicchio, M. A kinetic approach to oxygen radical absorbance capacity (ORAC): Restoring order to the

antioxidant activity of hydroxycinnamic acids and fruit juices. *Antioxidants* **2024**, *13* (2), 222.
(182) Liu, L.; Hudgins, W. R.; Shack, S.; Yin, M. Q.; Samid, D. Cinnamic acid: a natural product with potential use in cancer intervention. *International journal of cancer* **1995**, *62* (3), 345-350.
(183) Cavallini, L.; Valente, M.; Bindoli, A. Comparison of cumene hydroperoxide-and NADPH/Fe3+/ADP-induced lipid peroxidation in heart and liver submitochondrial particles: Mechanisms of protection by succinate. *Biochimica et Biophysica Acta (BBA)-Lipids and Lipid Metabolism* **1984**, *795* (3), 466-472.
(184) Wu, K.; Hou, H.; Shu, C. Thermal phenomena studies for dicumyl peroxide at various concentrations by DSC. *Journal of Thermal Analysis and Calorimetry* **2006**, *83* (1), 41-44.
(185) Miyake, Y.; Yokomizo, K.; Matsuzaki, N. Determination of unsaturated fatty acid composition by high-resolution nuclear magnetic resonance spectroscopy. *Journal of the American Oil Chemists' Society* **1998**, *75* (12), 1091-1094.
(186) Kamal‐Eldin, A. Effect of fatty acids and tocopherols on the oxidative stability of vegetable oils. *European Journal of Lipid Science and Technology* **2006**, *108* (12), 1051-1061.
(187) Nam, T.-g. Lipid peroxidation and its toxicological implications. *Toxicological research* **2011**, *27* (1), 1-6.
(188) Jia, C.-H.; Shin, J.-A.; Lee, K.-T. Effects of caffeic acid phenethyl ester and 4-vinylcatechol on the stabilities of oil-in-water emulsions of stripped soybean oil. *Journal of Agricultural and Food Chemistry* **2015**, *63* (47), 10280-10286.
(189) Wong, M.; Timms, R.; Goh, E. Colorimetric determination of total tocopherols in palm oil, olein and stearin. *Journal of the American oil chemists society* **1988**, *65* (2), 258-261.
(190) Hoops, S.; Sahle, S.; Gauges, R.; Lee, C.; Pahle, J.; Simus, N.; Singhal, M.; Xu, L.; Mendes, P.; Kummer, U. COPASI—a complex pathway simulator. *Bioinformatics* **2006**, *22* (24), 3067-3074.
(191) Guo, Y.; Amorati, R. The underrecognized role of the hydroperoxyl (HOO•) radical in chain propagation of lipids and its implication in antioxidant activity. In *Lipid Oxidation in Food and Biological Systems: A Physical Chemistry Perspective*, Springer, 2022; pp 115-132.
(192) Amorati, R.; Lynett, P. T.; Valgimigli, L.; Pratt, D. A. The Reaction of Sulfenic Acids with Peroxyl Radicals: Insights into the Radical‐Trapping Antioxidant Activity of Plant‐Derived Thiosulfinates. *Chemistry–A European Journal* **2012**, *18* (20), 6370-6379.